UTS UNIVERSITY OF TECHNOLOGY SYDNEY

Applying microfluidics for industrial production of stem cells

by Lin Ding

Thesis submitted in fulfilment of the requirements for the degree of

Doctor of Philosophy

under the supervision of Prof. Majid Ebrahimi Warkiani
Adjuvant Prof. Graham Vesey

University of Technology Sydney
Faculty of Engineering and Information Technology

August 2022

Certificate of Original Authorship

I, Lin Ding, declare that this thesis is submitted in fulfillment of the requirements for the award of Doctor of Philosophy, in the School of Biomedical Engineering, Faculty of Engineering and Technology at the University of Technology Sydney.

This thesis is wholly my own work unless otherwise reference or acknowledged. In addition, I certify that all information sources and literature used are indicated in the thesis.

This document has not been submitted for qualifications at any other academic institution.

This research is supported by the Australian Government Research Training program.

Signature: Production Note:
Signature removed prior to publication.

Date: 19-08-2022

Acknowledgement

'There is neither wine of eternity nor fountain of youth. Life is pointless. Death loomed over all, and the ground beneath us all was the same. Humanity will one day be ended by the explosion of the Sun'. Thought the 15-year-old me. 'However, knowledge can be everlasting. If I can do research, contribute to even just one building block of human knowledge, or become a dancing byte in the database. Eventually, the human race will travel across the universe and find another oasis.'

Therefore, I am very grateful to my supervisors, Majid Ebrahimi Warkiani and Graham Vesey, for allowing me to work on my favourite stem cells topic, opening the gate of research for me, and providing the guidance to pursue my dream. I want to thank the school, faculty, and university for giving me the space and freedom to do my research and achieve what I would not be able to succeed in other places. I will never forget my colleagues' support during the hard times, the days we pursued excellence in work and dreams together. I would also like to express my gratitude to my family and friends. They have been my strong backing from the beginning, and they gave me the courage to go through the degree. I really appreciate my collaborators. They taught and helped me during my projects, shaped my papers and brought them to a higher level.

The taste of victory may be bittersweet, but the aftertaste lingers forever, a reminder of the journey, the struggle, and the triumph.

Format of Thesis

The aim of this PhD thesis is to address the challenges faced by the stem cell industry using microfluidic devices. The thesis is presented in six chapters. In Chapter 1, an overview of the current stem cell production process is provided, along with a discussion of the industry's challenges. This is followed by a review of microfluidic devices used in stem cell research, along with potential applications in different processes of the stem cell industry. Chapters 2-5 present original research on the development and application of microfluidic devices to solve the challenges in the stem cell industry.

Chapter 2 describes the use of a high throughput microfluidic droplet generator to produce dissolvable and edible microcarriers for the cultivated meat industry, where no edible microcarriers are currently available. In Chapter 3, 3D printing technology is used to develop a microfluidic system for detaching stem cells from current commercial microcarriers and separating and concentrating cells for downstream applications. Industry-scale microcarriers detachment and harvesting rely on membrane-based technologies that cause significant cell loss.

Chapter 4 presents the development of a micromixer to homogeneously mix cryoprotectant and stem cells. This replaces the current industrial bulk mixing methods, which can potentially damage cells and cause batch-to-batch differences in the products. In Chapter 5, a static droplet array is used to evaluate the metabolism and senescence level of cells in industrial production culture.

Finally, Chapter 6 provides a summary of the thesis and highlights potential future works related to microfluidic applications in the stem cell industry. This thesis contributes to the development of innovative microfluidic devices that can address the challenges faced by the stem cell industry and potentially enhance the quality and efficiency of the stem cell-based products.

Table of Content

1. Chapter 1: Potential Applications of Microfluidic Devices in the Industrial Production of Stem Cells

1.1. Introduction

Stem cells represent a cutting-edge technology with the potential to revolutionise both the therapeutic and agricultural industries. They are cells which can renew themselves and differentiate into other cell types, attracting great interest in regenerative medicine, drug scanning and cellular agriculture. As our understanding of stem cells continues to deepen, the demand for them is increasing at an unprecedented rate. The current stem cell production process can be divided into two parts, upstream processing (USP) and downstream processing (DSP) [1, 2]. USP includes collecting samples from donors, establishing master cell banks, and working cell banks and expanding cells on a large scale. DSP includes harvesting cells from the culture, washing and concentrating them[3]. The stem cell therapy industry formulates and cryopreserves the cells until they are delivered and used in the clinics, while the cultivated meat industry composites the cells with other cell types seeded on scaffolds for the nutrients, taste, and texture before packaging [4].

The stem cell industry is advancing at a rapid pace, but it is also facing significant challenges in its production processes. The key limitations of the stem cell industry can be summarised into two major areas: yield and quality assurance [5, 6]. The current 60-year-old technologies are inadequate to meet the high demand for cell numbers required to provide effective treatment dosages and protein supplies. In fact, about 50% of cells are lost during production due to low detachment efficiency and frequent blocking/clogging of filtration devices [3, 4, 7]. This inconsistency in batch-to-batch product quality leads to unstable therapeutic outcomes and clinical trial failures. This is caused by the lack of production standards across the industry [1, 2] and old production technologies. These challenges result in increased costs of stem cell products, hindering people from enjoying the benefits of stem cells. Therefore, the stem cell industry urgently needs new technologies to address these challenges and improve stem cell yield and quality assurance.

Microfluidic technology is a promising solution to address the challenges in various fields of biotechnology. This technology utilizes small channels to precisely control the flow of liquids and has been found to have potential in a range of applications. In particular, microfluidic technologies have been used to separate [8], concentrate [9], mix [10] particles like cells,

generate droplets for cell culture [11] and analysis [12]. Additionally, these devices have been used to provide complex model [13] for cell studies and drug screening/testing [14]. Due to the miniaturisation and precision handling of fluid flow, microfluidic devices preserve the cells well during the handling process and provide better outcomes such as high processing efficiency, low-cost and clogging-free separation. This chapter provides an overview of the current industrial production process, the challenges faced by the existing stem cell industry, and the potential of microfluidic devices in stem cell research and their future applications in the industry.

1.2. Literature review

Stem cells are considered the next frontier in regenerative medicine, with the potential to treat, regenerate, or even replace malfunctioning or unhealthy tissues and organs. Recently, stem cells have also found application in the cultivated meat/lab-grown meat/cellular agriculture industry. This sector is generating significant interest due to the considerable reduction in environmental impact and ethical concerns surrounding animal farming. Several reviews have explored the application of stem cells in the progress of clinical trials [15-18] and the future of cultivated meat [19, 20]. Despite the increasing number of stem cell clinical trials, the scale of stem cell production in the industry remains inadequate due to limitations in production technologies and understanding of stem cells. [21, 22]. Challenges include the difficulties in purifying a uniform population of stem cells, which can reduce the safety and efficacy of therapeutic dosage [23] and limit stem cell recovery from tissue samples [24], that results in low post-transplanted stem cells survival rates and therapeutic outcomes [17, 20]; Stem cells are heterogeneous and express distinct characteristics [25], making the ability to isolate specific populations of stem cells critical for improving the quality of stem cell products [6]. Stem cells from other donors have potential to trigger the immune rejection of the recipient. Induced pluripotent stem cells (iPSCs) do not face this challenge, however, there are concerns about their reprogramming and differentiation protocol [15], as well as genome stability [26]. Microfluidics has the potential to improve iPSC reprogramming protocols and cell stability through targeted delivery of genes and controlled fluid delivery. In the cultivated meat industry, cost of culture medium [27], scale-up production method [4], differentiation [28] and scaffolding technologies [29] remain the leading challenges for bringing cultivated meat to dinner tables. Furthermore, current technologies rely heavily on animal-based products, which conflicts with the industry's original purpose. Microfluidics can be employed to develop low-

volume, high-throughput media optimization and differentiation protocols, as well as scaffold fabrication, to address these challenges.

Microfluidics is a rapidly evolving technology that enables the manipulation of small volumes of fluid in micron-scale channels. Microfluidic devices offer several advantages, such as high customisability, precise control of fluid flow and micro-particles, low consumption of reagents, and low production costs. These features make microfluidics an ideal choice for cell separation [30], single cell study [31], cell interactions and secretions studies [32], replacing the traditional cell sorting machines and plate- or well-based methods.

In this review, we provide an overview of the industrial production process of stem cells and examine various microfluidic devices utilized in stem cell research and production. We also highlight the limitations of current methods and discuss how microfluidic devices can overcome these challenges. Specifically, we cover the benefits and limitations of cell sorters via active and passive microfluidics, mechanical stimulus and measurements of cell properties by microfluidics, various types of organ-on-a-chip to study tissue behaviour, droplet-based microfluidics for manufacturing cells and scaffolds, and integrated devices for sorting, culturing, detecting, and purifying cells. Finally, we discuss the future potential of combining several microfluidic technologies to accelerate and overcome complex challenges in the industrial production of stem cells.

1.3. Stem cell production in laboratories and industry

The stem cells production processes are divided into upper stream production (USP) and downstream production (DSP) [1]. The USP stage involves the isolation of tissue samples from donors, followed by purification and the creation of a master cell bank (MCB). These cells are then used to generate a working cell bank (WCB), which can be expanded for downstream applications. In contrast, the DSP stage comprises the collection of the expanded cells, selection of target cells or their secretions, multiple washes, exchange into buffers for final formulation, and storage and transport of the final product (Fig.1.1). Mesenchymal stem cells (MSCs) are the most used cells in stem cell therapy and will be used as an example in this review.

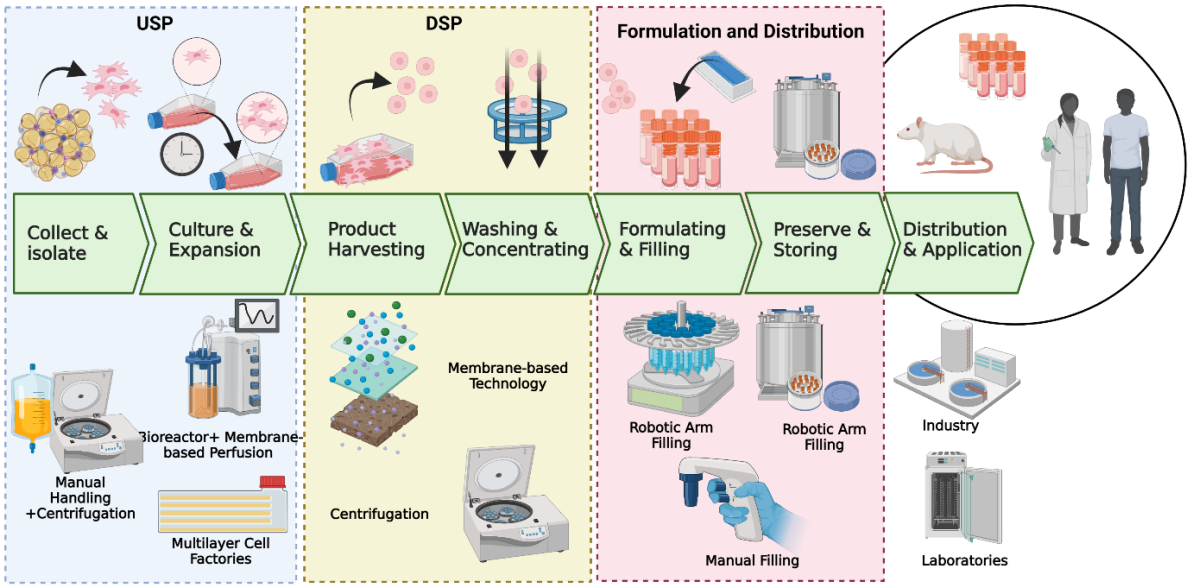

Fig. 1.1. A general process of stem cells production for therapeutic purpose. This process is normally divided into two parts, upper stream production (USP), Lower stream production (DSP) and formulation and distribution. There is no revolutionary in the cell culture and handling technologies used in this process for more than 50 years. Manual handling, cell loss, cell damage, and discontinuous process are the main challenge of the current industry.

1.3.1. Upstream production

The use of primary cells from donors remains the dominant source of stem cells in the industry. However, this practice raises concerns about the quality and variability of MSC-related products, which can be influenced by donor health, gender, genetics, and age. The need for a stable and consistent cell source is therefore a major demand in clinics. Unfortunately, there is no regulatory level standard procedure to for stem cell extraction process. This results in each company having their own approaches for isolation and production. Since there is a lack of standard procedures recommended by regulatory bodies in the stem cell industry, each company use their own approaches for isolation and production contributing to the variation in final products [6]. Recently, iPSCs have been explored as a potential source of MSCs, eliminating the need for biopsy samples from donors [33, 34]. Although this approach has not yet been widely accepted for clinical trials due to concerns about transgenic nature and iPSC stability, iPSC-induced MSCs offer the advantage of reduced heterogeneity between donors and fewer ethical issues. Ongoing research is investigating the feasibility of using iPSCs as an MSC cell source [35].

Among the various sources of MSCs, adipose tissue, bone marrow tissue and umbilical cord tissue are the most commonly used [36] due to the accessibility and higher cell availability. Isolating MSCs from these sources requires the depletion of unwanted cell types, which is

typically achieved through time-consuming, expensive, and error-prone methods such as blood cell/fat tissue lysis, gradient centrifugation, and/or fluorescence-/magnetic-activated cell sorting (FACS or MACS) [6, 24]. While stem cell-specific antibodies are often used in this step, they are expensive and can alter the cell surface structure. Additionally, the heterogeneous nature of stem cells means that they may not express the same markers, making the antibody-based method unreliable. Adipose-derived stem cells (ADSCs, MSCs in adipose tissue) have unique advantages in this regard. ADSCs are one of the few adherent cell types in the tissue. They can be isolated by culturing lysed adipose samples in a culture flask for a few passages without requiring antibodies binding [37, 38]. ADSCs are often obtained as a by-product of liposuction surgery, which is less traumatic than obtaining bone marrow derived MSCs (BMSCs) through aspiration from the bone marrow cavity of the hipbone. On the other hand, the extraction of BMSCs from bone marrow cells requires multiple steps and the antibody-based method is necessary due to the complicated composition of cells in bone marrow. The standard procedure involves density gradient centrifugation to obtain cell pellets, culture of cells on a culture flask to eliminate non-adherent cells, and further selection using specific surface markers [24]. However, this procedure is complicated and does not guarantee the purity and quality of the cells. Additionally, ADSC is more ethically accepted, and the source is more abundant than BMSCs. ADSCs can be cultured for about 12-15 passages on average, and it is crucial to stabilize the properties of cells in as few passages as possible to establish a master cell bank (MCB) for the production of therapeutic doses. One adipose sample may be enough to produce hundreds of therapeutic doses.

The static planar multilayer flask method remains the most used cell culture technique for industrial production of MSCs. [21]. This method limits the scale of manufacturing and has multiple disadvantages, including changes in cell fate, cell proliferation and differentiation ability, cell phenotype, and secretions [39, 40]. An alternative approach is to culture MSCs on microcarriers in dynamic bioreactor culture systems, which provide better control of physiological parameters such as nutrients, pH, and dissolved oxygen levels. Microcarriers are composed of various matrices and are typically spherical in shape, with diameters ranging from 100 to 300 μm. This technology offers cost-effective and homogeneous conditions for massive cell expansion, resulting in consistent cell product quality at a large scale [41, 42]. However, different cell types have different preferences of the substrate's properties, such as the hardness, surface charges, topography, and structure of the material [5, 21, 43]. The current microcarriers were not designed for the special needs of the stem cell industry. They also need to be improved

in terms of breakage during large-scale culture to reduce the chance of having microplastics in the final products. While the use of microcarriers is critical in the cultivated meat sector, the current options are prohibitively expensive, with production costs for 1 kg of meat reaching several thousand dollars. Furthermore, cells grown on microcarriers tend to form aggregates, making them difficult to detach and resulting in severe cell loss, sometimes approaching 100%. [44]. Despite the enormous potential of microcarriers in stem cell therapy and the cultivated meat market, large-scale studies on cell behaviour on microcarriers are scarce [5].

Microcarrier culture is becoming increasingly important due to its potential for high-density cell culture and improved cell growth. However, the culture standard for microcarriers varies depending on the cell type, and the protocol for microcarriers can differ among different research groups and enterprises as compared to traditional planar flask technologies. To increase productivity, some groups have implemented additional steps in the culture process, such as increasing impeller speed or agitating the microcarriers [45], or agitating the microcarriers [46]. Despite these developments, standardisation of the culture process is still needed, and further research is required to identify optimal culture conditions for various cell types. In addition, new microcarrier technologies based on surface substances and degradable microcarriers are currently being explored as potential alternatives to traditional microcarriers.[21].

MSCs are commonly cultured in α-MEM/DMEM supplemented with 10% fetal bovine serum (FBS) or human platelet lysate (HPL). [47]. However, the use of serum supplements can result in batch-to-batch variation due to donor-to-donor differences and increases the risk of contamination from pathogens in samples. [48, 49]. In response to these challenges, serum-free and xeno-free media have been developed, but their high cost has limited their widespread adoption in industry. Currently, there is no standard composition of media for MSC culture, and further discussion and confirmation are needed in this area. [21]. As such, ongoing research efforts are focused on identifying cost-effective and standardized culture media formulations that can support consistent MSC growth and differentiation.

1.3.2. Downstream production

The downstream production (DSP) includes four steps. The first step is cell harvesting from the culture flask, which involves enzymatic methods to detach the cells from their containers. In laboratory settings, the cells are centrifuged, washed by Dulbecco′s Phosphate Buffered Saline (DPBS), and cryopreserved by adding cryoprotecting agents. The problem here is the

harvesting process is a labour-intensive process and takes at least two hours to complete for a multilayer cell factory. Traditional centrifugation, which applies external forces to the cells can negatively impact the viability and recovery of cells [21]. It also increases the risk of contamination due to multiple open handling during these processes. Additionally, all cell therapeutic products must be produced under the current Good Manufacturing Practice (cGMP) guidelines, which require the cells to be produced in a clean room. However, the current DSP lacks standardisation, leading to variations in product quality. These issues emphasise the need for further optimization and development of DSP processes to ensure consistent and high-quality biotechnology products [21].

Cell harvesting in large-scale manufacturing is challenging due to the limitations of traditional centrifugation with manual handling. Several standard techniques have been developed, including dead-end filtration, tangential flow filtration (TFF), and continuous flow centrifugation [2, 50], to address these limitations. Dead-end filtration and TFF are both membrane-based technologies that harvest cells with size-based membrane filtration. However, dead-end filtration is not feasible for large-scale applications due to membrane clogging from high cell concentration [2, 3]. On the other hand, TFF avoids direct deposition of products on the membrane which hugely reduce the chance of clogging, extend the lifespan of the filter, and enable the potential for larger scale application [21]. However, TFF still has a high failure rate, compromises the viability of cells since blockage of the device cannot be completely eliminated [22]. Membrane fouling and clogging from TFF can cause cell death, changes in the fate of stem cells and reduced therapeutic potential [3, 22, 50], resulting in high cost due to expensive and time-consuming replacement. Continuous flow centrifugation is an advanced technology that combines washing and concentration in one step [51], reducing the chance of contamination [52] and the throughput can go up to 2000L/h. However, it can potentially damage the cells due to centrifugal forces like the traditional centrifugation [53] and is limited by the high cost and it is not optimised to harvest cells from microcarriers at large scale [2]. Cell harvesting cells from microcarriers share similar challenges cell harvesting from planar flask. Cells need to be separated from microcarriers, normally by TFF, followed by cell washing with centrifugation or membrane filtration. Harvesting cells from microcarriers is one of the major limiting factors of using microcarriers in the industry. Cells are harder to detach from microcarriers compared to planar flasks and it results in 20-50% cell loss during harvesting and in some cases can be up to ~100% [44, 54, 55]. Therefore, smart microcarriers with dissolvable or cell-releasing feature, such as temperature and UV sensitive microcarriers

[5] are being explored to address this issue. Also, better detachment technologies and protocols are urgently needed to optimise the cell harvesting processes in large-scale manufacturing.

The harvested and formulated stem cells are cryopreserved in liquid nitrogen until they are needed in the clinics. During this process, the formation of ice crystals can damage the cells and impede their performance after recovery [56]. To prevent this, cryoprotective agents (CPA) or cryoprotectants are added into the cells during cryopreservation. Currently, the most common CPA used is 10% Dimethyl sulfoxide (DMSO). It prevent water crystallisation and opens the cell membrane to balance the electrolytes inside and outside the cells during cryopreservation. However, exposing cells to high concentration DMSO or extended period may compromise the viability, stemness and differentiation potential of stem cells when the cells are [57, 58]. It might also induce severe adverse effects if taken by patients [59]. Therefore, the cryoprotective agents need to be mixed with cells precisely at a 1:9 ratio for the best protection of cells while maintaining minimum damage to them. The current benchmark technology for this application is robotic arms system, such as the Crystal® Filling Lines from Aseptic Technologies. However, the robotic arm system creates cell damage and significant batch-to-batch difference in the final products. It adds DMSO into cells in a bulk manner, exposing one portion of the cells to high concentration of DMSO and then fills into cryopreservation tubes and store the cells in temperature-controlled freezer every few hours [60]. Additionally, the system is expensive to maintain and operate. The only alternative method to robotic arm technologies is manual mixing. Manual mixing is not a viable alternative due to low throughput, risk of contamination, insufficient mixing, and the reliance on human labour. Therefore, improvements in cryopreservation process should target the mixing methods and improve the filling speed [60].

Unlike the pharmaceutical industry, the stem cell industry lacks quality control steps in its procedures. As we discussed earlier, the age and gender of donors [61, 62], tissue origin [62, 63], the passage of cells and even cells in the same batch [64-66] with different culture conditions [67] are heterogeneous, different protocols and production processes employed by different companies and laboratories further diversify the quality of stem cells [68]. Therefore, the lack of quality control and the inherent variability of MSCs contribute to inconsistent experimental results and clinical outcomes [69-71]. In order to address this issue, the International Society for Cellular Therapy (ISCT) released the well-recognised standard for characterising MSCs in 2008 [72]. However, this standard does not include criteria for evaluating the protein expression and cytokine secretion levels of cells, which are important

indicators of the stem cells potency and efficacy. While regulatory bodies such as Food and Drug Agency (FDA) allow for some flexibility in this matter [73], having a standard quality control procedure as part of the standard requirement of medicine is still desirable [6]. Some studies have proposed immunofluorescent staining of the surface markers as a quality control method [64, 73, 74], but these methods might not be sufficient due to the heterogeneity of cells and have to be combined with some functional attributes of the cells.

In all, the production of stem cells is a critical process that currently heavily relies on plastic/non-degradable culture substrates, membrane-based, and centrifuge-based technologies. Unfortunately, these methods present several limitations that cause reduced productivity and increased production costs. To address these challenges, innovative technologies that enhance the cell separation, detachment, washing, and mixing processes are urgently required. Furthermore, there is a pressing need to establish a universally accepted standard protocol for stem cell production. By enhancing the production process, it is possible to reduce the cost of production, which would ultimately translate into significant benefits for patients and consumers. These improvements are crucial in advancing stem cell research and facilitating the development of novel therapies for various diseases.

1.4. Different microfluidic devices used in stem cells research

Microfluidic devices have emerged as a key technology for addressing many of the challenges in the stem cell industry. Microfluidics is a technology that manipulate fluid in microliter level [75]. It is getting more and more attention due to its precise control of the fluid, low cost, high customisability, small footprint and its potential to perform experiments that other technologies cannot [76]. The discovery of particle behaviours in small channels dates back to the 1960s. Segre´ and Silberberg found that when 1mm particles pass through a 1cm cylinder channels, they were focused at certain positions of the channels rather than randomly dispersed [77, 78]. This phenomenon received little attention until the rapid development of micro-fabrication and micro-manufacturing technologies [30] such as soft lithography and 3D printing technologies, which allowed for fabrication of better resolution channels for manipulating microparticles. This discovery has led to further investigations for various purposes, such as isolating single cells for single cell resolution gene studies [79] and separating cells according to size difference [80]. Microfluidic devices provide higher efficiency, lower cost, lower consumption of reagents, and lower expertise needed for these applications while creating the possibility for executing new tasks that cannot be done before, such as large-scale single cell sequencing and

creating tissue or organ models in small scale. In this chapter, we categorised microfluidic devices as cell separators, cell stimulators/manipulators, droplet-based microfluidics, organ-on-a-chip, and integrated or other microfluidics, highlighting their potential to significantly improve the stem cell production process.

1.4.1. Cell separators

Stem cells is a very small subpopulation of cells in tissue samples. Stem cells constitute as little as 2% [81] of cells in adipose tissue and 0.02% in bone [82], while the cell tissues themselves contains up to 15 different cell types [24]. To isolate specific stem cell populations, researchers rely heavily on techniques such as fluorescence-activated cell sorting (FACS) [83-85], magnetic-activated cell sorting (MACS) [83, 86], or manual selection using microscopy [87]. These methods select the stem cells based on surface-specific markers and morphology, which have high specificity, but are suffering from low recovery rate of stem cells, high cost of reagents, antibodies, and equipment [24]. They are also limited by low scalability, limited selectivity, and high risk of contamination [88]. Moreover, some stem cells, such as mesenchymal stem cells (MSC) or iPSCs, lack definite surface markers that can identify them [73], limiting the effectiveness of marker-based selection. To overcome these challenges, novel approaches are being developed to isolate stem cells based on their functional characteristics or genetic profiles. These efforts are critical to advance the study and application of stem cells in regenerative medicine.

In recent years, microfluidic devices have undergone significant technological advancements that enable the separation of cells based on additional properties such as size, deformability, and surface charges. Microfluidic cell separations can be classified into two categories: passive and active methods. Active microfluidics integrate external energy sources such as electric fields, sound and magnetism with microchannels to control microparticles, while passive microfluidics rely mainly on channel designs, fluid forces and properties of the liquid flow to direct the particles. Active microfluidic devices offer monitoring of particles in real time [89] and precise control of individual particles and different fluid types [90]. However, the throughput of active microfluidic devices is generally low and there is a potential risk of damaging cells due to the external energies applied. Passive microfluidics on the contrary, have generally higher throughput and can be easily paralleled to further increase the throughput [89]. The energy consumption of passive devices is lower than active devices since the passive devices are purely driven by fluid flow. However, the separation resolution of passive devices is typically lower, providing less control over individual particles.

1.4.1.1. Active microfluidics

Active microfluidics are technologies that use external energy sources, such as magnetic, electronic or acoustic field, or optical methods [89] to manipulate the microparticles inside the channel. Cells or particles with different surface charges, cell density, electrical properties or size [91] experience varying levels of forces and can be therefore positioned in different areas, which can be used to separate cells and microparticles [23].

Dielectrophoretic (DEP) based microfluidic device is one of the most widely used active microfluidic systems. This type of device separates cells based on their size, density, and electronic properties. The earliest application of DEP on stem cells dates back to 1995. Talary, Mills [92] used a DEP device to purify peripheral blood stem cells (PBSC) from bone marrow samples, and a 5.9-fold enrichment was achieved. Adjusting the voltage of DEP device allows separation of different properties particles and also can manipulate particles in different ways. Simon, Li [93] used a DEP device to trap neural stem and progenitor cells (NPSCs) inside the electric field, wash off the undesired cells and then collect them by changing voltage (Fig. 1.2A). More recently, due to the development of microfabrication technologies, the purity and recovery rate of cells increase drastically compared to the old technologies. Song, Rosano [94] developed another dielectrophoretic based microfluidic device to purify cultured MSCs from the differentiated osteoblast, to obtain a pure population of MSCs with highest 96% recovery rate or 84% purity. Similarly, Flanagan, Lu [95] used DEP device to separate neural stem/progenitor cells (NSPC) from their surrounding differentiated cells in mouse embryo neural samples by the difference dielectric features of neurons and astrocytes. The recovery rate of NSPC is constantly higher than 95% in different embryonic stage samples. Another DEP device was used to separate NSPC with a 50% recovery rate and 1.4-fold enrichment by trapping them inside the field [96]. Although the recovery rate is low, the advantage of this device is it is capable of manipulate the cells inside the trap by altering the frequency of the device. Later, this technology was used to study the correlation between NSPC membrane charges and cell fates [97]. The biggest challenge for DEP in the industry is its throughput. A typical DEP device for cell separation proceeds samples at µL/min scale.

Besides DEP devices, magnetic, acoustic and optic-based microfluidics have also been used in stem cell separation. Plouffe, Mahalanabis [98] applied a magnetic field to a straight microfluidic channel to extract the anti-CD133 labelled haematopoietic stem cells (HSCs) and endothelial progenitor cells (EPCs) from whole blood in the microfluidic channel, with a 96% average recovery efficiency of both stem cell types (Fig. 1.2B). Zeng, Qiu [99] used the

IsoFlux™ commercial microfluidic cell sorter to purify Sca-1 labelled lung multipotent stem cells from mouse lung tissue (Fig. 1.2C). These two examples demonstrate the capability of microfluidic devices in stem cell isolation from raw blood and tissue samples with minimum loss. The results also showed better preserved cell viability and cell functions. Dykes, Lenshof [100] made an acoustic field size-based microfluidic device to separate PBSC from the peripheral blood mononuclear cells obtained from human donors. The recovery rate reached 98%, and 89% of the platelets were depleted (Fig. 1.2D). Zalis, Reyes [101] use an acoustic microfluidic device to separate live hESCs from dead hESCs with 88.1% purity. As for optical microfluidics, optical tweezer is a technology that precisely manipulates individual particles with high-energy laser beam. Wang, Chen [102] have combined optical tweezers in a microfluidic channel to sort GFP tagged hESC from non-tagged cells with a 90% recovery rate and 90% purity.

Active microfluidic devices have become a promising technology for isolating target cells from clinical samples with high separation resolution and precise control. This technology is particularly useful in the stem cell therapy and cultivated meat industry, where target cells like MSCs lack universal markers for purification. While active microfluidic devices typically have a relatively low throughput, they offer high separation efficiency, which is especially beneficial when separating stem cells from tissue samples that are already small in volume. Although the geometries and designs of active microfluidic devices are simple, they can be combined in series to increase the throughput of the system or reduce the loss of target cells. In the future, active microfluidic devices are likely to be developed for high volume processing in stem cell industry applications while maintaining high resolution separation from clinical samples.

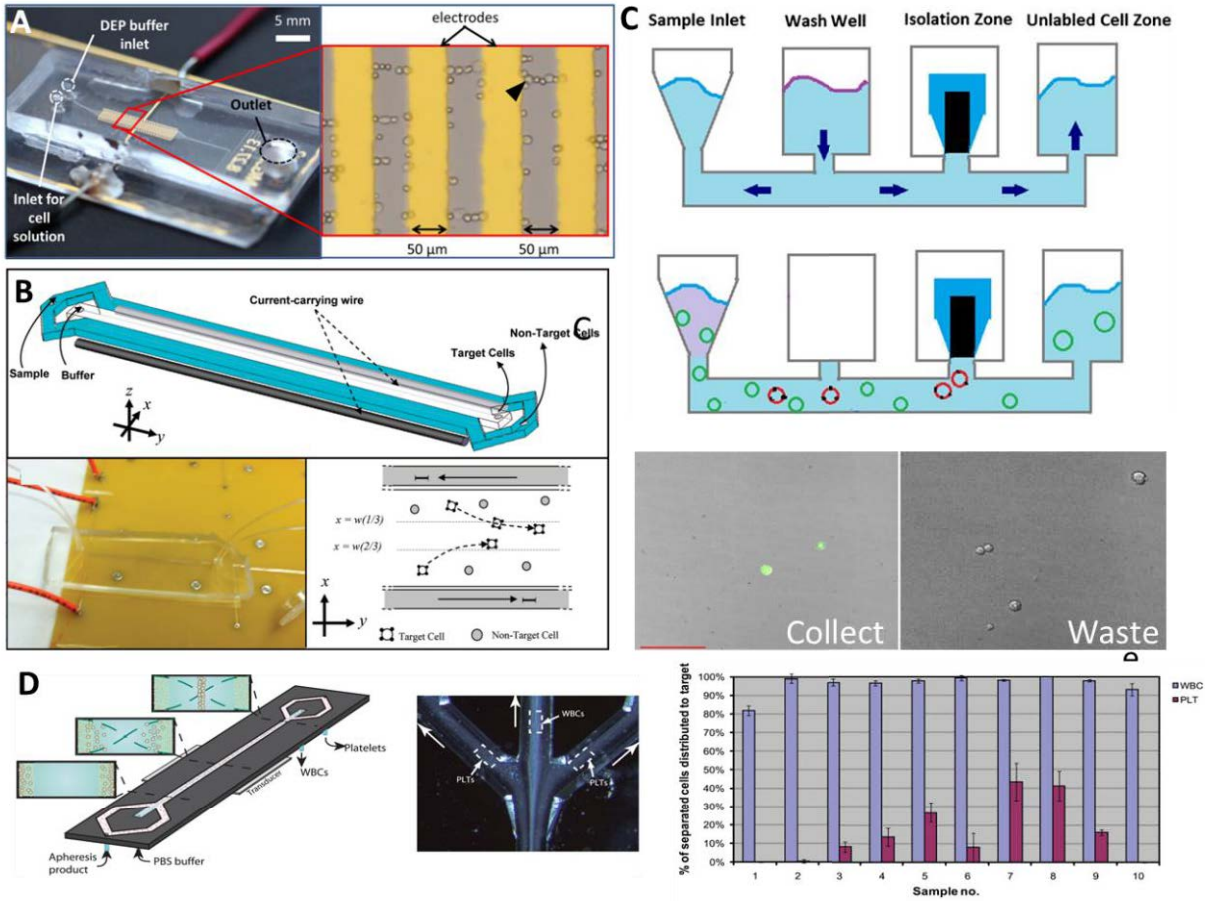

Fig. 1.2. Active microfluidic devices used for stem cell isolations. A) The Dielectrophoretic microfluidic chip (left) used to trap (right), wash and release NSPCs. Reproduced with permission [93] Copyright 2014, AIP Publishing. B) Magnetic microfluidic device can isolate target cell types with high recovery rate, but cell modification is needed. Reproduced with permission [98] Copyright 2012, American Chemical Society. C) Similar to DEP-based microfluidic devices, magnetic-based microfluidic devices can be operated in different ways to retain the cells in the device and perform washing together with isolation. Reproduced with permission [99] Copyright 2015, John Wiley and Sons. D) Acoustic microfluidic devices perform cell size-based separation due to the different reactions of particles responding to the same wave strength (left) with 805% overall recovery rate of white blood cells (WBC, right). Creative Commons CC-BY license [100]. Copyright 2011, the Authors. Published by PLOS.

Table 1.1. Active microfluidics for cell separation purposes

AUTHORS	TECHNIQUES	SAMPLES	TARGET CELLS	RECOVERY RATE	PURITY/ ENRICHMENT	THROUGHPUT
Talary et al 1995 [92]	DEP	Bone marrow sample from a donor	PBSC	///	5.9-fold enrichment	///
Song et al 2015 [94]		Mixed MSCs and osteoblasts	MSC	92%	84%	0.3 µL/min
Plouffe et al 2012 [98]		Whole blood from a donor	HSC, EPC	96%	81%	120 µL/min
Flanagan et al 2008 [95]		Cultured mouse neural sphere	NSPC	>95%		2 µL/min
Prieto et al 2012 [96]				50%	1.4-fold enrichment	2 µL/min
Simon et al 2014 [93]					13.2-fold	3 µL/min
Yoshioka et al 2018 [103]		Cultured MSC and Leukaemia cell lines	MSCs	29.1%	83.5%, 2.3-fold	///
Dykes et al 2011 [100]	Acoustic	PBMC from multiple donors	PBPC	98%	89% platelet depleted	20 µL/min
ZALIS, REYES [101]		Cultured hESCs	Live ESCs	42.3%	88.1%	100 µL/min
Vykoukal et al 2008 [104]	Magnetic	Adipose samples from donors	MSC	///	14-fold enrichment	1500 µL/min
ZENG, QIU [99] 2015		Digested mouse lung samples	Lung multipotent stem cells	///	96-99%	20 µL/min
Wang et al 2011 [102]	Optical tweezer	Mixed culture population	hESC	90%	90%	120/s

1.4.1.2. Passive microfluidics

Passive microfluidics can be divided into 4 types: hydrophoresis, pinch flow filtration, deterministic lateral displacement (DLD) and inertial microfluidics [89]. Among these four types of devices, hydrophoresis works at a narrow and low flow rate range, pinch flow filtration requires sheath flow to operate, and DLD suffers from high shear stress and frequent clogging [105]. Inertial microfluidics does not rely on sheath flow to operate, and it has the highest throughput among the four device types. It does not apply large shear stresses to the cells and the channels are large, which are not easily blocked and maintains a relatively high separation resolution. Also, there are only a few papers separating stem cells based on the other three types of devices. Therefore, in this chapter, we will only discuss inertial microfluidics as a separator device for stem cells.

1.4.1.2.1. Inertial microfluidics

Inertial microfluidics exploits the phenomena of microparticles moving towards their equilibrium positions inside a microchannel to separate particles with their properties such as size, morphology or density [30]. Inertial microfluidics only apply gentle forces to the cells, which have been shown to preserve the sensitive stem cell properties during the separation process [8, 65, 106]. This is appealing in stem cell extraction from the tissue of origin. As the first paper to use an inertial microfluidic device to purify stem cells, Hur, Brinckerhoff [107] used a straight microfluidic channel with an expanded ending to separate adrenal cortical progenitor cells from digested murine adrenal glands. Compared to the progenitor cells, the surrounding differentiated tissue was found to have higher cholesterol content and tend to form as a cluster of cells. Therefore, this device separated single cells from cell clusters based on their size and collected stem cells from the side outlets and the cell clusters from the middle outlets (Fig 1.3A). Lee, Rosano [106] demonstrated that a multi-outlet, rectangular spiral microfluidic device can be used to separate MSCs from undiluted mouse bone marrow samples with a 73.2% recovery rate. Compared to traditional cell extraction methods described above, using inertial microfluidics to purify stem cells from their tissue origin is label-free, high-throughput, clogging free, requires less manual handling, is simple and preserves high cell viability with a high recovery rate. The throughput of inertial microfluidic devices can be mL/min scale and can be further improved by paralleling these devices together without drastically increase the footprint of the system.

Stem cells can develop into different subpopulations with different physical properties and potential cell fate even under the same culture condition. Inertial microfluidics have been used

to distinguish different subpopulations of cells with their physical properties and study the cell secretion, gene expression and cell fate in each subpopulation. For example, Lee, Shi [65] used a multi-outlet rectangular spiral device to separate cultured bone marrow derived MSCs with different size and measured the physical properties of the sorted cells (such as elastic modulus, relative nuclear fluctuation, attached cell spread area, etc.). They found that cells with small size, low elastic modulus and high relative nuclear fluctuation are more undifferentiated and multipotent (Fig. 1.3B). The 'cell size-differentiation potential' correlation is also supported by other researchers. Yin, Yang [108] used a spiral microfluidic device to separate mesenchymal stem cells into three different size groups and found that these cells have distinct differentiation potencies and paracrine effects (Fig. 1.3C). The same spiral microfluidic device was used to separate the cells into big, medium and small sizes by altering the flow rate. The larger cells tend to differentiate into bone cells, the middle-size cells have higher potencies to differentiate towards chondrogenic cells [109] and adipogenic cells, while the small-size cell group remains most pluripotent. Moreover, large cells secrete more tropical factors such as IL-6, IL-8, and VEGF. A larger scale proteomic study is needed to support this result. Based on the findings of the study, this tool can be used for stem cell separation to study the subpopulations of cells as well as reducing the batch-to-batch difference of the therapeutic products, or selectively collecting the cells with higher therapeutic potential to treat patients.

Other applications could be in separating differentiated cells from stem cells. Depleting differentiated stem cells from undifferentiated cells will maintain the pluripotent stem cell population. On the other hand, depleting undifferentiated stem cells from differentiated cells is important for the safety of regenerative medicine, since direct administration of undifferentiated stem cells have the potential risk of tumorigenesis [71]. Song, Rosano [110] used a multi-outlet spiral chip with the shear flow to isolate neuronal stem cells from other non-neuronal cells in iPSC differentiation process. They recovered 93% of the neural stem cells based on the size differences. The multiple outlets of the device allows precise isolation of middle size neuronal cells from large cells and clusters and other small size cells. It is worth mentioning that using sheath flow in microfluidic devices facilitates the particle migrations inside the channel by reinforcing the force [111]; therefore, the devices using sheath flow normally have a smaller footprint than the sheathless devices. Also, sheath flow can potentially be used as a washing buffer in the system to perform washing and separation simultaneously. However, in cases where cell washing is not needed, Sheathless devices are preferred since there will be no consumption of sheath fluid. Guzniczak, Otto [112] has used a rectangular,

multi-outlet sheathless spiral device to separate iPSCs induced red blood cells from other cells in culture with more than 90% recovery and about 70% purity based on the deformability of the enucleated cells. In these above-mentioned cases, iPSC stem cells are larger than the other differentiated cells in the same tissue samples. In muscle tissue myotubes are multinuclear cells, whereas muscle stem cells (myoblasts) are smaller in size. Syverud, Lin [113] use the Labyrinth inertial microfluidic device to separate small mouse myoblasts (8-13μm) from adult muscle myotubes (16μm), fibroblasts (10-22 μm) and large undigested extracellular matrix residues. The results showed that 66.5% muscle stem cells were recovered from the inner outlet and demonstrate better myogenic differentiation potential than unsorted cells. Cell mitosis is also one of the reasons for size variation in the same cell population. Cells in a different stage of the cycle are different in size due to the alignment of chromosomes during mitosis metaphase. Therefore, Lee, Bhagat [114] used a multi-outlet spiral microfluidic device to synchronise cell cycles of MSCs based on size. MSCs were divided into three groups, 10, 15, 25 um groups corresponding to G0/G1, S and G2/M phase of the cells.

The inertial focusing phenomenon can be observed as long as the particles satisfy the condition where the particle size is larger than $0.07D_H$, where D_H is the hydraulic diameter of the channel [115]. This phenomenon still exists on a larger scale, but other factors such as gravity have to be considered [9]. Inertial focusing have been applied for separating particles larger than single cells such as cell aggregates and microcarriers. For instance, a two-outlet rectangular cross-section spiral was used to separate single neural stem cells from neurospheres. Since neural stem cells naturally form a neural sphere in culture, traditional enzymatic or mechanical detachment hugely damages cell viability. Therefore, the researchers gently separated the single neuron cells from enzyme-mixed neurospheres, by applying gentle inertial forces to detach the cells and obtain single neuron cells for distinguishing cell types in a cell population and clonal study [116]. Another simple straight channel with sheath fluid inlet and obstacle at the end was used to separate mESC spheroids into three different size groups [117]. The single line obstacles ensure the larger cells go only into the larger outlets, producing a 100% purity of small embryoid bodies population. Spiral microfluidic devices are beneficial in separating larger particles since the Dean forces in a curved channel is amplified hugely in larger channels [118]. Moloudi et al [8, 118] has used scaled-up, slanted two outlets microfluidic devices to separate detached MSCs from microcarriers (Fig 1.3D) and another one for perfusion culture of microcarriers with high recovery rate and well-preserved stem cell properties, such as surface markers expression and differentiation potentials.

Inertial microfluidic devices have been developed as one of the advanced methods for the separation of rare cells from blood samples and multiple commercial devices have been developed (Clearbridge BioMedics, Labyrinth Biotech Inc.), indicating that great potential has been recognised by the scientific community and the industry. Although inertial microfluidic devices have lower resolution than active microfluidic devices, the high throughput, low fabrication and operation cost, simple setting and channel structure make them an ideal candidate for cell separation, perfusion, and concentration purpose for larger volume applications. In the future, different channel designs, such as the different cross-sectional shapes of spirals can be explored to better meet the need of the stem cell industry, since rectangular and slanted spirals dominate in the research field, while other cross-sections designs have merely been explored. Also, integrating multiple inertial microfluidic devices in the system can reduce the loss during separation or increase the throughput for larger scale production. Lastly, fabrication of inertial microfluidics in a close-up system need to be addressed, before they can be successfully commercialised.

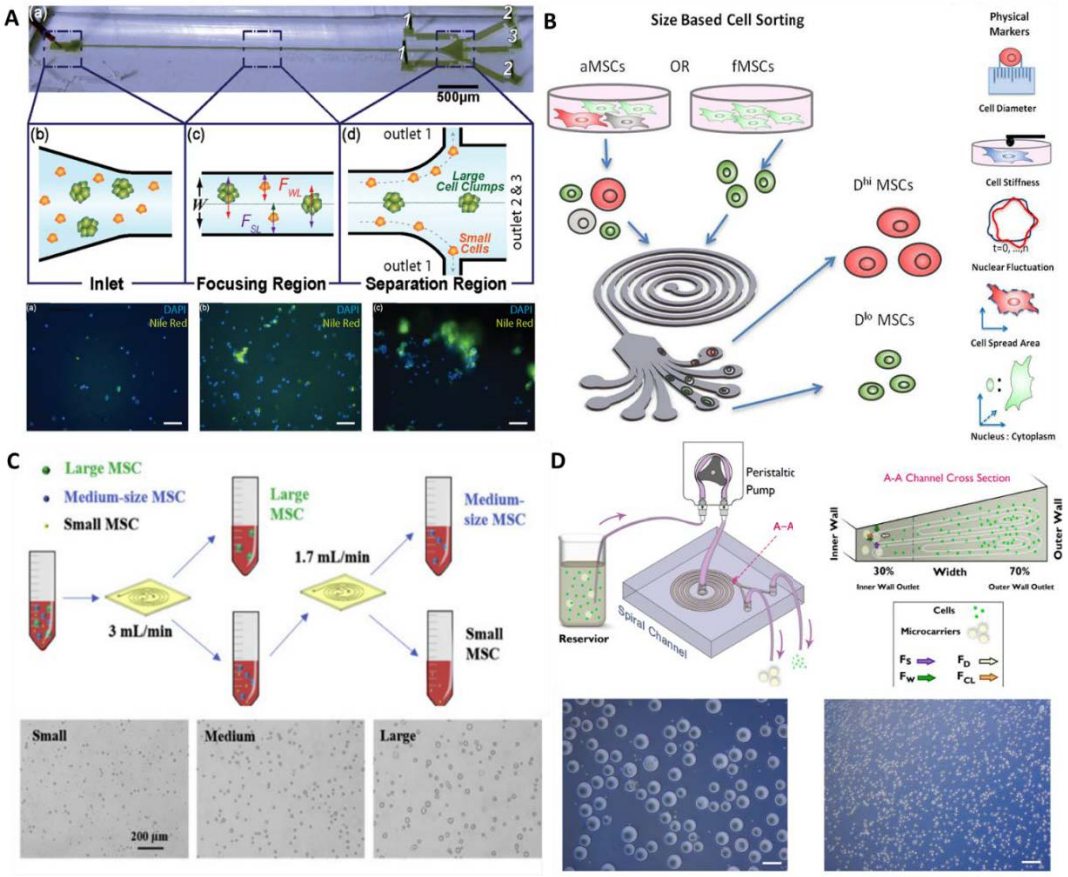

Fig. 1.3. Different types of inertial microfluidic devices used for Stem cell separation. A) straight channel inertial microfluidic devices (a) used to separate single adrenal cortical progenitor cells from surrounding cell clusters. The cells collected from different outlet are showed in (b) outlet 1, (c) outlet 2 and (c) outlet 3. Reproduced with permission [107]. Copyright 2012, the Authors. Published by PLOS.

Spiral microfluidic devices used to separate stem cells with different physical properties in two one step B) and two steps C). Reproduced with permission [65, 108] Copyright 2014, National Academy of Sciences. Copyright 2020, Elsevier. D) Scaled-up inertial microfluidic devices used for separation of MSCs from microcarriers. 97% of the beads can be collected from the inner outlet (bottom left) and 70% of cells collected in the outer outlet (bottom right). Creative Commons CC-BY license [9]. Copyright 2018, the Authors Published by Springer Nature.

Table 1.2. Inertial microfluidic devices for cell separation purposes

TECHNOLOGIES	CELL SOURCE	TARGET CELL TYPES	THROUGHPUT	EFFICIENCY	ENRICHMENT RATIO/PURITY
Rectangular spiral [116]	ganglionic eminences of E13 embryos from CD1 mice	Neural stem cells	1 mL/min	84%	67% purity[109]
Rectangular spiral [65]	Femur bone marrow of adult mice	MSCs	1.6 mL/min	73.2%+-1.5%	6+-0.4-fold increase from an initial purity of 2.2%+-0.5%
Straight channel [107]	Adrenal gland from mice	Adrenal cortical stem cells	60 uL/min	Not given	Not given
Slanted spiral [110]	Neural induction kit added iPSCs	Neural stem cells	3 mL/min	93%	2.1-fold increase
Rectangular spiral [119]	Commercialised umbilical cord blood	Cord blood CD34+ cells	1 mL/min	>90%	>70%
Slanted spiral [8]	Commercial MSCs with microcarriers	MSCs	30 mL/min	94% in two rounds	Not given
Slanted spiral [120]	Murine MSCs	dead MSCs	5 mL/min	75%	6 times higher senescence marker expression
Labyrinth Channel **[113]**	Mouse muscle tissue	Mouse muscle stem cells	1.8 mL/min	66.5%	2 folds increase, 84.8%

TECHNOLOGIES	CELL SOURCE	THROUGHPUT	APPLICATIONS
Rectangular spiral [114]	hMSCs	2.5 mL/min	cell cycle synchronisation for potential downstream research and applications.
Straight channel with obstacles [117]	mESCs	20 µL/min	Sorting of embryoid bodies with different sizes.
Slanted spiral [108, 109]	Commercial human bone marrow MSCs	1.5-4 mL/min	Investigate the correlation of physical properties of cells and differentiation potential, therapeutic potential
Slanted spiral [121]	Commercial human bone marrow MSCs	3 mL/min	Promote bone marrow regeneration with bigger size MSCs

1.4.2. Active and passive mechanical stimulation or cell manipulation devices

Active and passive microfluidics are also widely used to provide physical stimulations to the cells, study their behavioural changes or measure their physical properties. These devices are normally combined with signal readers or microscope to analyse the response of cells.

1.4.2.1. Active microfluidics

The external forces/stimulus applied by different microfluidic devices can be used to measure different properties of the cells. Nourse, Prieto [97] used the DEP device described in [96] to measure the cell size (based on the time cells spent to cross the measuring point), surface glycosylation and resting membrane potential to investigate their influence on the membrane capacitance and the correlation with NSCs cell fate. This type of devices is called microfluidic impedance flow cytometer (IFC), which have great potential in cell studies and have already attracted great interest in commercialisation (e.g., Pollen IFC of Amphasys). Song, Rosano [122], [123] used an IFC to distinguish and sort the MSCs with self-proliferation tendency and MSCs with adipocytes, osteoblasts differentiation tendency. Similarly, Gong, Petchakup [124] used a scaled-up IFC to characterise the differentiation potential of MSCs growing on microcarriers since adipogenic cells have higher lipid content and, therefore lower conductivity, and osteogenic cells have higher conductivity due to the higher calcium ions content on the cell membrane. The electrical properties of cells can also be linked to the expression level of specific genes as an indicator of cell behaviours (Fig. 1.4A). Crocetti, Beyer [125] used impedance flow cytometer to evaluate the expression level of TRPC1, a proliferation related gene which plays a key role in calcium uptake. These works all showed a strong correlation between electrical properties and cell proliferation and differentiation. IFC, as a non-invasive, non-damaging device, can be potentially applied in the bioprocessing industry for cell monitoring during culture. Gong, Petchakup [124], who demonstrated IFC for high throughput detecting the viability and differentiation potential of spheroids or cells attached to microcarriers, could be a very useful cell monitoring tool during the industrial production of stem cells. Similarly, the response of cells to acoustic field can be recorded to measure the size and density of cells as well [126]. However, there are not many applications showcased for stem cell applications.

1.4.2.2. Passive microfluidics

Passive microfluidic utilises the hydrodynamic forces generated by the channel geometry to relocate cells inside the channels. The inertial microfluidic channels can be used to mimic body fluid movements, which also applies inertial forces to the cells in our body. While the cells are being proceeded in the devices, different levels of shear forces are applied to the cells and their behavioural changes are recorded and observed.

Moledina, Clarke [127] made a microfluidic device with 5 culture chambers for perfusing media across the cultured mouse ESCs with different flow rates and compared the signalling and proliferation rate changes of cells in different chambers. This method depletes the endogenously secreted factors and allows the calculation of minimum paracrine ligands needed to direct the cells towards certain cell fate (Fig. 1.4B). Choi, Levy [128] used an hydrophoresis device, which is a device consisting of multiple ridges horizontal to the fluid direction, to separate the MSCs with stickier surface properties. Sticky cells tend to roll on the ridges of the device, while the non-sticky cells tend to follow the streamlines. With the help of this device, they found the mediator of cell rolling in the system and correlated MSC differentiation with the loss of adhesion. Otto, Rosendahl [129] combined a straight channel microfluidic chip with a camera to observe the relationship between the deformability of hHSC (introduced by inertial forces of the straight channel) and their cell-fate decision. Lin, Kim [130] built a serpentine cross microfluidic channel (deformability cytometry) study and characterised the physical properties of different subpopulation groups of stem cells with morphological changes. The serpentine channel applies Dean forces and inertial forces on the cells and forces them to change their morphology during the movement inside the channel. Different degrees of changes were recorded by the camera in microscope and used to characterise them into different subpopulations (Fig. 1.4C).

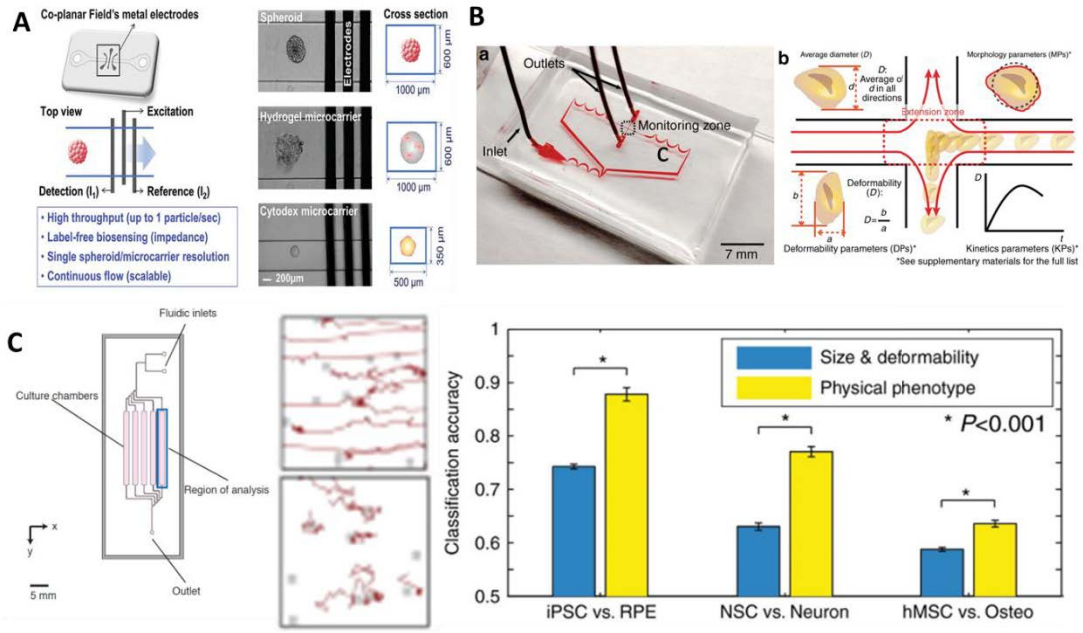

Fig. 1.4. The active and passive microfluidic devices used for cell stimulation and analysis. A) An impedance flow cytometer used for analysing the drug response and proliferation of microspheres/cells attached microcarriers in a continuous manner. Reproduced with permission [124]. Copyright 2021, John Wiley and Sons. B) a simple microfluidic channel to observe stem cells behaviours under paracrine effect and inertial flow. Reproduced with permission [127]. Copyright 2012, National Academy of Science. C) inertial microfluidic devices coupled with high-speed camera to record the deformability of cells under inertial forces. The cell density and secreted factor trajectories were recorded in lines (left) and the correlation between deformability and physical phenotypes (right). Reproduced with permission [130]. Copyright 2017, Springer Nature.

Table 1.3. Active and passive devices for cell stimulation and properties measurement

TECHNOLOGIES	CELL SOURCE	PURPOSE OF RESEARCH
DEP [97]	NSCs	Distinguish stem cells with different differentiation potentials by their electrical properties and isolate subpopulations
IFC [122, 123]	hMSCs	Separate stem cells with osteogenic and adipogenic potentials based on their membrane potential
IFC [131]	hMSCs	Induce stem cell differentiation by applying different level of electrical stimulation, and the electrical properties of cells can be measured
IFC [124]	hMSCs	Measure the electrical properties of cell spheroids to characterise their differentiation potentials
IFC [125]	hMSCs	Use IFC to detect electrical properties (Cation channel expression level) of cells and correlate them with proliferation potential
Straight channel [127]	mESCs	Observe autocrine and paracrine effects changes of cells under different flow rate
Straight channel [129]	hHSCs	Observe deformability of cells and their correlation with cell fate
Hydrophoresis [128]	Commercial MSCs	Investigate the correlation between cell adhesion and differentiation states
Slanted spiral [118]	Commercial MSCs	Recirculating MSCs in the microcarrier-based perfusion culture system
Serpentine channel [130]	Cultured iPSCs, NSCs, MSCs	Differentiate subpopulations of stem cells with different physical properties

1.4.3. Organ-on-a-chip (OOC)

Bringing a new drug into the market is a slow, lengthy and costly process [132]. All drug candidates undergo extensive preclinical assessment to avoid failures in clinical trials. High drug attrition in clinical trials are mostly due to the absence of highly reliable and predictable preclinical models [133]. Currently, pharmaceutical companies heavily rely on non-human animal models and 2-dimensional (2D) cell culture-based assays for pre-clinical drug screening. Although animal models provide vital information on the organ physiology, disease pathophysiology and drug screening, they fail to recapitulate the anatomical structures, development, disease symptoms and the actual human clinical response [134]. Moreover, animal models are genetically different from humans and are expensive, with ethical issues. The conventional 2D cell cultures of primary cells and immortalized cell lines lack the tissue-tissue or multi-organ interactions, cellular matrix and all the mechanical cues present in vivo [135]. Although the current 3D spheroids or organoid models constitute the relevant components, they do not always include physiologically relevant cues like dynamic flow, mechanical strain and multi-organ interactions, which all have significant impact on drug metabolism [136]. Therefore, there is an urgent need of advanced model systems that complement the existing preclinical models and reproduce physiologically relevant human response.

Microfluidic organ-on-chips (OOCs) technology is a rapidly-growing approach used in drug development and testing, as an alternative to the existing preclinical models [137] .OOCs are miniaturised microengineered physiological systems that recapitulate the key structural and functional features of human organs *in vitro* [138]. They offer controlled dynamic conditions, substrate, biochemical and mechanical cues that mimic the organ-level functions. Owing to the advantages offered by OOCs, numerous research groups have utilized it to develop models of lung, heart, gut, kidney, liver, marrow, brain, and other organ systems of human body [139-144]. Most OOCs incorporate co-culture of different cell types to study the interactions between different organs, which can be further expanded by integration of different organ-specific OOCs into one body-on-a-chip (BOC), to better understand the drug pharmacokinetics in human body [145] . The possibility of using patient specific cells or tissue samples to develop personalized OOCs that represent the physiology, pathology and genetics contributing to assess and develop treatments for a specific patient or individual has further drawn attention towards them (Table 1.4) [146].

Isolation procedure, limited supply and donor variability are major issues with primary human tissue samples [147]. Stem cells offer unlimited renewability with capability of self-regeneration and controllable differentiation into adult cell types of different tissues or organoids, making stem cell based OOCs models powerful alternatives for human disease modelling and drug testing with multiple organ system interactions [146, 148]. Recently, the use of stem cells in OOCs have drawn attention aiming to develop better models of effective drug screening and toxicity testing. With the use of stem cells, the human OOCs will help understand the differences in underlying pathophysiology between different patient groups, identify groups that are more susceptible to a specific disease, compare drug responses of individual patients and predict prognosis [149]. This will help to develop human tissue models to assess the most effective and safest therapies prior to clinical trials and animal models. Mesenchymal stem cells (MSCs) are usually the preferred option for researchers, as they are relatively easier to extract from adult tissue biopsies [150]. However, the variability of isolation, culture and differentiation protocols among different research groups lead to heterogenous phenotypes in MSCs population, which is a major limitation of using MSCs in OOCs [145]. Although embryonic stem cells (ESCs) offer consistent phenotype and unlimited differential potential than MSCs, they are ethically controversial and highly regulated as they must be derived from human embryos [145]. The limitations of generating large number of genetically diverse cell lines coupled with ethical issues make ESCs an inappropriate source of stem cells for disease modelling and drug studies. IPSCs on the other hand offer similar genetic background, morphology and surface marker expression as ESCs with no ethical concerns [151]. Furthermore, iPSCs offer the possibility of developing patient-specific models and drug studies by obtaining samples from donors with known disease phenotypes [145] (Fig. 1.5B). Organogenesis-on-a-chip developed from hPSCs can help overcome the limitations of human primary cells by generating highly ordered structures and tissues [152]. The types of stem cells that can be used as tissue source for OOCs is illustrated in Fig. 1.5A.

Different research groups have already developed an array of OOCs including blood vessels, heart, kidney, CNS, blood-brain-barrier, muscles and more using ESC- and iPSC-derived cells [149, 153] and demonstrated their potential. However, designing complex stem-cell based OOC devices can be time-consuming, and expensive; limited access to stem cell resources being another factor to consider. Recent advances in the OOCs technology have gained tremendous interest from scientific and pharmaceutical industry evident from the outburst of publications and industrial start-ups [135, 153-155]. OOCs offer better physiological

representation of human disease modelling and drug responses compared to existing preclinical models. iPSCs can also be genetically edited for specific mutations or introducing different variants associated with a disease, allowing the modelling of specific diseases and to identify novel therapeutic measures. In terms of multi-organ devices, it can be really challenging to maintain different scaffolds, making the flow rates, culture duration, mechanical and chemical cues for different cell types, making the system complex and challenging to all researchers. The inherent genetic variability of humans can lead to major differences in cell phenotypes and drug response, making the use of these models more challenging [156]. Also, culture and maintenance of stem cells is a laborious, expensive, challenging, and lengthy process with increased risk of contamination. The other issue is to ensure a fully differentiated and mature adult phenotype of a desired organ. iPSC derived cells often display a foetal phenotype which may lead to immature or poorly differentiated cells and large heterogeneity in phenotypes [148]. Thus, it is vital to establish standard stem cell based experimental protocols for individual patient and disease models to assess the individual's cellular response to drugs and other stimuli [153].

1.4.3.1. Stem cells-based organ-on-a-chip for Disease modelling

The stem-cell based OOC technology offers improved cell populations, structures, and environments which are more physiologically similar, and a microfluidic flow pattern is optimized to keep cells viable, differentiate and maintain polarity [157]. It is possible to differentiate them into a broad range of cell types with relatively high efficiency, including cardiomyocytes, hepatocytes, and distinct neuronal types [158]. They have become a good alternative for disease-specific or patient-specific cells. Different research groups have utilized stem cells that can differentiate to desired cell types with fairly authentic functionality. HiPSCs derived from healthy individuals and patients can be used to develop models of vasculature: human endothelial cells, vascular smooth muscle cells and pericytes, which can be integrated in the OOC platforms to develop in vitro models of blood vessels and study associated diseases[13]. Different cell types and cancer stem cells (CSCs) can be used to mimic the key factors of the tumour microenvironment (TME) to study the tumour growth, invasion and migration. By including CSCs, malignant cells with its TME can be invaded with myeloid cells, phagocytes, immune cells and tumour-associated fibroblasts [159]. The stem cell approach is particularly valuable for cardiac disease modelling because primary cardiac cells are difficult to access and maintain in culture as they are non-dividing cells [160]. Also, the tissues obtained from heart transplantation usually have abnormalities. Studies have shown the differentiation

of iPSC-derived hepatocytes (iPSC-HEPs) on a perfusable micropillar chip to generate controllable and mature spheroids, in situ with longer viability[161]. Musah et al. mimicked the development, filtration properties and disease characteristics of the glomerular capillary wall by co-culturing iPSC-derived podocytes with glomerular microvascular endothelial cells in a kidney-on-a-chip model [14]. Naumovska et al. developed a gut-on-a-chip model by differentiating iPSC into 3D-gut like tubules to model inflammatory responses observed in patients [162]. Similarly, different groups have developed and validated BBB-on-a-chip models by co-culturing iPSC derived endothelial cells with primary human brain pericytes and astrocytes [163, 164]. In addition, OOC can be applied to advanced disease models by combining them with patient-specific iPSCs eventually leading to more realistic patient-specific on-chip devices.

1.4.3.2. Stem cells-based organ-on-a-chip for Drug Screening

With OOCs, 3D cell culture can be controlled spatially and temporally, which is opening up new avenues of research on cancer invasion, extravasation, and drug response [159]. Tumors-on-chips have reduced drug development time and costs, as well as ethical issues associated with animal experiments. Through parallel cell encasements and chemical gradients of circulating drugs, organ-on-a-chip platforms can be made more powerful and capable of high-throughput drug screening[159]. In order to replicate the bloodstream-to-tissue transport of drugs, OOCs are vascularized by an endothelium layer. Liver is the main target organ for drug-induced toxicity due to its crucial role in drug metabolism and detoxification. Thus, several research groups have developed liver-on-a-chip to study the hepatotoxicity of new drugs[165]. A four-cell human liver acinus microphysiology system (LAMPS) was developed by Sakolish et al using primary human hepatocytes, iPSC-HEPs as well as three human non-parenchymal cell lines to observe the short-term and long-term effects of 8 different drugs [166]. The kidney-on-a-chip developed by Musah et al. was used to replicate the cancer drug Adriamicyn-induced injury and albuminuria Adriamicyn [14]. Similarly, Naumovska et al. used the iPSC derived 3D-gut like tubules to assess the inflammatory responses observed in patients using pro-inflammatory cytokines IL-1 β, IFN-γ and TNF-α [162]. To study the hepatic metabolism-dependent cardiotoxicity induced by clomipramine, an antidepressant drug, Yin et al. built an iPSC liver-heart OOC platform with iPSC differentiation into the OOC [167]. Oleaga et al. used their liver-iPSC-bsed heart OOC to investigate the cardiotoxicity of the drug cyclophosphamide [168]. Zhang et al. used their iPSC-based liver-heart OOC model to analyze the hepatotoxicity of Doxorubicin and Acetaminophen [169]. For cancer therapeutics, cancer

stem cells(CSC)-based models developed using the tumor samples or IPSCs can be a promising platform to analyze and identify the best chemotherapy agents with positive results and minimal side effects. By developing such models, the cancer community will be able to improve patients' quality of life, improve survival rates, and facilitate the testing of various new drug formulations [159]. The hiPSC-CM-based OOC technology reduces the cost and time of preclinical drug research by allowing the preliminary evaluation of libraries of drugs and the selection of compounds that are potentially active and safe[164].

The incorporation of stem cells into OOC models will lead to development of advanced preclinical models for identifying the best treatment for individual patients across large population suffering from same disease [155]. Furthermore, stem cells-based organoids can be integrated into the OOC platform to develop a more powerful “organoids-on-a-chip”, which has better maturity and functionality [136]. Standardising OOC models provides a comprehensive model for evaluation of treatment outcome and thus a potential scalable standard for cell therapy quality control, or cell line establishment standard.

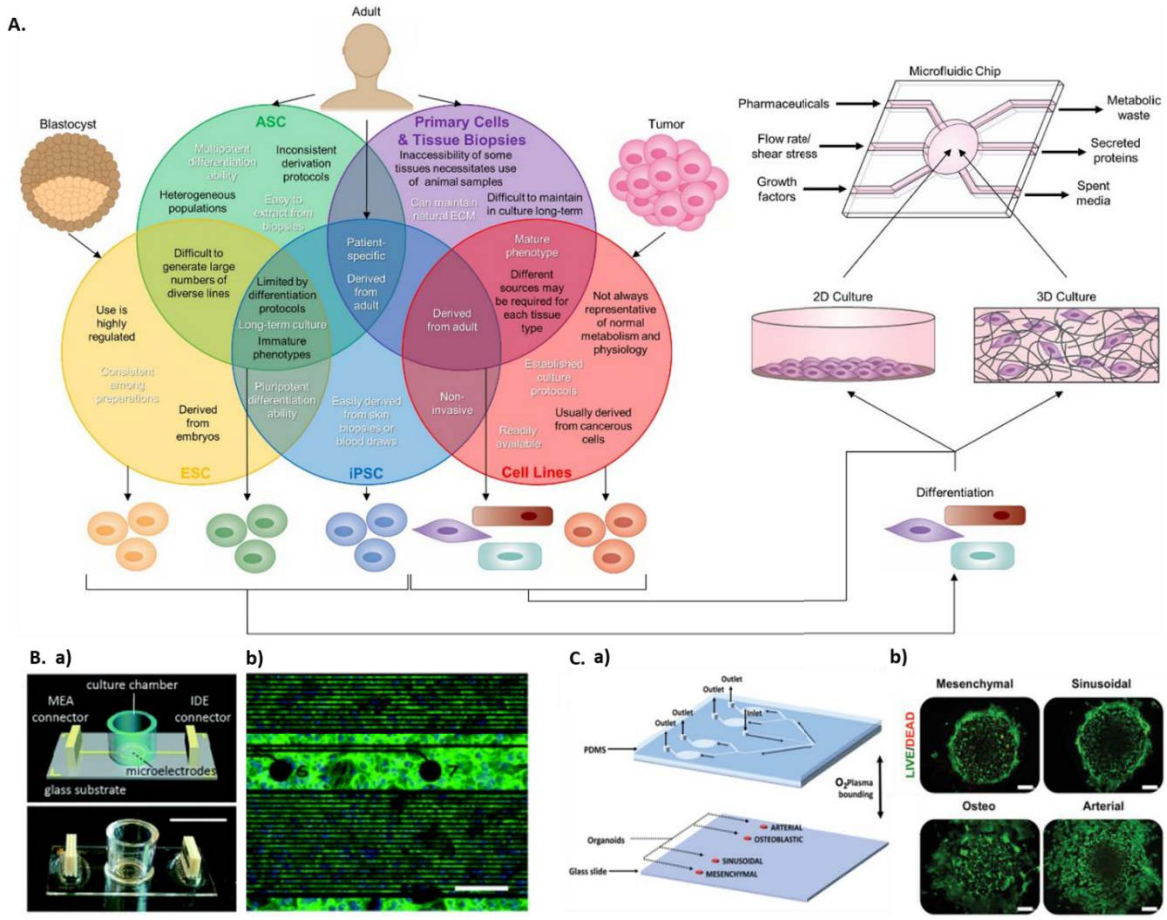

Fig 1.5. Stem cells organ-on-a-chip modelling. A) Tissue sources for organ-on-a-chip (OOC) devices. ESCs, iPSCs, and adult stem cells (ASCs) can be differentiated and integrated into OOC. The figure demonstrates the advantages (white) and limitations (black) for the use of different cell types in OOC

devices. Stem cells are readily available and have unlimited cell source. Despite the existing limitations, stem cells are a promising technology for integration into OOCs. (Reprinted with permission from [14]) B) (a) Schematic and picture of the fabricated chip for real-time monitoring of cardiac electrophysiology and contraction. (b) Fluorescence images of cultured human iPSC-CMs on the device (Hoechst: blue and cTnT: green) Scale bar: 100 μm. Reproduced with permission [145]. C) (a) Fabrication of the bone marrow-on-a-chip by bonding the PDMS layer with channels to a glass slide. (b) Live and dead staining of 4 different mesenchymal niches construct types on day 8. scale bar: 100 μm. Reproduced with permission [170].

Table 1.4. Organ-on-a-chip used for stem cell research

OOC	TARGET DISEASE/CONDITION	DRUG TESTED	STUDY DONE
Heart-on-a-chip	Hypertrophic changes	Isoprenaline	Signs of hypertrophic changes caused by mechanical and biochemical co-stimulation [171]
	Heart-pump functions	Isoproterenol	Recapitulate the kinetics of cardiac microtissue functions and validate the responses to electrical stimulation and dose-dependent inotropic drug administration [172]
	Heart failure and low blood pressure	Norepinephrine	A model with integrated sensors to record contractility and electrophysiology [170]
	Drug-induced changes in cardiac cell growth	Doxorubicin, Endothelin-1, Acetylsalicylic acid, Isoproterenol, Phenylephrine, Amiodarone	Cardiac spheroids, quantitative growth, and effects of different drugs [173]
	Drug-induced changes in heart rate	Isoproterenol	Heart rate and duration of rate correlated field potential [174]
	Changes in vascular permeability and drug-induced cardiotoxicity	TNF-α and Isoproterenol	Measurement of the TEER in the endothelial layer, the beating rate with corrected field potential duration [175]
Liver-on-a-chip	Drug-induced hepatotoxicity	Troglitazone	Assessment of albumin and urea production, viability, and nuclear size of hepatocytes [176]
	Drug-induced hepatotoxicity	Terfenadine, Troglitazone, Rosiglitazone, Tolcapone, Trovafloxacin, Pioglitazone and Caffeine	Compared iPSC-derived model with the primary human hepatocytes seeded model, their model is better in basic liver functions, drug pharmacokinetics, metabolism, and safety [166]
	Drug-induced hepatotoxicity	Acetaminophen	Effects of the drug on the differentiated liver organoids in situ [177]
Bone marrow-on-a-chip	Organ-level marrow toxicity to radiation	Granulocyte colony-stimulating factor (G-CSF)	Physiologically relevant, demonstrated the effects of γ-radiation and validated radiation countermeasure drug, G-CSF [178]
	Long-term in vitro bone marrow model		Long-term culture of primitive HSPCs in a dynamic condition [179]
	Interaction between infused hematopoietic stem and progenitor cells (HSPC), lymphoma and leukemic cells		Study of circulating normal and malignant hemopoietic cell-niche interactions [180]

	Radiation-induced toxicity	Radiation-protecting effects of two potential therapeutic proteins, G-CSF and bactericidal/ permeability-increasing protein (BPI)	Modelling haematopoiesis, response to radiation and its countermeasures [181]
Kidney-on-a-chip	Albuminuria and Podocyte injury	Adriamycin	Chip mimicked the structure and function of the kidney glomerular capillary wall in vitro [182]
BBB-on-a-chip	Normal physiological BBB and Neurodegenerative diseases	Mannitol and TNFα	Physiologically relevant human post-capillary venules, quantitative analysis of barrier function and endothelial cell behaviour [183]
	Neurological Disorders	TNFα, IL-1β and IL-8, Retigabine, Levetiracetam, Colchincine	Modelling inheritable neurological disorder and drug screening [184]
	Normal physiological BBB	Caffeine, Cimetidine, and Doxorubicin	Physiologically relevant perfusion, permeability assays, shear stress and drug testing [185]
	Human BBB physiology and pathology	Anti-brain tumor drugs (paclitaxel and bortezomib) and a neurotoxic peptide (amyloid β 1-42)	Barrier integrity with tight junction protein expression and multiple drug testing[186]
	Mechanistic studies of BBB disruption	Transforming growth factor beta (TGF-β1)	Tight junction protein expression, permeability and BBB disruption [187]
	Organophosphate neurotoxicity	Dimethyl methylphosphonate (DMMP, 97%), diethyl methylphophate (DEMP, 97%), diethyl cyanophosphonate (DECP, 90%), and diethyl chlorophosphate (DCP, 97%)	Organophosphate toxicity screening, transport across the barrier, inhibition of AChE activity following exposure [188]
CNS/PNS-on-a-chip	-Motor Neuron Disease such as Amyotrophic Lateral Sclerosis (ALS)	-Brain-derived neurotrophic factors (BDNF) and glial cell-derived neurotrophic factor (GDNF)	Neuro-vascular coupling to study pathogenesis of motor neurone disease [189]

	Motor Neuron Disease	Thapsigargin and Riluzole	Therapeutic effect of Riluzole concentration gradients on Thapsigargin-mediated neuronal damages[190]
	Neurovascular diseases, Hypoxic-ischemic brain injury	Glial cell-derived neurotrophic factor (GDNF)	Co-culture platform to investigate paracrine signalling in controlling endogenous neuronal behaviours in vivo. [191]
Muscle-on-a-chip	Hutchinson-Gilford Progeria Syndrome (HGPS)	Everolimus	Model reproduced key features of HGPS to study its pathogenesis and response to proposed therapeutic [192]
Multi-organs-on-a-chip	Normal human physiology	Pergolide, Rofecoxib, Valdecoxib, Bromfenac, Tienilic acid and Troglitazone	Co-cultured four autologous tissue models from iPSCs from the same healthy donor [193]
	Drug Toxicity in multiple organs	Pergolide, Rofecoxib, Valdecoxib, Bromfenac, Tienilic acid and Troglitazone	Multi-organoid 'body-on-a-chip' system for integrated drug studies [194]
	Hepatic metabolism-dependent cardiotoxicity	Clomipramine	Multi-organoids-on-a-chip model replicating human organ-specific functions, drug metabolism and responses at multi-organ level [167]
	Cardiotoxicity and hepatotoxicity	Cyclophosphamide	Replicates in vivo crosstalk between heart and liver, evaluation of cardiotoxicity and hepatotoxicity [168]

1.4.4. Droplet microfluidics

1.4.4.1. Single cell analysis

Droplet-based microfluidics has been extensively used in the study of single cells in recent years. Cells can be easily compartmentalised in individual droplets for downstream applications by utilizing the sub-nanolitre level compartments and narrowed channels. This technology hugely increases the resolution and reduces the cost of single cell analysis.

Traditionally, cell and molecular biology studies are performed in bulk samples, analysing the average signal of a whole population. In recent years, researchers have shown the importance of studying cells and their characteristics at single cell resolution to avoid masking cellular diversity, functionality and behaviour [31, 195]. This finding gives rise to a new term called cell heterogeneity, which is one of the main roadblocks to the translation of stem cell research into practical therapy. Cellular heterogeneity exists in every cell population [196, 197], particularly in stem cells compared to differentiated cell groups. Due to their differentiation potential, stem cells are heterogeneous even in the same batch of cells. This can potentially lead to false judgment of therapeutic or research outcomes. For instance, transplantation of a small population of undifferentiated stem cells with the majority of differentiated cells has the potential risk of developing teratoma. Therefore, studying individual cells in a cell population is necessary to unmask the low levels of important cell properties that might be covered up by the bulk analysis results [198]. The following reviews have discussed the cell application on different aspects including genome [199], epigenome [200], transcriptome [201], metabolome [202], proteome [203, 204] and multi-omics [25]. This review focuses on discussing the single-cell microfluidic tools applied in stem cell research.

Microfluidic-based single-cell analysis tools are divided into two types: droplet generator and droplet array. Droplet generators encapsulate individual cells into droplets by alternating liquid and oil phases in micrometre level channel. This method generates millions of droplets/min, with about 10% droplets containing a single cell [205]. However, the droplet generator cannot handle a small sample size due to the requirement of minimum starting volume, similar to a flow cytometer [206]. Static arrays encapsulate cells into individual chambers or wells by injecting cell solutions into microchamber arrays. It allows multi-omic studies and monitoring of single cells, while the throughput and scale (number of droplets produced) are limited. Active microfluidic devices provide precise control of a single particle inside the fluid or droplet that contain a single cell. The accessibility and controllability of the single cell are

better, but the throughput is lower, associated with risks of cell damage caused by the external forces applied [207].

Droplet generator has become a hot topic in recent years. The high throughput feature attracts great interest in large-scale cell encapsulation for sequencing and molecular studies. Droplet generators are commonly used with DNA or RNA barcoded beads to capture the genetic material of the lysed single cell in the droplet. Each barcoded bead has a unique sequence to allow identification of the genetic material of each cell during reading. This method was first developed by Klein, Mazutis [205], to study the heterogeneity in mESCs and has now been adopted worldwide for single cell analysis (Fig. 1.6A). For example, Rotem, Ram [208] use the same concept and technology to distinguish and identify the sub-population of mESCs by characterising chromatin profiles of cells by binding the DNA content of each cell to their own unique barcoded beads and performing next-generation sequencing (NGS). Izzo, Lee [209] use droplet generators to sequence the scRNA of mouse haematopoietic stem cells (mHSCs). The sequencing results provided deeper insight into the effect epigenomic regulation genes have on the differentiation landscape of mHSCs. De Micheli, Laurilliard [210] used the 10X genomics sequencing kit to sequence the RNA of mouse muscle stem cells before and after injury. The populations involved in muscle regeneration was identified and the key paracrine factors involved in muscle regeneration were identified. This can be potentially useful not only for muscle regeneration purpose, but also for speeding up the cultivated meat production process. Single cell capturing can be used to do long-term culture or spheroids development. An, Liu [211] encapsulated single MSCs in microgels to generate single MSCs-derived spheroids for bone regeneration. Compared to multiple cells encapsulation which will be discussed in the following section, single cells encapsulation allows direct intravenous injection due to the small size. It also reduces the chance of clearing out by the host in allogenic injection (Fig. 1.6B).

Droplet arrays can be divided into two types; one type of array encapsulates the cells within a droplet during cell solution injection and is therefore named as a static droplet array (SDA). The other type of array contains ten to thousands of individual cell-sized traps, allowing perfusion of cells with high trap occupancy, called cell trapping array (CTA). Since the cells are physically put in compartments, SDA can be used for cell-cell interaction and secretion studies. Sikorski, Caron [212] developed a static droplet array (SDA) with multiple inlets for adding reagents during the experiment. They investigated the heterogeneity of individual hESCs reactions to the addition of FBS and found that OCT4 expression correlated to foetal bovine serum (FBS) presence, which affects the cell morphology, growth, and differentiation

(Fig. 1.6C). To improve the sensitivity of qPCR in low input RNA, Zhong, Chen [213] developed an SDA with a heating plate to study the heterogeneity of B2M, Nodal and Fzd4 gene expression in single hESCs. SDA has also been combined with a pumping system to provide long-term culture study of single cells. Dettinger, Frank [214] made a 48 chambers SDA to study the differentiation of primary HSCs under the presence of Macrophage colony-stimulating factor (M-CSF) cytokine. Lecault, VanInsberghe [215] used an SDA device to track the proliferation of HSCs and investigate the cell response to exposure time of growth factors over time. On the contrary, a CTA does not have a separate environment for each cell, thus, studies that require an individualised environment are not feasible. However, the footprint of CTA is much smaller than SDA, and large scale screening of cells is easier in CTA. Skelley, Kirak [216] developed a static array for trapping and pairing two different types of cells to study cell-cell interaction and provide a chance for cell fusion for reprogramming. This device contains maximum of 6000 traps and they obtained about 70% paring efficiency in an 8×4 mm space. Kobel, Burri [217] developed an algorithm for automatically detecting single cells within a static array, and it is capable of tracking dividing cells and recording different fluorescent signals of cells. Faley, Copland [218] use CTA to trap chronic myeloid leukaemia patient-derived HSCs and treat the cells with dasatinib, a cancer-treating drug, to investigate the apoptosis and motility of the cells after treatment. This demonstrates the potential application of CTA in clinical applications such as personalised treatment and industrial applications such as drug screening.

There are also some single cell microfluidic studies using other platforms, such as active microfluidic systems to manipulate the cells individually. Zhou, Basu [12] isolated mESCs in a static array with electrodes built under the traps. The electrodes were used to measure the change of electrical properties of the cells during differentiation (Fig. 1.6D). This device was used to investigate the same problem as to Song, Wang [123], who built an impedance microfluidic flow cytometer channel to measure the electro-properties of differentiation states of mESCs. The static array yields more sensitive results than the cytometer, due to the better positions of electrodes and more precise measurements. DEPArray (DEP-based microfluidic device) is another example. Silvestris, Cafforio [219] used DEPArray to isolate oogonial stem cells (OSCs) from tissue fragments and select the OSCs based on the fluorescent tag and the morphology of the cells. They found that the levels of marker expressed by individual cell is a direct indication of their differentiation capacity. The external forces applied by active microfluidic devices can be strong enough to be used as an active trap for cells. Evander,

Johansson [220] used an acoustic microfluidic device to trap single NSCs inside the channel, allowing perfusion culture and study of single cell or cell clusters (Fig. 1.6E).

As we discussed in the earlier section, currently, there is no standard quality control tests for stem cell products, even though the heterogeneity of stem cells is vast. Unsuccessful clinical trials can be partially attributed to the heterogeneity of cells. Although there are papers suggesting universal standards to quantify the immune-modulatory properties of cGMP-produced MSCs [64], insight of stem cell product quality has never been provided at the single cell level. Likewise, a comparison of the stem cells from different cell sources can be beneficial for quality control of products and standardising the cell sources. Stem cell therapy industry require homogeneous product quality and a well-characterised single muscle cell profile can be useful as a cell line selection standard. Given the fast and low-cost manner of droplet-based microfluidics and especially the easy manipulation mode of SDA devices, new stem cell quality control methods can be developed around it. It can provide a more detailed analysis and a better understanding of the batch-to-batch difference of the products, which would then improve the clinical outcome of stem cell therapy.

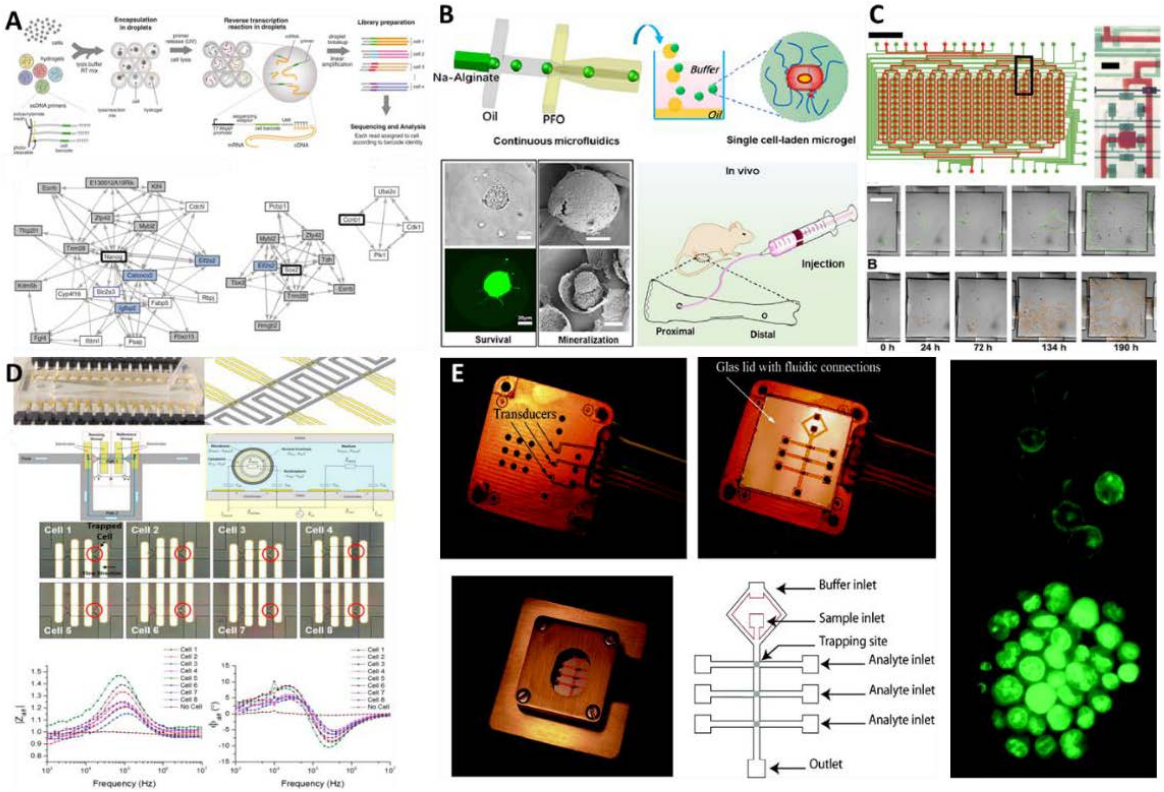

Fig. 1.6. Droplet-based microfluidic devices used or single stem cell analysis and studies. A) Droplet generator-based single cell sequencing (top) reveal pluripotency related gene in ESCs (bottom). Reproduced with permission [205]. Copyright 2015, Elsevier. B) Single cell-encapsulated microgel (top) used for regenerative medicine showed a lower clear out rate in the injection site (bottom). Reproduced with permission [211]. Copyright 2020, Elsevier. C) Static droplet array (top) allows better long-term culture and tracking of single stem cells derived colony (bottom). Reproduced with permission [212]. Copyright 2015, John Wiley and Sons. D) A static droplet array coupled with electric field (top) to measure the differentiation state of ESCs. 8 cells were individually trapped, and the impedance magnitude and phase were measured overtime (bottom). Reproduced with permission [12]. Copyright 2016, Elsevier. E) Acoustic-based single cell traps (left) allow long-term perfusion study of single NSCs, perfusing acridine orange staining over time (right). Reproduced with permission [220]. Copyright 2007, American Chemical Society.

Table 1.5. Droplet-based microfluidic devices for single cell analysis

TECHNOLOGIES	THROUGHPUT	CELL TYPES	APPLICATIONS
Droplet generator	100 uL/h	mESCs	Developed droplet generator for RNA-sequencing and study the heterogeneity in subpopulations of ESCs [205]
	N.A.	murineHSCs	Use RNA-sequencing to study the differentiation landscape of HSCs, correlate DNA methylation with differentiation [209]
	N.A.	ESCs	Use DNA sequencing to study subpopulations of ESCs classified by different chromatin states [208]
	100 uL/h	MSCs	Single cell encapsulation in hydrogel for bone regeneration[211]
SDA	160 chambers	hESCs	Long-term analysis of correlation between cell proliferation and cell marker expression [212]
	20 chambers	hESCs	On-chip PCR analysing absolute mRNA level in single cell [213]
	48 chambers	MurineESCs	Precise control of single cell microenvironment for long-term tracking study. [214]
	1600 chambers	mHSCs	Controlled microenvironment for single cell proliferation study [215]
CTA	700-6000 traps	mESC	Cell fusion with chemical and electrical methods [216]
	2048 traps	hHSCs	A tool with an algorithm to track cell division and cell phase [217]
	440 traps	hHSCs	Test cancer drug response with patent-derived stem cells [218]
DEP array	N.A.	mESCs	Measure the difference of electrical properties of individual cells and their differentiation potentials after time [12]
	8 DEP cages	Oogonial stem cells	Single cell isolation from tissue and observe the relationship between marker expression level and differentiation potential [219]
Acoustic microfluidics	3 acoustic traps	NSCs	Demonstrate the potential to trap single cell, single spheroid and perfuse different media [220]

1.4.4.2. Droplet generators for microcarriers and microtubes manufacturing

The high-throughput, customisable and stable nature of droplet generators is also of great interest in the field of chemical synthesis such as microcapsule and microcarrier production. Traditionally, microcarriers are produced by water-in-oil emulsification. This method is simple and effective but results in huge size variation of microcarriers and a huge waste of material (the microcarriers producing efficiency can be lower than 50% [221]). They also have limited control over the material and modification that can be performed on microcarriers. The emergence of droplet generators hugely reduces the waste of materials in a large scale, reduces the size variation and simplifies the post-processing steps. Also, the appliance of droplet generators enables production of combined materials, or microcarriers/microtubes with complicated structures and shapes. The material of microcarriers is one of the keys determining factors in choosing droplet generator designs. For example, Alginate microcarriers require at least two sample inlets to allow mixing of Alginate acid and Calcium solution on-chip and allow gelation of material on a chip [222]. At the same time, gelatine can have only one sample inlet [11, 223, 224] and the microcarriers can be crosslinked or gelated later.

Droplet generators are highly customisable. They can make variable sizes microcarriers which allows culturing of monolayer cells, or multiple smaller microcarriers embedded in cell spheroids that become the extracellular matrix [225] of cells to increase the nutrient and oxygen supply. They can also be used to produce fibres-like or sphere structures to encapsulate cells. These different technologies are used to serve the different purpose of research or achieve different aims during culture. Most commonly, droplet generators are used to produce mono-size microcarriers [11, 224, 226, 227], encapsulated spheroids [222, 223, 228-232] or microfibres [233-236] for large scale cell culture. One of the main advantages of using a droplet generator is to produce low-cost, mono-sized microcarriers. Rogers, Haskell [11] built a step emulsification droplet generator to make mono-size Gelatine methacryloyl (GelMA) microcarriers in large-scale. The microcarriers produced pass through an on-chip UV device to gelate the microcarriers, and the cost of production is 0.01 USD/cm^2 (Fig. 1.7A). The flexibility of the device allows the production of microcarriers to process fragile materials or integrate multiple components which traditional emulsification technologies cannot. For example, Allazetta, Hausherr [226] and Dashtimoghadam, Fahimipour [227] used flow focusing droplet generators to encapsulate growth factors into the microcarriers, which were then slowly released during cell culture to direct stem cells differentiation (Fig. 1.7B, 7C).

Another unique application of droplet generators is cell encapsulation. Stem cells can be treated as one of the materials during the droplet generation process to create a local stem cell niche-like environment for research purposes [232]. For example, Alessandri, Feyeux [237] used a microfluidic droplet generator to encapsulate multiple hNSCs in one hydrogel to improve the cell proliferation and differentiation in culture. Liu, Wang [231] used droplet generators to encapsulate pancreatic endocrine cells and culture them into functional islet organoids, demonstrating a robust and scalable method of stem cell organoid generation. Chan, Zhang [232] encapsulate MSCs in alginate-arginine-glycine-aspartic acid (-RGD) to generate MSCs spheroids. The main advantage of using this material is that after culturing the MSCs in a niche-like microenvironment, the -RGD shell of the generated spheroids can be dissolved within a short time, exposing the MSC spheroids for downstream application. Besides the benefits of encapsulating cells for better cell culture, encapsulation of stem cells is also a safe and effective method to deliver stem cells to injury site as a regenerative therapy, since delivering cells alone without encapsulation results in cell loss and cell death after engraftment [223, 230]. Therefore, researchers have showcased using droplet generators to encapsulate different stem cells such as cardiomyocytes [230], MSCs [222, 228], endoderm Stem cells [229], etc to treat different conditions in animal models. Zhao, Liu [223] encapsulated bone marrow MSCs in hydrogel with growth factors to differentiate the cells after engraftment, which showed significant promotion of osteogenesis of stem cells (Fig. 1.7D). Kankala, Zhao [238] developed porous microcarriers, which allow better nutrients and oxygen delivery for mouse myoblast cells (C2C12 cell line) delivery and culture and the results showed facilitated cell growth and differentiation. These results showed that droplet generators can potentially be used to produce microcarriers for large-scale culture, but also has the potential to be applied in the formulating and filling process, to make encapsulated stem cells for better delivery of therapy. Moreover, growth factors can be encapsulated into the microspheres and released slowly [223], which can improve the outcome of stem cell therapy. It is worth mentioning that Alessandri, Feyeux [237] fabricated the whole droplet generator device by 3D printing technology. 3D printing allows fabrication of complicated microfluidic structures with low-cost, fast turnover rate and simpler post-fabrication treatment. As the printing resolution of printers advances these days, 3D printing can be one of the future main technologies to rapid prototype and manufacture microfluidic devices.

Other types of microcarriers can be produced to achieve different aims. Fibres-like carriers is one other type of cell carrier that attracted great interest. Encapsulating or growing cells on

long fibres is efficient to produce large cell mass with good homogeneity. Cell spheroids limit the nutrient supply to the cells in the core of the sphere, while fibres encapsulated cells have a constant diameter and can therefore supply nutrients evenly[235]. Fibre-like structure is also suitable for mimicking a different microenvironment compared to microcarriers (Fig. 1.7E). For cells with extending morphology like neural stem cells, better morphology, and cell-cell interaction [233] were reported with microfibres culture (Fig. 1.7F).

The promising potential of droplet generators in microcarriers has attracted a lot of attention in the stem cell industry. CellFiber Ltd have already started using droplet generators to produce microcarriers and microfibres for cell culture purposes. Currently, harvesting cells and cellular products from microcarriers is still a major challenge in the stem cell bioprocessing industry. Droplet generators show a promising future of producing mono-size, xeno-free and cell type-specific microcarriers. It is also critical to provide dissolvable and edible solutions for the stem cells industry, to reduce potential microplastic residues in the final product and to meet the food and therapeutic goods standard. Moreover, more and more papers and products are showing higher cell expansion rate, better treatment outcome of implantation by having porous structure in the microcarriers [239]. This has also been made feasible by microfluidic devices [240]. Industrial scale production of microcarriers with droplet generators are still under research. The current mL/min scale is far beyond enough for industrial need. However, paralleling multiple microfluidic devices or setting up multiple microfluidic devices for microcarriers production is feasible due to the low production cost.

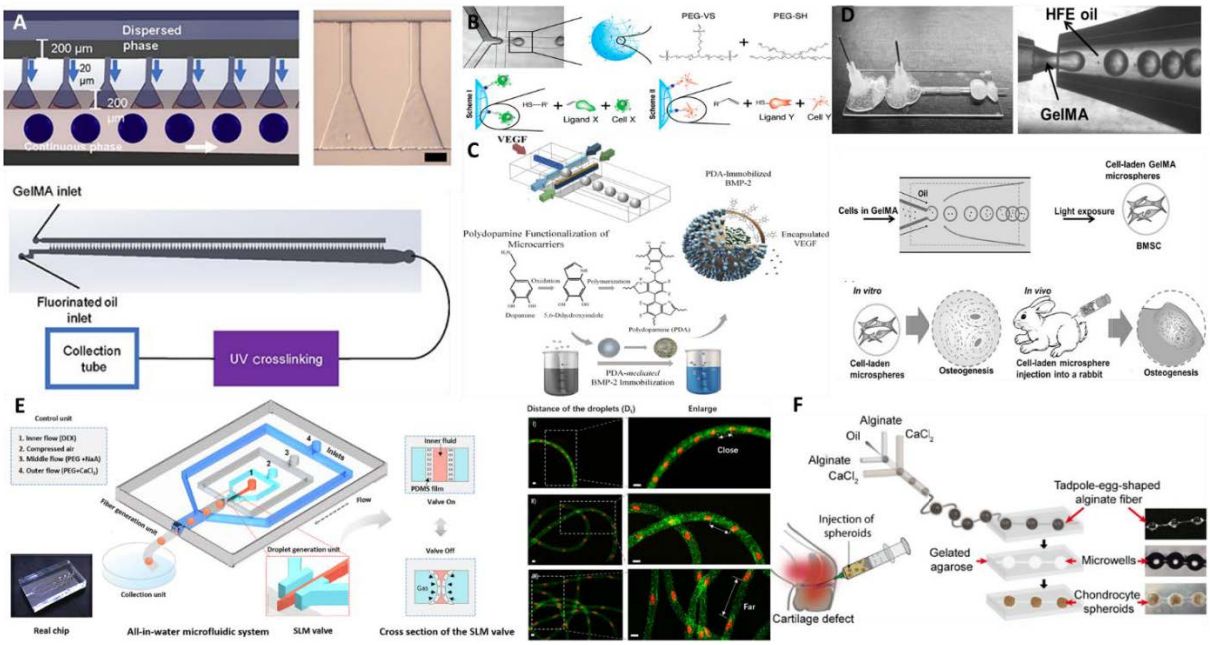

Fig. 1.7. Scaled-up droplet-based technologies used for microcarriers production/cell encapsulation. A) A step-emulsification droplet generator used for large-scale production of gelatine microcarriers. Reproduced with permission [11]. Copyright 2021, Oxford University Press. Droplet generator platforms can be customised to add different surface ligands B) or growth factors C) in the microcarriers to promote attachment, proliferation and differentiation of different cell tyeps. Reproduce with permission [226]. Copyright 2013, American Chemical Society. Creative Commons CC-BY license [227]. Copyright 2020, the Authors, published by Springer Nature. D) Encapsulated cells for cell therapies increase the cell retention rate and improve the therapeutic outcome. Reproduced with permission [223]. Copyright 2016, John Wiley and Sons. E) Cells-ladened microfibres provide different microenvironment compared to microcarriers. Reproduced with permission [234]. Copyright 2021, American Chemical Society. F) Tadpole-Egg-shaped microspheres generated by droplet generators for therapeutic purpose. Reproduced with permission [236]. Copyright 2019, American Chemical Society.

Table 1.6. Droplet-based microfluidic devices for microcarriers production

TYPE	MATERIAL	TYPE	CELLS	MATERIAL THROUGHPUT	PURPOSE
Microcarriers	GelMA	Step emulsification	hMSCs	5-30 mL/h [241]	Large-scale, low-cost microcarriers production for stem cells expansion [11]
	Gelatine crosslinked with genipin	Flow focusing	hMSCs	2.5uL/min	Dissolvable microcarriers for stem cells expansion [224]
	PEG	Flow focusing	ESCs	4 uL/min	Produce microcarriers with appropriate ECM that can direct stem cell differentiation [226]
	PLGA	Co flow	MSCs	5 uL/min	Growth factors integrated microcarriers for differentiation of stem cells [227]
	Gelatine crosslinked with PEG	Cross flow	hMSCs (bone)	NA	Injectable encapsulated cells to promote articular cartilage tissue regeneration [228]
	Alginate Calcium	Cross flow	hMSCs (dental)	200 uL/h	Injectable encapsulated cells to promote articular cartilage tissue regeneration [222]
	Alginate Calcium	Flow focusing	hMSCs	13 uL/min	Control the microenvironment of hMSCs and induce differentiation for research [232]
	Alginate Calcium	Co flow	hNSCs, dental MSCs	N.A.	Study stem cell behaviours in a 3D manner [242]
	GelMA	Co-flow with electrostatic field	hMSCs (bone)	100-2000 uL/h	Injectable encapsulated cells for osteogenic tissue construct [223]
Encapsulation	Alginate calcium	Co-flow with electrostatic field (?)	hEndoderm stem cells	NA	Proliferate and differentiate somatic cells from stem cells for transplantation [229]
	PEG-based hydrogel	Co-flow	hiPSCs with NHCF-V cells	NA	Make stem cell organoids for potential tissue regeneration purposes [231]
	PEG, Dextran	Flow focusing and co-flow	hiPSCs	0.1-0.4 ul/min	Produce biocompatible porous microcarriers for better nutrients supply of cells and transplantation [238]

Fibres	PLGA	Co flow	C2C12	N.A.	Encapsulate neural cells in hydrogels to produce 3D stem cell niches [237]
	Alginate Calcium	Co-flow	hNSCs	20 mL/h	Provide new encapsulation methods and scaffold structures for improved tissue engineering outcomes [243]
	GelMA	Cross flow	C2C12, hMSCs	50 uL/min	Build encapsulated stem cell fibres for reconstructing neural fibres in vivo [233]
	GelMA	Co-flow	MSCs		Encapsulate MSCs with pancreatic cells to provide a immune-suppressive, favourable environment for pancreatic cells survival and function [244].
	Collagen	Cross flow	Pig ADSCs	0.2 mL/h	Encapsulate MSCs for clinical treatment. Cells went through multiple clinical handling process and the cells maintained their potential for therapy [245].
	Dextran, Alginate Calcium	Flow focusing and co-flow	Pancreatic endocrine progenitor cells	2 uL/min, 40uL/min	A potential source of small-diameter vascular grafts [235]
	Alginate Calcium	Co-flow	mMSCs	5-40 uL/min	Make stem cell organoids for potential tissue regeneration purposes [231]
	Alginate Calcium	Co-flow	hMSCs	4-10 mL/h	Produce biocompatible porous microcarriers for better nutrients supply of cells and transplantation [238]

1.4.5. Integrated and other microfluidic devices

In addition to the above-described technologies, there are some other microfluidic devices used in less-explored fields or made for specific applications, yet they showed outstanding performance in their purpose or have great potential in the future and are therefore worth mentioning. For example, by miniaturising the culture chamber of cells, the delivery of pluripotent mRNA into the cells to transfer somatic cells into iPSCs [246, 247]. Taking one step forward, Singh, Suri [248] used a straight microfluidic channel to reprogram iPSCs and flush the channel with slow fluid flow to wash away the un-reprogrammed cells. These technologies use only a simple micrometre level channel with cells culturing inside. However, compared to the traditional methods of using large culture vessels like T-25 flasks or petri dishes, these microfluidic chambers used much less reagents and time (12 days compared to 28 days of traditional method) to convert somatic cells into iPSCs, with a higher efficiency [246, 247]. In recent years, the benefits of using microfluidic devices to differentiate and reprogramme iPSCs have been demonstrated across multiple studies [249]. The precise control of microenvironment, ease of manipulation and tracking the conditions of cells maximised the outcome of current protocols and provided chances to develop more efficient protocols around these new advanced system [249]. Another example of using microfluidic miniaturisation is the image cytometer developed by Kamei, Ohashi [250]. The image cytometer consists of image analysis technology with arrays of straight microfluidic channels. It was used to quantitatively monitor the characteristics of ESCs in different conditions. This array is straightforward to make with low-cost, yet the analysis capacity is much higher compared to a flow cytometer. Lyu, Chen [251] used a microfluidic gradient generator to feed different concentrations of growth factors into the BMSCs and transplant the differentiated cells into mouse models to observe the regenerative outcome. Similar to organ-on-a-chip devices, gradient generators can be helpful in drug testing, personalised medicine and the cell line development process.

Another common type of microfluidic device used in the chemical and cosmetic industries but is yet to be applied in the stem cell industry is the micromixer. Micromixers are a type of microfluidic device that allows complete mixing of different solutions in a short time. It can also be used in stem cell research by mixing stem cells with immunomagnetic beads for cell type selection. Tan, Suzuki [252] used a 3D micromixer to incubate cells and antibody-coated microbeads to isolate MSCs from a mixture of MSCs and epithelial cells. The high mixing

efficiency of micromixers and small channels allow better interaction between cells and microparticles and therefore increase the chance of binding.

In the active and passive microfluidic sections, we discussed integrated active or passive microfluidic devices for higher throughput and separation of particles of different sizes. Integrating different types of microfluidic devices in the same system assembles a multifunctional platform for more complex and diverse real case applications. Wu, Hsu [253] developed an integrated microfluidic system with a laser detector, micromixers, and magnetic sorting device to identify and separate HSCs from mimicked mixed blood cells. With the combination of different technologies, the stem cells can be potentially purified from the original sample within this one palm-size device. Kane, Moreno [254] built a micro-culture chamber array to accommodate NSCs and used an automatic control system to monitor the growth conditions of the cells inside to grow and differentiate them into dopaminergic neurons for Parkinson's disease treatment. Due to the high-resolution manipulation features, active microfluidics is very popular in the integrated microfluidics field (Fig. 1.8A). This paralleling and automated system has also demonstrated the potential large-scale application in the industry. Sun, Teng [255] combined droplet-based cell sorter with electrode droplet fusing and sorting systems to culture, mix, analyse and sort the HepaRG hepatocyte progenitor cells. They mixed the cells with a toxicity assay kit to demonstrate the HepaRG cell's functionality was affected by treatment with the kit and detected by on-chip ELISA, showing the strong capability of the device as a chemical sensor (Fig. 1.8B). Sakuma, Nakahara [256] combined two piezoelectric actuators with a sheath-flow including straight channel to read Young's modulus of MSCs spheroids and sort the spheroids with different mechanical characteristics. Integrating active microfluidics with droplet-based microfluidics provides precise single cell manipulation and properties measurement. Fan, Chen [257] combined active microfluidics, droplet generator and CTA to build a microfluidic system for single cell trapping and electrical properties measurement (Fig. 1.8C). Using CTA combined with an electrical field, Valero, Post [258] developed a microfluidic system for single cell electroporation, introducing a DNA vector for gene modification. This method allows higher efficiency cell transfection (>75%) than traditional bulk methods (1-11% [259]), and it can be potentially used to transfect cells in a larger size for cell therapy in the industry.

Overall, compared to traditional bulk methods, microfluidic devices provide a miniaturised platform to manipulate liquid with lower cost, lower consumption, less labour needed, and better outcomes. Integrating multiple microfluidic devices in one system can perform multiple

functions or reinforce the advantages of the microfluidic devices [89]. All these characteristics can be of great use in the stem cell industry. The stem cell industry requires a closed-up production line for stem cell products. Therefore, integrating individual microfluidic devices into a closed microfluidic system would be recommended. For example, an integrated straight microchannel with sheath flow and spiral channel system can be used to wash and concentrate the cells in one system. Connecting a DEP array after hydrophoresis microfluidic device will enable for high throughput (3 μL/min compared to DEP or hydrophoresis alone), and high purity isolation of stem cells [260] from the tissue origin (Fig. 1.8D).

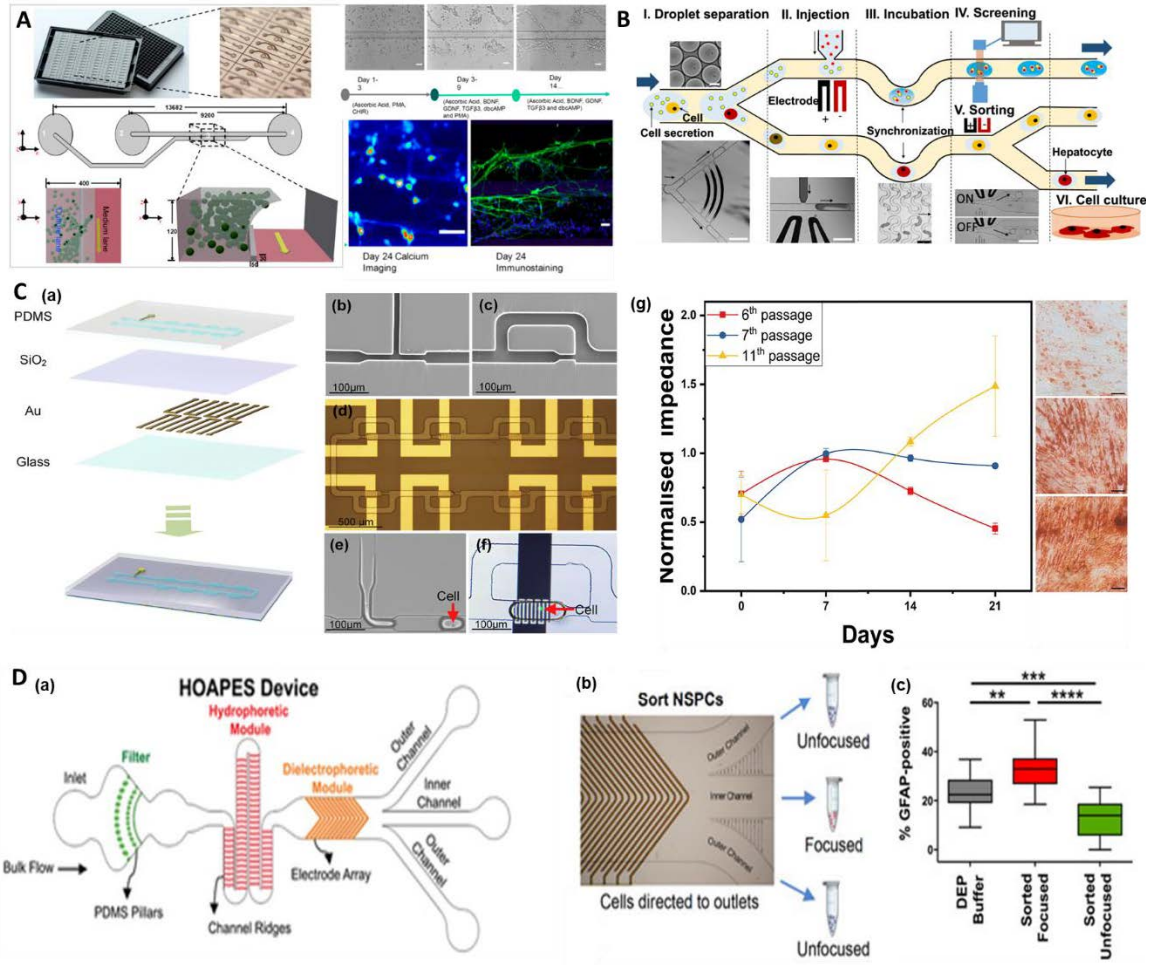

Fig. 1.8. Microfluidic devices that are hard to categorised and integrated microfluidic devices used for stem cell research. A) Computer controlled microfluidic array (left) for automated NSCs culture and cell fate modification. The cells cultured at day 1, 4, 7 after seeding, firing event recorded by calcium imaging and immunofluorescent staining are showed on the right. Creative Commons CC-BY license [254]. Copyright 2019, the Authors, published by Springer Nature. B) A droplet generator coupled with chemical sensor to analyse the secreted product while retrieving the cells for cell line establishment. Reproduce with permission [255]. Copyright 2020, American Chemical Society. C) A droplet generator, a static droplet array combined with electrical field to perform single cell culture overtime and track the relationship between membrane voltage and differentiation potential. (b)-(d) the droplet generator, SDA unit and circuits below the SDA. (e) the droplet generation process and (f) the cell-containing droplet in SDA. The right figure shows the osteogenic differentiation of cells and impedance

measured overtime. 6^{th}, 7^{th} and 11^{th} passage cells with Alizarin Red staining (Osteogenic cells staining) are showed on the top, middle and bottom right figure. Reproduce with permission [257]. Copyright 2019, Elsevier. D) (a and b) a DEP array + hydrophoresis microfluidic device to improve the throughput of device and (c) purity of isolated NSCs. Reproduced with permission [260]. Copyright 2019, AIP Publishing

Table 1.7. Other microfluidics and integrated microfluidic devices

TECHNOLOGIES	CELLS	PURPOSES
Straight channel as mini bioreactor [246, 247]	iPSCs	Use microfluidic channels to generate iPSCs.
Straight channel as mini-bioreactor [248]	iPSCs and ESCs	Use microfluidic channels to select iPSCs and ESCs based on the adhesive properties.
Gradient generator [251]	MSCs	Find out the appropriate concentration to induce stem cells differentiation for transplantations
Microchannel + image analysis [250]	ESCs	Use microfluidic channels to isolate characterise the ESCs in different chemical environments.
3d micromixers[252]	hMSCs	Increase the chance of immune-affinity binding of cells and antibody-coated microbeads.
Microfilter [261]	HSCs	Use microfilter to perform size-based purification of stem cells.
Integrated microfluidic devices		
Micromixer + magnetic sorter [253]	HSCs	Integrated microfluidic system for purification of specific cell types
Organ-on-a-chip microarrays [254]	NSCs	Automatic controlled cell culture and differentiation system
Droplet generator + active microfluidics [255]	HepaRG	Use a droplet-based sorter as a chemical sensor to detect chemical secretion level after treating the cells with toxicity assay kits.
Active microfluidics + inertial microfluidics [256]	MSCs	On-chip spheroids sorting and measurement of Young's modulus
Active microfluidics + cta [257]	MSCs	Measurement of single cell electrical properties for differentiation potential study
Active microfluidics + cta [258]	MSCs	Single cell genetic modification
Active microfluidics + passive microfluidics [260]	NSCs	high throughput, high purity isolation of stem cells

1.5. Hypothesis

Over the past three decades, the mass manufacturing of adherent cells has remained stagnant due to technological limitations. This has led to several problems, including labour-intensive processes, high risk of contamination, cell loss during operations, expensive and hard-to-access equipment and material, lack of standard production procedures, and high requirements for speciality. As a result, the products obtained from these processes often have batch-to-batch differences, leading to inconsistent therapeutic outcomes and unaffordable costs for patients. Microfluidic technology offers precise, customised, scalable and low-cost solutions for liquid handling. These advantages provide the potential possibility to integrate into the current industrial stem cell production process to reduce the cost, risk of contamination, and specialists needed and increase the safety and stability of products.

1.6. Aims

In this thesis, the aim was to employ various microfluidic devices to overcome existing challenges during the manufacturing process of mesenchymal stem cells (MSCs), and muscle stem cells (myoblast) including producing dissolvable microcarriers for large-scale stem cell culture, developing an integrated microfluidic system for harvesting and concentrating cells from microcarriers-bioreactor culture, mixing cells and cryoprotectant in a homogenous and continuous manner, and monitoring culture condition and quality control in bioreactor at single-cell level. The use of microfluidic devices can improve the automaticity, reduce labour interference, cost of devices and chance of contamination of the production processes.

Aim 1: Create a high-throughput microfluidic droplet generator capable of producing edible microcarriers for use in the cultivated meat and stem cell therapeutic industries. With an additional 20 billion people projected to be born on Earth by 2050, the current farming industry will soon be unable to meet the growing demand for protein, having already reached maximum capacity and consuming 38.5% of habitable land and 8% of total water consumption. Cultivated meat, an alternative protein source produced through lab-grown meat technology, has been suggested as a viable alternative, but high production costs, including microcarriers cost, have so far prevented its widespread adoption. There is currently no market for microcarriers designed specifically for cultivated meat. The muscle stem cells grown on these microcarriers often have low

harvesting efficiency and there is a potential risk of microplastic contamination in the final product. To address this issue, this study will utilise a microfluidic droplet generator to produce edible microcarriers using off-the-shelf food ingredients, which can also be applied to the therapeutic stem cell industry.

Objectives:

- Design a new high throughput droplet generator CAD model.
- Optimise the production flow rate and process with different droplet sizes.
- Develop the crosslinking protocol for generated microcarriers.
- Culture muscle stem cells C2C12 on the microcarriers compared with commercial microcarriers.
- Validate the growth rate, proliferation, and differentiation potential of C2C12 cells on the microcarriers.

Aim 2: Develop an integrated microfluidic device to harvest the MSCs from microcarriers with less labour cost, shorter time, lower contamination risk and cell loss. Harvesting cells from microcarriers is one of the major limiting factors of microcarriers application in the stem cell industry. Microfluidic devices have been demonstrated as one of the potential candidates to address this challenge, but there is no integration system of microfluidic device designed for simple adaptation in the industry. Here 3D printing technology was applied to perform rapid prototyping of an integrated microfluidic system for cell harvesting. The system can be easily integrated into any current industrial system with two peristaltic pumps and three tubes. It performs cell detachments from microcarriers, separation from microcarriers and cell concentration in one gadget.

Objectives:

- Use 3D printing technologies to fabricate micromixers and inertial microfluidic devices that can be used to process.
- Test the micromixers and inertial microfluidic devices with microcarriers and microbeads to mimic cell and microcarriers' movement.
- Combine the whole setup and optimise the working conditions with microcarriers and microbeads.
- Validate the system with mesenchymal stem cells attached to microcarriers.
- Characterise the cells harvested by the system, quantify their stem cell properties, and compare them to membrane-based technologies harvested cells.

Aim 3: Reduce the batch-to-batch difference in the products and lower the cost of cryopreservation by using a micromixer in the cell-cryoprotectant mixing process instead of manual handling or a robotic arm platform.

Cryopreservation is the final step of stem cell production before the cryostorage of the product. Conventional methods of adding cryoprotecting agents (CPA) into the cells can be manual or use robotic arms to further store the solution in liquid nitrogen at the operator's disposal. However, a challenging issue with these methods at industrial-scale production is the inappropriate mixing method of cells and CPA, leading to damage of cells, intermittent feeding, the batch-to-batch difference in products, and occasionally cross-contamination. Therefore, this chapter proposed an alternative way to overcome the abovementioned challenges: a highly efficient micromixer for low-cost, continuous, labour-free, and automated mixing stem cells with CPA solutions.

Objectives:

- To design a novel micromixer CAD file with high mixing efficiency.
- Perform simulation to simulate and predict the mixing efficiency and pressure at a flow rate in the micromixer.
- Validate the mixing efficiency with food dye and cells with membrane-based staining.
- Mix mesenchymal stem cells with cryoprotectant, cryopreserve the cells and compare the cell properties after thawing with manual mixing control.

Aim 4: Use a static droplet microfluidic device to assess the metabolomic profile of a single muscle cell in bioreactor culture and use it to build a model for predicting bioreactor conditions on a large scale.

Monitoring bioreactors is an essential process in stem cell production. The current industry relies on bulk measurements of pH to assess proliferation and nutrient consumption in the bioreactor, and based on this, to provide a model of the bioreactor status. However, this bulk measurement is inaccurate since it reacts slowly and measures the pH of the entire bioreactor rather than local changes in pH. Therefore, the models are imprecise. Our goal is to develop a bioreactor cell culture model for the cultivated meat industry using single-cell metabolomic data acquired by measuring single-cell pH secretion with a static droplet microfluidic device. Since the metabolomic data is measured locally at a single-cell level, the model can predict the culture condition more accurately.

Objectives:

- To design a simple-to-operate static droplet microfluidic device with the potential to operate labour-free.
- Measure single Muscle stem cell lactate secretion level with the microfluidic droplet device and fluorescent pH dye as an indicator of lactate secretion. Compare the single cells lactate secretion level across different culture periods.
- Build a prediction model with this single cell secretion profile and compare it with current industrial models.

2. Chapter 2- Scalable microfluidic-based production of edible microcarriers for cultivated meat industry (Aim 1)

Cultivated meat has recently emerged as a promising alternative protein source. However, its availability is hindered by the high cost of cell expansion and the use of non-edible materials in the production process. Microcarriers are currently the only option for low-cost, large-scale adherent cell culture. Traditional microcarrier production methods rely on random emulsification, which yields microcarriers of varying sizes and requires filtration, leading to significant product waste. Additionally, the non-edible and non-dissolvable materials used in current microcarriers limit their applicability in the cultivated meat industry and pose a significant challenge to stem cell therapy. To address these issues, we developed a high-throughput microfluidic device that produces mono-size, edible, and dissolvable microcarriers. Our fully dissolvable microcarriers demonstrated superior cell attachment compared to commercial microcarriers and resulted in a 30-fold increase in cell number. This innovative approach represents a significant step forward in the development of sustainable and scalable cell-based meat production systems.

2.1. Introduction

With the global population on the rise, there is an increasing demand for food production that is putting a significant strain on limited farmland. The projected increase in population to 10 billion [262] could see the average animal protein supply per person drop to just 22g/day, a stark contrast to the current average of over 100g/day [263]. Animal farming is already operating at maximum capacity, consuming 38.5% of habitable land [264] and 8% of human water while emitting 18% of the greenhouse gasses [265]. In light of these challenges, there is an urgent need for alternative protein sources.

One such alternative is cultivated meat, which can be produced by growing muscle cells in large-scale bioreactors. This method of meat production requires significantly less environmental footprint and human labor compared to traditional animal farming. Typical cultivated meat bioprocessing includes four steps: isolation of muscle stem cells (MuSCs) from tissue biopsy sample, expansion of MuSCs in a large-scale bioreactor, differentiation of MuSCs into mature muscle cells, and lastly, assembly of muscle cells with other cell types into scaffold as the final product [4, 19, 29]. This technology simplifies the meat production process, shortens the production period, and reduces the environmental footprint and labour cost. However, cultivated meat technologies are not ready to reach the market yet. There are a couple of significant limitations, including the high cost and lack of proper edible microcarriers in the field.

Microcarrier is a micrometre-level matrix that supports adherent cell growth in large-scale culture. Compared to the planar flask, the large surface area to volume ratio and capability of culture cells in the Z dimension makes them an ideal candidate for large-scale cell production [4]. Producing microcarriers on a large-scale hugely relies on emulsification technologies. With the very well optimised conditions in the industry, the microcarriers produced still have huge size variations. This causes cell clumping during culture and therefore need to be filtered before use which results in huge waste of culture [266]. The current non-edible microcarriers options have a potential risk of having non-edible materials, such as leach and broken parts of microcarriers left in the final product [267]. This is one of the major concerns of microcarrier application in recent years since microplastic is getting more and more attention publicly. The current

microcarriers also lead to a huge cell loss during production, due to the incompetent enzymatic treatment or clogging and loss during the filtration process [4]. This cell loss can be more than 50% [268, 269], depending on the cell types and microcarriers used. Meanwhile at the large-scale, the recovery rate of cells from microcarriers has batch-to-batch variations [266]. A new technology called microfluidic droplet generator has been recently used to generate microcarriers in large scale with small size variations [11, 224] to address this challenge. The customisable droplets and channel designs also enable high throughput production and the incorporation of additional features such as adding slow-release growth factors [227] or customised cell type-specific ligands [226].

Microfluidic technologies have opened new avenues to produce microcarriers. Despite this, there are currently no commercially available microcarriers specifically designed for cultivated meat [4]. Although they are used to produce dissolvable microcarriers for therapeutic purposes, the materials and methods can be optimised to produce edible microcarriers for the cultivated meat industry. In this paper, we used a scaled-up microfluidic device to make gelatine-based edible microcarrier for MuSCs expansion. Gelatine-based microcarriers were generated under 45 ℃, crosslinked with glutaraldehyde and blocked with glycine. C2C12 mouse myoblasts were cultured on our microcarriers, directly compared with commercial microcarriers Cytodex3. Our microcarriers showed comparable attachment and growth rates to the commercial microcarriers but outstanding harvesting rates due to the material used. The microcarriers and technology we developed in this work have the potential to accelerate the translation of cultivated meat to the market by solving the scalability, cost-effectiveness, and toxicity issues.

In this paper, we used a scaled-up microfluidic device to make gelatine-based edible microcarrier for MuSCs expansion. Gelatine-based microcarriers were generated under 45 ℃, crosslinked with glutaraldehyde and blocked with glycine. C2C12 mouse myoblasts were cultured on our microcarriers, directly compared with commercial microcarriers Cytodex3. Our microcarriers showed comparable attachment and growth rates to the commercial microcarriers but outstanding harvesting rates due to the material used. The microcarriers and technology we developed in this work have the potential to accelerate the translation of cultivated meat to the market by solving the scalability, cost-effectiveness, and toxicity issues.

2.2. Materials and methods

2.2.1. Microfluidic droplet generator design and fabrication

The microfluidic droplet generators are designed and fabricated as previously described [206, 270]. Briefly, a mould of the device was designed in Solidworks and printed in MiiCraft Ultra 50 (MiiCraft, Taiwan) resin printer, with 50 μm slicing and 1.2 seconds curing time. Then the print was taken out, washed with Isopropyl Alcohol (IPA) three times, and dried with an air nozzle. The mould was further cured by a UV light box and soaked in IPA for 4 hours to further clear the remaining resin on the surface. Lastly, the surface of the mould was plasma treated for 2 minutes before salinisation to create a non-attaching surface for easier peeling of Polydimethylsiloxane (PDMS).

2.2.2. Experimental setup and microcarriers production

An OB1 microfluidic flow controller (Elve Flow, France) and compressed air source were used to inject the gelatine (Collagen X, Australia). Span 80 (Sigma Aldrich, Australia) added mineral oil (Sigma Aldrich, Australia) into the device, as shown in Fig. 2.1. To ensure the gelatine was not gelling during the experiment, the experiment was carried out under 65℃. The collected MCs were placed at 4℃ to gelate without changing the shape and merging. A large volume of cold water was added to the samples, and the microcarriers were then allowed to sediment into the water phase. The MCs were soaked in 1% Glutaraldehyde (GTA) for 30 minutes and repeatedly washed with DPBS (Gibco, Australia). To prevent excessive GTA from affecting cells, Glycine (Sigma Aldrich, Australia) is used to block GTA by soaking microcarriers in 0.025 mg/mL glycine solution overnight. Before using for cell culture, the MCs were washed with 70% ethanol once and DPBS twice.

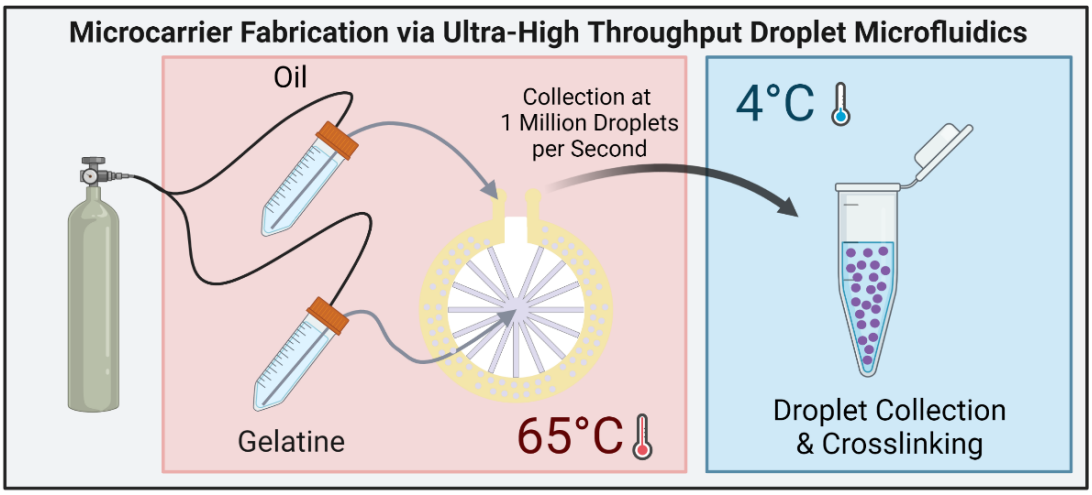

Fig. 2.1 The experimental setup of this work. The droplet generation process happens in a 65 ℃ oven to keep gelatine in a liquid state with consistent viscosity. Then the MCs were immediately put in 4℃ to keep the shape and structure identical and allow the crosslinking to happen at this temperature.

2.2.3. Cell culture and seeding

C2C12 muscle myoblast cell line was kindly provided by Vow Ltd. The cells are cultured in DMEM F12 (Gibco, Australia) media supplied with 20% FBS (Gibco, Australia) and 1% Penicillin-streptomycin (Gibco, Australia). The cells were harvested when they reached 80% confluence with the TrypLE enzyme (Gibco, Australia) and seeded on the microcarriers with a ratio of roughly four cells/MC, as a standard used in research and industry. Cytodex 3 (Cytiva, USA) MCs were used as a control, and the cells were cultured with MCs for five days on a shaker at 75 rpm. Cells were seeded in 6 well plates coated with Poly(2-hydroxyethyl methacrylate) (Sigma Aldrich, Australia). The microcarriers were counted, size-measured and used at a concentration of 11 cm^2 surface area/mL media, corresponding to Cytodex 3 usage.

2.2.4. Attachment rate, viability, and expansion of cells on MCs

After cells were seeded on MCs, samples were taken after 20, 40, 60, 120, 180 minutes, 6 hours and 24 hours to count the attachment rate of cells via the following equation: $Attachment\ rate = (N_{seed} - N_{count})/N_{seed}$. Cells were harvested from the MCs after five days via adding TrypLE express (Gibco, Australia) and incubated in the incubator for 10 minutes. The viability of cells was measured by staining with a live/dead staining kit (Abcam, Australia) and run through CytoFlex S (Beckman Coulter, USA) flow cytometer. The cells were harvested after five days and counted

with a haemocytometer. The expansion ratio was calculated with the following equation $Expansion\ rate = N_{day5}/N_{seed}$.

2.2.5. Differentiation and characterisation of cell markers

To differentiate MuSCs into mature muscle cells, the cells cultured on MSCs were harvested, seeded on six-well plates at 500,000 cells/well, and cultured with DMEM-F12 supplemented with 2% horse serum. After four days, the cells were harvested and fixed with 2% GTA for 30 minutes. Then, the cells were permeabilised with 0.1% Triton-X 100 for 15 minutes, followed by blocking the cells with 5% BSA for 1 hour. Primary antibodies, including anti-myogenin, anti-myoD and anti-Myh-1 (Thermofisher, Australia), were added to the cell solutions and incubated at 4 ℃ overnight. Then, secondary antibodies were added to the cells and incubated in the dark for one hour. Between each step, the cells were washed three times with DPBS. The cells were then imaged with IX70 fluorescent microscope (Olympus, Japan), and pictures taken with different fluorescent filters were combined in Cellsens software (Olympus, Japan).

2.2.6. SEM (Scanning Electronic Microscopy) imaging of cells

The MCs, and MCs with cells attached were fixed with 2% GTA for 30 minutes and washed with DPBS 3 times. Then the MCs were soaked in 60%, 80% and 100% ethanol for 30 minutes progressively, and the samples were loaded on a stub, coated with Au/Pd at 15 nm thickness. Then the MCs were imaged with SUPRA 55 (Zeiss, Germany) SEM, with 15kV electron high tension.

2.3. Results and Discussions

2.3.1. Principle of droplet generation and characterisation of device operation

In this study, we utilized a microfluidic droplet generator based on step-emulsification to produce droplets of gelatine material. The operation of this type of droplet generator is primarily driven by Laplace pressure, Plateau–Rayleigh instability of the disperse flow [271], and gravity. In contrast to other droplet-based microfluidic devices such as flow-focusing droplet generators, which rely on continuous flow, our system operates by flowing gelatine material out of a nozzle, resulting in the formation of an enlarged

head and a narrowed neck due to Laplace pressure. Surface tension then causes the droplets to detach from the flow, a phenomenon known as Plateau–Rayleigh instability. The continuous phase, in our case the oil flow, does not play a role in droplet generation [272] but rather provides a lateral force to push away microcarriers and maintain a consistent droplet size [271].

Therefore, the oil pressure was maintained constant at 150 mbar, and gelatine pressure was changed to obtain constant sizes microcarriers (MCs). We maintained a constant oil pressure of 150 mbar and varied the gelatine flow pressure. Droplet sizes were most consistent when the pressure of gelatine was 70 mbar (Fig. 2.2A). StarPlus microcarriers showed a significant size difference compared to Our gelatine MCs while Cytodex3 MCs were similar in size to ours (Fig. 2.2B, C). The size comparison showed that although we are using a 3D printed mould to fabricate the droplet generator, which has lower precision compared to photolithography mould, the size of the MCs is still very consistent and comparable with the commercial MCs. The size variation can be further reduced by using a photolithography mould. Another reason causing size variation in our MCs is the high viscosity of gelatine material. High viscosity caused inconsistency in droplet size. Compared to another gelatine-based MC (Fig. 2.2 D), our gelatine MCs are significantly more uniform in size. The high dispersed flow pressure in the 105-150 mbar group caused inconsistency in the droplet sizes and created many nanometre sizes droplets, which made the droplet suspension cloudy (Fig. 2.2 E). The 70-150 mbar group showed excellent size consistency, but there were two different types of surface topography in the MCs, one with a smooth surface and one with a microporous surface, which can be improved by optimizing the operation conditions. Using an air pressure pump improved the consistency of droplet size. Other pressure sources, such as peristaltic pumps, caused pulsation in the system, resulting in droplet size variations. Although syringe pumps provide stable pressure, their production is limited to the size of syringes and is not continuous. Our production method allowed us to produce microcarriers for as low as 1.5 Australian dollars/million MCs (Table 2.1). Previous studies [11, 224] have demonstrated the production of dissolvable/edible MCs using Gelatine Methacryloyl and genipin as crosslinking agents, which are more expensive than ours and have smaller production scales. Although they can benefit the stem cell therapy industry, they are not suitable for the cultivated meat industry.

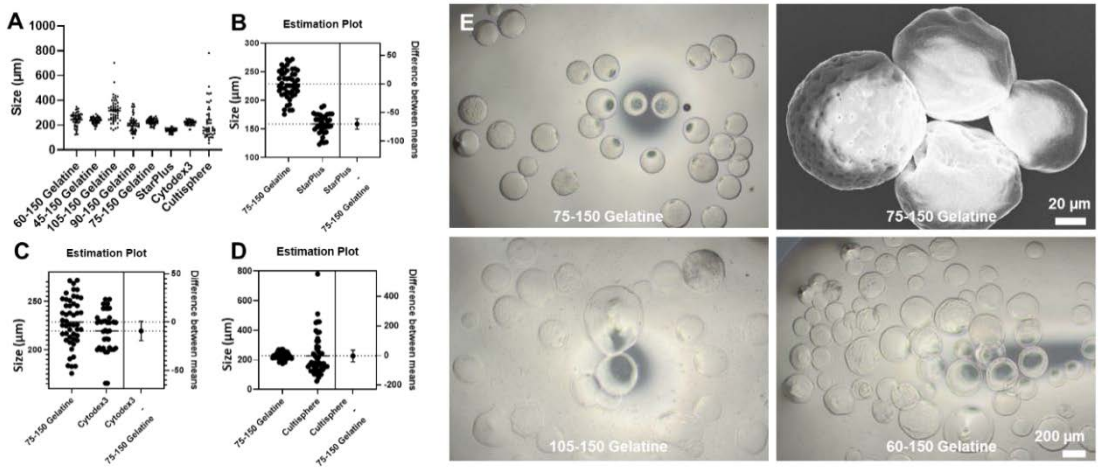

Fig. 2.2. The optimisation of the microcarriers production process. A) The effect of changing dispersed flow pressure on droplet size and comparison of our gelatine MCs and the commercial MCs. B)-D) The size comparison of gelatine MCs with commercial MCs. B) There is a significant difference between Gelatine MCs and StarPlus analysed by paired t-test, but no significant difference between Gelatine MCs and C) Cytodex3. D) Compared to another Gelatine-based MC Cultisphere, our gelatine MCs are significantly more regular. E) The MCs are generated by different pressure of the dispersed flow. 75-150 mbar pressure gives the smallest droplet size variation. The SEM images showed that gelatine MCs could be microporous.

Table 2.1. Comparing the features of gelatine MCs with the commercial MCs. Data taken from the official documents of the products.

Features	Percell Cultisphere	Corning microcarriers	Cytiva Cytodex3	Gelatine microcarriers
Cost (AUD/Million MCs)	34	76	30	1.2
Diameter (µm)	130-380	125-212	120-180	120-140
Edible materials	×	×	×	√
Dissolvability (Cell loss)	×	×	×	√

2.3.2. MCs cell culture and expansion

The microcarriers produced were used to compare with other commercial MCs, including StarPlus (SoloHill, Australia), Cyodex3 (Cytiva, USA), an startup product Unitantrix (Tantti, Taiwan), and another gelatine-based MC, Cultisphere (Cytiva, USA). Fig. 2.3A shows the 24h attachment rate of all the commercial MCs and our gelatine MCs. Cytodex3 (98.65±0.56%) has the best C2C12 attachment rate across the 24h counting period. Followed by our Gelatine MCs (96.67±0.90%), Cultisphere (93.47±2.55%), Unitantrix (94.74±3.31%) and Starplus (88.336±7.00%). Eventually,

all MCs have overall 90% attachment rate after 24h, showing a logarithmic increase in the attachment rate. Attachment rate is a critical parameter for MCs. Every cell can potentially expand 3-10 times during culture. Low attachment rate leads to slower cell expansion even under optimal culture conditions.

Then, Cytodex3 was chosen to be the control in the following experiment since it is one of the most commonly used microcarriers in research and industry, and also the best performing microcarriers that can be purchased at large scale. Fig. 2.3B showed the MTS results of C2C12 cultured on gelatine MCs and Cytodex3 MCs over 5 days. Paired t-test results (P=0.4140) showed no significant difference in the two groups, indicating a comparable growth in the two groups. Fig. 2.3C and 3D showed the expansion of cells on the MCs at different days. The morphology of C2C12 cells were similar on both MCs, indicating no phenotypic changes of cells on gelatine MCs.

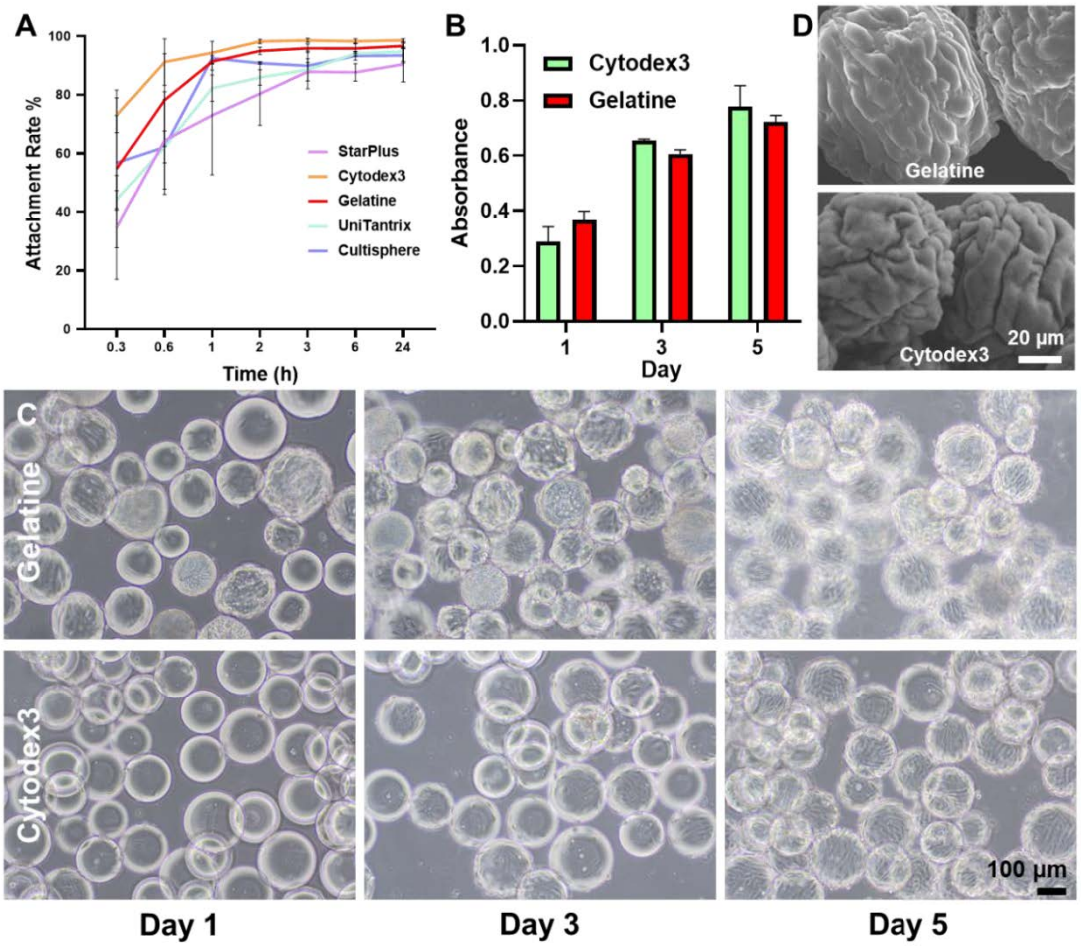

Fig. 2.3. Cells attachment efficiency and cell culture performance on our gelatine microcarriers compared to other commercial microcarriers. A) Comparison of C2C12 cell attachment with 4

different types of commercial MCs. C2C12 have best attachment rate on Cytodex3 microcarriers, followed by gelatine microcarriers. B) The MTS assay of cells growing on Gelatine MCs compared to Cytodex3. There is no significant difference between the two groups. C) Proliferation of cells on gelatine and Cytodex3 MCs overtime, show normal morphologies on both MCs and both MCs started clumping at day 5, indicating over-confluence of cells. D) SEM pictures of cells growing on both microcarriers, showing the microcarriers were fully covered, indicating a good homogeneity of microcarrier surface.

After cell expansion, TrypLE express was used to detach cells from MCs by taking out the culture media as much as possible and replace with an equal volume of enzyme and incubate at 37 ℃ shaker for 5 minutes. Three types of cells were used in this experiment: MuSCs, the main cell type in meat, fibroblast, a primary supportive cell type in meat [27, 273] and human MSCs, the main cell type used in the therapeutic industry and the adipocytes progenitor. Fig. 2.4A shows Cytodex3 MCs still had many attached cells on the surface, while Gelatine MCs had no cells left on the surface after 5-minutes incubation. Fig. 2.4B demonstrated that Gelatine MCs yielded a higher fold increase of different types of cells compared to Cytodex3. Across all different cell types, Cyodex3 has 4.67±0.13, 6.68±1.328, and 5.08±0.74 folds increase, while gelatine MCs have 5.20±0.412, 18.39±2.49, and 10.87±1.46 folds increase with MSCs, fibroblasts and MuSCs. MuSCs and fibroblasts have a higher yield compared to MSCs because MuSCs and fibroblasts can be overgrown to obtain higher cell numbers, while the secretion profile of MSCs is important. Therefore, the MSCs were harvested when they had a single confluent layer of cells to avoid cell death due to clumping. When the MuSCs were seeded at 1 cell/MC concentration, Cyodex3 yielded 21.23±3.81 folds cells, and gelatine MCs yielded 28.11±5.60 folds cells, indicating lower requirement for resources. The problem with cell detachment of Cyodex3 was probably caused by the different cell attachment strategies applied in the MCs. Cytodex3 has positive surface charges, which are favoured by the cells [4], and cells are therefore hard to be detached from them. On the other hand, Gelatine MCs are typically slightly negative. They attract the fibronectin inside the FBS [274], an important extracellular component that facilitates cell attachment, and are dissolvable by TrypLE [275]. The viability of the harvested cells was then assessed using a flow cytometer, revealing no significant difference (P=0.0853) between the two groups, as shown in Fig. 2.4C.

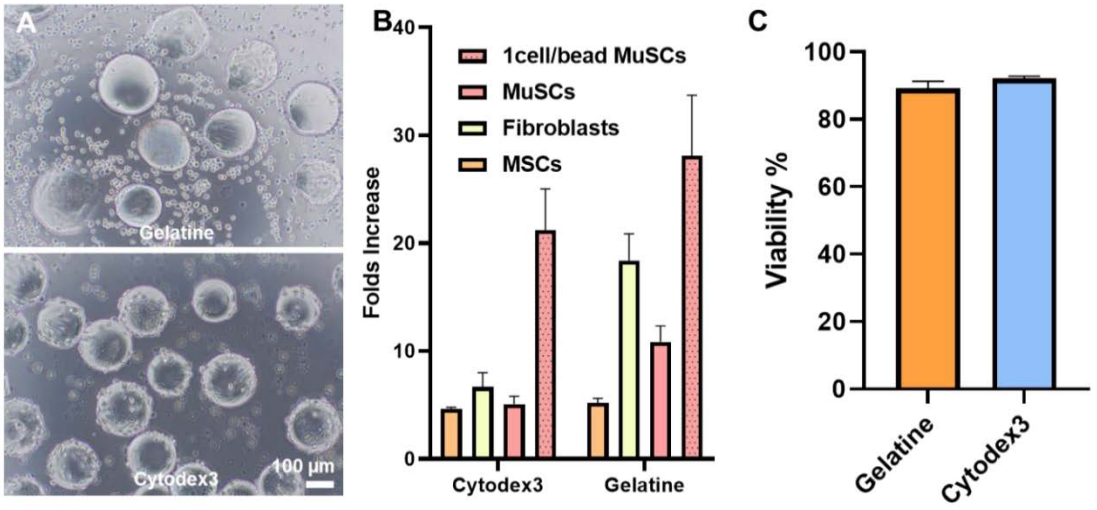

Fig. 2.4 Head-to-head comparison of microcarriers performance with the Cytodex 3 in cell harvesting performance. A) After 5 minutes enzyme treatment, many cells were attached to the Cytodex3 MCs while all cells on gelatine MCs had detached. B) The fold increase of cells harvested from gelatine MCs is significantly higher than Cytodex3. C) The viability of the cells was examined by staining with live/dead cells staining and proceeded through flow cytometer. Good viability of cells was preserved in both gelatine and Cytodex3 cell groups.

2.3.3. Cell Differentiation

In Fig. 2.5A and Fig. 2.5B, we evaluated the differentiation potential of C2C12 cells cultured on gelatine and Cytodex3 microcarriers. The myoblast differentiation potential was examined by harvesting the cells, reseeding them on well plates and staining them with myogenesis regulator MyoD. MyoD triggers myocyte differentiation and myotube formation [276, 277] indicating the preservation of differentiation capability. Fig 2.5B showed that after four days culture in differentiation media, the C2C12 cells cultured on gelatine and Cytodex 3 microcarriers expressed myocyte markers Myh-1 and formed myofibers, as observed by multi-nuclei cells with Hoechst staining. The size of the cells in Fig. 2.5A was larger than in Fig. 2.5B, and the elongated, large cell morphology was indicative of myogenesis. These results demonstrate that C2C12 cells cultured on gelatine microcarriers are capable of differentiating into myotubes.

In the field of cultivated meat, there are two approaches for processing cells after they are cultured on microcarriers: harvesting and seeding on other scaffolds or using the microcarriers themselves as edible scaffolds. Our gelatine microcarriers have the potential to be used as direct scaffolding, given their edible nature. In Fig. 2.5C, we

observed C2C12 differentiation on microcarriers, with expression of Myh-1 in both groups and high expression of myocyte fusion regulator Myogenin, which controls myofiber fusion, size, and numbers [278, 279]. The staining on both MCs overlapped and present in yellow. indicating the potential application of our gelatine microcarriers in direct scaffolding for cultivated meat. This has the potential to greatly reduce costs by eliminating the need for enzymatic treatment and filtration, cell washing, and scaffolding costs. It provides an alternative solution to address the biggest challenge in the industry: the high cost of cultivated meat production.

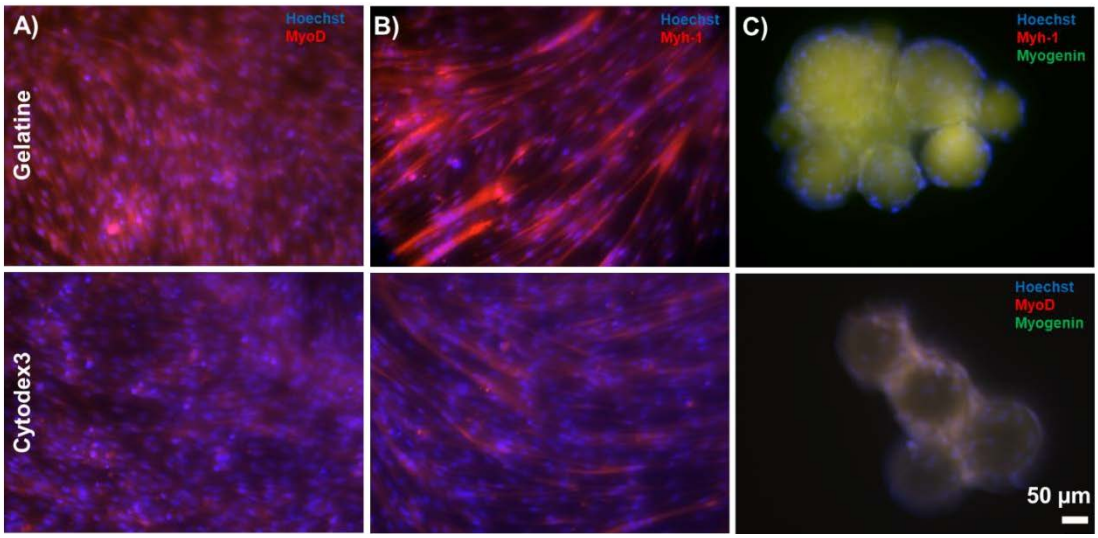

Fig. 2.5 The C2C12 cells reserve their properties during and after the microcarriers culture. A) C2C12 cells differentiated on the microcarriers, showed that the cells can be potentially used as a direct scaffold for cultivated meat industry. B) the differentiated cells after harvesting from microcarriers and reseeded on culture flask. Clear myotubes were observed in both groups and the morphology of muscle fibres were well preserved. C) the myoblast markers showed that the myoblast properties can be maintained during the culture.

2.3.4. Surface markers expression of MSCs

Surface markers expression of MSCs is an essential criterium for assessing the maintenance of MSCs properties [280]. MSCs typically express CD73, CD90 and CD105 encoded proteins on the cell membrane. Fig. 2.6 results showed that the MSCs cultured on both MCs express a high level of these three markers. CD34 is a stem cell marker typically expressed in some MSCs (depending on cell source) in vivo. However, after passaging in culture flasks to establish cell lines, CD34 turns into a negative marker [281, 282]. CD45 is a pan-haematopoietic cell marker not expressed in MSCs [283]. The MCs did not alter the expression level of these two negative markers. These

results indicate that same as Cytodex3, gelatine MCs do not change the cell properties of MSCs in culture.

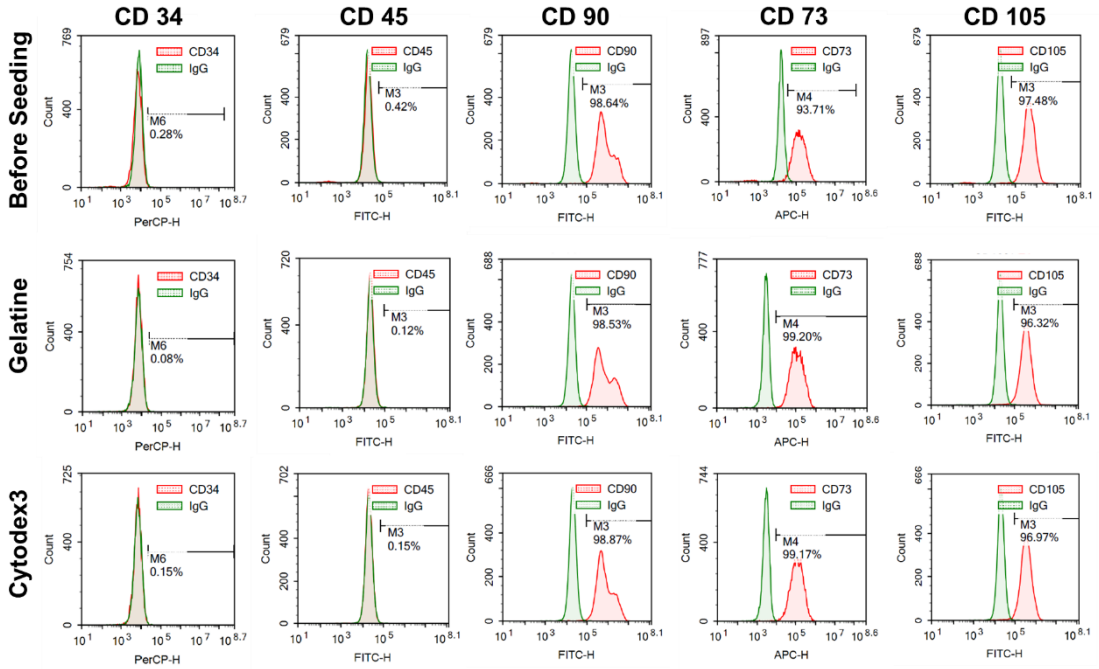

Fig. 2.6 The expression of positive and negative surface markers of MSCs on different microcarriers.

2.4. Conclusion

In this work, we presented a microfluidic device capable of continuously producing gelatine-based edible MCs at a rate of 1 million/s. The cost of production is as low as 1.2 Australian dollars/million MCs now and is expected to decrease further at a larger scale. The microcarriers showed comparable attachment to the commercial microcarriers and extraordinary growth of MuSCs, fibroblasts and MSCs. At the meantime, cell viability, differentiation potentials and cell-specific markers expression were well maintained. The dissolvability of the microcarriers significantly reduces the cost of filtration and loss of cells due to this process. C2C12 cells cultured on the gelatine microcarriers maintained the key regulator genes expression, and direct differentiation on MCs enabled them to be used directly as a scaffold as part of the end product, further reducing the cost of cultivated meat production.

3. Chapter 3: A modular 3D printed microfluidic system for continuous cell harvesting in large-scale bioprocessing (Aim 2)

Mesenchymal stem cells (MSCs) are a promising cell type for regenerative medicine, but scaling up their production for clinical use remains a major challenge in the field. Microcarrier-based culture has emerged as a leading strategy, but the associated costs and cell loss during the harvesting process are major concerns. Here, we describe an integrated microfluidic system, fabricated using 3D printing technology, that effectively detaches cells from microcarriers, separates cells from microcarriers, and concentrates cells for downstream applications. Importantly, our system preserves cell viability, gene expression, proliferation, and therapeutic properties, enabling seamless and cost-effective scaling of MSC production for clinical translation.

Author contribution statement

For the paper entitled 'A modular 3D printed microfluidic system: a potential solution for continuous cell harvesting in large-scale bioprocessing' by Ding L., Razavi Bazaz S., Asadniaye Fardjahromi M., McKinnirey F., Saputro B., Banerjee B., published in the journal of 'Bioresources and Bioengineering', Lin did major contribution to the work as first author, in particular he planned and executed the experiments, analysed and explained the results, drafted and finalised the manuscript.

Production Note:
Signature removed
prior to publication.

Sajad Razavi Bazaz

Production Note:
Signature removed
prior to publication.

Mahsa Asadniaye Fardjahromi

Production Note:
Signature removed
prior to publication.

Flyn McKinnirey

Production Note:
Signature removed
prior to publication.

Brian Saputro

Production Note:
Signature removed
prior to publication.

Balarka Banerjee

Production Note:
Signature removed
prior to publication.

Graham Vesey

Production Note:
Signature removed
prior to publication.

Majid Ebrahimi Warkiani

RESEARCH Open Access

A modular 3D printed microfluidic system: a potential solution for continuous cell harvesting in large-scale bioprocessing

Lin Ding[1†], Sajad Razavi Bazaz[1†], Mahsa Asadniaye Fardjahromi[1,2†], Flyn McKinnirey[3], Brian Saputro[3], Balarka Banerjee[3], Graham Vesey[3] and Majid Ebrahimi Warkiani[1,4*]

Abstract

Microfluidic devices have shown promising applications in the bioprocessing industry. However, the lack of modularity and high cost of testing and error limit their implementation in the industry. Advances in 3D printing technologies have facilitated the conversion of microfluidic devices from research output to applicable industrial systems. Here, for the first time, we presented a 3D printed modular microfluidic system consisting of two micromixers, one spiral microfluidic separator, and one microfluidic concentrator. We showed that this system can detach and separate mesenchymal stem cells (MSCs) from microcarriers (MCs) in a short time while maintaining the cell's viability and functionality. The system can be multiplexed and scaled up to process large volumes of the industry. Importantly, this system is a closed system with no human intervention and is promising for current good manufacturing practices.

Keywords: Microfluidics, Modular microfluidic system, Mesenchymal stem cells, 3D printing, Bioprocessing

†Lin Ding, Sajad Razavi Bazaz and Mahsa Asadniaye Fardjahromi contributed equally as first authors

*Correspondence: majid.warkiani@uts.edu.au

[1] School of Biomedical Engineering, University of Technology Sydney, Sydney, NSW 2007, Australia
Full list of author information is available at the end of the article

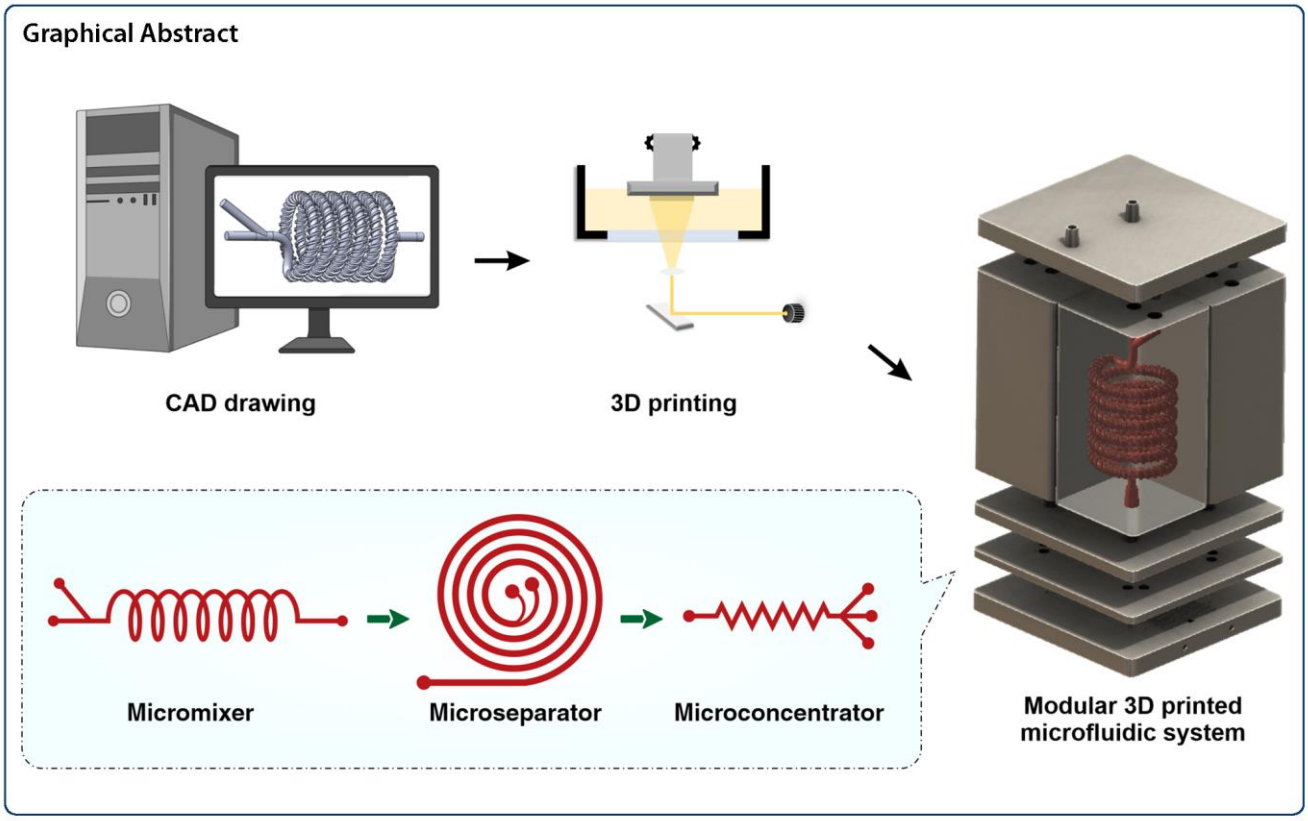

Introduction

Microfluidics, a science of precise fluid handling within the network of channels, has shown great promise in manipulating cells and particles. Microfluidics has attracted significant attention in biology and medical research due to their unique features including low price, high throughput, high customisability, and energy-efficiently compared to other technologies (Wang and Dandy 2017; Figeys and Pinto 2000). For example, micromixers have been used in chemicals synthesis and microparticle coating (Vasilescu et al. 2020). Multiple microfluidic devices, especially spiral microfluidic channels, have been demonstrated to separate or concentrate cells based on particle sizes (Xiang et al. 2019; Nivedita et al. 2017).

To date, microfluidic devices are widely used in laboratories but one of the major limitations for applying microfluidics in the industry is its customisability (Yi-Qiang et al. 2018). For instance, in the stem cell bioprocessing industry, each company has its own manufacturing protocol. The lack of standard procedure is one of the reasons for the low yield of cell products and the inconsistent clinical outcome of stem cell therapy (Jossen et al. 2018; Schnitzler et al. 2016). Although microfluidic devices have been applied in the stem cell bioprocessing industry as cell separator and concentrator in a labour-free, low-cost, and high-throughput manner (Moloudi et al. 2018, 2019), the lack of modularity and integrity makes them hard to be applied in the bioprocessing industry. Microfluidic devices are normally made from polydimethylsiloxane (PDMS) by soft lithography. Compiling these single microfluidic devices together to increase the throughput requires multiple external tubing and diverters to meet the industrial need, and testing and modifying them to meet the demand requires a huge amount of time and effort. 3D printing technology can be a good solution for this inadequacy. In recent years, the advances in 3D printing technologies have made it increasingly appealing for producing microfluidic devices (Bhattacharjee et al. 2016). The resolution of 3D printing allows direct construction of microfluidic channels with micrometre-level features, and the study and treatment of 3D printed resin enable the production of soft-lithography mould in a few hours (Vasilescu et al. 2020; Razavi Bazaz et al. 2019). Although 3D printing technologies are not the solution for large-scale manufacturing of microfluidic devices, their potential to modify changes and fabricate microfluidic devices in a few hours is unique and valuable for the industry. This feature hugely decreases the cost and time needed for rapid prototyping and building integrated microfluidic systems.

In the stem cell industry, microcarriers (MC)-based culture systems are a promising candidate for maximising cell manufacturing on a large scale. MCs facilitate massive cell expansion at a lower cost and allow control of cell culture parameters in a homogenous condition to produce consistent quality cell products at a large scale (Fardjahromi et al. 2020; Chen et al. 2020). Despite the enormous advantages of microcarrier-based technologies in maximising cell production, harvesting cells from MCs still faces challenges with high product quality and yield (Chen et al. 2013). The common method for harvesting is detaching cells with digestive enzymes and separating them from MCs using membrane-based filtration or centrifugation (Chilima et al. 2018; Tavassoli et al. 2018). Membrane-based filtration separates the cells with a physical porous filter. Clogging filters is the major limitation of this method (Schnitzler et al. 2016; Zydney 2016). In addition, membrane fouling has been shown to cause cell death, cell fate changes, and reduce the therapeutic potential of harvested cells (Chilima et al. 2018; Zydney 2016; Rodrigues et al. 2018). Centrifugation-based methods, particularly continuous flow centrifugation, are another alternative method for separating cells from MCs (Schnitzler et al. 2016). The advantage of this method is that it washes cells during separation, but the centrifugation process is time-consuming, potentially causing cell damage (Joseph et al. 2016). In addition, the continuous washing and centrifuging process cost more reagents and disposables (Serra et al. 2018). Hence, a continuous, clogging-free, highly efficient, and low-cost harvesting method is severely lacking in this area.

Herein, in this paper we report an integrated 3D printed modular microfluidic system containing two micromixers, one spiral separator, and one zig-zag concentrator. We used this system to detach and separate mesenchymal stem cells (MSCs) from MCs and eventually concentrate them in a smaller volume for downstream processing. At first, each module was characterised using cells and microbeads in different volume fractions and flow rates to obtain the optimum condition for the MSC harvesting. Then, the viability, proliferation, and therapeutic properties of MSCs harvested with our proposed integrated system were compared with the manual method, i.e., Millipore filtration. The results indicate that the developed microfluidic device is a promising candidate for automated MSCs harvesting and concentrating from MCs. In the end, we demonstrated that the system could be multiplexed to process samples with higher throughput.

Materials and methods

Device fabrications

For the fabrication of microfluidic devices using additive manufacturing, different techniques exist. Fused Deposition Modelling (FDM), Stereolithography (SLA), Digital Light Processing (DLP), two-photon polymerisation (2PP), Multijet, and wax printing are all capable of fabricating microfluidic devices. For the creation of complex microfluidic devices, however, DLP and wax printing methods show more promise in this regard. The fabrication process of these two methods is illustrated in Additional file 1: Fig. S1. The wax 3D printing method is a multi-step process, and the printed microfluidics are inherently fragile and prone to fault and error. As an alternative, DLP method has been selected for the current study because of its accuracy, precision, fast turnaround time, and the ability to fabricate robust complex microfluidic channels (Chai et al. 2021; Ding et al. 2022). Design selection consideration is introduced in detail in Additional file 1: Section S1.

The micromixers were designed in Solidworks 2018 × 64 edition (SolidWorks Corporation, USA) and fabricated with a high-resolution DLP resin printer (MiiCraft II, Hsinchu, Taiwan), with the layer thickness of 50 μm. BV-007 resin was used, which is an acrylate-based resin containing 80–95% acrylate components and 10–15% photoinitiator and additives (Razavi Bazaz et al. 2020a). After printing, the micromixers were carefully removed from the build plate, washed with isopropyl alcohol, and dried by air nozzle. This process was repeated three times to prevent uncured resin from clogging the channels. Then, the micromixers were cured by 450 nm UV light in a UV-curing chamber. The design and dimension of the micromixer are shown in Additional file 1: Fig. S2.

The spiral chip and zig-zag channel were produced as previously described (Razavi Bazaz et al. 2020a; Ding et al. 2022). Briefly, the devices were designed by SolidWorks and printed by the MiiCraft II 3D printer with a 10-μm layer thickness. Then the devices were rinsed with IPA and dried with an air nozzle three times. These devices were further post-processed by UV light in a UV-curing chamber and then bound to a PMMA sheet with a double-sided tape (ARclear®, Adhesive Research). Next, Tygon tubes (Tygon tubing, inner diameter: 0.50″, outer diameter: 0.90″) were used as connections of inlets and outlets to connect each part. Finally, the printed parts were then connected in series, as shown in Fig. 1.

Characterisation of micromixer module

The performance of the micromixer has been evaluated using numerical (described in detail in Additional file 1: Sections S2, and S3 explained the detail of mixing index calculation) and experimental results. To verify the mixing efficiency of the mixers, food dye (1 mL in 49 mL DI water) and pure DI water were loaded in 50-mL syringes and injected into the mixer with syringe pumps at

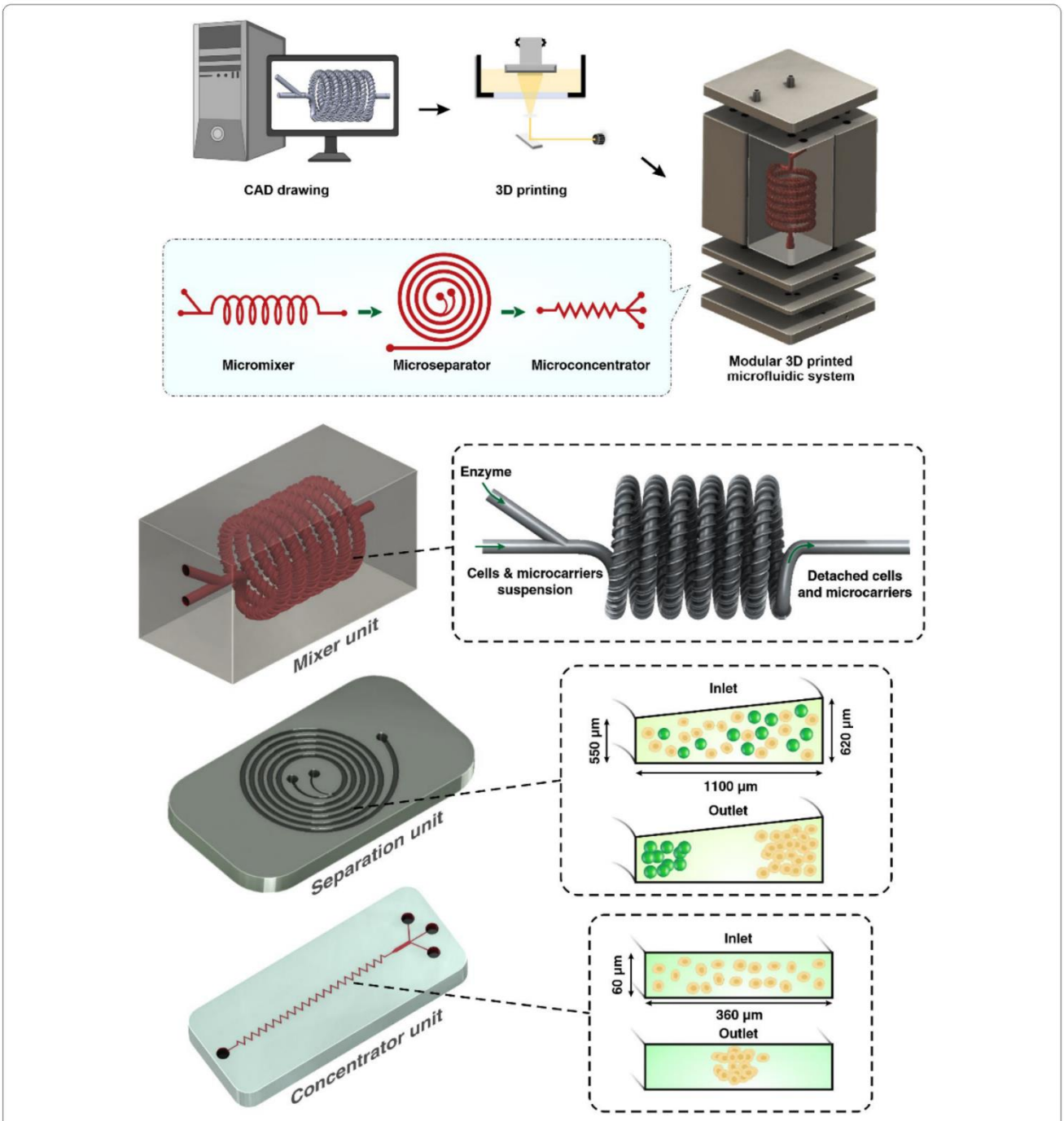

Fig. 1 Schematic representation of the modular microfluidic system. The whole system was built by 3D printing technology. The system comprises two micromixers, a micro separator, and a zig-zag channel connected vertically to detach cells from MCs, separate cells from MCs, and dewater the harvested cells. The adherent cells on MCs were detached from MCs through enzymatic treatment and gentle mechanical force inside of mixer channels. Cells and MCs were then collected separately from spiral outlets and concentrated using the zig-zag concentrator unit. The dimension of the micromixer is shown in Additional file 1: Fig. S1

different flow rates. The syringes were connected to the Tygon tubes with precision syringe tips (0. 0. 50″ Long Tip, Adhesive Dispensing Ltd, UK). The pictures of the mixed liquid before and after going through the mixing units were taken by Olympus IX73 microscope (Olympus, Japan). The pictures were then analysed, and the degree of experimental mixing efficiency in these channels was compared with numerical results obtained using

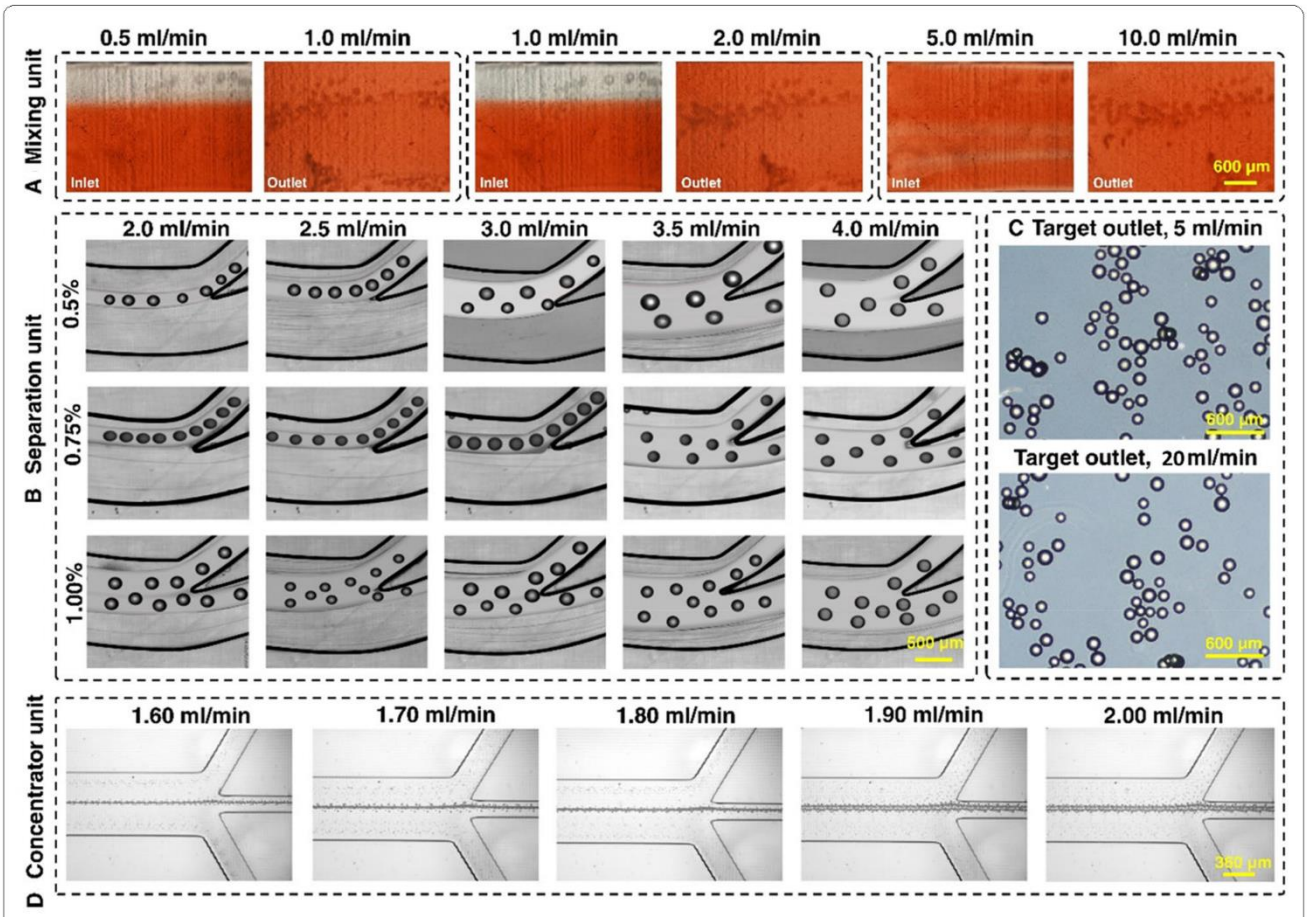

Fig. 2 Characterisation of the microfluidic harvesting system using food dye, MCs, and fluorescent microparticles. **A** The micromixer reached 95% mixing efficiency with a 1:2 fluid flow mixing ratio. **B** The spiral microfluidic device can be operated at a flow rate of 3 mL/min with 0.75% v/v% microcarrier concentration. **C** The micromixers and spiral apply gentle forces to the microcarriers, and no breakage of microcarriers happened even when the flow rate was 6 times higher than the operation flow rate. **D** The zig-zag channel focuses 15 um beads from 1.6 to 2 mL/min with a 100% recovery rate

The experimental results of the mixing index with pure water and food dye for various flow rate ratios are illustrated in Fig. 2A. The mixing efficiency of the device was higher than 95% (Additional file 1: Fig. S5) at the flow rate ratio of 1 mL/min:2 mL/min. Hence, the total flow rate of 3 mL/min was chosen as an optimised flow rate for cell harvesting. Based on the method described in Additional file 1: Section S1, the experimental mixing index is 82.7%. The discrepancy between simulation and experimental results can be attributed to the difficulties of imaging 3D printed channels with microscopy and the addition of extra noise in the picture due to the unsmooth surface of the micromixer (Rouhi et al. 2021). The micromixers have no splitting, obstacles, or sharp turning, which are appropriate for processing cells without damaging them.

Working principle of the microseparator module

The focusing position of microparticles inside a curved microfluidic channel is affected by two forces, inertial lift force (F_L) and Dean drag force (F_D) (Amini et al. 2014):

$$F_L = \rho\left(\frac{U_{max}}{D_h}\right)C_L a^4, \tag{1}$$

$$F_D = 5.4 \times 10^{-4}\pi\mu De^{1.63}a. \tag{2}$$

F_L is affected by the density of fluid ρ, the hydraulic diameter D_h (which can be calculated by $4A/P$, $A =$ channel cross-section and $P =$ perimeter of the channel), the maximum fluid velocity U_{max} which is approximated as $2 \times U_f$ (U_f is the average velocity), C_L which is a constant named dimensionless lift coefficient number and is dependent on the channel Reynolds number ($Re = \rho U_f D_h/\mu$, μ is the viscosity of the liquid) and the

diameter of particles a. F_L consists of two forces: shear-gradient and wall-induced lift force. Shear gradient lift force pushes the particles towards the wall due to the velocity difference between the middle area and the side area of the channel. When the particles move close to the wall, the wall lift force pushes the particles away. The balancing point of inertial equilibrium position contributed to the lift force is where these two forces balance each other (Razavi Bazaz et al. 2020c).

In a curved channel, the channel's curvature causes the inner wall (IW) fluid to flow faster than the outer wall (OW) due to the shorter distance travelled. This transverse fluid flow creates another force that affects the focusing position of the particles, which is the Dean drag force (F_D). F_D is defined in Eq. (2), where $De = Re\sqrt{D_h/2R}$ is the Dean number, and R is the radius of curvature; it describes the strength of F_D. According to Eqs. (1) and (2), the forces applied to the particles are proportional to the particle size ($F_L \propto a^4, F_D \propto a$). Therefore, different particle sizes have different focusing positions across the channel cross-section, and they can be collected through separate outlets (Mihandoust et al. 2020; Ozbey et al. 2019).

In a normal spiral channel, the particles inside the channel need to follow the rules of $Cr > 0.07$, where $Cr = a/D_h$ to be affected by the inertial forces inside the channel. In a scaled-up microfluidic channel, the increase in D_h results in a reduction of absolute flow velocity compared with a normal microfluidic channel. Therefore, the secondary forces applied to the microparticles were weaker, and the Cr value in the scaled-up microfluidic channel was much higher than the microfluidic channels ($Cr > 0.17$) (Moloudi et al. 2019; Carlo 2009).

Another factor that affects particle focusing is channel rigidness. There is no swelling or channel inflation in rigid channels compared to traditional PDMS chips; thus, the scaled-up device should have theoretically a lower Cr. Also, larger particles are more likely to be affected by mass and gravity since they are not neutrally buoyant (Moloudi et al. 2019), adding another variable despite flow velocity; the variable sizes of particles would also increase the difficulty in the channel design. When MCs and cells pass through the channels, focusing MCs near the IW causes the MSCs to be dispersed in the channel due to the large size difference between MCs and cells (MCs size are 150–220 μm, and MSCs are 15–20 μm). However, since large particles occupy the inner channel, the particle–particle interaction can stop some of the MSCs from going out through the inner outlet (Moloudi et al. 2018). Considering all these factors, in this study, we have designed the channel with a trapezoidal cross-section and heights of 550 μm and 620 μm, and a width of 1100 μm. This spiral chip has 6 loops and a slightly slanted enlarged inlet size to prevent clogging of MCs at the beginning of the channel (Fig. 1).

Working principle of the microconcentrator module

The zig-zag channel relies on inertial, and Dean drag forces to focus the MSCs at the centre of the channel. When Reynolds number of the channel falls in the intermediate range $1 < Re < 100$, the fluid flow is laminar, between Stokes and turbulent flow regimes. Therefore, inertial forces focus the randomly dispersed particles toward certain equilibrium positions after a sufficiently long channel length. As explained above, shear-gradient and wall-induced lift force are the main forces affecting the particle focusing in straight channels, and they both contribute to the overall inertial lift force F_L. Straight channel relies on the difference in particle sizes to focus the particles at different positions ($F_L \propto a^4$). In zig-zag channels, Dean force F_D is introduced differently compared to the spiral microfluidic channel. The interchanging channel direction creates a mismatch of fluid flow velocity in an alternating pattern and introduces Dean force, accelerating the focusing of particles inside the channel.

A zig-zag channel has three focusing modes across different flow rates. When $F_L < F_D$, the particles focus at the side of the channels. When $F_L > F_D$, the particles were focused in the middle of the channel due to due to the strong F_L. When $F_L \sim F_D$, particles are in the transition mode. For the aim of this study, MSCs need to satisfy the condition of $F_L > F_D$. One primary advantage of the zig-zag channel is its operating ranges of flow rates, i.e., it can focus particles at the centre over a wide range of flow rates. After careful evaluations, the zig-zag channel with a cross-section of 360 μm × 60 μm, 60° angle has been proposed to concentrate cells after the spiral microfluidic device. To avoid clogging of zig-zag channels caused by the remaining MCs in the target outlet, some obstacles were planted at the target outlet of the spiral to ensure no MCs could enter the zig-zag channel.

Pressure balance of microfluidic system

Combining multiple microfluidic devices in one system requires careful arrangement to balance the fluid flow and pressure change. An electronic circuit was used as an analogy for our system to understand better the fluid behaviour in the system (Additional file 1: Fig. S5). These microfluidic devices resemble the resistors that reduce the pressure input from the pumps, similar to the voltage drop in an electronic circuit (Oh et al. 2012). Keeping the flow rate and pressure stable according to the following equation is the key point of the successful operation of this system:

$$Q = \frac{\pi {R_H}^4}{8\mu}\frac{\Delta p}{L}, \quad (3)$$

where Q is the volumetric flow rate, R_H is the hydraulic resistance of the channel, μ is the viscosity, Δp is the pressure drop, and L is the channel length. In a serial circuit, Q (which is current I in the electronic circuit) remains constant in each device, thus $Q_{spiral} = Q_{mixer1} = Q_{mixer2}$. Q_{mixer1} has two inputs, one from the peristaltic pump, and one from the syringe pump. In a parallel circuit, the current of the circuit $Q_{mixer} = Q_{inlet1} + Q_{inlet2}$. The working flow rates of micromixers and zig-zag channels are more flexible, while the spiral microfluidic device only works under a specific flow rate. To achieve this flow rate, we change the flow rate of the two pumps according to $Q_{spiral} = Q_{inlet1} + Q_{inlet2}$. The outlet's resistance of the spirals affects the focusing of the MCs in the inner outlet. Therefore, the fluid pressure of the zig-zag channel must be balanced with the pressure-damping channel connecting to the inner outlet of the spiral device. This pressure-damping channel needs to have the same hydraulic resistance R_H to the zig-zag channel, which can be calculated by Eq. (4) (Oh et al. 2012):

$$R_H = \frac{8\eta L}{\pi D_h}, \quad (4)$$

where η is the viscosity and L is the finite length of the channel. Since D_h of the channel is fixed and $R_H \propto 8L$, changing the length of the pressure-damping channel to reach R3 = R4 balances the pressure of the system and would not affect the particle focusing positions in the spiral channel (Additional file 1: Fig. S6). This system potentially eliminates the debris larger than cells through spiral channel, and removes debris smaller than the cells through the zig-zag channel.

Evaluation of different modules with fluorescent microbeads and microcarriers

The maximum capacity and optimal flow rate of the spiral microfluidic device was determined by passing a different concentration of MCs through the device across a range of flow rate. As shown in Fig. 2B and Additional file 1: Fig. S6, from 2.0 to 4.0 mL/min, the focusing position of the MCs gradually shifts to the outer outlet. Noticeably, 3.0 mL/min is the critical flow rate that runs under high throughput while still focusing the MCs at the inner outlet. MCs with a concentration higher than 1% escape from the outer outlet even at a lower flow rate. However, MCs with a concentration of 0.75% can be sufficiently removed from the inner outlet at a flow rate of 3 mL/min. At the flow rate of 3 mL/min (2 mL/min from the bioreactor, 1 mL/min from the enzyme reservoir), the fluid mixing efficiency reached 95% after the first micromixer (Additional file 1: Fig. S4). The addition of the enzyme from the syringe pump inlet of the micromixer dilutes the sample.

The microcarrier concentration used for cell culture was 1.29% v/v% (1 g in 80 mL media). Therefore, MCs' volume and concentration for cell harvesting before entering the microfluidic gadget were set to 70 mL to reach 0.75% when the sample arrived at the spiral microfluidic chip. The volume was calculated by the following equations: target concentration (0.75%)/dilution factor in micromixer (2/3)/concentration in culture (1.29%) × volume in culture (80 mL). As such, 40 mL of TrypLE was added since there was 30 mL of media inside the bioreactor after 50 mL of supernatant was taken away. The flow rate was set at 2 mL/min from the bioreactor and 1 mL/min TrypLE from the syringe pump, so the total flow rate of 3 mL/min fluid proceeded into the spiral. To demonstrate the inertial forces in the system do not damage the MCs, we passed MCs through the two micromixers and one spiral chip setup under a 20 mL/min flow rate. The results showed that the gentle forces applied by the micromixer do not change the shape and size of the MCs (Fig. 2C). Various inertial microfluidic channel designs can be used in this application as evidenced in our previous publications (Moloudi et al. 2018). In this study, we have showcased a rigid channel in the processing of large particle through the power of 3D printed inertial microfluidics.

The zig-zag channel was responsible for further concentrating the harvested cells. Since it was connected to the outer outlet of the spiral, the operation flow rate of the zig-zag channel needed to match the flow rate of the outer outlet of the spiral. The zig-zag concentrator was tested with 15 and 20 μm beads across different flow rates. The results showed that from 1.6 to 1.9 mL/min, the beads were concentrated 100% in the middle outlet (Fig. 2D). The beads were concentrated ~3.5 times, with ~70% of the volume removed, indicating good dewatering efficiency of the device.

Application showcase

Harvesting MSCs from bioreactor using the microfluidic system

To investigate the efficiency of the microfluidic gadgets on cell detachment, the cells were stained with Hoechst before passing through the mixer. To ensure the complete detachment of cells in the micromixers, a one-inlet micromixer was added at the end to increase the interaction of cells and enzyme under the same mixing efficiency (Vasilescu et al. 2020). Figure 3A shows microcarrier-cell suspension before cell harvesting in which cells covered the whole surface of MCs. The growth of healthy MSCs

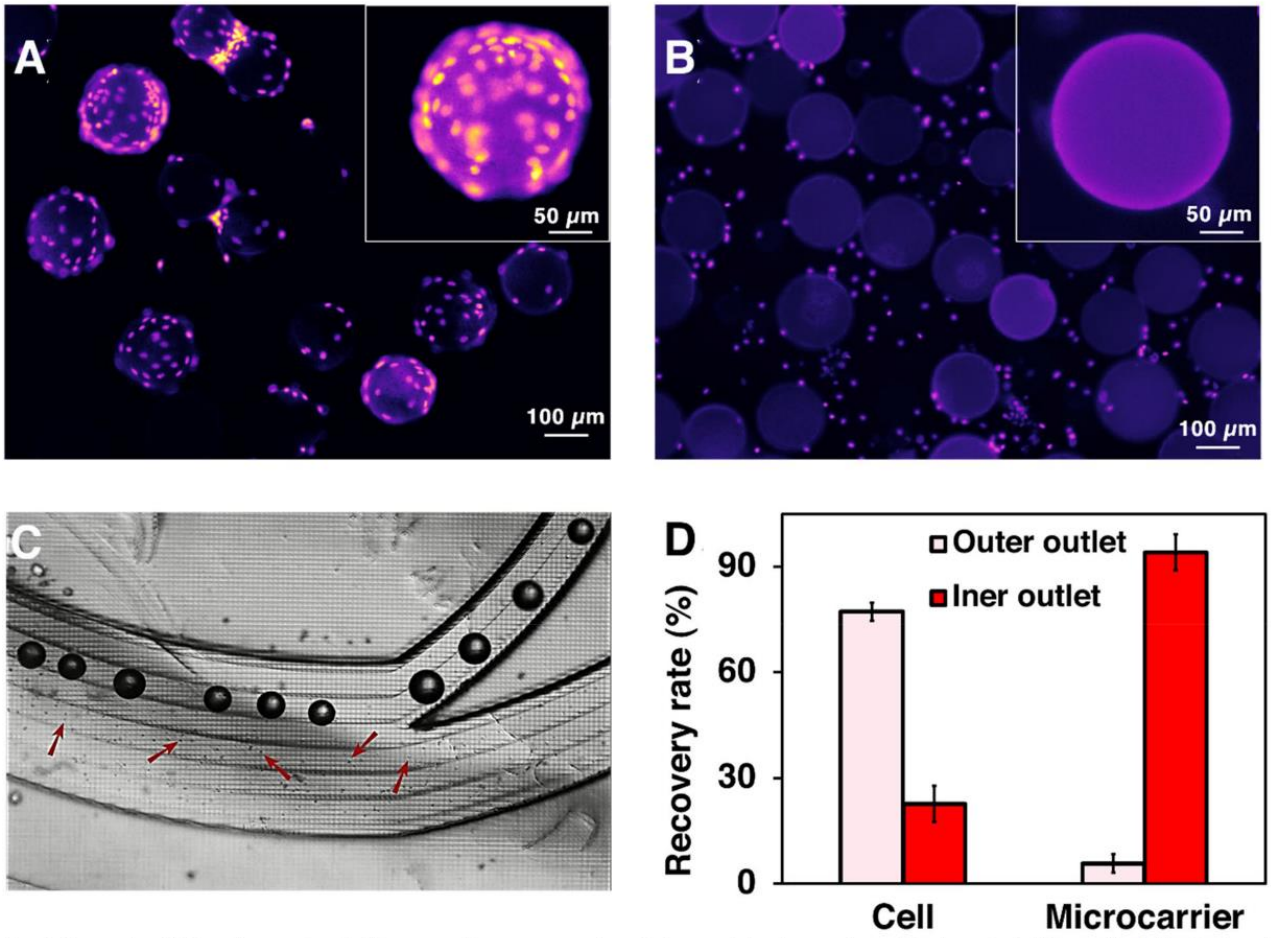

Fig. 3 Harvesting MSCs with our microfluidic system. The concentrating efficiency of the zig-zag channel is shown in Additional file 1: Fig. S9. **A** and **B** Fluorescent microscopy images of cells–MCs before and after passing through the mixer. Cell nuclides were stained with Hoechst. **C** Separation of cells and microcarriers through the spiral chip. Cells and MCs were separated through different channels based on their size difference. **D** The recovery rate of cells and MCs after passing through the spiral chip in one round. The liquid collected from the inner outlet of the spiral was collected and performed a second-round running through to further recover the cells. The two-round separation results are shown in Additional file 1: Fig. S8

on MCs commonly leads to cell–MCs aggregation (Ferrari et al. 2012) (Additional file 1: Fig S7). Therefore, to prevent the blockage of microfluidic devices, the cells–MCs suspension was incubated with enzyme for 5 min in the incubator to detach these aggregates. Figure 3B shows the MSCs were detached from MCs' surface by enzymatic treatment and gentle mechanical force after passing through the micromixers.

The media containing detached cells and MCs from the micromixers were then passed through the spiral. Later, they were collected separately from two outlets (Fig. 3C). 94.11% of MCs were successfully removed in the first round of separation. $76.62 \pm 2.1\%$ and $17.21 \pm 0.6\%$ cells were recovered from the OW outlet in the first and second pass, respectively, and $6.16 \pm 1.80\%$ cell loss through the IW outlet at the end of the process (Fig. 3D, Additional file 1: Fig. S8). The sum of yield (sum of cells harvested from the OW outlet over the total cell harvest from all outlets) can reach ~ 94%. Adding some obstacles at the outlet leads to 100% of the microcarrier removal rate, making it ready for clinical applications. Additional file 1: Fig. S9 shows the tight focusing band of MSCs in the middle outlet and the removal of small debris in the outer outlets. The cell solutions were collected from the outer outlets, and no cell was found in the waste outlet. Cells were concentrated 4.5 times compared to the pre-filtered samples. Although the counting results showed that the recovery rate was higher than 100%, a small number of cell loss could potentially happen due to the heterogeneity, clumping of cells, or attachment to the tubing or channel walls.

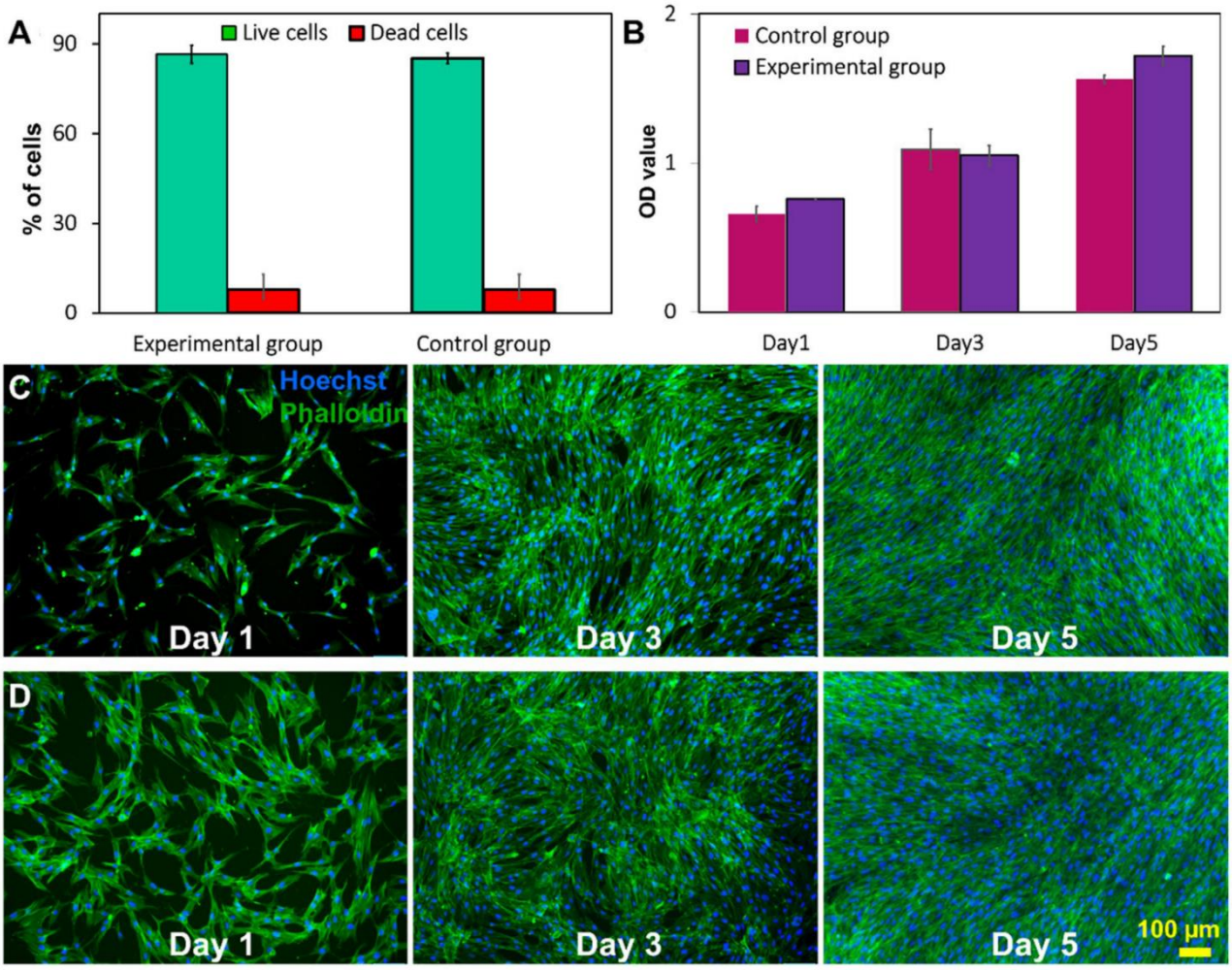

Fig. 4 Viability and proliferation of MSCs after harvesting process. **A** The viability of cells harvested by the microfluidic system and filtration method. Cell viability did not change significantly compared with the control group. Data are presented as mean ± SEM (****p value < 0.0001, $n \geq 3$). **B** MTS viability/proliferation rate of harvested cells. The morphology and proliferation rate of MSCs of the two groups were also compared with DAPI/phalloidin staining via **C** filtration group and **D** microfluidic group on 1st, 3rd, and 5th day of culture. F-actin filaments were visualised via FITC labelled phalloidin (green) and nuclei with DAPI (blue)

MSCs viability and proliferation after microfluidic cell harvesting

Cell viability was assessed immediately after harvesting. The live and dead staining results indicate that the microfluidic device did not compromise the viability of cells (Fig. 4A). MTS (3-(4,5-dimethylthiazol-2-yl)-5-(3-carboxymethoxyphenyl)-2-(4-sulfophenyl)-2H-tetrazolium) assay illustrating the metabolic activity of cells harvested by the device is also similar to the control. In the microfluidic group, the absorbance of media at 490 nm wavelength increased over time which indicates that cells have slightly higher metabolic activity than the control group, although the difference is not significant (Fig. 4B). Cell attachment, morphology, and proliferation were evaluated by staining the post-harvesting cells using DAPI and phalloidin. The fluorescent microscopy images in Fig. 4C and D indicate cells harvested with the microfluidic device have comparatively better cell attachment (Additional file 1: Fig. S10) than the control group on the first day of culture. After 3–5 days of culture, both groups of cells were confluent in the wells, and no significant difference in the growth rate was observed. Additionally, cells maintained their spindle morphology after harvesting with the device, and the size of cells was around 13–17 μm in both groups. The number of harvested cells after 1, 3, 5 days of cell seeding was counted by ImageJ to verify the MTS results. The results confirm that the microfluidic

system does not affect cell attachment and growth after harvesting (Additional file 1: Fig. S10).

Stem cell properties and therapeutic properties of the harvested MSCs

To confirm the stemness and multipotency of the harvested cells, the MSC surface markers were evaluated and trilineage differentiation was performed. CD90, CD73, and CD105 were stained with fluorescent antibodies (ThermoFisher, Australia) staining and counted by a flow cytometer (CytoFLEX LX, Beckman Coulter, USA). Figure 5A shows 98%, 100%, and 100% of the cells express CD90, CD73, and CD105, respectively, confirming the well-preserved MSCs identity. To assess the multipotency of cells after harvesting, cells were stained with Oil Red, Alizarin Red, and Alcian Blue staining after treating

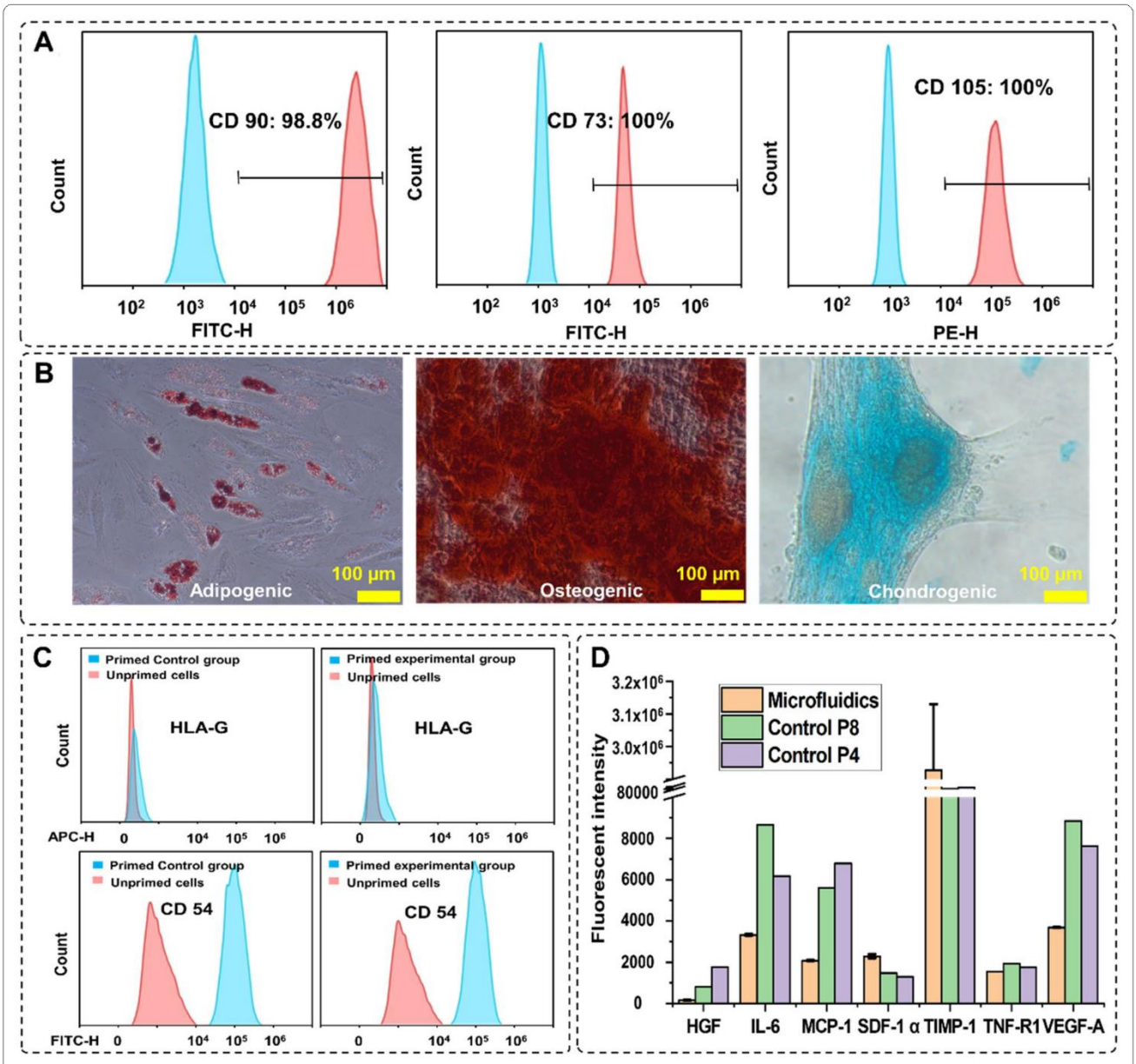

Fig. 5 MSCs characterisation after harvesting. **A** Expression of the MSCs surface markers CD90, CD73, and CD105 after 3 passages of indicated cells preserve their stemness after harvesting. **B** Multipotency assay of harvested cells using Oil red (left), Alizarin red (middle), and Alcian blue (right) showed the cells maintained their capacity to differentiate into different cell types. **C** The expression level of the surface therapeutic proteins of the experimental group. The changes in the expression level of HLA-G and CD54 were similar in both groups. **D** Comparison of the cytokine secretion profile of MSCs harvested from the microcarriers with microfluidic system and the passage 4, passage 8 planar flask cultured cells

with adipogenic and osteogenic/chondrogenic induction media, respectively (Fig. 5B). Formation of bright red stain calcium deposits stained by Alizarin Red S confirmed osteoblastic phenotype of cells. Additionally, presence of red lipid droplets stained by Oil Red O verified the adipocyte phenotype, and the blue glycosaminoglycan complex staining showed the presents of chondrogenic cells. These results indicate that cells retained their differentiation potential.

The therapeutic effect of harvested MSCs is verified by staining the surface therapeutic proteins and analysis of the cytokines in the cultured supernatant. Figure 5C shows the changes in the expression level of the surface therapeutic proteins after priming with TNF-α and IFN-Ɣ for 24 h. HLA-G is a protein that prohibits the growth of lymphocytes, which expression level does not change with priming (Nasef et al. 2007; Selmani et al. 2009; Najar et al. 2012). The expression level of HLA-G in both microfluidic and control groups remained constant after priming. CD54 (iCAM) is a T-cell activation-related protein that is sensitive to inflammation, and the expression level of this protein increased significantly after priming (Rubtsov et al. 2017; Tang et al. 2018). Figure 5C shows that the expression level of CD54 increased 100% after priming in both groups. These results prove that there is no significant difference in the therapeutic properties of the MSCs after proceeding through the microfluidic device. Next, using the Custom ProcartaPlex Multiplex immunoassay panel, we analysed the secretion profile of the harvested cells compared to the secretion profile of cells passaged stably in multilayer cell factories. The results showed that the harvested cells expressed a similar or lower level of HGF, IL-6, CCL2, VEGF-A, and TNF-RI compared to the passage 4, passage 8 multilayer cell factory grown controls, the expression level of SDF-1 alpha and TIMP-1 are much higher than the control group (Fig. 5D).

Multiplexing the microfluidic harvesting system for large-scale application

A multiplexed system was built with the same printing protocols to demonstrate the capability of scaling up the microfluidic system for large-scale applications. The system consists of five layers (Fig. 6); the first layer is the fluid splitting layer; it has one inlet for cell and microcarrier solutions to enter the system and another inlet for the digestive enzyme with a flow rate of 8 mL/min for the cell and microcarrier solution and 4 mL/min for the enzyme. These two inlets split the total flow into four even sets and enter the 4 micromixers evenly in the second layer. The micromixers have inserted holes for the pins to anchor the positions and prevent leakage. The flow rate in each micromixer is 3 mL/min for detaching cells from MCs. The third layer is the spiral layer, with a pin inserted into the outlet of the micromixers. The solutions collected from each of the two micromixers were evenly split into two spiral microfluidic devices, and each spiral received 3 mL/min liquid flow to separate cells from MCs. Then, the fourth layer, a splitting layer was used as the bottom layer of the spiral. Two holes were opened at the outlets of the spirals, and this layer was bonded with the fifth layer spiral layer with double adhesive tape. Lastly, a whole 3D printed layer with 4 zig-zag channels and pressure-damping channels was attached to the splitting layer with double adhesive tape. The inner outlets of each spiral are connected to one pressure-damping channel, and the outer outlets of each spiral are connected to one zig-zag channel. The cross-sectional area ratio of the inner and outer outlet is 2:3; the flow rate of the outer outlet is, therefore 1.8 mL/min for each spiral. As shown in Fig. 2, the zig-zag channel can focus the cells from 1.4–1.9 mL/min. This flexible working range of the zig-zag channel ensures the cells focus on the middle outlet of the device and reduce the requirement of precision of the pressure-damping channel. The total flow rate of the cell outlet was 7.2 mL/min, while the MCs outlet was 4.8 mL/min.

Discussion

The merits of microfluidic devices, such as low-cost, high throughput, labour-free, customisability, and energy efficiency, meet the need of the bioprocessing industry. Recently, multiple attempts have been made to bring microfluidic devices to solve the challenges associated with bioprocessing. However, microfluidic devices are still facing difficulty in accommodating and integrating themselves in the bioprocessing industry. In this manner, 3D printing technology can be used as a bridge to connect microfluidic devices and the bioprocessing industry. The one-step fabrication method of 3D printing technology (printing and washing) allowed us to test 16 zig-zag channels with different dimensions, six different inertial concentrator designs and three micromixers.

In our proposed microfluidic system, cells detachment, separation, and concentration–time are short, 5 min for incubation and 20 s for passing through the system with a total length of < 5 cm. This short processing time could effectively minimise the negative impact of enzymatic treatment on the cell membrane and enhance attachment and growth of harvested cells (Fig. 4), indicating well-preserved cell membrane integrity and functionality. Although the damages caused by enzymatic treatment can be reversible (Tsuji et al. 2017), it takes a few passages for the cells to recover and is not feasible for clinical applications.

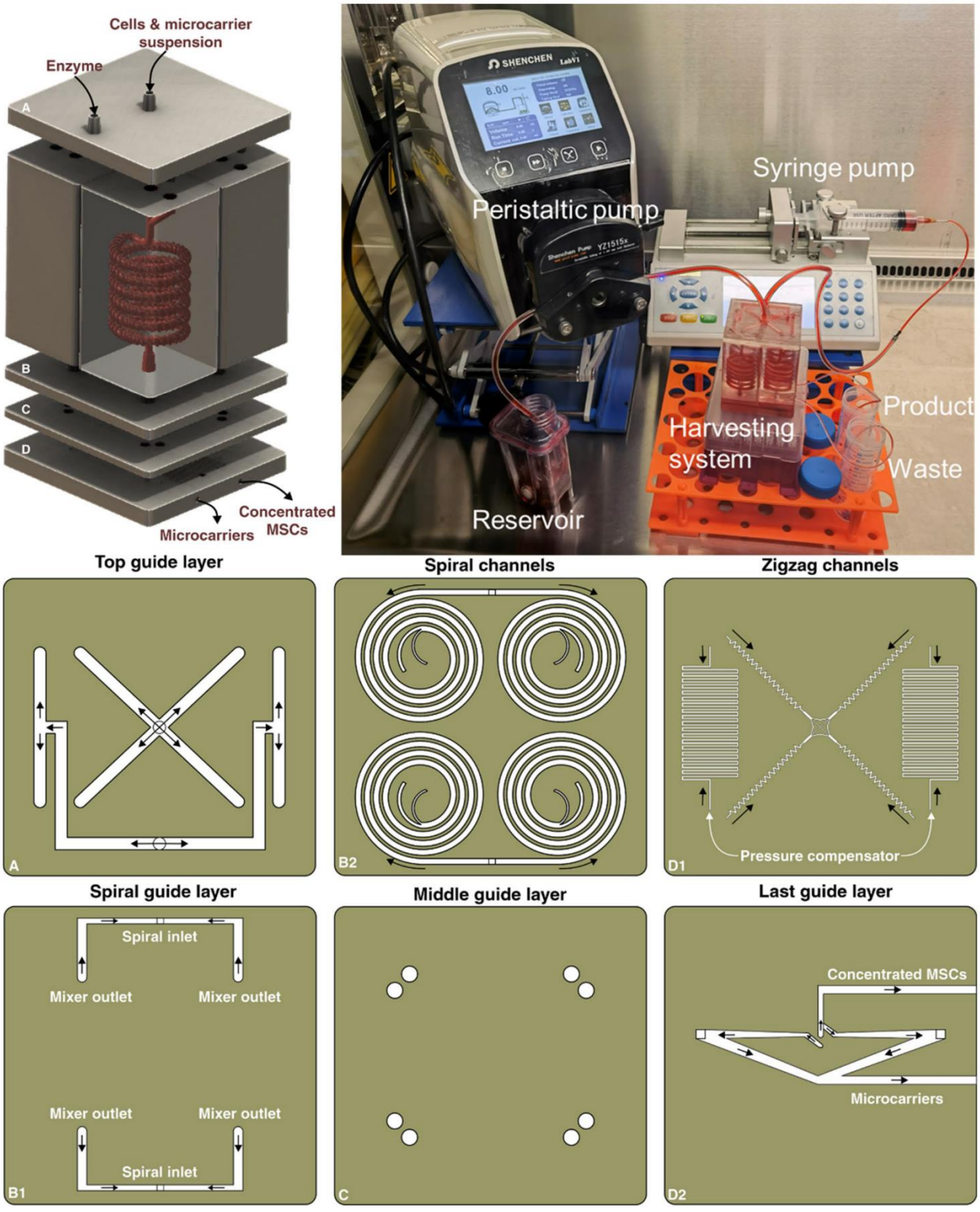

Fig. 6 The setup and components of each layer. The multiplexing system consists of five layers: a top guide layer to distribute the liquid evenly into the micromixers; a micromixers layer that detaches MSCs from MCs; a spiral layer separating MSCs and MCs; a middle guide layer that provided a base for spiral and zig-zag channels and a zig-zag channel and pressure-damping channel layer that concentrate the MSCs. The cells and MCs are left from the outlets, respectively

The results of cell viability and MTS assays indicate that the viability and proliferation rate of the microfluidic-harvested cells are the same as the control. This is in agreement with the results reported by Nienow et al. (2016), who suggested that agitating cell–MCs suspension facilitates cell detachment while not compromising cells' properties and viability. As expected, the cells maintain their differentiation potential trilineage (Fig. 5D), their size, spindle morphology (Fig. 4D), and surface markers expression (Fig. 5A). The size and morphology of the cells are important indicators of the cell potencies and secretion profile since different sizes MSCs were shown to have a different expression levels of differentiation promotor/inhibitor genes and different secretion levels of therapeutic factors (Yin et al. 2018, 2020; Lee et al. 2014).

Our experiment showed that the anti-inflammatory surface proteins expression level of the harvested cells during the subsequent subculture had no difference compared to the control group (Fig. 5C). This indicates that the cells preserved their therapeutic properties after the process, and the microfluidic system is safe for the industrial production of stem cells for clinical purposes. The high secretion level of SDF-1α and TIMP-1 proteins suggest strong potential in therapeutic applications. However, these results are not enough to draw the conclusion of whether this harvesting method alters cytokine secretion levels of the MSCs. Previous works show that the topography of the culture system (Leuning et al. 2018) and shifting from 2 to 3D culture (Russell et al. 2018) influenced the cytokine expression level of cells. Ng and Wang (2021) showed that even growing cells on different types of microcarriers influence the secretion profile. Therefore, the secretion profile changes caused by our 3D printed modular harvesting system require further characterisation. These results showed that the cells harvested with our 3D printed modular microfluidic system preserved all the cell properties with no cytotoxic effect, and damage caused by the material, or the hydrodynamic forces was observed.

With the aid of 3D printed technologies (Additional file 1: Section S6), our microfluidics system has multiple advantages over the current laboratory and industrial adherent cell harvesting methods. This microfluidic system requires only two pumps to trigger, and no complicated tubing and valve is needed. This system is cGMP compatible and the design of the system ensures negligible risk of contamination (Tamura et al. 2012; Caruso et al. 2014); The device can be operated in a continuous manner, which is particularly suitable for industrial-scale application (Castilho and Medronho 2002); The system can be used as a single unit system for lab-scale production or easily scaled-up by paralleling the devices together for large volume processing; Other microfluidic devices can also be integrated to perform other functions such as quality control of cellular products (Ding et al. 2021). With the small device footprint, reaching 2 L/min flow rate requires 100 chips, and the total volume would be only 1 m^3. It will take 25 min to harvest 50 L MCs. The small footprint allows easy integration into any current-available system, 3D printing technologies allow easy and rapid prototyping of customised fluidic interconnects at a low cost to aid the industrial integration (Ho et al. 2015).

On the other hand, our system shows clear advantages over TFF (Schnitzler et al. 2016) with its clogging-free operation manner. This important feature reduces the production cost since the device does not need frequent membrane replacement and maintenance and can be single used due to the low-cost. Also, the low flow rate in each individual unit of our device ensures the cells are not suffering from shear stress like TFF, resulting in cell damage (Cunha et al. 2015). Moreover, this system can be integrated into other enzymatic detachment methods or even enzyme-free cell detachment procedures as well. In recent years, frontier research about smart MCs shows that thermosensitive MCs and soluble MCs have great potential in future cell culture (Tamura et al. 2012; Kalra et al. 2019; Hanga et al. 2021). Proceeding these MCs through our microfluidic gadget may increase exposure to light and heat while benefiting from the agitation of fluid flow. In our multiplexing design, we showcased the first multiplexed modular microfluidic system. The system is built in a nonlinear and modular manner which has not been showcased before. This rapid, low-cost prototyping is not possible without 3D printing technology.

Conclusion

In this paper, we proposed a 3D printed modular microfluidic system consisting of three modules, which are micromixer, microseparator, and microconcentrator, to detach and separate MSCs from MCs. Each module was produced with direct SLA printing, creating highly accurate 3D structures with a low cost and a simple, rapid manufacturing process. Operating at the throughput of 3 mL/min, this microfluidic gadget can detach the cells fully from MCs with 5 min incubation time and 20 s proceeding time through the device, removing 100% of the MCs from cells solution while recovering 77% of cells in one round. The cells passing through the device were viable proliferative with preserving their differentiation potential. More importantly, the therapeutic potential of the cells was well preserved. Our scaled-up version shows that the current system has the potential to apply in the stem cell industry in cGMP compatible manner. Compared to the current system, this gadget is operated in high throughput and clogging-free manner. It simplifies

the cell harvesting procedure, minimises the damage and chance of contamination to the cells, and reduces the overall production cost on a large scale. Furthermore, this system is flexible and can potentially be modified to fit with any microcarrier and bioreactor to produce various cell types and products.

Abbreviations
MSCs: Mesenchymal stem cells; MCs: Microcarriers; TFF: Tangential flow filtration; cGMP: Current good manufacturing practice; MTS assay: 3-(4,5-Dimethylthiazol-2-yl)-5-(3-carboxymethoxyphenyl)-2-(4-sulfophenyl)-2H-tetrazolium Assay; FDM: Fused Deposition Modelling; SLA: Stereolithography; DLP: Digital light processing; 2PP: Two-photon polymerisation; IW: Inner wall; OW: Outer wall.

Supplementary Information

The online version contains supplementary material available at https://doi.org/10.1186/s40643-022-00550-2.

Additional file 1. The design criteria, methodology and simulation sections of the microfluidic system, methodology of cell culture and properties measurement, supplementary figures of the microfluidic system characterisation and MSCs characterisation post-harvesting.

Acknowledgements
Not applicable.

Author contributions
In this work, LD, SRB and MAF contributed to manuscript writing, experimental design and execution. FM, BS and BB contributed to part of the experimental execution and validation of data. GV and MEW provided the idea and supervision of the work. All authors read and approved the final manuscript.

Funding
Not applicable.

Data availability
All data that support the findings of this study are included within the article and Additional file 1.

Declarations

Ethics approval and consent to participate
Not applicable.

Consent for publication
Not applicable.

Competing interests
Flyn McKinnirey, Brian Saputro and Graham Vesey are currently employed by Regeneus company. The other authors have no other relevant affiliations or financial involvement with any organisation or entity with a financial interest in or financial conflict with the subject matter or materials discussed in the manuscript apart from those disclosed.

Author details
[1]School of Biomedical Engineering, University of Technology Sydney, Sydney, NSW 2007, Australia. [2]School of Engineering, Macquarie University, Sydney, NSW 2109, Australia. [3]Regeneus Ltd, Paddington, Sydney, NSW 2021, Australia. [4]Institute of Molecular Medicine, Sechenov University, Moscow 119991, Russia.

Received: 21 February 2022 Accepted: 13 May 2022
Published online: 06 June 2022

References

Amini H, Lee W, Di Carlo D (2014) Inertial microfluidic physics. Lab Chip 14(15):2739–2761
Bhattacharjee N et al (2016) The upcoming 3D-printing revolution in microfluidics. Lab Chip 16(10):1720–1742
Cai G et al (2017) A review on micromixers. Micromachines 8(9):274
Caruso SR et al (2014) Growth and functional harvesting of human mesenchymal stromal cells cultured on a microcarrier-based system. Biotechnol Prog 30(4):889–895
Castilho LR, Medronho RA (2002) Cell retention devices for suspended-cell perfusion cultures. Tools and applications of biochemical engineering science. Springer, Berlin, pp 129–169
Chai M et al (2021) Biocatalytic micromixer coated with enzyme-MOF thin film for CO2 conversion to formic acid. Chem Eng J 426:130856
Chen AK-L, Reuveny S, Oh SKW (2013) Application of human mesenchymal and pluripotent stem cell microcarrier cultures in cellular therapy: achievements and future direction. Biotechnol Adv 31(7):1032–1046
Chen X-Y et al (2020) Recent advances in the use of microcarriers for cell cultures and their ex vivo and in vivo applications. Biotechnol Lett 42(1):1–10
Chilima TDP, Moncaubeig F, Farid SS (2018) Impact of allogeneic stem cell manufacturing decisions on cost of goods, process robustness and reimbursement. Biochem Eng J 137:132–151
Cunha B et al (2015) Filtration methodologies for the clarification and concentration of human mesenchymal stem cells. J Membr Sci 478:117–129
Di Carlo D (2009) Inertial microfluidics. Lab Chip 9(21):3038–3046
Ding L et al (2021) An easy-to-operate method for single-cell isolation and retrieval using a microfluidic static droplet array. Microchim Acta 188(8):1–11
Ding L et al (2022) Giardia purification from fecal samples using rigid spiral inertial microfluidics. Biomicrofluidics 16(1):014105
Fardjahromi MA et al (2020) Mussel inspired ZIF8 microcarriers: a new approach for large-scale production of stem cells. RSC Adv 10(34):20118–20128
Ferrari C et al (2012) Limiting cell aggregation during mesenchymal stem cell expansion on microcarriers. Biotechnol Prog 28(3):780–787
Figeys D, Pinto D (2000) Lab-on-a-chip: a revolution in biological and medical sciences. Anal Chem 72(9):330A-335A
Hanga MP et al (2021) Expansion of human mesenchymal stem/stromal cells (hMSCs) on temporary liquid microcarriers. J Chem Technol Biotechnol 96:930–940
Ho CM et al (2015) 3D printed microfluidics for biological applications. Lab Chip 15(18):3627–3637
Joseph A et al (2016) A scale-down mimic for mapping the process performance of centrifugation, depth and sterile filtration. Biotechnol Bioeng 113(9):1934–1941
Jossen V et al (2018) Manufacturing human mesenchymal stem cells at clinical scale: process and regulatory challenges. Appl Microbiol Biotechnol 102(9):3981–3994
Kalra K et al (2019) Developing efficient bioreactor microcarrier cell culture system for large scale production of mesenchymal stem cells (MSCs). Cytotherapy 21(5):S73
Lee WC et al (2014) Multivariate biophysical markers predictive of mesenchymal stromal cell multipotency. Proc Natl Acad Sci 111(42):E4409–E4418
Leuning DG et al (2018) The cytokine secretion profile of mesenchymal stromal cells is determined by surface structure of the microenvironment. Sci Rep 8(1):7716
Mihandoust A et al (2020) High-throughput particle concentration using complex cross-section microchannels. Micromachines 11(4):440
Moloudi R et al (2018) Inertial-based filtration method for removal of microcarriers from mesenchymal stem cell suspensions. Sci Rep 8(1):12481
Moloudi R et al (2019) Scaled-up inertial microfluidics: retention system for microcarrier-based suspension cultures. Biotechnol J 14(5):1800674
Najar M et al (2012) Immune-related antigens, surface molecules and regulatory factors in human-derived mesenchymal stromal cells: the expression and impact of inflammatory priming. Stem Cell Rev Rep 8(4):1188–1198
Nasef A et al (2007) Immunosuppressive effects of mesenchymal stem cells: involvement of HLA-G. Transplantation 84(2):231–237
Ng EX et al (2021) Dissolvable gelatin-based microcarriers generated through droplet microfluidics for expansion and culture of mesenchymal stromal cells. Biotechnol J 16(3):2000048

Nienow AW et al (2016) Agitation conditions for the culture and detachment of hMSCs from microcarriers in multiple bioreactor platforms. Biochem Eng J 108:24–29
Nivedita N, Ligrani P, Papautsky I (2017) Dean flow dynamics in low-aspect ratio spiral microchannels. Sci Rep 7:44072
Oh KW et al (2012) Design of pressure-driven microfluidic networks using electric circuit analogy. Lab Chip 12(3):515–545
Ozbey A et al (2019) Inertial focusing of cancer cell lines in curvilinear microchannels. Micro Nano Eng 2:53–63
Razavi Bazaz S et al (2019) Rapid soft lithography using 3D-printed molds. Adv Mater Technol 4(10):1900425
Razavi Bazaz S et al (2020a) 3D printing of inertial microfluidic devices. Sci Rep 10(1):5929
Razavi Bazaz S et al (2020b) Obstacle-free planar hybrid micromixer with low pressure drop. Microfluid Nanofluid 24(8):61
Razavi Bazaz S et al (2020c) Computational inertial microfluidics: a review. Lab Chip 20(6):1023–1048
Rodrigues CA, Nogueira DE, Cabral JM (2018) Next-generation stem cell expansion technologies. Cell Gene Ther Insights 4(8):791–804
Rouhi O et al (2021) Numerical and experimental study of cross-sectional effects on the mixing performance of the spiral microfluidics. Micromachines 12(12):1470
Rubtsov Y et al (2017) Molecular mechanisms of immunomodulation properties of mesenchymal stromal cells: a new insight into the role of ICAM-1. Stem Cells Int 2017:6516854
Russell AL, Lefavor RC, Zubair AC (2018) Characterization and cost-benefit analysis of automated bioreactor-expanded mesenchymal stem cells for clinical applications. Transfusion 58(10):2374–2382
Schnitzler AC et al (2016) Bioprocessing of human mesenchymal stem/stromal cells for therapeutic use: current technologies and challenges. Biochem Eng J 108:3–13
Selmani Z et al (2009) HLA-G is a crucial immunosuppressive molecule secreted by adult human mesenchymal stem cells. Transplantation 87(9 Suppl):S62–S66
Serra M et al (2018) Advancing manufacture of human mesenchymal stem cells therapies: technological challenges in cell bioprocessing and characterization. Curr Opin Chem Eng 22:226–235
Tamura A et al (2012) Temperature-responsive poly(N-isopropylacrylamide)-grafted microcarriers for large-scale non-invasive harvest of anchorage-dependent cells. Biomaterials 33(15):3803–3812
Tang B et al (2018) The therapeutic effect of ICAM-1-overexpressing mesenchymal stem cells on acute graft-versus-host disease. Cell Physiol Biochem 46(6):2624–2635
Tavassoli H et al (2018) Large-scale production of stem cells utilizing microcarriers: a biomaterials engineering perspective from academic research to commercialized products. Biomaterials 181:333–346
Tsui Y-Y, Yang C-S, Hsieh C-M (2008) Evaluation of the mixing performance of the micromixers with grooved or obstructed channels. J Fluids Eng 130(7):071102
Tsuji K et al (2017) Effects of different cell-detaching methods on the viability and cell surface antigen expression of synovial mesenchymal stem cells. Cell Transplant 26(6):1089–1102
Vasilescu SA et al (2020) 3D printing enables the rapid prototyping of modular microfluidic devices for particle conjugation. Appl Mater Today 20:100726
Wang L, Dandy DS (2017) A microfluidic concentrator for cyanobacteria harvesting. Algal Res 26:481–489
Xiang N et al (2019) Precise size-based cell separation via the coupling of inertial microfluidics and deterministic lateral displacement. Anal Chem 91(15):10328–10334
Yin L et al (2018) Microfluidic label-free selection of mesenchymal stem cell subpopulation during culture expansion extends the chondrogenic potential in vitro. Lab Chip 18(6):878–889
Yin L et al (2020) Label-free separation of mesenchymal stem cell subpopulations with distinct differentiation potencies and paracrine effects. Biomaterials 240:119881
Yi-Qiang F et al (2018) Applications of modular microfluidics technology. Chin J Anal Chem 46(12):1863–1871
Zydney AL (2016) Continuous downstream processing for high value biological products: a review. Biotechnol Bioeng 113(3):465–475

Publisher's Note

A modular 3D printed microfluidic system: a potential solution for continuous cell harvesting in large-scale bioprocessing

Lin Ding[1, Ψ] Sajad Razavi Bazaz[1 Ψ], Mahsa Asadniaye Fardjahromi[1,2Ψ], Flyn McKinnirey[3], Brian Saputro[3], Balarka Banarjee[3], Graham Vesey[3], Majid Ebrahimi Warkiani[1,4*]

[1]School of Biomedical Engineering, University of Technology Sydney, NSW, 2007, Australia

[2]School of Engineering, Macquarie University, Sydney NSW, 2109, Australia

[3]Regeneus Pty Ltd, Paddington, Sydney, NSW, 2021, Australia

[4]Institute of Molecular Medicine, Sechenov University, Moscow, 119991, Russia

[Ψ] These authors contribute equally

*Contact

Majid Ebrahimi Warkiani (majid.warkiani@uts.edu.au)

School of Biomedical Engineering, University Technology Sydney, Sydney, New South Wales 2007, Australia

Supplementary information section

S1. Microfluidic system design consideration

Based on previous developments of scaled-up microfluidic devices [1-3], here, we used a 3D printed scaled-up modular microfluidic system consists of two micromixers, one spiral inertial separator, and one zig-zag concentrator to detach and separate cells from microcarriers (MCs) and dewater the cells. The micromixers in this system assisted cell harvesting by mixing the MCs and enzyme sufficiently and inducing mild mechanical force, reducing the cell detachment time. 3D passive micromixer has been utilised in this system owing to its high mixing efficiency, adaptable flow rate range, adequate cross-sectional channel size, and gentle forces applied to the cells. MCs were found to be fragile and have the risk of breakage in stirring bioreactor [4], but they remained intact even under high flow rate in our micromixers (Fig. 2C), and no clogging of channels was observed [5-7]. For the same reasons, spiral microfluidics was chosen due to the large channel dimension and gentle forces it applied to the microparticles and in the last step, the zig-zag channel was used to concentrate the cells due to its high dewatering efficiency and flexible working flow rate range. In addition, the spiral channel extracts larger particles out of the cell solution, and zig-zag channel removes smaller debris like microplastics of the culture flask, cell debris or MCs fragments (Fig. 2) which might trigger immune rejection [8] of the patients. These two devices worked together to remove particles and debris that are bigger or smaller than the cells.

S2. Numerical simulation of the micromixer

To characterise the performance of the micromixer, the fluid behaviour in the micromixer was simulated using COMSOL Multiphysics 5.5 [5]. Two equations, Navier-Stokes, and continuity equations (Eqs. (1) and (2)), which are regarded as the governing equations for laminar, incompressible Newtonian fluid, were used to calculated velocity and pressure distribution in the channel:

$$\nabla . V = 0 \tag{1}$$

$$\frac{\partial V}{\partial t} + \rho(V.\nabla)V = -\nabla P + \mu\nabla^2 V \tag{2}$$

where V is the velocity vector (m/s), ρ is the fluid density (kg/m^3), μ is the dynamic viscosity (N·s/m^2), and P is the pressure (Pa). The fluid velocity and pressure in Eq. (2) can then be used to model the mass transport of the fluid by the convection-diffusion equation (Eq. (3))

$$\frac{\partial c}{\partial t} + (\mathrm{V}.\nabla)\mathrm{c} = \mathrm{D}\nabla^2 c \tag{3}$$

where c is the fluid concentration (Mol/m^3), D is the diffusion coefficient (m^2/s).

To evaluate the performance of the micromixer, mixing index was introduced:

$$MI = 1 - \sqrt{\frac{\frac{1}{N}\sum_{i=1}^{N}(c_i - \bar{c})^2}{{\sigma^2}_{max}}} \tag{4}$$

$${\sigma^2}_{max} = \bar{c}(1 - \bar{c}) \tag{5}$$

where N is the total number of the cross-section mesh elements, ${\sigma^2}_{max}$ is the maximum variance of mixture concentrations at the specific cross-section along the channel, c_i is the concentration of species for each of the mesh elements, and $\bar{c}$ is the average value of c_i. The value of $\bar{c}$ is related to the inlet volume ratio, which is 2:1 in our case, and it is equal to 0.66 [9].

S3. Calculation of experimental mixing index

To extract the experimental values of the mixing index, an image processing software (Fiji, NIH, USA) has been used. Grayscale values of the images along a line parallel to the channel width at the inlet and outlet were extracted from the pictures. These values were then normalized using Eq. (6).

$$I_i = \frac{I_i^* - I_{min}^*}{I_{max}^* - I_{min}^*} \tag{6}$$

where the actual intensity is represented by I_i^*, and the minimum and maximum values of intensity at the inlet (unmixed fluid) are given by I_{min}^* and I_{max}^*, respectively. The experimental value of the mixing index is then calculated using Eq. (9).

$$MI_{experimental} = 1 - \frac{ME}{ME_{no\ mixing}} \tag{7}$$

Here, ME and $ME_{no\ mixing}$ were calculated using Eqs. (10) and (11).

$$ME = \sqrt{\frac{1}{N}\sum_{i=1}^{N}\left(\frac{I_i - \bar{I}}{\bar{I}}\right)^2} \tag{1}$$

$$ME_{no\ mixing} = \sqrt{\frac{1}{N}\sum_{i=1}^{N}\left(\frac{I_{min,max} - \bar{I}}{\bar{I}}\right)^2} \tag{92}$$

where N is the number of pixels in the inlet or outlet image along a line parallel to the channel width, $\bar{I}$ is 0.5, and $I_{min,max}$ can be 0 or 1, respectively.

S4. Cell culture in culture flask and bioreactor

Human adipose-derived mesenchymal stem cells were supplied by Regeneus Ltd. The cells used in this study were in passage 8. The cryopreserved cells were thawed and cultured in complete media made of α-MEM (Gibco, Australia) supplemented with 10% Human Platelet Lysate (HPL, COOK Regentec, US) in a 37°C incubator with 5% CO_2 before seeding on microcarriers.

Star-Plus MCs were sterilised by autoclaving according to the manufacturer's instruction and then were suspended with a density of 12.5 mg/ml prior to cell seeding. MCs were transferred to the 100 ml PBS mini bioreactor (PBS biotech, USA), and the cells were seeded at a concentration of 2.0×10^6 cells/g MCs in the bioreactor. The bioreactor was placed at 37 °C humidified bioreactor with 5% CO_2. To improve cell attachment, the bioreactor was first operated at 15 rpm for the first 24 hours and then increased to 24 rpm to attain near-full suspension of MCs-cells suspension. Cell propagation on MCs proceeded for 7 days. After that, cells were harvested by the traditional filtration method and the proposed 3D printed integrated microfluidic system. To visualise the number of attached cells on the MCs after cell harvesting, the cells were stained with Hoechst staining (Miltenyi Biotec, Australia) and observed by fluorescent microscope (Olympus IX73, Olympus, Japan). Briefly, 1 mL of the cultured microcarrier-cell suspension was taken out from the bioreactor, rinsed with PBS, and then fixed by 4% paraformaldehyde (Sigma Aldrich, Australia) for 20 min. Then the cells-attached MCs were washed with PBS and stained with Hoechst for 30 min.

S5. Cells characterisation after passing through microfluidic devices

S5.1 Cell viability assay and proliferation assay

The viability of cells after harvesting was evaluated by live and dead cells viability assay kit (ab115347, Abcam, UK) and viability profile for control and experimental group was assessed via flow cytometry (CytoFLEX LX, Beckman Coulter, USA) according to the manufacturer's instructions. The proliferation rate of harvested cells was quantified by MTS. To this aim, 2×10^4 cells/well were seeded in three wells of the 24 well plates, and after 1, 3, and 5 days of cell seeding, the proliferation rate of cells was examined by MTS reagent containing serum-free medium according to the manufacturer's protocol (Progmo, Australia). The absorbance was measured at 450 nm using a Tecan Spark multimode microplate reader (Tecan, Switzerland).

To further quantified cell proliferation, the cells (2×10^4 cells/well) were seeded on a 24-well plate and on the 1st, 3rd, and 5th day of culture, cell nuclei and F-actin filaments were stained with DAPI and FITC-labelled phalloidin, respectively. Cells were visualised using Olympus IX73 microscope (three fields of view per replicate; three replicates; Olympus, Japan). Then the number of cells for each sample was counted manually using ImageJ.

S5.2 Identification of cell phenotype

To evaluate the microfluidic harvesting system's long-term effect on the stem cell, the surface markers of MSCs were stained by fluorescent antibodies. 3×10^4 cells were seeded in 24-well plates and incubated at 37°C and 5% CO2. When cells reached near 80% confluence, they were labelled with monoclonal antibodies CD90-FITC, CD105-PE, and CD73-FITC (Abcam, Australia), fixed by 4% formaldehyde (Sigma Aldrich, Australia) and analysed by CytoFLEX flow cytometer and FlowJo software (BD, USA).

S5.3 Trilineage differentiation

The harvested cells were seeded in 24-well plates with a density of 3×10^4 cells/well. The detail method was reported in our previous work [10]. Briefly, three days after culture, the media was

replaced with StemPro™ Osteogenesis differentiation media (Gibco, Australia) for osteogenic and differentiation, StemPro™ Chondrogenesis differentiation media (Gibco, Australia) for chondrogenic and StemPro™ adipogenic differentiation media (Gibco, Australia) for adipogenic differentiation. After 21 days, the osteoblasts property of cells was verified by Alizarin Red staining (Sigma Aldrich, Australia). The cells first were fixed with 70% ethanol for 1 hour, washed with deionized water several times, then stained with alizarin red s solution, and incubated at room temperature for 1 hour. The cells treated with chondrogenic and adipogenic differentiation media were stained with Alcian Blue and Oil Red O (Sigma Aldrich, Australia) staining respectively. Both group of cells were fixed with 4% formaldehyde for 1 hour, and then Oil Red staining was added into the adipocytes for 30 minutes staining and Alcian Blue was added into the chondrocytes and stain the cells overnight. Finally, the cells were washed with deionized water three times, and the stained matrix was observed by a light microscope (Olympus, Japan).

S5.4 Surface proteins responses to cytokine stimulation

The harvested cells were seeded into a 6 well plate at the concentration of 5×10^4 cells/ml in complete media. After cells reached 50% confluence, the cells were treated with priming media containing α-MEM with 5% HPL, 10ng/mL TNF-α, and 100ng/mL IFN-γ recombinant proteins (Stem cell technologies, USA). The unprimed cells (treated with α-MEM and 5 % HPL) were used as a control. After 24 hours, cells were harvested and centrifuged at 800 G for 7 minutes. The supernatant was discarded, and the cell pellet was resuspended in 1mL of cold DPBS (2-8 °C) and stained with CD54 (iCAM) and HLA-G antibodies (Biolegend, Australia). The labelled cells were analysed via a CytoFLEX LX flow cytometer system and CytExpert software.

S5.5 Cytokine secretion study

To assess the characteristics of MSCs secreted protein, MSCs were assessed under normal culture conditions and after harvesting from the microfluidics system. Analytes, including HGF, IL-6, MCP-1, VEGF-A, SDF-1α, TNFR1, and TIMP-1 were measured using the Custom ProcartaPlex Multiplex immunoassay (Thermo Scientific, Australia). ProcartaPlex is a Luminex-based multiplex assay that utilizes magnetic beads with antibodies directed against distinct analytes in one assay, enabling the measurement of many analytes at one time. Assays were performed as per the manufactures' instructions. Briefly, MSCs were defrosted and spun at 10,000g for 2 minutes; spun sample supernatant is bound with detection antibodies added, conjugated with Streptavidin-PE, and the fluorescent intensity of each sample was read on a MAGPIX 200 (Luminex Corporation, US) reader.

S6. Additive manufacturing for device fabrication

In our system, all microfluidic devices were fabricated by 3D printing. 3D printing is the only choice to fabricate such spatial designs in a short time due to the high customisability, high accuracy, and potentially labour-free manufacturing process. Stacking of PDMS [11], laser cutting [12] or micromilling [13] have limited capability of fabricating 3D structures, and they are expensive and labour-intensive. An alternative fabrication method is direct 3D printing of microfluidic devices, which have great potential in the industry due to their rigid nature, highly customisable design, cost-effective, and rapid manufacturing process [14-16]. These devices required manual aligning and binding and are therefore prone to human error. Micromixers with such complex geometry can only be made using sacrificial moulds or direct printing, similar to the one that we used in previous study [17]. However, sacrificial moulds do not have high quality (limited on the accuracy of the printer) and hugely rely on experienced users to produce, it has an extended processing time, and excessive PDMS material is needed. Therefore, in this paper, we employed the SLA 3D printer to directly print the micromixer, shortening the cost, time, and effort needed to fabricate the device with the same spatial and precise geometry. With this printing procedure, the micromixer and spiral chip can be fabricated within a few hours and require only very simple post-processing steps, which can be automatically proceeded by washing and curing machine to further reduce labour cost.

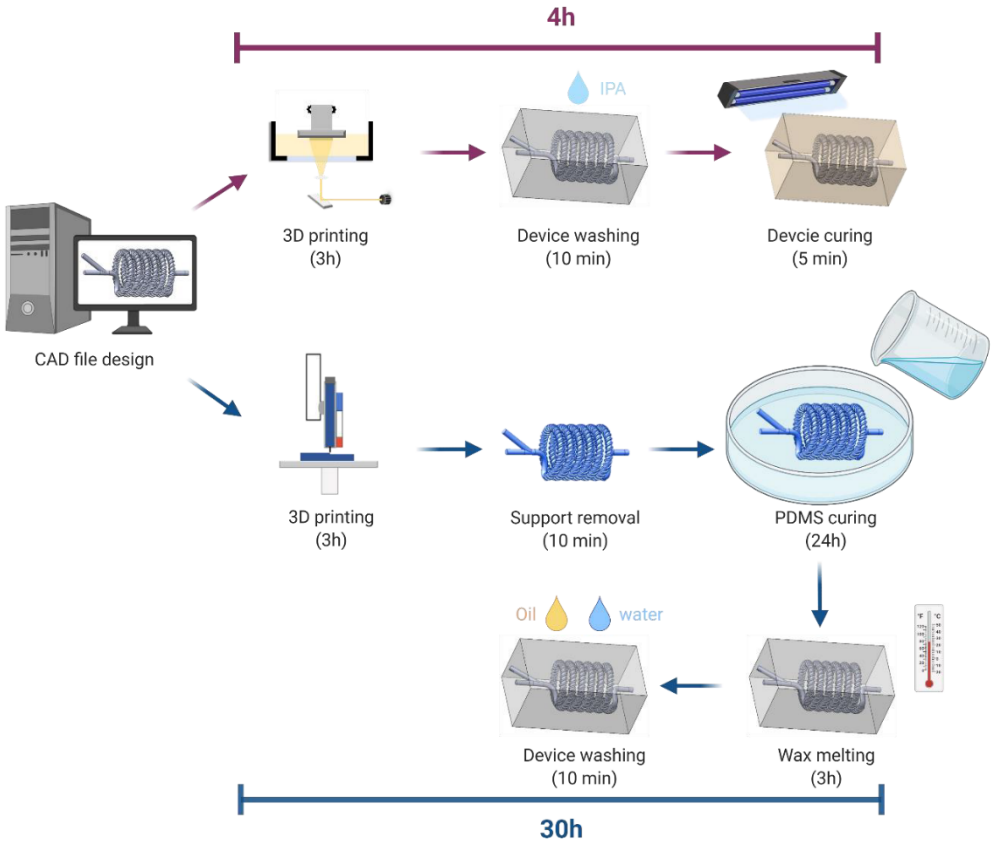

Fig. S1. Direct printing of 3D micromixers hugely reduces the time needed for fabricating time compared to wax printing method.

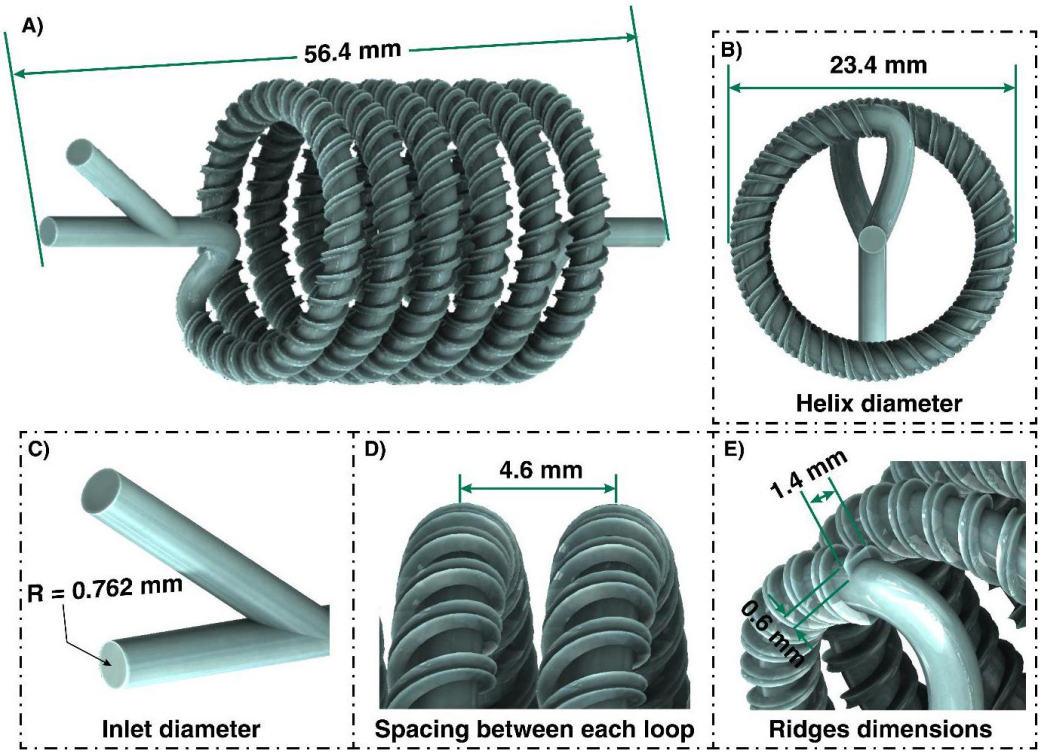

Fig. S2. Dimensions of threaded micromixer used for detachment of cells from microcarriers

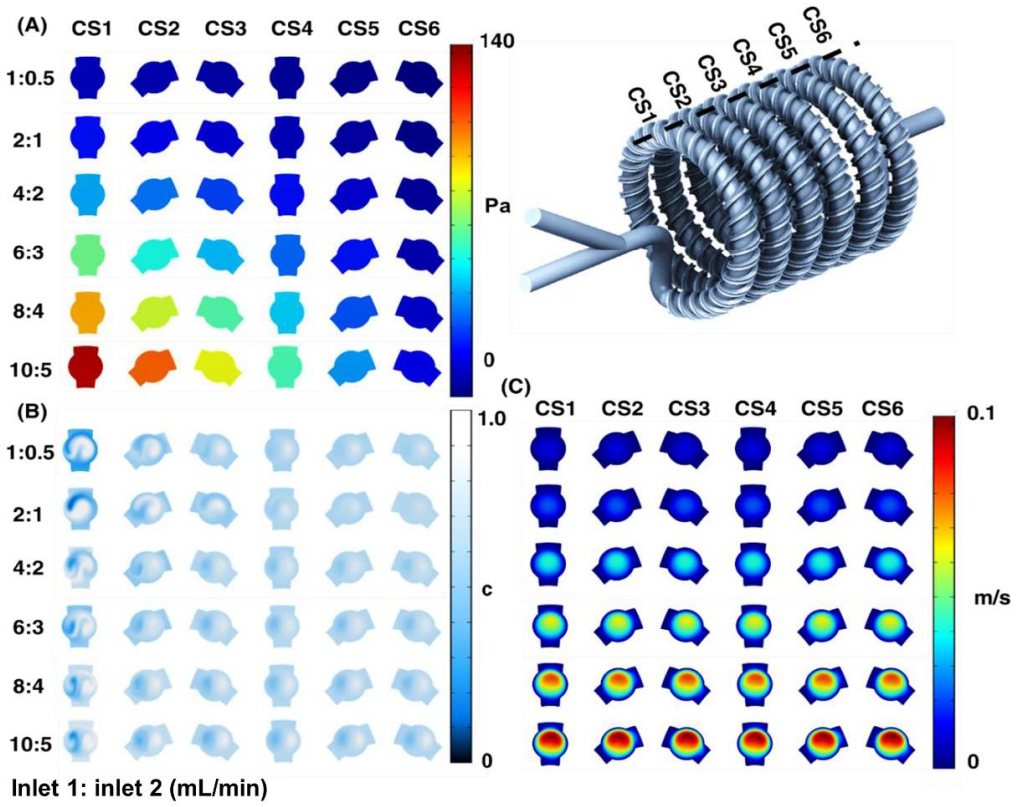

Fig. S3. The simulation results of the micromixer demonstrating A) a constant pressure drop across different flow rate. B) The different mixing strategies at different flow rate, and the mixing of different species across the channel, and C) the velocity profile across the channel.

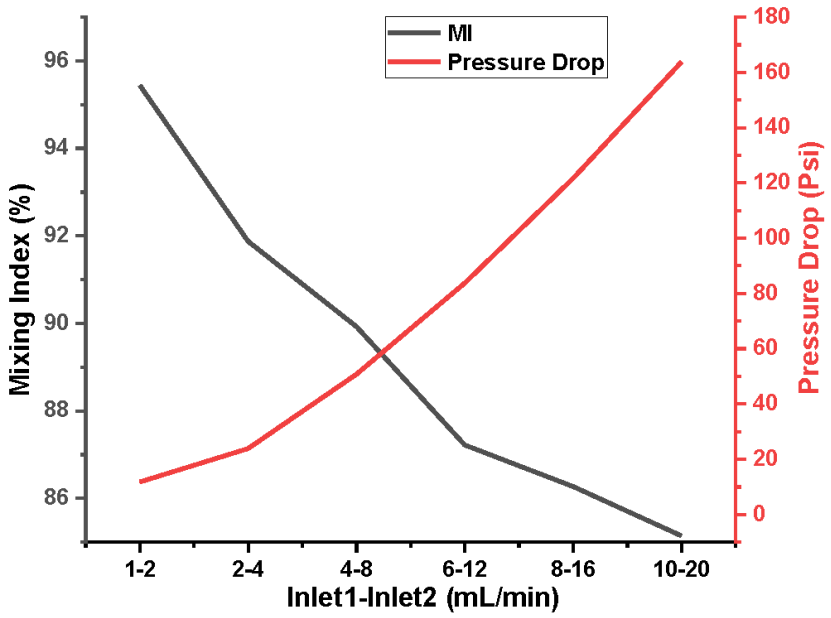

Fig. S4. The mixing index and pressure drop of the micromixer at different flow rates. The results showed that the mixing index was as high as 95% when the micromixer was operated at a total flow rate of 3 mL/min.

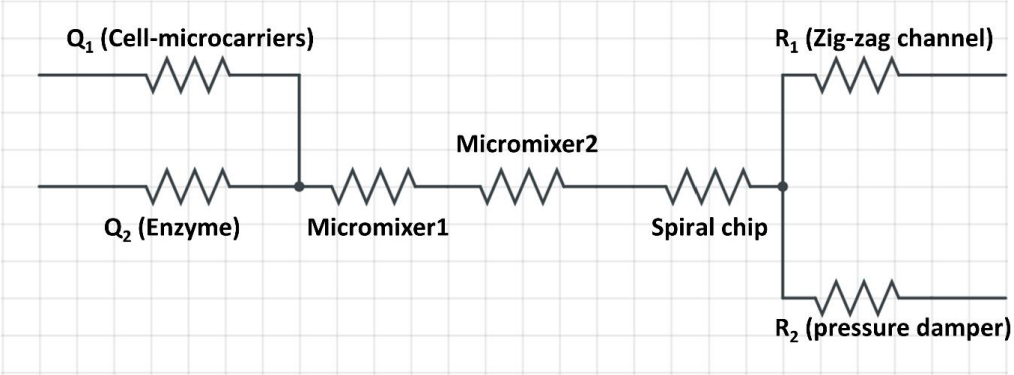

Fig. S5. Electric circuit analogy of our system. The serial connection of devices ensures the flow rate was constant in every device. The flow rate is controlled by Q_1+Q_2.

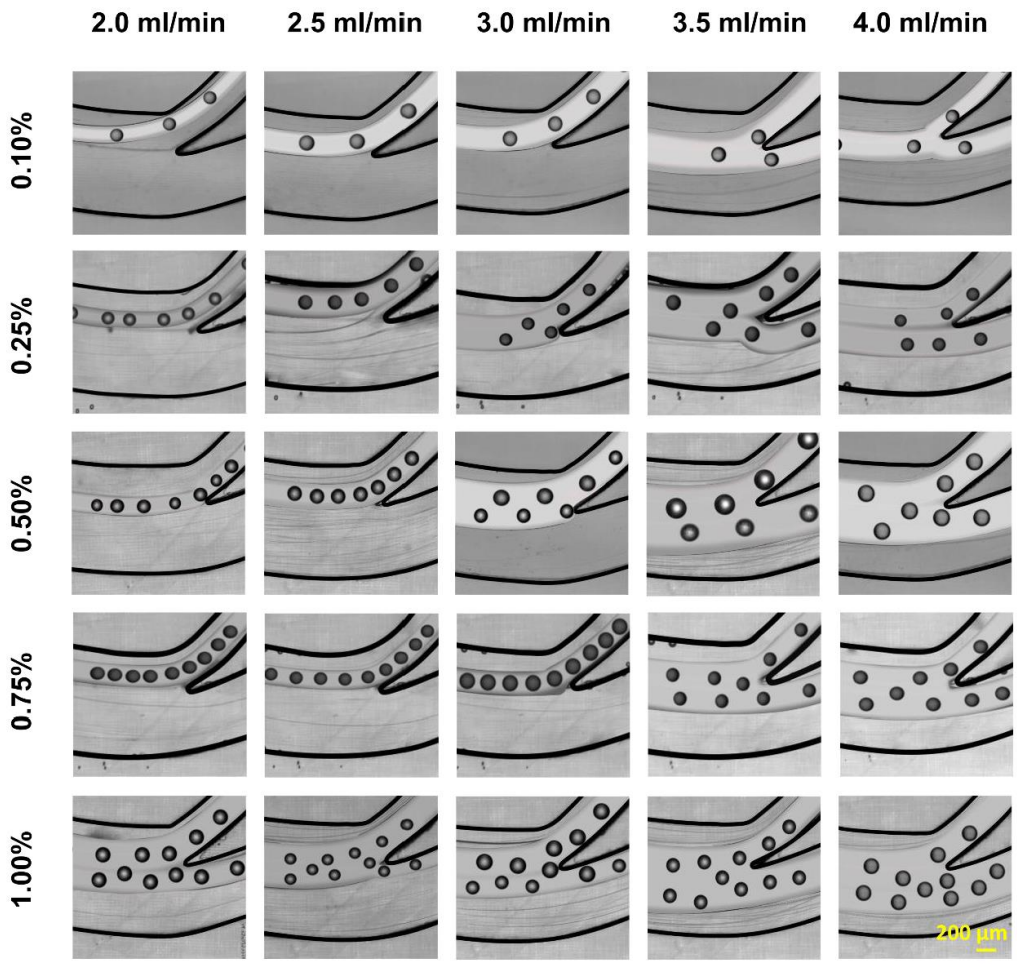

Fig. S6. Spiral device characterization with different concentration of microcarriers under different flow rates. The results showed that when the concentration reached 1% the microcarriers cannot be focused on the inner wall. And the flow rate above 3.5 mL/min cause the particles to disperse even under low concentration. The images were made by stacking the video with Z project, standard-deviation mode in ImageJ to visualise the focusing bands, and the microcarriers were added manually later to represent the concentrations and trajectories.

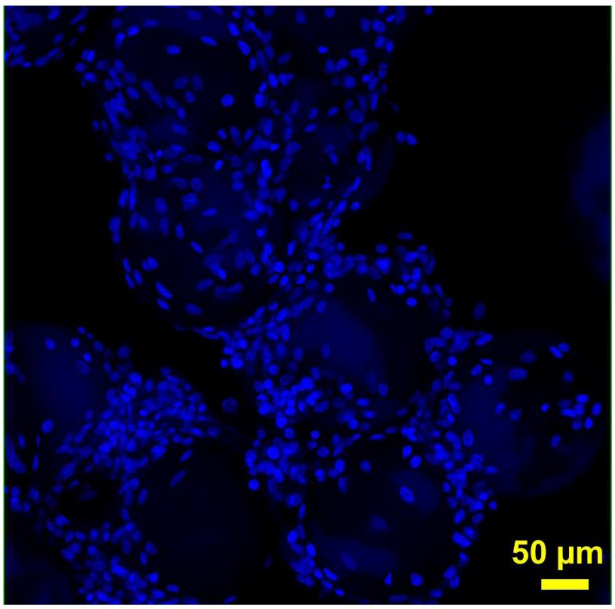

Fig. S7. Confocal microscopy images of aggregated microcarriers before cell harvesting.

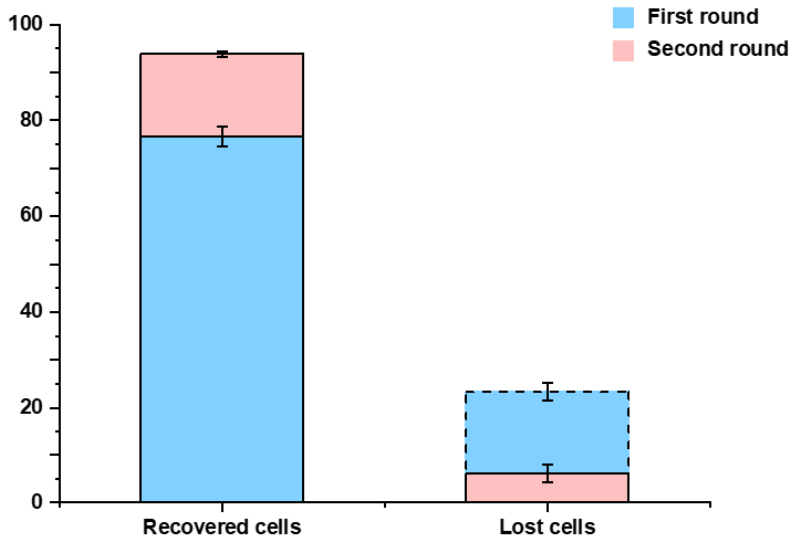

Fig. S8. The total recovery rate of first and second round purification add-up to be 98.83% in total. The blue dashed area of the lost cells was the cells recovered by the second-round separation.

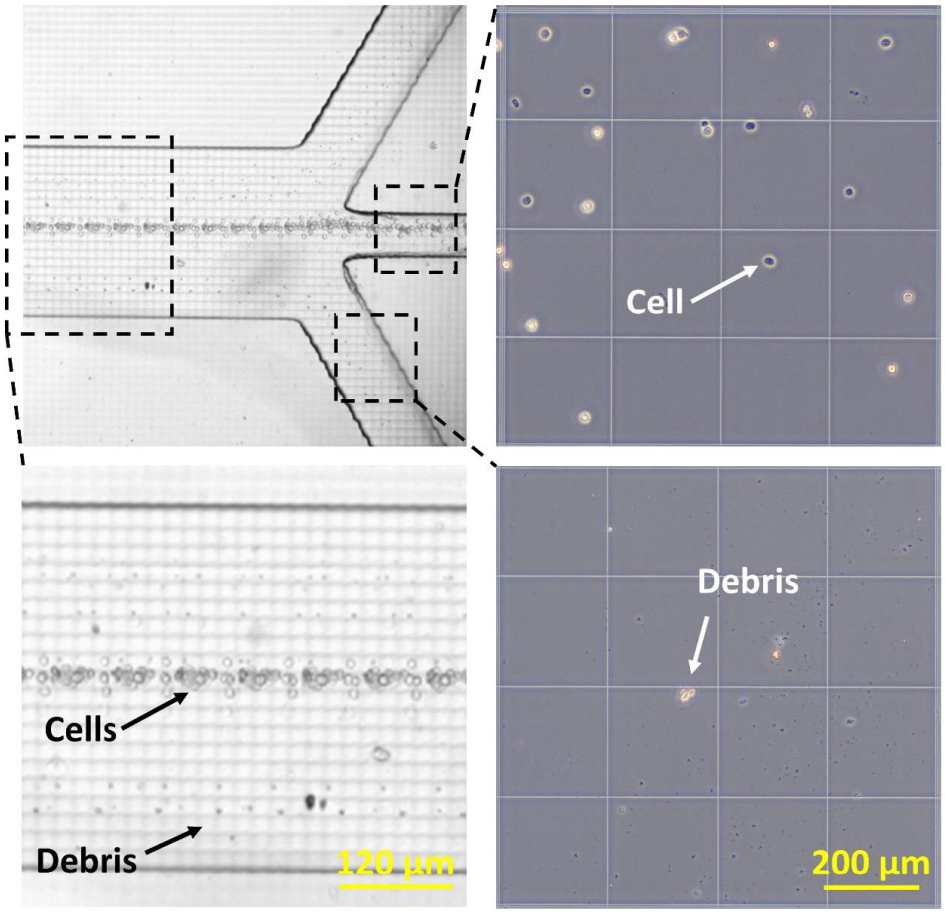

Fig. S9. The concentrating results of MSCs in the zigzag channel. The results showed that the cells were concentrated for about 4.5 times, and the recovery rate was about 99.9%.

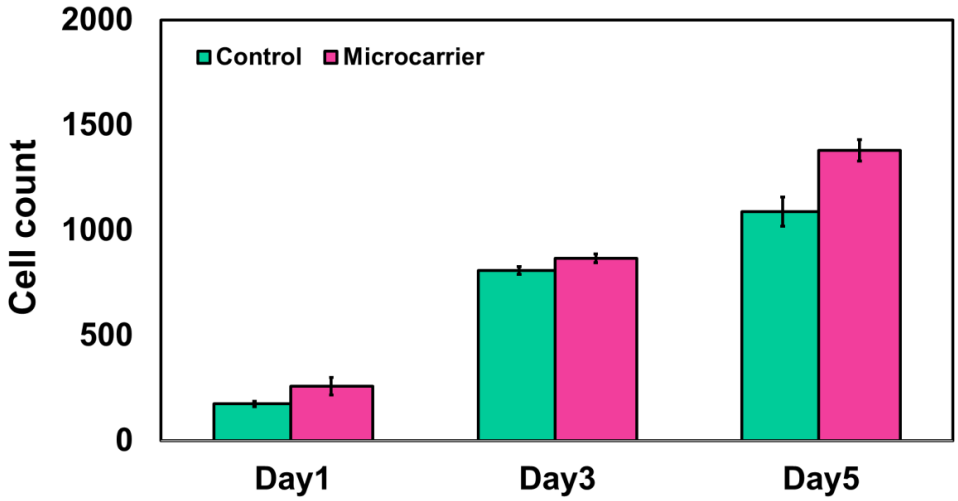

Fig. S10. Comparison of the cell attachment after harvesting by counting the number of cells in the pictures in ImageJ.

References

1. Moloudi, R., et al., *Scaled-up Inertial Microfluidics: Retention System for Microcarrier-based Suspension Cultures.* Biotechnology journal, 2019. **14**(5): p. 1800674.
2. Moloudi, R., et al., *Inertial-Based Filtration Method for Removal of Microcarriers from Mesenchymal Stem Cell Suspensions.* Sci Rep, 2018. **8**(1): p. 12481.
3. Kwon, T., et al., *Microfluidic Cell Retention Device for Perfusion of Mammalian Suspension Culture.* Sci Rep, 2017. **7**(1): p. 6703.
4. Gupta, P., et al., *Optimization of agitation speed in spinner flask for microcarrier structural integrity and expansion of induced pluripotent stem cells.* Cytotechnology, 2016. **68**(1): p. 45-59.
5. Cai, G., et al., *A review on micromixers.* Micromachines, 2017. **8**(9): p. 274.
6. Nguyen, N.-T. and Z. Wu, *Micromixers—a review.* Journal of micromechanics and microengineering, 2004. **15**(2): p. R1.
7. Capretto, L., et al., *Micromixing within microfluidic devices*, in *Microfluidics*. 2011, Springer. p. 27-68.
8. Langille, S.E., *Particulate matter in injectable drug products.* PDA J Pharm Sci Technol, 2013. **67**(3): p. 186-200.
9. Viktorov, V., M.R. Mahmud, and V. Carmen, *Numerical Analysis of Fluid Mixing in Three Split and Recombine Micromixers at Different Inlets Flow Rate Ratio.*
10. Fardjahromi, M.A., et al., *Mussel inspired ZIF8 microcarriers: a new approach for large-scale production of stem cells.* 2020. **10**(34): p. 20118-20128.
11. Cha, J., et al., *A highly efficient 3D micromixer using soft PDMS bonding.* Journal of micromechanics and microengineering, 2006. **16**(9): p. 1778.
12. Xiang, N., et al., *A Multilayer Polymer-Film Inertial Microfluidic Device for High-Throughput Cell Concentration.* Anal Chem, 2019. **91**(8): p. 5461-5468.
13. Taheri, R.A., V. Goodarzi, and A. Allahverdi, *Mixing Performance of a Cost-effective Split-and-Recombine 3D Micromixer Fabricated by Xurographic Method.* Micromachines, 2019. **10**(11): p. 786.
14. Bazaz, S.R., et al., *Obstacle-free planar hybrid micromixer with low pressure drop.* 2020. **24**(8): p. 1-15.
15. Riche, C.T., et al., *Flow invariant droplet formation for stable parallel microreactors.* Nature communications, 2016. **7**(1): p. 1-7.
16. Kang, H., *5. J. Lee, IK Ko, C. Kengia, JJ Yoo, A. Atala.* Nat. Biotechnol, 2016. **34**: p. 312-319.
17. Rafeie, M., et al., *An easily fabricated three-dimensional threaded lemniscate-shaped micromixer for a wide range of flow rates.* Biomicrofluidics, 2017. **11**(1): p. 014108.

4. Chapter 4-Rapid and continuous cryopreservation of stem cells with a 3D micromixer (Aim 3)

In the stem cell industry, cryopreservation is the crucial final step before the cryostorage of the product. However, conventional methods of adding cryoprotecting agents (CPA) to the cells have various limitations in industrial-scale production, including insufficient mixing of cells and CPA, which can damage the cells, create batch-to-batch variations, and cross-contamination. To address these issues, this study proposes a highly efficient micromixer for low-cost, continuous, and automated mixing of stem cells with CPA solutions. Our results show that this micromixer provides a more homogenous mixing of cells and CPA than manual mixing methods, while preserving the stem cell properties, including surface markers, differentiation potential, proliferation, morphology, and therapeutic potentials. This approach offers a promising solution for overcoming the challenges of cryopreservation in large-scale stem cell production.

4.1. Introduction

Stem cell cryopreservation is the last step of the stem cell production process, before storing and delivering the cell products to the clinics for stem cell treatment. This process is carried out by mixing cryoprotectant (or cryoprotecting agent, CPA) and cells in a defined ratio. At the moment, Dimethyl sulfoxide (DMSO) is the most commonly used CPA in MSCs cryopreservation [284, 285], due to the high cell viability and conservation of stem cell properties after thawing. DMSO permeabilises cell membrane, minimises dehydration of the cells and prevent overconcentrating of solutes inside the cells [206, 286-288] to protect cells from water crystallisation. However, exposure to high concentration of DMSO and long-term exposure to DMSO causes detrimental osmotic shock to the cells and might be lethal to them [289-292]. Therefore, minimising the exposure of DMSO to cells [60] and controlled mixing of DMSO and cells is critical for protecting cells during the freezing process.

Currently, the standard technique for mixing large volumes of MSCs with CPA is robotic arms technologies, such as the robotic filling line from Aseptic technologies. In this system, cells are handled in a completely sealed and sterile environment, which meets the current good manufacturing practice (cGMP) needs. Nonetheless, in the robotic arm system, DMSO is pre-mixed with cells in a bulk manner before aliquoting the cell-DMSO solutions into the cryopreservation tubes. This means 100% DMSO is added into the cell solution in a large mixing tank, where direct exposure to high concentration DMSO is, as described above, lethal to the cells. Then the cells are stored in the large mixing tank for up to 2 hours until all the cells are gradually filled into cryopreservation tubes and moved to the temperature-controlled freezer. DMSO changes cell permeability within minutes [293] and the uneven mixing and temporary storage under room temperature causes significant batch-to-batch differences [60] in the MSC products. They can potentially affect the clinical outcome of the cell treatment. The only alternative method, also the most common method used in laboratories, is manual mixing. Manual mixing imposes human error which increases the chance of contamination. It has exceptionally low throughput which also leads to batch-to-batch quality differences at a large scale. Therefore, there is an enormous need for novel technologies that can introduce CPA into cells homogenously [60].

Microfluidic devices can be the perfect solution to mix CPA and cells. They are miniaturised channels used to manipulate liquid inside the channels, possessing low-cost, disposable, and simple operation features and can be easily implemented in different conditions [293]. There were attempts to implement sheath flow-added straight channels to replace the media of the cells to CPA-added media. The advantage of these devices is cell washing happens while CPA is added to the cells, yet the throughputs were only μL/min level [292, 294], which has no potential in industrial application. Among the microfluidic devices, micromixers are miniaturised fluid mixing devices that have attracted significant attention in recent years due to their efficiency and high throughput mixing of a small amount of liquids [295]. They are extensively used in biomedical diagnosis, food and pharmaceutical industries, drug development, and chemical synthesis [296, 297]. Broadly, micromixers are divided into active and passive categories. Active micromixers rely on external energy input such as thermal, acoustic, magnetic, or electric fields to disturb the fluids and achieve high mixing efficiency. Active mixers have a relatively simple structure and high mixing efficiency. But compared to passive micromixers, active micromixers broadly require stirrers, air interface, fine-tuning, integrated electrodes, heaters, and external energy sources, which have low energy efficiency and could be detrimental to some biological samples [295-297]. Therefore, passive micromixers are preferred by the industry. Passive micromixers have complex structures compared to active ones. The complex structures enhance molecular diffusion and chaotic advection and improve the mixing efficiency vividly. In general, passive mixers offer unignorable benefits, including better accessibility, simple fabrication, low cost, high reliability, and easy integration with other systems [296-298].

Therefore, to optimise the stem cells cryopreservation process in the industry, here, we have presented a novel 3D printed microfluidic mixer for efficiently mixing CPA with MSCs in a high throughput manner (Fig. 4.1). The micromixer was firstly characterised by mixing food dye and water, and mixing cells with cytoplasmic staining. The properties of cells cryopreserved by mixing with DMSO in the micromixer were then compared with manual mixing control. The results showed that the presented setup managed to preserve the critical stem cell criteria [285] including viability, growth rate, and phenotype of the cell without changing the properties and differentiation potential.

Although we demonstrated the application of the device here with a small sample size (<5 mL cells), the 3D-printed micromixer has the potential to perform large-scale cryopreservation. It can also be easily integrated into other microfluidics systems [206, 299] or the current industry system at a low cost.

4.2. Material and Methods

4.2.1. Micromixer design and Fabrication

The micromixer was fabricated as previously described [299]. Briefly, SolidWorks 2018 ×64 (SolidWorks Corporation, USA) was used to design the micromixer. The micromixer was then converted into an STL file and fabricated with Clear Resin V4 (RS-F2-GPCL-04) via a Form2 SLA 3D printer (Formlabs, USA). The layer thickness of the print was set at 50 μm to ensure parts have high quality. After printing, the micromixers were carefully removed from the build plate, and the support was cut off by a scalpel and scissors. The device was then washed thoroughly with Isopropyl Alcohol (IPA) three times to prevent the uncured resin from blocking the channel and dried by an air nozzle. Lastly, the device was further cured by a 450 nm UV light in a UV-curing chamber for stabilisation. The channel dimension is shown in Fig. S4.1.

4.2.2. Governing equations and boundary conditions

Laminar flow holds as Reynolds number ($Re = \frac{\rho U d}{\mu}$) does not exceed 700 for the present case. Therefore, assuming incompressible, isothermal, and steady-state Navier-Stokes equation (Eq. (1a)) coupled with the continuity equation (Eq. (1b)) governs the flow field:

$$\rho(u \cdot \nabla)u = -\nabla P + \mu \nabla^2 u, \tag{1a}$$

$$\nabla \cdot u = 0, \tag{1b}$$

Where fluid density and dynamic viscosity are assumed to be $\rho = 998\ kg/m^3$ and $\mu = 8.9 \times 10^{-4}\ Pa \cdot s$, respectively. First, the flow field is solved for the velocity vector field, u, and pressure, P. Then the concentration distribution, c, is calculated by the stationary convective-diffusive transport equation (Eq. (2)):

$$(u \cdot \nabla)c = D\nabla^2 c, \tag{2}$$

with $D = 2 \times 10^{-9}\, m^2/s$ being the diffusivity coefficient between the fluids. The inlets are assigned the uniform velocity boundary conditions with the 1 to 9 ratio for the CPA ($\Delta c = 1\, mol/m^3$) to the cell media. The outlet is set to zero pressure. The remaining boundaries are considered to be no-slip and no-flux walls. COMSOL Multiphysics, a commercially available software based on finite element method was utilized to simulate and predict the laminar mixing of the solutions within the micromixer. Unstructured grid was generated for the entire domain with several boundary layers.

4.2.3. Mixing index

To evaluate the mixing performance of the device, the mixing index or $M.I.$ is defined by assessing the standard deviation of the concentration (σ):

$$M.I. = 1 - \sigma = 1 - \sqrt{\frac{1}{n}\sum_{i=1}^{n} \times \left(\frac{c_i - \underline{c}}{\underline{c}}\right)^2}, \tag{3}$$

where n is the number of sampling points, c_i denotes the molar fraction of samples, and $\underline{c}$ represents the totally mixed molar fraction.

4.2.4. micromixer characterisation

The mixing efficiency was experimentally characterised in two ways. The first characterisation was done by passing red food dye and DI water through the micromixer in a 1:9 mixing ratio at different flow rates. Pictures were taken after the fluids became steady at the inlet and before the outlet of the micromixer. The pictures were then analysed, and the degree of experimental mixing efficiency in these channels was compared with numerical results obtained using Comsol Multiphysics.

The second characterisation was done by mixing cells with a membrane-staining dye. CellBrite® Cytoplasmic Membrane Dyes (Biotium, USA) was firstly characterised by mixing with cells at different concentrations (0.1 µL to 5 µL/million cells/mL). The dye stained the cells seconds after they come into contact. Therefore, a low concentration that cannot stain all the cells (0.5 µL/mL) was used to evaluate mixing efficiency, since even mixing will stain more cells than uneven mixing (although uneven mixing might stain some cells with higher fluorescent intensity). The selected concentration was then added into DMSO (Gibco, Australia), and the dye-added DMSO was mixed with cells

either manually or through micromixer at 1:9 ratio. Then the cells were collected, analysed by microscope and CytoFLEX LX flow cytometer (Beckman Coulter, USA) to record the level of staining of individual cells. The results were compared with a manual mixing CPA and cells, and statistical differences were compared by Two-way ANOVA in Prism (GraphPad, USA).

4.2.5. Cell culture

P7 MSCs were kindly provided by Regeneus. The cells were cultured on T25 (Falcon, USA) flasks with α-MEM (Gibco, Australia) supplied with 10% human platelet lysate (In vitro Technologies, Australia) and passaged 2 times before this experiment to eliminate the impact of cryopreservation. Then, the cells were harvested at 90% confluence with TrypLE enzyme (Invitrogen, Australia) and centrifuged at 500g for 5 minutes to replace the enzyme with Fresh culture media (90% α-MEM and 10% human platelet lysate) at a concentration of 1 million cells/mL.

4.2.6. Experimental setup

The experimental setup is illustrated in Fig. 1A. The cells and DMSO solutions were loaded into 3mL syringes (BD plastic) and connected to the device with Tygon tubings (John Morris, Australia). Two syringe pumps (Fusion Touch, Chemyx Inc) were used to hold these two syringes separately and the flow rate ratio was fixed to 9 to 1 for cells and DMSO syringes. The cells were collected from the outlet by a cryopreservation tube and placed in Mr. Frosty (Sigma Aldrich, Australia) inside the -80℃ freezer immediately. Five control groups were made by adding and pipetting 100 µL of DMSO in 900 µL cells in fresh culture media. One group was put into Mr. Frosty (Thermo Scientific, Australia) immediately after mixing, two groups were left at room temperature (RT) for 30 minutes and 60 minutes, the last two groups were left in 4℃ fridge for 30 minutes and 60 minutes before putting into Mr. Frosty. This was to mimic the cell damage caused by long-term incubation with DMSO. All groups of cells were left in the freezer for one week before thawing for cell characterisations.

4.2.7. Cell characterisations

The cells were defrosted by the standard rapid thawing method, which is to place and stir the tubes in a 37℃ water bath until defrosted [300]. The cryopreserved cells were characterised by their post-thawing viability, growth rate, morphology, stem cell

surface markers staining, trilineage differentiation and immunoproteins staining. The thawed cells were stained with live and dead staining (Abcam, Australia) for 10 minutes in a dark room and proceeded through a flow cytometer to evaluate the viability. To assess the growth rate, the thawed cells were seeded in a 6-well plate at the concentration of 10,000 cells/mL and the media was replaced the next day to wash off dead cells. Images of 5 random positions in each well were taken every day to measure the cell doubling time, and three days later, the cells were stained with live and dead staining. Fluorescent pictures were taken by an IX 70 fluorescent microscope (Olympus, Japan).

To confirm the stem cell properties via surface markers staining, the thawed cells were harvested by TrypLE after culturing and passaging three times. They were washed by DPBS for two times, and fixed with 100 µL methanol (Sigma Aldrich, Australia) in a -20 ℃ freezer for 10 minutes. After that, the cells were washed twice with DPBS and resuspended in 100 µL DPBS with 10 µL anti-CD73-FITC, anti-90-FITC and anti-105-PE antibodies (miltenyi biotec, Australia) and incubated at a 4 ℃ fridge for 1h, according to the manufacturer's protocol. Then the cells were proceeded through CytoFLEX LX flow cytometer and the results were analysed in CytExpert (Beckman Coulter, USA).

Differentiation potential of the cells was confirmed by culturing the cells in 6 well plates with Osteogenic, Chondrogenic and Adipogenic differentiation media (Gibco, Australia) for 21 days, with the media replaced every three days. On the 21st day of culture, the cells were washed three times with DPBS before being fixed by 70% ethanol (osteogenic cells) and 4% paraformaldehyde for 1 h at room temperature. Then, the cells were washed three times with deionised water, and stained with Alizarin Red (osteogenic cells), Oil Red (adipogenic cells) and Alcian Blue (chondrogenic cells, all staining purchased from Sigma-Aldrich, Australia) respectively. The osteogenic and adipogenic cells were stained for 1 h before washing the remaining staining off with deionised water, and chondrogenic cells were stained overnight. The cells were imaged by a bright-field microscope (Olympus, Japan).

The therapeutic properties of the cells were verified by priming the MSCs with cytokines stimulation and staining the change of expression level of the

immunoproteins. The MSCs were seeded in 6 well plates after thawing. When the cells reached 50% confluence, priming media containing 10ng/mL TNF-α protein and 100ng/mL IFN-γ protein (Stem cell technologies, USA) were added to the wells, and incubated in the incubator for 24 hours. Then, the cells were harvested and resuspended in 1 mL cold DPBS and stained with HLA-G and iCAM antibodies (Biolegend, Australia) for 1 hour. The cells were then proceeded through CytoFLEX LX flow cytometer, and the results were analysed in CytExpert.

4.3. Results

4.3.4. Design principles of the micromixer

Fig. 4.1 illustrates the principle of micromixing and how the flows are guided through the micromixer structures. The design consists of two back-to-back circles with average diameters of $18\,mm$ with manifolds of $d = 1.5\,mm$ twisted through the channels' winding shape. The initial stage begins with introducing the stem cells solution and the CPA into their inlet manifolds. The micromixer's volume and footprint are ~ 668 mm^3 and 11×22×41 mm^3, respectively.

Mixing at the micro-scale is often achieved by a common technique called split and recombination (SAR) [301]. Here, a group of five different SAR components, namely one-sided, middle-sided, and double-sided screws, are arranged sequentially. Fig. S4.1 shows the shape of the SAR units comprised of at least one division and reunion of flow that undergoes a swirling path to induce vortices and mass transport. Moreover, the double-sided unit takes advantage of the third dimension to ensure efficient 3D mixing. After conducting a preliminary analysis, the best combination of the units and their order was selected.

The unique design of the 3D micromixer allows the velocity to change effectively across the fluid's path required to achieve high-performance mixing. Fig. 4.2A depicts the flow shifts along the channel and the lateral migration of the mass at a high Reynolds number of 550. The joints between each unit show that fluid tends to follow its previous path due to the fluid inertia and the micromixer's curvature. This is known as the Coanda effect, and in the present case, it significantly enhances the mixing efficiency as a consequence of strong chaotic flow.

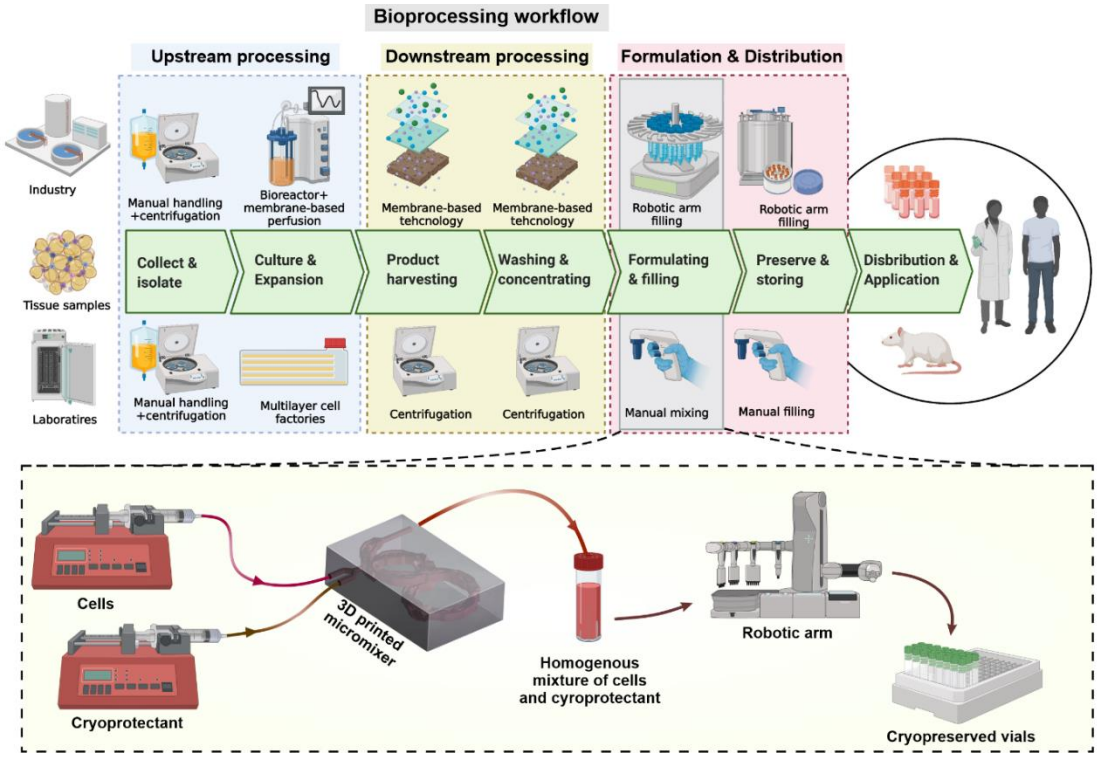

Fig. 4.1. Stem cell production process and the potential application of our proposed micromixer during this process. The micromixer can be either integrated into the current robotic arm system to perform homogenous mixing of stem cells and cryoprotectants or used separately in laboratories to increase the speed of cell-cryoprotectant mixing.

4.3.2. Effect of Reynolds number on mixing performance

The mixing efficiency over a wide range of Re was explored to evaluate the performance of the micromixer and the mixing mechanism. As Re increased from 1 to 60, the effect of convection becomes predominant over the diffusion. There is also around 5% fluctuation in the $M.I.$ between $Re = 30 - 100$, which is due to the nature of the flow where the two inlets meet and create disturbances. The geometry of the junction and the flow rate ratio might reflect on the flow state, creating discontinuities in the mixing performance. Fig. 4.2B illustrates the dispersion of concentrations along the channel walls for these Reynolds numbers. As shown in Fig. 4.2C, the mixing index is above 94 percent for $Re < 1$ regardless of the operational condition. This relatively low-speed, also corresponding to low-Peclet ($Pe = \frac{Ud}{D}$), flows are the most suitable condition for the diffusion-based mixings, where lateral transport occurs within the time frame of the main flow. That is, $Re = 0.1$ in Fig. 4.2B shows a gradual gradient of concentration as a manifestation of the diffusion mechanism.

Before the critical Re of 60, mixing is accomplished mainly through diffusion. Most passive micromixers use geometric-based manipulations of fluids, such as curvature-induced Dean flows [285] and out-of-plane translation, which are associated with convection and proportional to $U^{1.63}$. Accordingly, as the Reynolds number exceeds 100, convective mixing outweighs diffusion. Thus, $M.I.$ experiences a sharp growth for Re ranging from 100 to 550, after which it almost remains constant. Here, the convection-based concentration contours in Fig. 4.2B further confirm the proposed micromixer can achieve efficient mixing within a shorter mixing length. Overall, the proposed micromixer can efficiently maintain a mixing quality above 82% in a vast range of Re.

4.3.3. Pressure and shear stress inside the micromixer

Shear stress level within the channel is an important factor that needs to be evaluated, especially when proposing a new system that involves sensitive biological materials, including stem cells. High shear stress may jeopardise the cell viability at high Re. Considering a simplified model, the shear stress in a square duct is given as [302]:

$$\tau_s = \mu \cdot \dot{\gamma} = \frac{6\mu Q}{h^3} = \frac{6\mu^2}{\rho h^2} Re, \quad (4)$$

where $\dot{\gamma}$ is the shear rate, Q is the flow rate, and h is the height of the square cross-section. It is evident from Eq. (4) that the analytical shear stress linearly depends on the flow condition or Re with a slope of $\alpha = \frac{6\mu^2}{\rho h^2} = 7.62 \times 10^{-4}$ as a function of fluid properties and geometry.

In the peripheral blood system, the reported values for τ_s are approximately less than $0.1\ Pa$ considering both small and large capillaries. While in the cardiovascular system, τ_s is on the order of $6\ Pa$ for physiological or exercise conditions [303, 304]. This can have a considerable impact on the metabolic response, behaviour, viability or stem cell fates if they experience the stress for a significantly long time, i.e., longer than an hour [305, 306]. It took less than 2 seconds for the cells to pass through the micromixer, which is far shorter than the above-mentioned conditions. As a result, the maximum shear stress is calculated over the range of studied Re and the trend is shown in Fig. 4.2D. As discussed earlier, the shear stress was expected to change by Re linearly. However, the value of the α in the numerical model was calculated 14.6-fold higher

using the equation provided for the straight duct. This difference stems from the complexity of the geometry under the study that causes high efficiency mixing but at the cost of slightly higher shear stress.

Input energy is another criterion of using high-throughput microfluidic devices for cell applications. Micromixer design is the crucial factor in controlling it [301]. Pressure consumption defines the trade-off between the throughput and efficiency. The amount of pressure consumed in the proposed micromixer is illustrated in Fig. 4.2E. Owing to the small secondary flows at $Re < 100$, a linear relationship was obtained for the pressure usage, whereafter it was estimated via a quadratic function as a result of large vortical patterns. It was then postulated that the proposed mixer design required a relatively low pressure of less than $0.9\ kPa$ to mix the biological solutions efficiently and safely.

The cross-sectional concentration laminae and shear stress can better represent how the tortuous design of the micromixer induces swirls and vortices. Fig. 4.2F illustrates the shear stress and concentration gradient on the cut-planes intersecting each screw-shaped component and perpendicular to the main flow. The chaotic flow created in every region of the micromixer implied that the cells and reagents can be efficiently mixed (the shear stress can be also presented by the vorticity ($\nabla \times u$)). Flow stretched and folded from the moment the two solutions met each other, and the effect continued along the channel most dominantly within the screw-shaped units. Moreover, the highest stress grew mainly near the walls because of the high-velocity gradient, yet this effect is small in the proposed micromixer due to the large cross-sectional area of the channel.

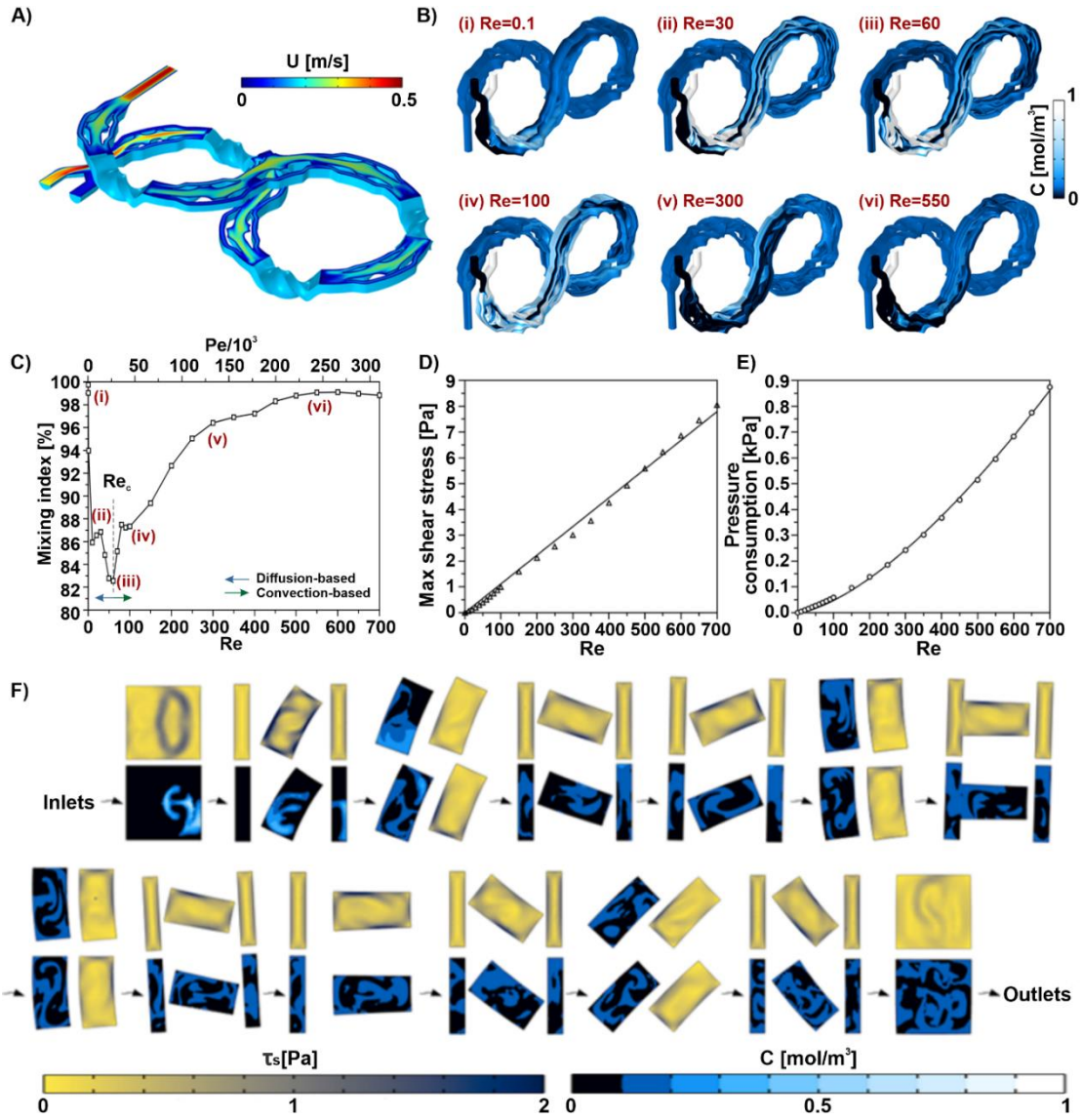

Fig. 4.2. Simulation results demonstrate the mixing performance, pressure, and shear stress in the micromixer. A) Velocity changes on the mid-plane at Re=550. The alteration of pathways and the complex geometry induce velocity shifts and thus, chaotic, and secondary flows. B) The concentration distributions on the micromixer's walls at different Re, representing the mixing mechanisms. C) The calculated mixing index at various operational Reynolds numbers. The corresponding Re to minimum M.I. is known as the critical Reynolds (ReC), representing the mixing mechanism's transition from diffusion to convection. D) The maximum shear stress during the mixing as a criterion for cell viability. Although it exceeds the physiological limit of 6 Pa, short exposure time as well as a small coverage area allow most of the cells stay alive at the end of the mixing cycle. E) Pressure usage at different Reynolds numbers highlights the relatively small pressure requirement. F) The changes in concentration and shear stress distribution at cross-sections inside all 12 units at Re=550. The dispersion of 0.1 mol/m^3 entails the effectiveness of the device.

4.3.4. Mixer characterisation

The mixing efficiency of the micromixer was first characterised via mixing of food dye and water. To test the device performance, we have used three different flow rates while

maintaining the flow rate ratios as 1:9 (Fig. S4.2). The results show that the micromixer can fully mix the samples, with a mixing efficiency of more than 85% across all flow rates. At very slow flow rates, the dominant fluid regime was Stokes and samples had enough time to properly mix with each other. At high flow rates, however, the fluid behaviour became more chaotic. Given the special geometry of the micromixer, it could still mix the samples well at extremely high flow rates and non-laminar flow regime.

Fig. 4.3 shows the results of mixing efficiency characterised by mixing cells and cytoplasmic dye. The lipophilic cytoplasmic membrane dye stains the cells immediately after contact (Fig. S4.3). Therefore, reducing the concentration of staining used can showed the effectiveness of staining better. Fig. S4.3 shows the effect of different concentrations of cytoplasmic dye staining on 1 million cells/ml. Above 1 μL/mL concentration, all cells were stained immediately after adding the staining. When the staining concentration was reduced to 0.5 μL/mL, some cells remained unstained even after 20 minutes of incubation. Theoretically, a micromixer should provide more homogenous staining of cells due to the high mixing efficiency and the continuous mixing feature. This was proved by mixing dye added DMSO and cells in the micromixer, the idea is illustrated in Fig. 4.3A. Fig 4.3B shows the flow cytometry results of membrane dye mixing. The cells processed by micromixer has a smaller area of distribution, and almost all cells (99±0.13% cells of over 3000 events) were stained with the dye, while the manual mixing control has only 67±4.11% of cells stained. The box plot in Fig. 4.3B shows the cells in the micromixer group were stained more homogeneously than the manual mixing control group since the stained cells distributed in a smaller region than control group in X-axis (FITC-stained). The difference between the two groups was significant ($p<0.001$). Fig. S4.4 are the microscopic images of cells from these two groups, and the results aligned with Fig. 4.3B.

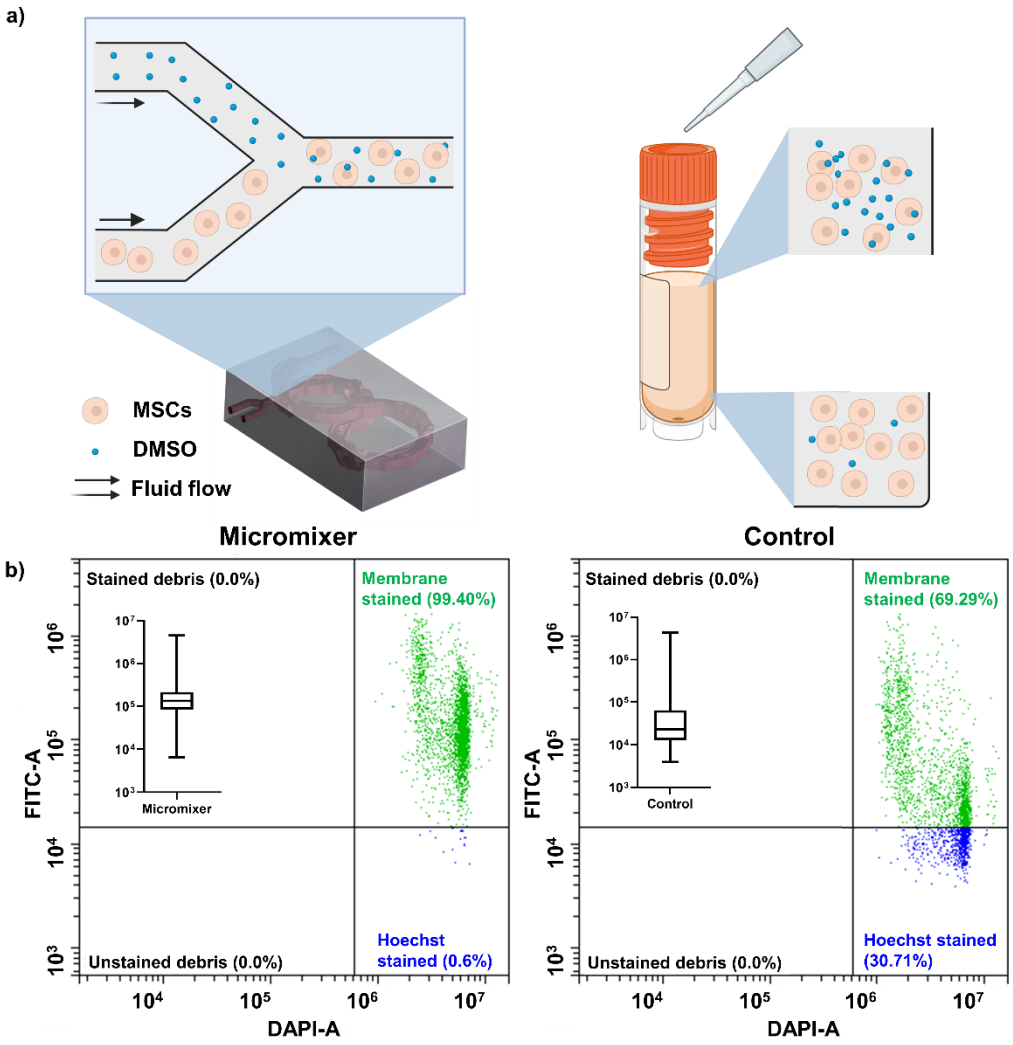

Fig. 4.3. Cytoplasmic dye was added into DMSO to verify the homogeneous mixing of micromixer experimentally A) Schematic illustration of the mixing strategies between micromixer and manual mixing. The micromixer introduced DMSO into cells at a constant ratio while manual mixing faces challenges of uneven distribution of DMSO at the beginning B) The flow cytometry results of cells mixed with cytoplasmic dye-DMSO in two methods, micromixer (left) and manual mixing (right). The inserted box plots show the level of FITC staining of each cell were summarised in box plot. The results show that the cells in the micromixer groups were more evenly stained than the manual mixing group, and the difference of distribution was significant ($p<0.001$).

4.3.5. Cells characterisation

Viability, morphology, proliferation, differentiation potential and surface protein expression are the key parameters to evaluate the effect of cryopreservation methods for MSCs [285]. Therefore, passage 9 MSCs was used to verify the capability of the device to mix cells and CPA in the correct ratio to protect the cells during cryopreservation.

Fig. 4.4A and 4.4B show that the cells' viability and proliferation rate were similar to the instant cryopreserved control group, indicating that the micromixer and handling process did not damage the cells. Meanwhile, the RT and 4 ℃ groups showed time-dependent reduction of cell viability and growth rate, and the microfluidic group had significantly higher viability and proliferation rate compared to them. Fig. 4.4C compares the cell morphology of all groups after three days in culture. The micromixer processed group showed similar size and spindle, fibroblast-like shapes to the instant cryopreserved control group, indicating the morphology, structure and integrity of the cells were not altered. Live and dead staining of cells after 3 days in culture show that the attached cells were healthy cells with no long-term damage caused by the device (Fig.4.4A). There was no change in cell morphology after exposure to DMSO for 30 and 60 minutes, however the number of dead cells in 30- and 60-minutes incubation groups increased compared to the control group, which was stored in the -80℃ freezer immediately after mixing. Fig. 4.4C and D also show an increased cells size in RT and 4 ℃ groups, indicating potential loss of stem cell pluripotency [65, 108].

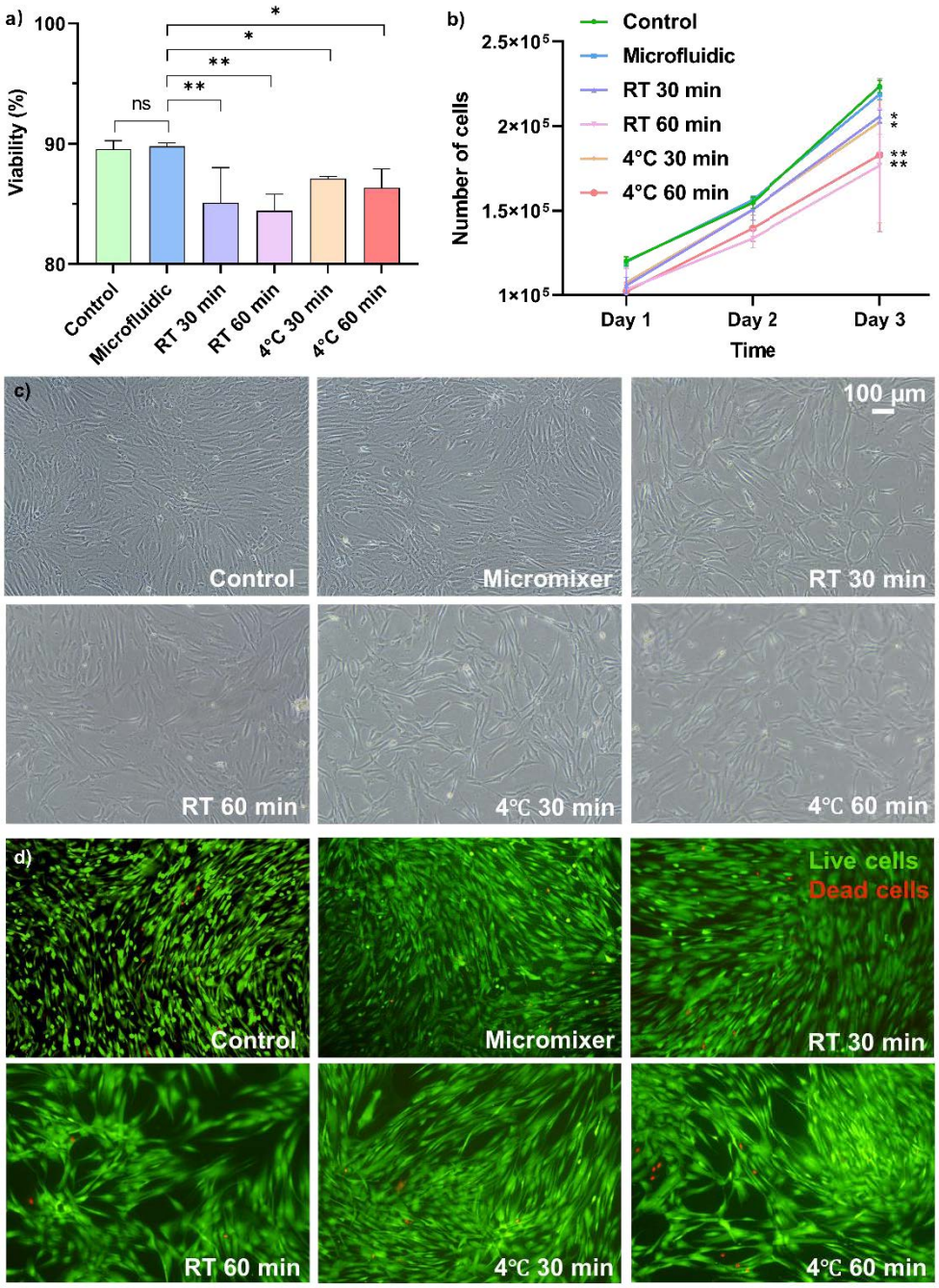

Fig. 4.4. Cell viability and proliferation rate after exposing cells to DMSO under different conditions before cryopreservation. A) Post-thawing viability of cells in different groups. Viability of each group is: 89.79±0.28% for microfluidic group, 89.55±0.69% for instant mixing control group, 85.10±2.92% and 84.44±1.38% for RT 30, 60 min groups and 87.09 ±0.19%, 86.35±1.56% for 4℃ 30- and 60-min groups B) Growth rate of cells after seeding them in 6 well plates for 3 days, micromixer and instant preserved control groups had significantly higher growth rate than the other groups ($p<0.001$). C) Cell morphology and D) live and dead staining in 6 well plates on day 3 show mixing the cells and CPA in the micromixer does not damage the cell viability, morphology, and phenotype of cells.

The stem cell properties were verified by surface marker staining, trilineage differentiation, and surface immunoproteins staining. After three passages, the cells were harvested and stained by fluorescence-tagged antibodies, and the results showed that the MSCs preserved their stem cells properties (Fig. 4.5A). Trilineage differentiations showed the cells preserved their differentiation potentials (Fig. 4.5B), as indicated by the Alizarin Red-stained mineralised matrix of the osteoblasts, Alcian Blue-stained glycosaminoglycan complex of chondrocytes and Oil Red-stained lipid vacuole of adipocytes. HLA-G and iCAM are two surface-expressed immunoproteins responsible for interacting with the immune system. HLA-G is an immune prohibitor that should remain low after priming, while iCAM is an immune-promotor that increases the immune activity after priming. Fig. 4.5C shows that the micromixer-processed cells are expressing the surface proteins at a similar level to the control group, indicating the therapeutic potential of the MSCs is well-preserved.

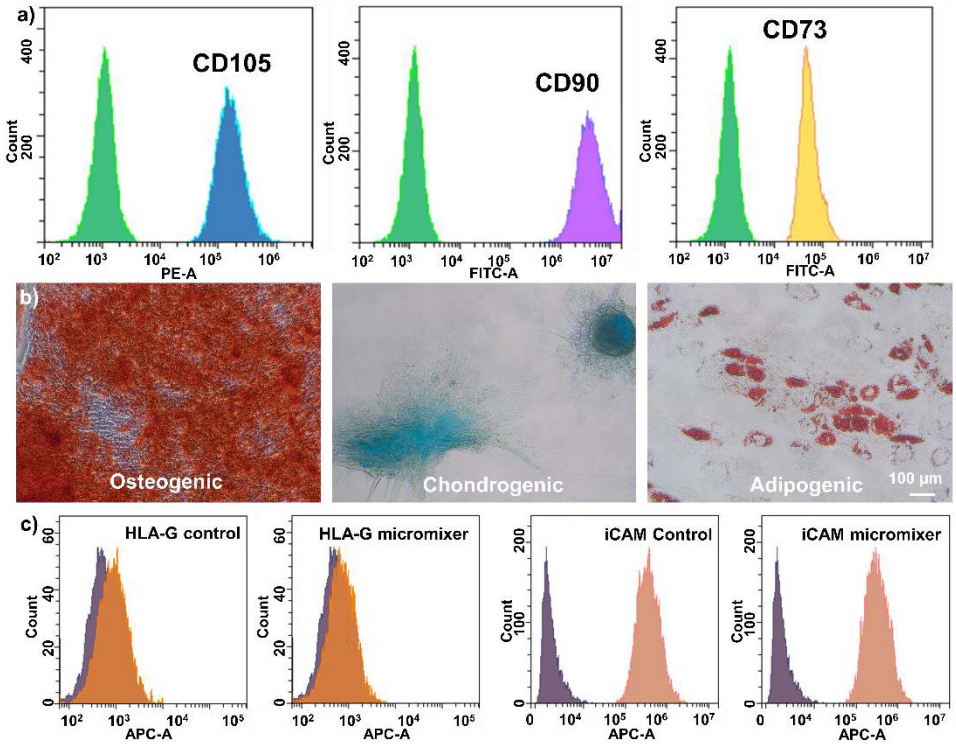

Fig. 4.5. Characterisation of stem cell properties after thawing. A) The micromixer-cryopreserved cells preserved their MSCs identities, expressing all 3 MSCs surface markers. B) The osteogenic, chondrogenic and adipogenic cells showed that the micromixer-cryopreserved cells also maintained the differentiation potentials. C) Comparison of the expression levels of the surface therapeutic markers in the control and microfluidic groups, showing the therapeutic properties of the MSCs passed through micromixer were not hampered.

4.4. Discussion

The debate on using cryopreserved or fresh cultured MSC for patient treatment has continued for many years. CPAs were found to damage the cell viability, integrity, structure, therapeutic potential when they were used at a high dosage and were left with the cells for an excessive period [36, 284, 285, 307]. These damages caused by cryopreservation are one of the reasons for unsuccessful clinical trials [308]. For example, low cell viability MSCs failed to treat chronic inflammatory disorder in an clinical study [309], and cryopreservation-induced cytoskeleton damage reduced the T cell activation capacity of MSCs [310]. Luckily, the cell damage caused by cryopreservation is reversible. There are attempts to reverse or avoid the cell damage caused by cryopreservation by recovering and culturing the stem cells for a few passages before administration or use the MSCs without cryopreservation [36, 285, 311]. The outcomes were successful, but this method increases the cost of cell culture consumables, limits the therapeutic window (the treatments need to be carried out according to the confluence of the cells) and accessibility to small clinics, and create the need for cell culture-related technicians.

Thus, cryopreservation of MSCs remains one of the standard procedures in MSC treatment, and more optimisation of this process is urgently need [308]. Especially in the bulk mixing process, a high concentration of DMSO added into the cells results in the instant formation of large pore on the cell membrane [312] and a large proportion of cell death [289-291], which can be the main reason for the batch-to-batch difference of the products in the industry at the moment. Here, we used a novel micromixer to continuously mix up CPA and MSCs to improve the cryopreservation process. We employed a new method to demonstrate the homogenous and continuous micromixer mixing by processing cells with cytoplasmic dye added DMSO in the micromixer. Our results showed that the cells processed by our micromixer have a significantly more homogeneous mixing than manual mixing group (Fig. 4.3). In this paper, we used a total flow rate of 1 mL/min to characterise the micromixer and cells. This flow rate sits at a diffusion-based dominant regime in the mixing index graph (Fig. 4.2C), where the mixing efficiency is high enough to create a homogenous sample at the channel output. Viability of cells stays as high as 90% after passing through the device and cryopreserved by Mr. Frosty for one week (Fig. 4.4A), and the growth rate (Fig. 4.4B),

morphology (Fig. 4.4C), and in-culture viability (Fig. 4.4C) are indistinguishable from the control. Since this is a small lab-scale experiment, we believe that a difference in viability can be observed when it comes to large-scale, where mixing is harder to happen and cells are exposed to high concentration DMSO for a longer period, as shown in Fig. 4.4. The well-preserved stem cell identity was verified by the three MSC surface markers staining (Fig. 4.5A). the MSCs differentiation potential was confirmed by trilineage differentiation (Fig. 4.5B) and most importantly, the immunoproteins expression level in response to stimulations was unaffected (Fig. 4.5C). This indicates that the device and the whole handling process had no mitigation of the cell properties. DMSO was found to exert heat while mixing with cells [313, 314], which might cause damage to the cells in large volumes. The small mixing volume and large surface-to-volume ratio of the mixer can potentially help release the heat [315], and although it is hard to prove, the cell properties measurement results indicated that there is no damage caused by fusion heat. The manufacturing method is robust and can tolerate high pressures up to 300 psi or more without any trace of channel disruption or crack propagation. It has been proved that MSCs can proceed in microfluidic devices with flow rate as high as 30 mL/min without damaging the cells [8]. Also, the potential of this device is not limited to mixing DMSO and stem cells, it can be used to mix cells with other reagents at any given ratio.

The micromixer possesses multiple advantages compared to the current CPA mixing methods. First, this micromixer has high mixing efficiency, and it can reach 99% at high Re, which ensures the complete mixing of DMSO with cells in a short time in the correct ratio. The cells only take 0.5 seconds to pass through the whole system, which minimizes the potential damage to the cells caused by shear forces or micromixer. The simple setup, designs, and small footprint of the device gives a low faulty rate to the system and can be easily integrated into any current industrial system in a closed-up manner by connecting the devices and bioreactors/cell containers with a peristaltic pump. This closed system meets the need of the current Good Manufacturing Practice (cGMP), which requires no human interference in the cell manufacturing process. Lastly, the device has the potential to increase the throughput to fit industrial applications by increasing the flow rate and paralleling multiple devices. As shown in

Fig. 4.2C, the mixing index of the micromixer stays above 90% across multiple flow rates.

4.5. Conclusion

This paper described a novel micromixer to mix stem cells and CPA for the stem cell industry. This device offers a labour-free, rapid, evenly, and continuous mixing, which the current methods cannot achieve. We used cytoplasmic dye to show the micromixer can mix cells and CPA more homogenous than manual mixing, with minimum cell damage introduced during the process. Our results showed that cells processed by the micromixer have well-preserved viability, morphology, and cell growth right after thawing. Stem cell properties such as surface markers, differentiation potentials, and immunoproteins expressions that respond to stimulants were well preserved. These results strongly support the fact that our device can be adapted by the bioprocessing industry and has the potential to be used for numerous clinical applications.

Supplementary information section

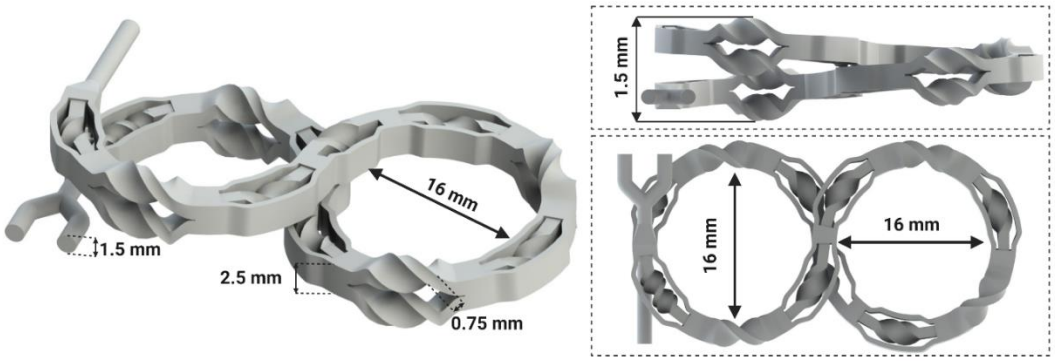

Fig. S4.1 The design and dimension of the micromixer. Mixing units used in the proposed design each has unique geometry and functionality, hence flow characteristic.

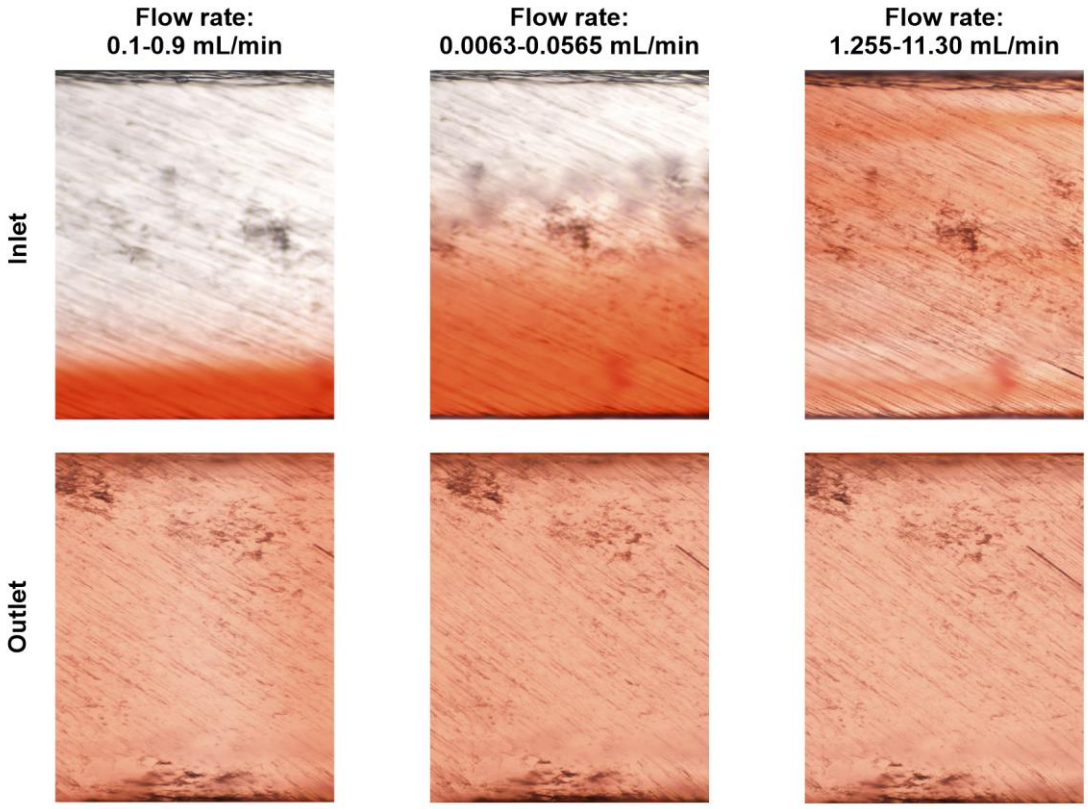

Fig. S4.2 The results of food dye mixing with DI water characterise the mixing efficiency of micromixer in real case. The figures of the outlet showed homogenous mixing of food dye across different flow rates.

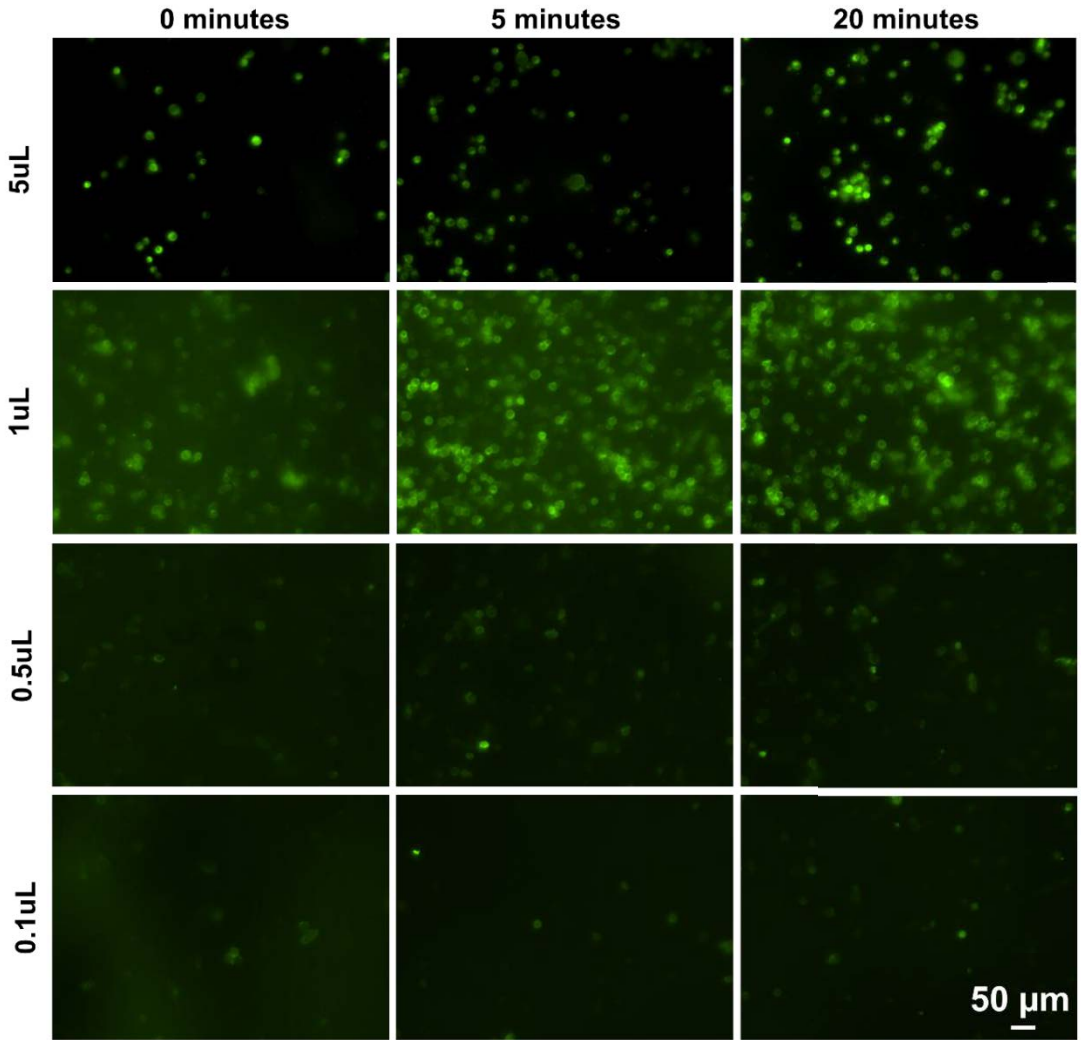

Fig. S4.3 Characterisation of cytoplasmic dye concentration before using it for mixing experiment. The results showed that above 1 µL/million cells/mL, the cells are overstained from 0 minutes. Therefore 0.5 µL/million cells/mL was used to characterise the micromixer.

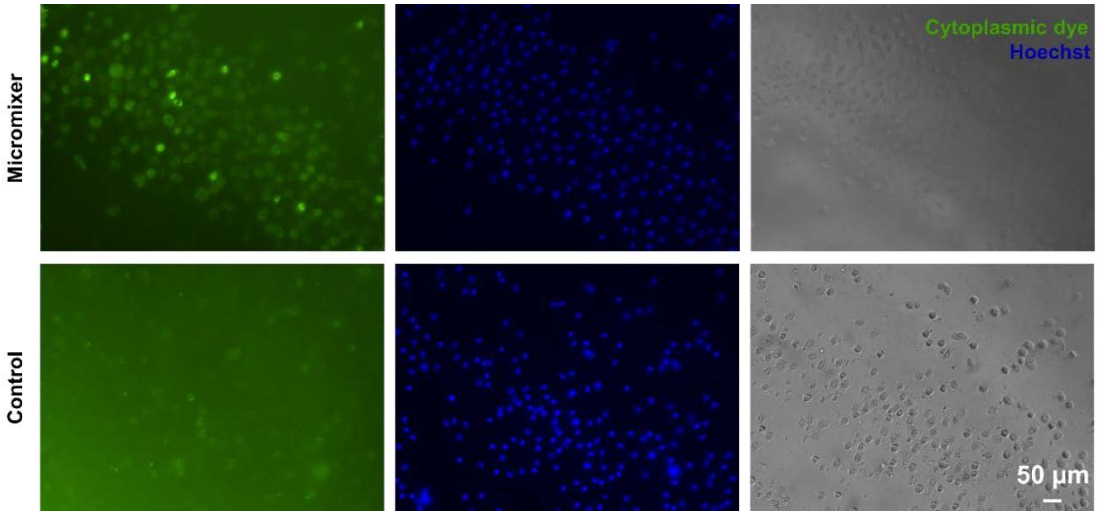

Fig. S4.4 The micromixer mixing group and manual mixing group control cells after 15 minutes of staining. Results showed that most of the cells in micromixer groups are stained by both Hoechst and cytoplasmic dye, while many cells in the manual control groups are not stained with cytoplasmic dye.

5. Chapter 5- Precise prediction and modelling of bioreactor culture condition with microfluidic-based single cell metabolomic analysis (Aim 4)

In large-scale cell cultivation, monitoring bioreactor conditions is essential to ensure the maintenance of healthy cells and production of high-quality cell products. However, the cultivated meat industry, being a relatively new industry, lacks standard criteria for bioreactor monitoring. In this study, we presented a microfluidic-based single cell metabolism detection method that allows for precise monitoring of localized lactate production in cells. This method provides highly sensitive and accurate metabolomic information about cells' behavior in different parts of the bioreactor, potentially offering high-resolution data for bioreactor monitoring and predictions.

5.1. Introduction

The cultivated meat industry has experienced rapid growth since the first proof-of-concept product was developed in 2013. Over 100 companies have been established, raising a total of 1.8+ billion dollars by 2021 [316]. Despite this progress, the industry is not yet ready for commercialisation. As a novel industry in the agricultural field, most of the production process and technologies are adapted from the stem cell therapy industry. This includes obtaining cells from animal tissue samples, establishing cell banks, and expanding cells on a large scale. Then the cells are harvested from culture vessels, differentiated into mature cells and composite with other cell types onto the scaffold and packaged into the final products [316]. Bioprocessing control in each step is crucial for high-quality and consistent production [317]. However, the cultivated meat industry lacks a standard for bioprocessing control, as does the therapeutic sector. Although some studies [318-320] proposed cell quality standards for stem cell therapy, these rely heavily on manual operation and are difficult to integrate into a fully automated cGMP production process and they have not yet been widely accepted.

Among all the parameters, Lactate level is one of the most critical criteria in bioprocessing monitoring [321]. as it can negatively impact cell proliferation and metabolism [322, 323]. Therefore, it is essential to maintain stable lactate production levels for large-scale bioprocessing. In animal muscle cells, lactate plays a more complicated role. Previous studies have shown that intracellular lactates of muscle cells increase dramatically after differentiation [324]. In contrast, lactate can suppress proliferation and promote myoblast differentiation [325, 326], increasing the number and size of myotubes formed and helping in regeneration [327]. Lactate also increases the generation of reactive oxygen species (ROS) [326], which leads to cell ageing and apoptosis. Aged cells lose their potential to differentiate [328]. Monitoring and measuring pH in the production process can be a good indication of the healthiness and differentiation stage of muscle cells. Current lactate monitoring relies on measuring the change in pH. Electrochemical and optical sensors are the two primary sensors used [329]. Electrochemical sensors provide accurate and real-time monitoring of bioreactor conditions, but the sensor is fragile and bulky. Optical sensors have a smaller footprint and are therefore easier to miniaturise and integrate into different bioreactor systems, yet the accuracy of optical sensors is not ideal. Meanwhile, both sensors are used to

measure the pH level in bulk, which means that measuring the metabolism of individual cells in the bioreactor or local pH level is impossible. This is particularly important since a slight pH change can significantly impact the viability and concentration of cells [329]. Only local, small fraction pH measurements can be fast and sensitive enough to detect the changes before cells are damaged. There are microfluidic sensors available for measuring pH at local scale or small sample size [330, 331] (including commercial sensors from PreSens Co.). The accuracy of the sensors are hugely improved, but there are no sensors available for measuring local pH at a single cell level. The development of such sensors could enable more precise and sensitive monitoring of bioprocessing and provide insights into cell behaviour at a more granular level.

In this study, we present a microfluidic-based approach with automation potential for monitoring lactate production in individual muscle stem cells. Our method is simple to operate and involves the use of a pH-sensitive dye to detect single-cell lactate secretion (Fig. 5.1). By analysing and comparing lactate secretion across cells cultured for different durations, we were able to correlate lactate secretion levels with cellular senescence. Importantly, this approach provides a more precise and sensitive means of monitoring lactate production levels in bioreactors. Our findings demonstrate the potential for this method to accurately predict lactate production levels in large-scale bioprocessing and provide insights into cellular behaviour at a single-cell level.

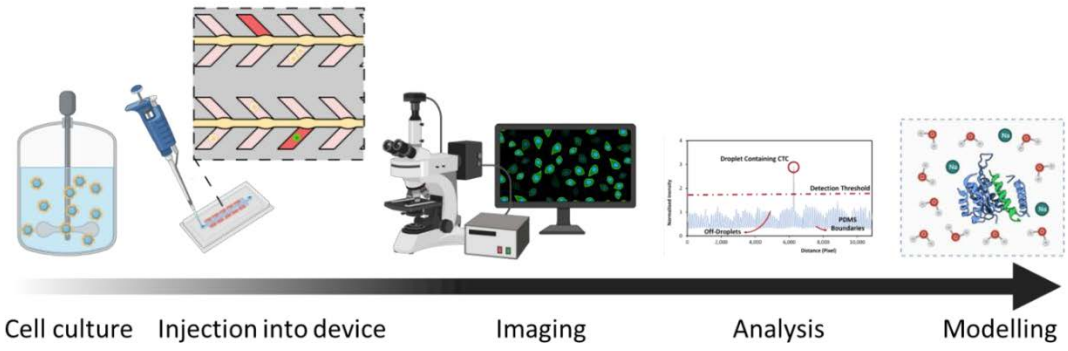

Fig. 5.1. The workflow of this paper. Cells were harvested and injected into the device to evaluate the lactate secretion at the single cell level, and the information was collected and analysed by an in-house MATLAB program which would be used to build a model for bioreactor culture.

5.2. Materials and methods

5.2.1. Device design and fabrication

A microfluidic static droplet array device (SDA) was designed with AutoCAD (AutoDesk, USA). The device contained 800 droplet chambers in total, and the volume of each chamber/trap was 125 pL. The mould of the device was designed and fabricated by mask-less lithography. Silicon wafers were prepared, spin-coated with 35 μm thickness SU8-2050 (Microchem Co., USA), and the design was developed with μPG101 lithography machine (Heidelberg, Germany) post-processed according to the manufacturer's instruction. Then, the patterned wafer was treated with tri-chloro (1H, 1H, 2H, 2Hperfluoro-octyl) silane (Sigma-Aldrich, Australia) via chemical deposition in a vacuum chamber to coat a hydrophobic film on the surface of the mould for easier fabrication of devices.

The devices were fabricated using polydimethylsiloxane (PDMS, Sylgard 184, Dow Corning, USA). PDMS elastomer was mixed thoroughly with the curing agent in a 10:1 ratio, poured onto the mould, placed in a petri dish, and degassed in a vacuum chamber. Then, the mould was left in a 65 ℃ oven for one h before peeling off the device. The Inlet and outlet of the device were punched with a 0.75 μ m biopsy punch, and 0.8 mm cover glass was used to bond to the channel via plasma treatment with 4 minutes vacuum and 2 minutes plasma.

5.2.2. Cell culture and differentiation

Mouse C2C12 myocyte cell line was kindly provided by Vow Ltd. Cells were cultured in T24 flasks and seeded in 6 well plates for different culture days at a seeding density of 500,000 cells/well. DMEM/F12+ Glutamax was supplemented with 20% Foetal bovine serum, and 1 % penicillin & streptomycin (all from Gibco, Australia) were used as the media for C2C12 culture. Cell differentiation was triggered by changing the culture media from FBS supplemented to 2% horse serum-supplemented media. Cells were cultured at 37℃ with 5% CO2 supply.

5.2.3. Single cell metabolomic measurement

The inlet and outlet of the device were taped with scotch tape (3M, Australia) and left in a vacuum chamber for two h before use. The gas permeability of PDMS and the

scotch tape allowed the channel to be temporarily vacuumed after taking out of the vacuum chamber. Then, the cells were harvested, stained with Hoechst and Viobility fixable cell apoptotic dye (both 1 uL/mL, Miltenyi Biotec, Australia) was used to stain the cells for 15 minutes in the incubator. The cells were counted, and 15,000 cells were taken out, centrifuged, and resuspended in 10 μL pHrodo fluorescent pH indicator solutions (1 uL pHrodo solution in 10 uL of DMSO provided in the same kit, added into 1 mL of fresh DMEM F12, Glutamax+. ThermoFisher, Australia). The cells were then immediately injected into the freshly taken-out device. Due to the vacuum environment inside the device, the cell solution would be taken in automatically. Then the middle channel of the device was sheathed with mineral oil (Sigma Aldrich, Australia) to prevent evaporation, and the device was left inside the incubator for 30 minutes before imaging.

5.2.4. Image analysis

After 30 minutes of incubation, the cells were taken out and imaged with an IX70 fluorescent microscope (Olympus, Japan). All pHrodo pictures (mCherry channel) and Viobility pictures (FITC channel) were taken at 10×, 500 ms exposure time without changing any other fluorescent intensity settings, while Hoechst was taken at 30 ms exposure (DAPI channel). All pictures were saved without burning in information and then proceeded through our MATLAB program (MathWorks, USA) for intensity analysis. The images were firstly cut by ImageJ (National Institute of Health, USA) to pick out the chambers, and the fluorescent intensity of each chamber was picked up and recorded in MATLAB, output into an excel file. The values of multiple experiments were plotted in histograms for further analysis and comparison.

5.3. Results and discussions

5.3.1. Cell trapping efficiency and experiment operation

To visualize the cell trapping process, we used a high-speed camera to record the procedure, and the resulting footage is presented in Fig. 5.2A. In this process, the cell solutions were represented by food dye and were automatically drawn into each individual trap within a rapid timeframe of 2 seconds. Once the cell solutions were loaded, we introduced oil into the middle channel, causing the liquid to break into multiple static droplets. This sheathing step helps to isolate the individual cells within

each trap, enabling precise and controlled analysis of single cells. The cell trapping and sheathing process presented here can be readily adapted for use with a variety of different cell types and can enable high-throughput screening of single cells, with potential applications in regenerative medicine and tissue engineering.

The single cell trapping efficiency of the device was firstly characterised by injecting a different concentration of cell solutions. The occupancy of the individual traps in the device should follow a Poisson distribution, with a theoretical single cell trapping efficiency of around 37.5% for approximately 300 single cells trapped in the device. As the cell concentration increased, the number of traps with multiple cells increased. While at low cell concentration, the chance of having empty droplets increased and the chance of having multiple cells in one chamber decreased (Fig. 5.2B). Decreasing the cell concentration resulted in lower overall chamber utility rates but improved the single-cell utility rate [206]. Fig. 5.2C shows that when the concentration of cells decreased to 20 cells/μL (20,000 cells/mL), the cell utility rate can be as high as 90%. In other words, although most of the chambers were empty, 90% of the cells were trapped in the chambers as a single cell, making it easy for software to analyse. Therefore in this experiment, the experiments were carried out with 20 cells/μL concentration.

In this work, we present an improved version of our previously published SDA [206]. Our previous design operate relying on the smaller resistance of the chambers' inlet compared to the main channel. The droplets stayed only inside the chambers without penetrating to the next chamber due to the surface tension and the sudden decrease of chamber size at the hydrophobic air gap. The device can be operated without permanent bonding, and no pre-treatment is needed, but sometimes the chambers are not 100% filled, and it is not suitable for culture because the air plug formed in the air gap might gradually move out during culture and the droplets in neighbouring chambers will merge in one. In this work, we introduce a new design that utilizes the gas permeability of PDMS and scotch tape on the inlet and outlet to create a temporal vacuum inside the channels, which enables the liquid to fill every single pocket efficiently. The chambers remain stationary during culture, and droplet size stays more consistent after culture.

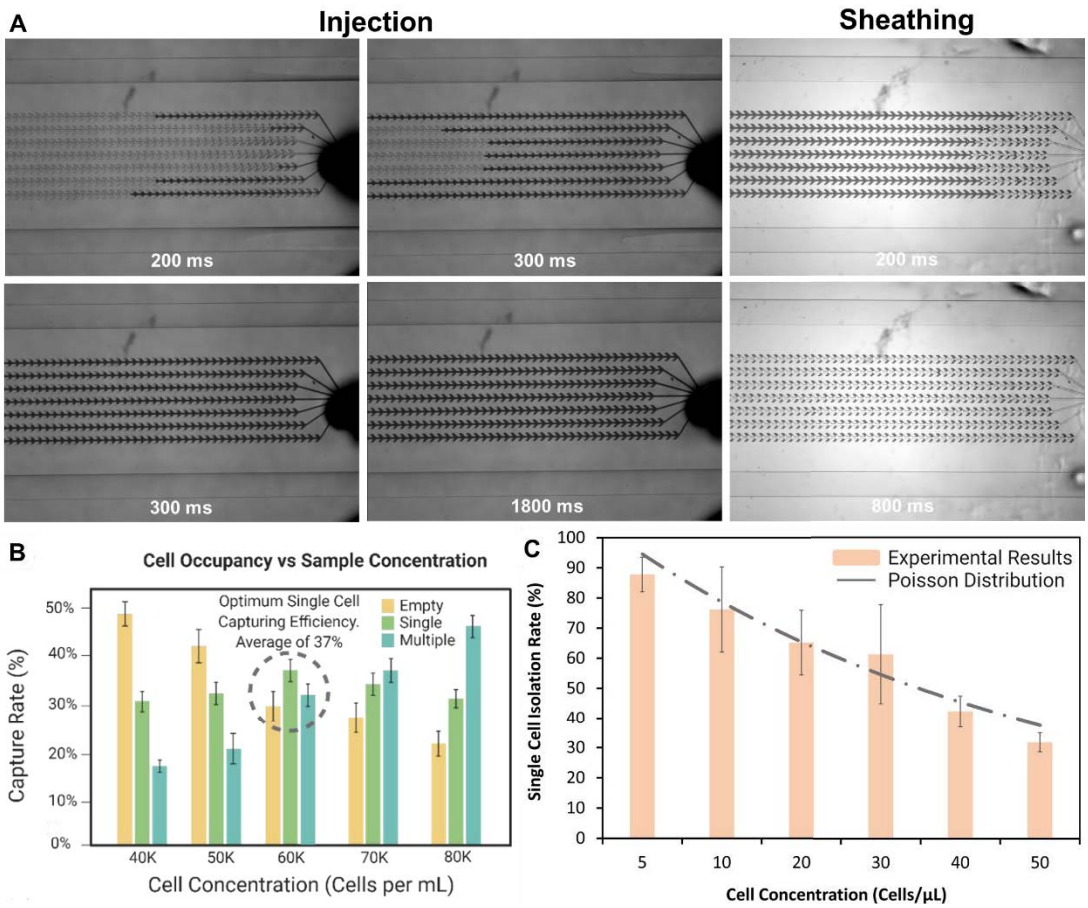

Fig. 5.2. Device performance and image analysis process. A) the injection and sheathing process of the workflow, takes less than 3s operation time. B) Single cell trapping efficiency reached highest when the cell concentration reached 50-60 cells/µL C) The single cell trapping efficiency can increase to almost 100% when the concentration of cell solution is low. While the trap occupancy decreases, reducing cell solution concentration results in low cell loss and maximising cell usage.

5.3.2. Device optimisation for secretion analysis

Fig. 5.3A showed the picture analysis process after imaging. The positions of droplets array were defined, and the fluorescent intensity of each pixel was recorded. The highest point of each peak, which corresponding to the fluroescent light of the cells, was picked up and recorded as the value of the chamber and plotted as a graph shown in the software processing part. Meanwhile, the program was set to normalise the fluorescent intensity of each PDMS device based on the fluorescent intensity of the area between the wells. This eliminates the error when comparing results across different SDAs and experiments. In our study, a value above 2.1 was considered as 'on' for lactate production. This value was determined by calculating the average value across multiple experiments and empty control. The 'off' droplets, which were affected by potential cell

metabolism, solubilised CO2, and autofluorescence of media, had an average value of 1.5. The empty control was set as 0.

The fluorescent intensity level of the droplets is dependent on droplet sizes and incubation time. Smaller droplets provides quicker and more efficient detection [332]. Larger droplets exceeding 0.75 nL do not exhibit detectable levels of lactate secretion within 30 minutes of incubation time. Droplets sized at 0.125 nL, on the other hand, display high sensitivity in detecting lactate secretion levels, as evidenced by their wide distribution range in fluorescence intensity (Fig. 5.3B). Longer incubation times lead to increased lactate production (Fig. 5.3C), but also an increase the fluorescent intensity of empty droplets suggesting signal oversaturation. Prolonged incubation of cells also led to over-estimation of the number of high-lactate secretion cells. The results showed that 15 minutes of incubation is adequate for identifying lactate secreting cell population, and 30 minutes of incubation can highlight differences in secretion level among positive cells. Based on these findings, a 0.125 nL chamber size device and 30 minutes incubation time were applied in the subsequent experiments.

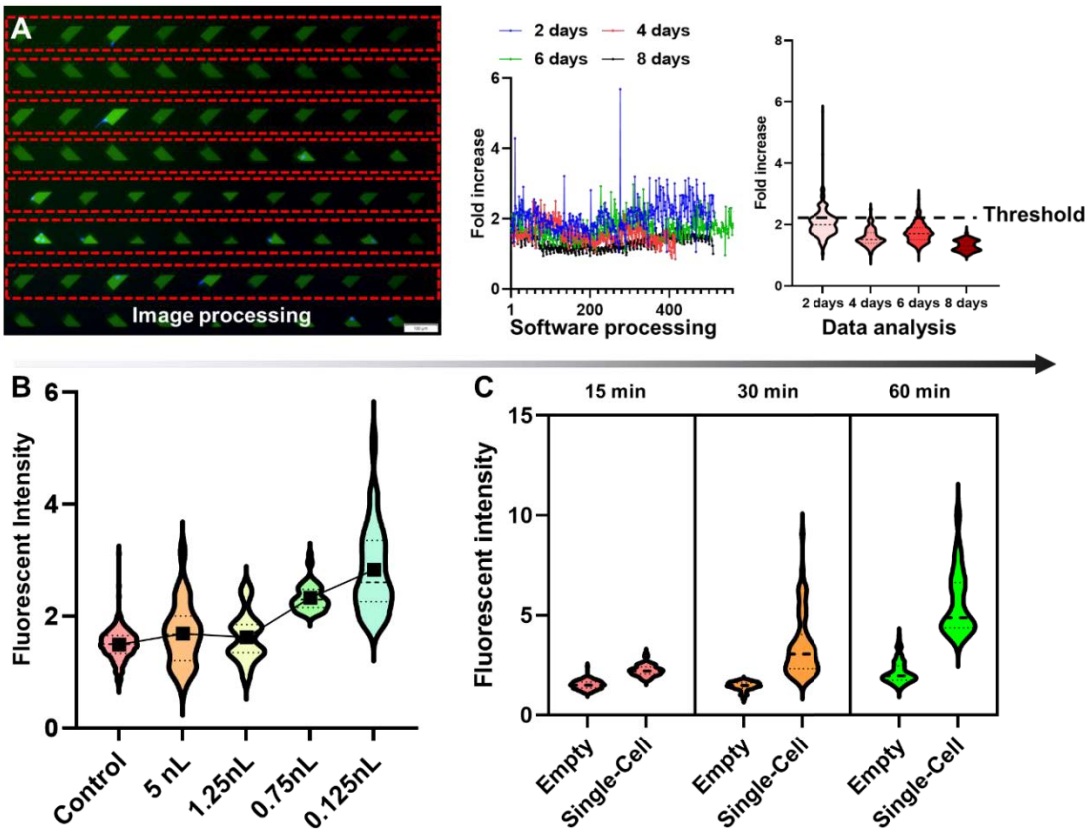

Fig. 5.3. A) The imaging area was selected in ImageJ and processed automatically in the MATLAB program, and results were analysed in statistical software like Prism. B) the fluorescent intensity of the C2C12 cells in different sizes traps after 30 minutes incubation. The line shows the means of intensity level increased when the size of droplets decreased. C) The fluorescent intensity of C2C12 cells 0.125 nL sizes traps.

5.3.3. Lactate secretion level and culture times

The effects of culture duration on single cell lactate secretion levels in C2C12 cells was investigated first. C2C12 cells were cultured for 2, 4, 6 and 8 days, and the lactate secretion level were measured. The results in Fig. 5.4A showed a significant reduction in lactate secretion in C2C12 cells for 8 days, indicating potential damage to the cells. The mean lactate secretion levels for days 2, 4, 6, and 8 were 2.039, 1.571, 1.73, and 1.314, respectively, and significant differences were observed among the groups ($p<0.001$) (Fig. 5.4B). Fig. 5.4C and 5.4D showed that day 4 had a significant drop in % of 'on' droplets, and the fold increase of 'on' droplets was smaller than day two cells. However, the fold increase and the number of % 'on' droplets on day 6 increases again, to a similar level on day 2. This can be an indication of the early differentiation of myoblasts [325, 326] while day four cells might be in an exponential growth stage. Although the mean value of 'on' droplets in each group is closer (2.414, 2.232, 2.313 for days 2, 4 and 6), there is still a significant difference among them ($p<0.001$). Further investigations on the correlation between pH and cell growth, cell death and cell differentiation are needed.

In order to improve the accuracy and efficiency of image analysis in the context of cell metabolism, a deep-learning programe based on MATLAB to perform prediction of cell metabolism in different days of culture is needed and comparison between current commercial prediction model can be conducted.

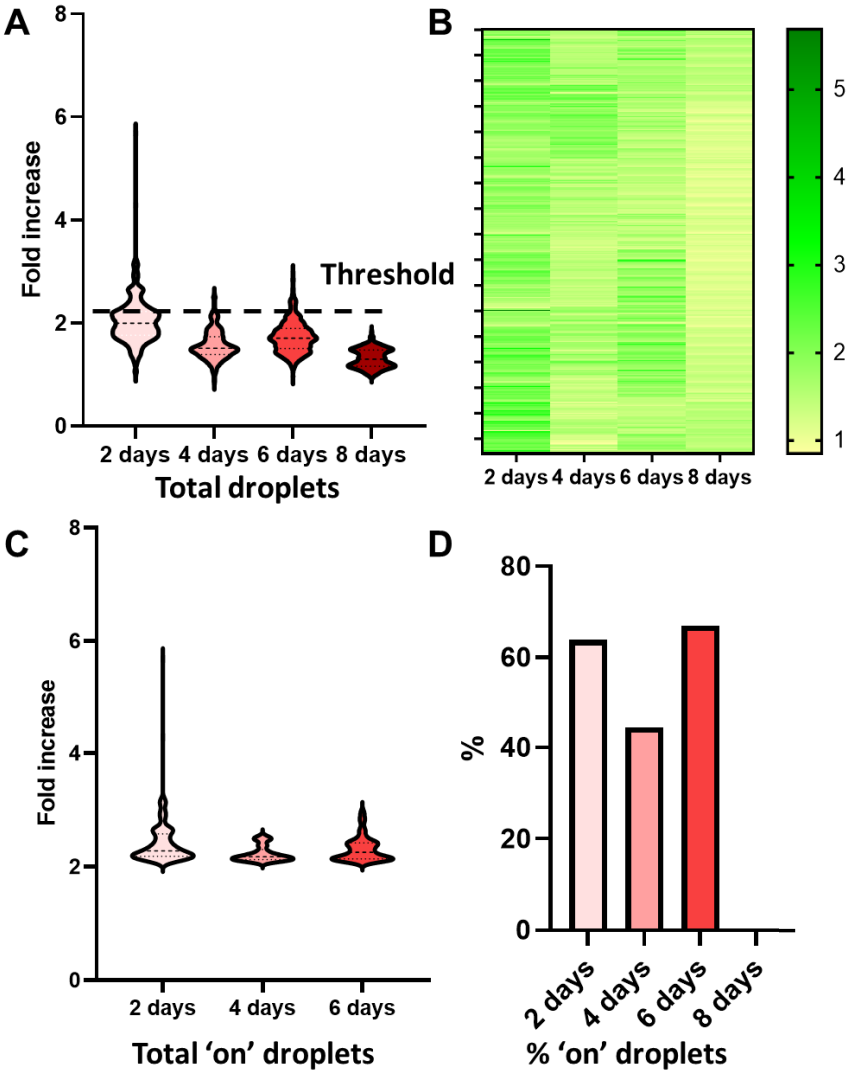

Fig. 5.4. Comparison of lactate secretion level over different days culture. A) the fluorescent intensity of all droplets analysed on different days. B) The heat of 400 'on' droplets from different groups showed the frequency of 'on' droplets each day. C) although the mean values are closed, the distribution of 'on' droplets have significant differences from each other according to student t-test results ($p<0.0001$). D) % of 'on' droplets on different days, showing that day two and day six have more than 60% of cells secreting lactate while day four has only about 40 %.

6. Conclusion and future perspective

Stem cell research remains a complex and dynamic field, with much still to be discovered regarding the proliferation, metabolism, and therapeutic mechanisms of stem cells. However, microfluidic devices have proven to be powerful tools for advancing our understanding of stem cells at a higher resolution. By allowing for the precise manipulation and observation of stem cells, microfluidic devices have enabled the identification and isolation of stem cell subpopulations, providing insight into their unique roles and behaviour within the broader cell group. Single-cell studies conducted in microfluidic devices have further highlighted inherent differences between subpopulations of cells, shedding light on their individual contributions to overall stem cell behaviour. Moreover, the use of organ-on-a-chip models has provided researchers with a more accurate representation of cellular behaviour and interaction, allowing for a better understanding of stem cell function in the context of human physiology. Inertial and active microfluidics have also proven to be effective in identifying and isolating stem cells and their subpopulations while facilitating the application of external stimuli. These advances not only improve our understanding of stem cells but also have the potential to address current manufacturing challenges in the stem cell industry (Fig. 6.1). This thesis showcases four applications of microfluidic technologies in stem cell research, highlighting their potential to accelerate progress towards the clinical application and scale-up production of stem cells.

In this thesis, four microfluidic devices were developed to address various challenges in stem cell research and production, as depicted in Fig. 6.1. Chapter 1 provided an overview of the stem cell production process and the existing microfluidic devices employed in stem cell research. Chapter 2 presented a low-cost, high-throughput microfluidic system for producing edible microcarriers for the cultivated meat industry, enabling large-scale production of stem cells in this sector. Chapter 3 developed a cell-harvesting device that can efficiently detach and separate cells from microcarriers while concentrating them for downstream processing. The separation device demonstrated minimal clogging and high efficacy. Chapter 4 introduced a micromixer to mix harvested stem cells continuously and effortlessly with cryoprotectant to improve the quality of cells preserved, potentially leading to enhanced therapeutic outcomes and product consistency. Additionally, a static droplet microfluidic device was developed

to assess the lactate secretion level of individual muscle cells in chapter 5. This data can be used to create an accurate model for large-scale bioreactor culture to optimize the cell culture outcomes.

In the stem cell industry, there is a pressing need for efficient processes such as mixing, separating, dewatering, and centrifuging. Microfluidic devices have shown significant promise in executing these processes on a laboratory scale. In particular, inertial microfluidics and droplet-based microfluidics have demonstrated high-throughput capabilities for perfusing cells-attached microcarriers and producing uniform-sized microcarriers, respectively. These devices offer advantages in terms of price, scalability, simplicity, and energy efficiency without damaging the cells. However, the adoption of microfluidic devices on an industrial scale remains limited, and further case studies are needed to demonstrate their feasibility and cost-effectiveness. Due to their high customisability, microfluidic devices can be integrated into current systems, and their advantages can be combined to achieve multiple outcomes. For instance, sheath flow added inertial device and sheathless spiral channel can be combined to wash and concentrate ceawlls simultaneously. Micromixers, an area of untapped potential in the bioprocessing industry, could enable precise, automated mixing, particularly for stem cell cryopreservation and final product formulation, where precise, labour-free mixing is required. As microfabrication technologies continue to advance, microfluidic technologies will play a critical role in stem cell research and industry. Moreover, similar technologies used in stem cell therapy could be applied to increase the number of cells acquired from tissue samples, produce microcarriers, wash, and harvest cells, which all serves to improve the efficiency and quality of production and reduce costs in the cultivated meat industry.

The use of microfluidic devices has had a transformative impact on stem cell research, but there is still much room for improvement in stem cell production at an industrial scale. Any advances in the production process could have a significant impact on both the industry and the medical sector. Microfluidic devices are particularly promising due to their scalability, automation potential, and ability to manipulate multiple parameters with precision. As a result, they may be able to overcome the current challenges in the stem cell production process and potentially supplant existing technologies in the near

future. More research is needed to fully realize the potential of microfluidic devices in stem cell production, but they represent a promising avenue for innovation in this field.

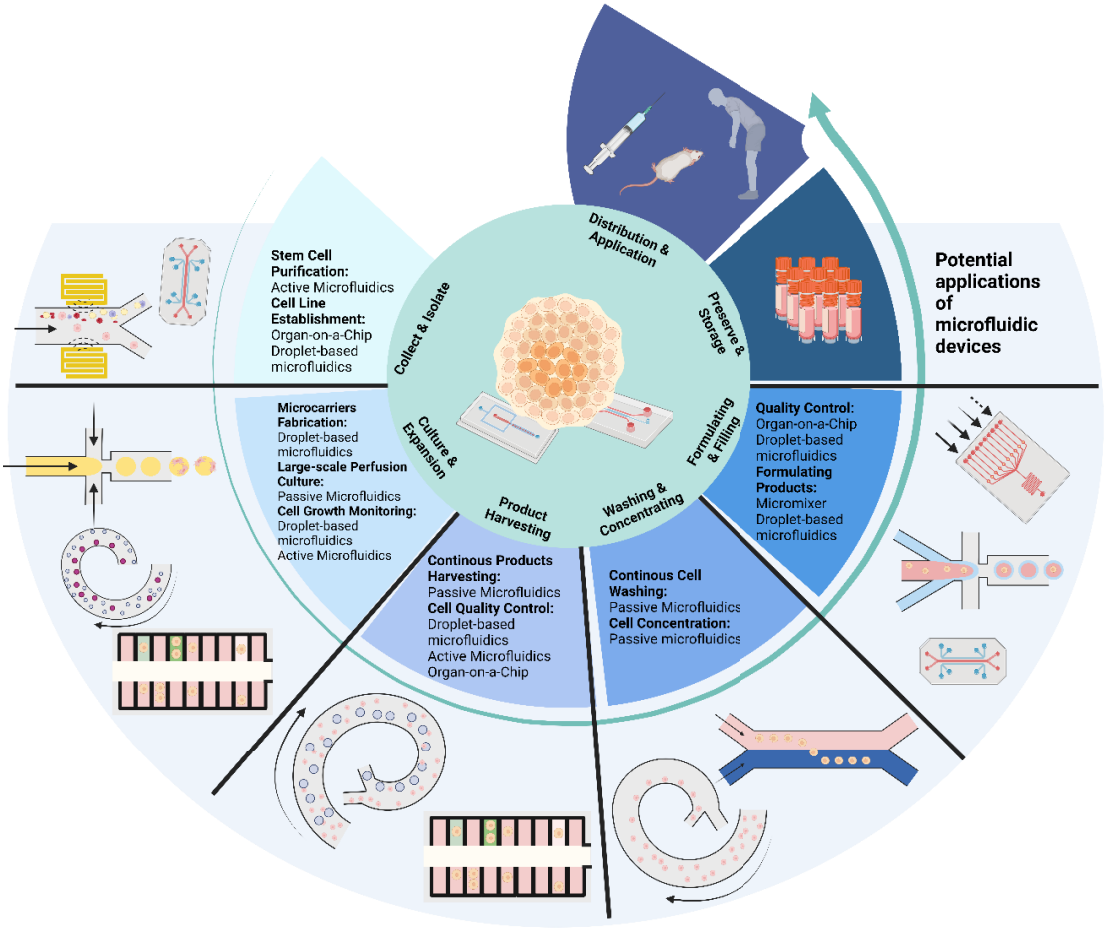

Fig. 6.1. Potential applications of microfluidic devices in the industrial production processes of stem cells. Microfluidic devices have low-cost, scalable, low-energy consumption, labour-free and precise manipulation of fluid features. These attributes address the challenges of the current industry and can potentially bring significant improvement to low-down the cost, set a universal standard procedure and improve the outcome for stem cell therapies.

7. Research outputs

Thesis related publications:

1. **Lin Ding,** Sajad Razavi Bazaz, Mahsa Asadniaye Fardjahromi, Flyn McKinnirey, Brian Saputro, Balarka Banerjee, Graham Vesey, Majid Ebrahimi Warkiani. " A modular 3D printed microfluidic system: a potential solution for continuous cell harvesting in large-scale bioprocessing". *Bioresources and Bioprocessing,* 9.1 (2022): 1-16. DOI: 10.1186/s40643-022-00550-2
2. **Lin Ding,** Payar Radfar, Meysam Rezaei, and Majid Ebrahimi Warkiani. "An easy-to-operate method for single-cell isolation and retrieval using a microfluidic static droplet array." *Microchimica Acta* 188, no. 8 (2021): 1-11. DOI: 10.1007/s00604-021-04897-9
3. **Lin Ding,** Reza Moloudi and Majid Ebrahimi Warkiani. "Bioreactor-based adherent cells harvesting from microcarriers with 3D printed inertial microfluidics", invited book chapter for *Bioreactors-Method and Protocols 2nd edition,* (2022) DOI: 10.1007/7651_2021_444
4. **Lin Ding,** Sajad Razavi Bazaz, Jesus Shrestha, Hoseyn A. Amiri, Sima Mas-Hafi, Balarka Banerjee, Graham Vesey, Morteza Miansari, and Majid Ebrahimi Warkiani. "Rapid and Continuous Cryopreservation of Stem Cells with a 3D Micromixer." *Micromachines* 13, no. 9 (2022): 1516. DOI: 10.3390/mi13091516
5. Payar Radfar, **Lin Ding,** Laura Rodriguez de la Fuente, Hamidreza Aboulkheyr, David Gallego-Ortega, Majid Ebrahimi Warkiani. "Rapid Metabolomic Screening of Cancer Cells via High-Throughput Static Droplet Microfluidics. " *Biosensors and Bioelectronics* 223, 114966. DOI: 10.1016/j.bios.2022.114966
6. Sajad Razavi Bazaz, Fateme Mirakhorli, Zahra Lotfibakalani, **Lin Ding,** Hossein Ahmadi Nejad Joushani, Jesus Shrestha, Peter J. Ralph, Majid Ebrahimi Warkiani. "Membrane-less microfiltration using microfluidics." Under review in *Environmental Science & Technology.*
7. **Lin Ding,** Payar Radfar, Alan Lam, Steve Oh, Majid Ebrahimi Warkiani, 'A scalable microfluidic-based production of dissolvable/edible microcarriers for stem cell industry', under preparation for *Biotechnology Journal*.

8. **Lin Ding,** Jesus Shrestha, Yaqing Wang, Payar Radfar, Zhixi You, Majid Ebrahimi Warkiani. " Potential Applications of Microfluidic Devices in the Industrial Production of Stem Cells", under preparation for *Biotechnology Advances.*
9. **Lin Ding,** Payar Radfar, Steve Oh, Majid Ebrahimi Warkiani, "Precise prediction and modelling of bioreactor culture condition with microfluidic-based single cell metabolomic analysis", under preparation for *Biosensors and Bioelectronics*.

Publications with other collaborators:

1. **Lin Ding,** Sajad Razavi Bazaz, Timothy Hall, Graham Vesey, & Majid Ebrahimi Warkiani. "Giardia purification from faecal samples using rigid spiral inertial microfluidics". *Biomicrofluidics*, 16(1), (2022) 014105. DOI: 10.1063/5.0069406
2. Steven Vasilescu, Shayan Khorsandi, **Lin Ding,** Sajad Razavi Bazaz, Reza Nosrati, Debra Gook, and Majid Ebrahimi Warkiani. "A microfluidic approach to rapid sperm recovery from heterogeneous cell suspensions." *Scientific reports* 11, no. 1 (2021): 1-11. DOI: 10.1038/s41598-021-87046-9
3. Alexey S. Rzhevskiy, Sajad Razavi Bazaz, **Lin Ding,** Alina Kapitannikova, Nima Sayyadi, Douglas Campbell, Bradley Walsh, David Gillatt, Majid Ebrahimi Warkiani, and Andrei V. Zvyagin. "Rapid and label-free isolation of tumour cells from the urine of patients with localised prostate cancer using inertial microfluidics." *Cancers* 12, no. 1 (2019): 81. DOI: 10.3390/cancers12010081
4. Jesus Shrestha, Maliheh Ghadiri, Melane Shanmugavel, Sajad Razavi Bazaz, Steven Vasilescu, **Lin Ding,** and Majid Ebrahimi Warkiani. "A rapidly prototyped lung-on-a-chip model using 3D-printed molds." *Organs-on-a-Chip* 1 (2019): 100001. DOI: 10.1016/j.ooc.2020.100001
5. Tohid Mahmoudi, Abbas Pirpour Tazehkand, Mohammad Pourhassan-Moghaddam, Mohammadreza Alizadeh-Ghodsi, **Lin Ding,** Behzad Baradaran, Sajad Razavi Bazaz, Dayong Jin, and Majid Ebrahimi Warkiani. "PCR-free

paper-based nanobiosensing platform for visual detection of telomerase activity via gold enhancement." *Microchemical Journal* 154 (2020): 104594. DOI: 10.1016/j.microc.2020.104594

6. Jesus Shrestha, Sajad Razavi Bazaz, **Lin Ding,** Steven Vasilescu, Sobia Idrees, Bill Söderström, Philip M. Hansbro, Maliheh Ghadiri, and Majid Ebrahimi Warkiani. "Rapid separation of bacteria from primary nasal samples using inertial microfluidics." *Lab on a Chip* 23, no. 1 (2023): 146-156. DOI: 10.1039/D2LC00794K
7. Payar Radfar, **Lin Ding**, Hamidreza Aboulkheyr Estarabadi, Majid Ebrahimi Warkiani. "A microfluidic approach for enrichment and single-cell characterisation of circulating tumour cells from peripheral blood". Invited book chapter for *Microfluidic Systems for Cancer Diagnosis 2022,* under review.
8. Steven Vasilescu, **Lin Ding,** Farin Yazdan Parasat, Reza Nosrati, Majid Ebrahimi Warkiani. "A biomimetic microfluidic selection platform providing improved sperm quality metrics compared to swim-up". Under review in *Microsystems & Nanoengineering*

Patent submitted:

Payar Radfar, **Lin Ding,** Majid Ebrahimi Warkinai. Australian patent " Static Droplet Generator", AU2021902248A

Conferences presentations:

1. **Lin Ding,** "Edible and digestible microcarriers for cultivated meat production." In *Bioprocessing network Conference,* p.63, Bioprocessing network, 2022.
2. Payar Radfar, Lin Ding, Majid Ebrahimi Warkiani, "Biodegradable and customised microcarriers for efficient and scalable culture of adherent cells", *ISCT 2023 Paris*, International Society for Cell & Gene Therapy, Accepted.
3. **Lin Ding,** Mahsa Asadniaye Fardjahromi, Sajad Razavi Bazaz, Mohsen Asadnia, Graham Vesey, and Majid Ebrahimi Warkiani. "A 3D printed modular microfluidic device for large scale cell harvesting from bioreactors." In 23rd

International Conference on Miniaturized Systems for Chemistry and Life Sciences, *MicroTAS 2019*, p. 602-603. Chemical and Biological Microsystems Society, 2019.

4. **Lin Ding,** Mahsa Asadina Fardjahromi, Reza Moloudi and Majid Ebrahimi Warkiani. "Inertial-based Microcarrier-Cell Retention and Particulates Matter Contamination in Bioprocessing" In Australia and New Zealand Nano and Microfluidics Symposium 2019, *ANZNMF 2019*

8. References

1. Jossen, V., et al., *Manufacturing human mesenchymal stem cells at clinical scale: process and regulatory challenges.* Applied microbiology and biotechnology, 2018. **102**(9): p. 3981-3994.
2. Schnitzler, A.C., et al., *Bioprocessing of human mesenchymal stem/stromal cells for therapeutic use: current technologies and challenges.* Biochemical Engineering Journal, 2016. **108**: p. 3-13.
3. Zydney, A.L., *Continuous downstream processing for high value biological products: a review.* Biotechnology and bioengineering, 2016. **113**(3): p. 465-475.
4. Bodiou, V., P. Moutsatsou, and M.J. Post, *Microcarriers for Upscaling Cultured Meat Production.* Front Nutr, 2020. **7**: p. 10.
5. Tavassoli, H., et al., *Large-scale production of stem cells utilizing microcarriers: A biomaterials engineering perspective from academic research to commercialized products.* Biomaterials, 2018. **181**: p. 333-346.
6. Sensebe, L., M. Gadelorge, and S. Fleury-Cappellesso, *Production of mesenchymal stromal/stem cells according to good manufacturing practices: a review.* Stem Cell Res Ther, 2013. **4**(3): p. 66.
7. Derakhti, S., et al., *Attachment and detachment strategies in microcarrier-based cell culture technology: A comprehensive review.* 2019. **103**: p. 109782.
8. Moloudi, R., et al., *Inertial-Based Filtration Method for Removal of Microcarriers from Mesenchymal Stem Cell Suspensions.* Sci Rep, 2018. **8**(1): p. 12481.
9. Moloudi, R., et al., *Scaled-Up Inertial Microfluidics: Retention System for Microcarrier-Based Suspension Cultures.* Biotechnol J, 2019. **14**(5): p. e1800674.
10. Vasilescu, S.A., et al., *3D printing enables the rapid prototyping of modular microfluidic devices for particle conjugation.* Applied Materials Today, 2020. **20**: p. 100726.
11. Rogers, R.E., et al., *A scalable system for generation of mesenchymal stem cells derived from induced pluripotent cells employing bioreactors and*

degradable microcarriers. Stem Cells Transl Med, 2021. **10**(12): p. 1650-1665.
12. Zhou, Y., et al., *Single cell studies of mouse embryonic stem cell (mESC) differentiation by electrical impedance measurements in a microfluidic device.* Biosens Bioelectron, 2016. **81**: p. 249-258.
13. Cochrane, A., et al., *Advanced in vitro models of vascular biology: Human induced pluripotent stem cells and organ-on-chip technology.* Advanced Drug Delivery Reviews, 2019. **140**: p. 68-77.
14. Musah, S., et al., *Mature induced-pluripotent-stem-cell-derived human podocytes reconstitute kidney glomerular-capillary-wall function on a chip.* Nat Biomed Eng, 2017. **1**.
15. Amabile, G. and A. Meissner, *Induced pluripotent stem cells: current progress and potential for regenerative medicine.* Trends Mol Med, 2009. **15**(2): p. 59-68.
16. Squillaro, T., G. Peluso, and U. Galderisi, *Clinical Trials With Mesenchymal Stem Cells: An Update.* Cell Transplant, 2016. **25**(5): p. 829-48.
17. Baldari, S., et al., *Challenges and Strategies for Improving the Regenerative Effects of Mesenchymal Stromal Cell-Based Therapies.* Int J Mol Sci, 2017. **18**(10).
18. Wraith, J.E., et al., *Mucopolysaccharidosis type II (Hunter syndrome): a clinical review and recommendations for treatment in the era of enzyme replacement therapy.* Eur J Pediatr, 2008. **167**(3): p. 267-77.
19. Guan, X., et al., *Bioprocessing technology of muscle stem cells: implications for cultured meat.* Trends Biotechnol, 2021.
20. Choudhury, D., T.W. Tseng, and E. Swartz, *The Business of Cultured Meat.* Trends Biotechnol, 2020. **38**(6): p. 573-577.
21. Jossen, V., et al., *Manufacturing human mesenchymal stem cells at clinical scale: process and regulatory challenges.* Appl Microbiol Biotechnol, 2018. **102**(9): p. 3981-3994.
22. Rodrigues, C.A., D.E. Nogueira, and J.M. Cabral, *Next-generation stem cell expansion technologies.* Cell and Gene Therapy Insights, 2018. **4**(8): p. 791-804.
23. Shields, C.W.t., C.D. Reyes, and G.P. Lopez, *Microfluidic cell sorting: a review of the advances in the separation of cells from debulking to rare cell isolation.* Lab Chip, 2015. **15**(5): p. 1230-49.
24. Xavier, M., R.O. Oreffo, and H. Morgan, *Skeletal stem cell isolation: A review on the state-of-the-art microfluidic label-free sorting techniques.* Biotechnology advances, 2016. **34**(5): p. 908-923.
25. Kucinski, I. and B. Gottgens, *Advancing Stem Cell Research through Multimodal Single-Cell Analysis.* Cold Spring Harb Perspect Biol, 2020.
26. Martins-Taylor, K. and R.H. Xu, *Concise review: Genomic stability of human induced pluripotent stem cells.* Stem Cells, 2012. **30**(1): p. 22-7.
27. O'Neill, E.N., et al., *Considerations for the development of cost-effective cell culture media for cultivated meat production.* Compr Rev Food Sci Food Saf, 2021. **20**(1): p. 686-709.
28. Lee, K.Y., H.X. Loh, and A.C.A. Wan, *Systems for Muscle Cell Differentiation: From Bioengineering to Future Food.* Micromachines (Basel), 2021. **13**(1).

29. Bomkamp, C., et al., *Scaffolding Biomaterials for 3D Cultivated Meat: Prospects and Challenges.* Adv Sci (Weinh), 2022. **9**(3): p. e2102908.
30. Zhang, J., et al., *Fundamentals and applications of inertial microfluidics: a review.* Lab on a Chip, 2016. **16**(1): p. 10-34.
31. Yin, H. and D. Marshall, *Microfluidics for single cell analysis.* Curr Opin Biotechnol, 2012. **23**(1): p. 110-9.
32. Qian, T., E.V. Shusta, and S.P. Palecek, *Advances in microfluidic platforms for analyzing and regulating human pluripotent stem cells.* Curr Opin Genet Dev, 2015. **34**: p. 54-60.
33. Lian, Q., et al., *Functional mesenchymal stem cells derived from human induced pluripotent stem cells attenuate limb ischemia in mice.* Circulation, 2010. **121**(9): p. 1113-23.
34. Villa-Diaz, L.G., et al., *Derivation of mesenchymal stem cells from human induced pluripotent stem cells cultured on synthetic substrates.* Stem Cells, 2012. **30**(6): p. 1174-81.
35. Toh, W.S., et al., *Advances in mesenchymal stem cell-based strategies for cartilage repair and regeneration.* Stem Cell Rev, 2014. **10**(5): p. 686-96.
36. Moll, G., et al., *Cryopreserved or Fresh Mesenchymal Stromal Cells: Only a Matter of Taste or Key to Unleash the Full Clinical Potential of MSC Therapy?* Adv Exp Med Biol, 2016. **951**: p. 77-98.
37. Dykstra, J.A., et al., *Concise Review: Fat and Furious: Harnessing the Full Potential of Adipose-Derived Stromal Vascular Fraction.* Stem Cells Transl Med, 2017. **6**(4): p. 1096-1108.
38. Oberbauer, E., et al., *Enzymatic and non-enzymatic isolation systems for adipose tissue-derived cells: current state of the art.* Cell Regen, 2015. **4**: p. 7.
39. Yim, E.K. and M.P. Sheetz, *Force-dependent cell signaling in stem cell differentiation.* Stem Cell Res Ther, 2012. **3**(5): p. 41.
40. Zhao, W., et al., *Effects of substrate stiffness on adipogenic and osteogenic differentiation of human mesenchymal stem cells.* Mater Sci Eng C Mater Biol Appl, 2014. **40**: p. 316-23.
41. Fardjahromi, M.A., et al., *Mussel inspired ZIF8 microcarriers: a new approach for large-scale production of stem cells.* 2020. **10**(34): p. 20118-20128.
42. Chen, X.-Y., et al., *Recent advances in the use of microcarriers for cell cultures and their ex vivo and in vivo applications.* 2020. **42**(1): p. 1-10.
43. Perez, R.A., et al., *Biomaterials control of pluripotent stem cell fate for regenerative therapy.* 2016. **82**: p. 234-293.
44. Van Beylen, K., I. Papantoniou, and J.M. Aerts, *Microcarrier Screening and Evaluation for Dynamic Expansion of Human Periosteum-Derived Progenitor Cells in a Xenogeneic Free Medium.* Front Bioeng Biotechnol, 2021. **9**: p. 624890.
45. Ye, G., A.W. Nienow, and F. Alberini, *Quantitative Measurements of the Critical Impeller Speed for Solid‐Liquid Suspensions.* Chemical Engineering & Technology, 2019. **42**(8): p. 1643-1653.
46. Nienow, A.W., et al., *A potentially scalable method for the harvesting of hMSCs from microcarriers.* Biochemical Engineering Journal, 2014. **85**: p. 79-88.

47. Martin, C., et al., *Revisiting MSC expansion from critical quality attributes to critical culture process parameters.* 2017. **59**: p. 231-243.
48. Spees, J.L., et al., *Internalized antigens must be removed to prepare hypoimmunogenic mesenchymal stem cells for cell and gene therapy.* Mol Ther, 2004. **9**(5): p. 747-56.
49. Panchalingam, K.M., et al., *Bioprocessing strategies for the large-scale production of human mesenchymal stem cells: a review.* Stem Cell Res Ther, 2015. **6**: p. 225.
50. Chilima, T.D.P., F. Moncaubeig, and S.S. Farid, *Impact of allogeneic stem cell manufacturing decisions on cost of goods, process robustness and reimbursement.* Biochemical Engineering Journal, 2018. **137**: p. 132-151.
51. Schnitzler, A.C., et al., *Bioprocessing of human mesenchymal stem/stromal cells for therapeutic use: current technologies and challenges.* 2016. **108**: p. 3-13.
52. Sartorius Stedim Biotech, *kSep systems (data sheet).* 2017: p. 1-4.
53. Joseph, A., et al., *A scale-down mimic for mapping the process performance of centrifugation, depth and sterile filtration.* Biotechnol Bioeng, 2016. **113**(9): p. 1934-41.
54. Derakhti, S., et al., *Attachment and detachment strategies in microcarrier-based cell culture technology: A comprehensive review.* Mater Sci Eng C Mater Biol Appl, 2019. **103**: p. 109782.
55. Mawji, I., et al., *Challenges and opportunities in downstream separation processes for mesenchymal stromal cells cultured in microcarrier-based stirred suspension bioreactors.* Biotechnol Bioeng, 2022. **119**(11): p. 3062-3078.
56. Singh, B., G. Mal, and S.K. Singla, *Chapter 18 Vitrification: A Reliable Method for Cryopreservation of Animal Embryos.* Methods Mol Biol, 2017. **1568**: p. 243-249.
57. Kita, H., et al., *Dimethyl sulfoxide induces chemotherapeutic resistance in the treatment of testicular embryonal carcinomas.* Oncol Lett, 2015. **10**(2): p. 661-666.
58. Chetty, S., et al., *A simple tool to improve pluripotent stem cell differentiation.* Nat Methods, 2013. **10**(6): p. 553-6.
59. Alessandrino, P., et al., *Adverse events occurring during bone marrow or peripheral blood progenitor cell infusion: analysis of 126 cases.* Bone Marrow Transplant, 1999. **23**(6): p. 533-7.
60. Thirumala, S., W.S. Goebel, and E.J. Woods, *Manufacturing and banking of mesenchymal stem cells.* Expert Opin Biol Ther, 2013. **13**(5): p. 673-91.
61. Golpanian, S., et al., *Effect of aging on human mesenchymal stem cell therapy in ischemic cardiomyopathy patients.* J Am Coll Cardiol, 2015. **65**(2): p. 125-32.
62. Hass, R., et al., *Different populations and sources of human mesenchymal stem cells (MSC): A comparison of adult and neonatal tissue-derived MSC.* Cell Commun Signal, 2011. **9**: p. 12.
63. Trivanovic, D., et al., *Mesenchymal stem cells isolated from peripheral blood and umbilical cord Wharton's jelly.* Srp Arh Celok Lek, 2013. **141**(3-4): p. 178-86.
64. Menard, C., et al., *Clinical-grade mesenchymal stromal cells produced under various good manufacturing practice processes differ in their*

immunomodulatory properties: standardization of immune quality controls. Stem Cells Dev, 2013. **22**(12): p. 1789-801.
65. Lee, W.C., et al., *Multivariate biophysical markers predictive of mesenchymal stromal cell multipotency.* Proc Natl Acad Sci U S A, 2014. **111**(42): p. E4409-18.
66. Whitfield, M.J., W.C. Lee, and K.J. Van Vliet, *Onset of heterogeneity in culture-expanded bone marrow stromal cells.* Stem Cell Res, 2013. **11**(3): p. 1365-77.
67. Burnouf, T., et al., *Human platelet lysate: Replacing fetal bovine serum as a gold standard for human cell propagation?* Biomaterials, 2016. **76**: p. 371-87.
68. Yaffe, M.P., S.A. Noggle, and S.L. Solomon, *Raising the standards of stem cell line quality.* Nat Cell Biol, 2016. **18**(3): p. 236-7.
69. Shi, Y., et al., *Induced pluripotent stem cell technology: a decade of progress.* 2017. **16**(2): p. 115-130.
70. Temple, S. and L. Studer, *Lessons Learned from Pioneering Neural Stem Cell Studies.* Stem Cell Reports, 2017. **8**(2): p. 191-193.
71. Trounson, A. and C. McDonald, *Stem Cell Therapies in Clinical Trials: Progress and Challenges.* Cell Stem Cell, 2015. **17**(1): p. 11-22.
72. Dominici, M., et al., *Minimal criteria for defining multipotent mesenchymal stromal cells. The International Society for Cellular Therapy position statement.* Cytotherapy, 2006. **8**(4): p. 315-7.
73. Galipeau, J., et al., *International Society for Cellular Therapy perspective on immune functional assays for mesenchymal stromal cells as potency release criterion for advanced phase clinical trials.* Cytotherapy, 2016. **18**(2): p. 151-9.
74. Wuchter, P., et al., *Standardization of Good Manufacturing Practice-compliant production of bone marrow-derived human mesenchymal stromal cells for immunotherapeutic applications.* Cytotherapy, 2015. **17**(2): p. 128-39.
75. Mark, D., et al., *Microfluidic lab-on-a-chip platforms: requirements, characteristics and applications*, in *Microfluidics based microsystems*. 2010, Springer. p. 305-376.
76. Neethirajan, S., et al., *Microfluidics for food, agriculture and biosystems industries.* Lab Chip, 2011. **11**(9): p. 1574-86.
77. Segre, G. and A. Silberberg, *Behaviour of macroscopic rigid spheres in Poiseuille flow Part 1. Determination of local concentration by statistical analysis of particle passages through crossed light beams.* Journal of fluid mechanics, 1962. **14**(1): p. 115-135.
78. Segre, G. and A. Silberberg, *Radial particle displacements in Poiseuille flow of suspensions.* Nature, 1961. **189**(4760): p. 209.
79. Hassanzadeh-Barforoushi, A., et al., *Static droplet array for culturing single live adherent cells in an isolated chemical microenvironment.* Lab Chip, 2018. **18**(15): p. 2156-2166.
80. Warkiani, M.E., et al., *Ultra-fast, label-free isolation of circulating tumor cells from blood using spiral microfluidics.* Nat Protoc, 2016. **11**(1): p. 134-48.
81. Bora, P. and A.S. Majumdar, *Adipose tissue-derived stromal vascular fraction in regenerative medicine: a brief review on biology and translation.* Stem Cell Res Ther, 2017. **8**(1): p. 145.

82. Alvarez-Viejo, M., et al., *Quantifying mesenchymal stem cells in the mononuclear cell fraction of bone marrow samples obtained for cell therapy.* Transplant Proc, 2013. **45**(1): p. 434-9.
83. Fong, C.Y., et al., *Separation of SSEA-4 and TRA-1–60 labelled undifferentiated human embryonic stem cells from a heterogeneous cell population using magnetic-activated cell sorting (MACS) and fluorescence-activated cell sorting (FACS).* Stem Cell Reviews and Reports, 2009. **5**(1): p. 72-80.
84. Borchin, B., J. Chen, and T. Barberi, *Derivation and FACS-mediated purification of PAX3+/PAX7+ skeletal muscle precursors from human pluripotent stem cells.* Stem cell reports, 2013. **1**(6): p. 620-631.
85. Buesen, R., et al., *Embryonic stem cell test remastered: comparison between the validated EST and the new molecular FACS-EST for assessing developmental toxicity in vitro.* Toxicological sciences, 2009. **108**(2): p. 389-400.
86. Freund, D., et al., *Comparative analysis of proliferative potential and clonogenicity of MACS ‐ immunomagnetic isolated CD34+ and CD133+ blood stem cells derived from a single donor.* Cell proliferation, 2006. **39**(4): p. 325-332.
87. Colter, D.C., I. Sekiya, and D.J. Prockop, *Identification of a subpopulation of rapidly self-renewing and multipotential adult stem cells in colonies of human marrow stromal cells.* Proc Natl Acad Sci U S A, 2001. **98**(14): p. 7841-5.
88. Diogo, M.M., C.L. da Silva, and J.M. Cabral, *Separation technologies for stem cell bioprocessing.* Biotechnol Bioeng, 2012. **109**(11): p. 2699-709.
89. Yan, S., et al., *Hybrid microfluidics combined with active and passive approaches for continuous cell separation.* Electrophoresis, 2017. **38**(2): p. 238-249.
90. Zhu, P. and L. Wang, *Passive and active droplet generation with microfluidics: a review.* Lab Chip, 2016. **17**(1): p. 34-75.
91. Sivaramakrishnan, M., et al., *Active microfluidic systems for cell sorting and separation.* 2020. **13**: p. 60-68.
92. Talary, M., et al., *Dielectrophoretic separation and enrichment of CD34+ cell subpopulation from bone marrow and peripheral blood stem cells.* Medical and Biological Engineering and Computing, 1995. **33**(2): p. 235-237.
93. Simon, M.G., et al., *Increasing label-free stem cell sorting capacity to reach transplantation-scale throughput.* Biomicrofluidics, 2014. **8**(6): p. 064106.
94. Song, H., et al., *Continuous-flow sorting of stem cells and differentiation products based on dielectrophoresis.* Lab Chip, 2015. **15**(5): p. 1320-8.
95. Flanagan, L.A., et al., *Unique dielectric properties distinguish stem cells and their differentiated progeny.* Stem Cells, 2008. **26**(3): p. 656-65.
96. Prieto, J.L., et al., *Frequency discretization in dielectrophoretic assisted cell sorting arrays to isolate neural cells.* Lab on a Chip, 2012. **12**(12): p. 2182-2189.
97. Nourse, J., et al., *Membrane biophysics define neuron and astrocyte progenitors in the neural lineage.* Stem Cells, 2014. **32**(3): p. 706-716.
98. Plouffe, B.D., et al., *Clinically relevant microfluidic magnetophoretic isolation of rare-cell populations for diagnostic and therapeutic monitoring applications.* Anal Chem, 2012. **84**(3): p. 1336-44.

99. Zeng, L., et al., *Isolation of lung multipotent stem cells using a novel microfluidic magnetic activated cell sorting system.* Cell Biol Int, 2015. **39**(11): p. 1348-53.
100. Dykes, J., et al., *Efficient removal of platelets from peripheral blood progenitor cell products using a novel micro-chip based acoustophoretic platform.* PloS one, 2011. **6**(8).
101. Zalis, M.C., et al., *Label-free concentration of viable neurons, hESCs and cancer cells by means of acoustophoresis.* Integr Biol (Camb), 2016. **8**(3): p. 332-40.
102. Wang, X., et al., *Enhanced cell sorting and manipulation with combined optical tweezer and microfluidic chip technologies.* Lab Chip, 2011. **11**(21): p. 3656-62.
103. Yoshioka, J., et al., *Label-Free Rapid Separation and Enrichment of Bone Marrow-Derived Mesenchymal Stem Cells from a Heterogeneous Cell Mixture Using a Dielectrophoresis Device.* Sensors (Basel), 2018. **18**(9).
104. Vykoukal, J., et al., *Enrichment of putative stem cells from adipose tissue using dielectrophoretic field-flow fractionation.* Lab Chip, 2008. **8**(8): p. 1386-93.
105. Liu, Z., et al., *Rapid isolation of cancer cells using microfluidic deterministic lateral displacement structure.* Biomicrofluidics, 2013. **7**(1): p. 11801.
106. Lee, L.M., et al., *Label-free mesenchymal stem cell enrichment from bone marrow samples by inertial microfluidics.* Analytical methods, 2018. **10**(7): p. 713-721.
107. Hur, S.C., et al., *Label-free enrichment of adrenal cortical progenitor cells using inertial microfluidics.* PloS one, 2012. **7**(10).
108. Yin, L., et al., *Label-free separation of mesenchymal stem cell subpopulations with distinct differentiation potencies and paracrine effects.* Biomaterials, 2020. **240**: p. 119881.
109. Yin, L., et al., *Microfluidic label-free selection of mesenchymal stem cell subpopulation during culture expansion extends the chondrogenic potential in vitro.* Lab Chip, 2018. **18**(6): p. 878-889.
110. Song, H., et al., *Spiral-shaped inertial stem cell device for high-throughput enrichment of iPSC-derived neural stem cells.* Microfluidics and Nanofluidics, 2017. **21**(4): p. 64.
111. Hou, H.W., et al., *Isolation and retrieval of circulating tumor cells using centrifugal forces.* Sci Rep, 2013. **3**: p. 1259.
112. Guzniczak, E., et al., *Purifying stem cell-derived red blood cells: a high-throughput label-free downstream processing strategy based on microfluidic spiral inertial separation and membrane filtration.* Biotechnol Bioeng, 2020.
113. Syverud, B.C., et al., *Label-Free, High-Throughput Purification of Satellite Cells Using Microfluidic Inertial Separation.* Tissue Eng Part C Methods, 2018. **24**(1): p. 32-41.
114. Lee, W.C., et al., *High-throughput cell cycle synchronization using inertial forces in spiral microchannels.* Lab Chip, 2011. **11**(7): p. 1359-67.
115. Di Carlo, D., et al., *Continuous inertial focusing, ordering, and separation of particles in microchannels.* Proc Natl Acad Sci U S A, 2007. **104**(48): p. 18892-7.
116. Nathamgari, S.S., et al., *Isolating single cells in a neurosphere assay using inertial microfluidics.* Lab Chip, 2015. **15**(24): p. 4591-7.

117. Lillehoj, P.B., et al., *Continuous sorting of heterogeneous-sized embryoid bodies.* Lab Chip, 2010. **10**(13): p. 1678-82.
118. Moloudi, R., et al., *Scaled‐up Inertial Microfluidics: Retention System for Microcarrier‐based Suspension Cultures.* Biotechnology journal, 2019. **14**(5): p. 1800674.
119. Guzniczak, E., et al., *Purifying stem cell‐derived red blood cells: a high‐throughput label‐free downstream processing strategy based on microfluidic spiral inertial separation and membrane filtration.* 2020. **117**(7): p. 2032-2045.
120. Chen, Z., et al., *High-throughput and label-free isolation of senescent murine mesenchymal stem cells.* Biomicrofluidics, 2020. **14**(3): p. 034106.
121. Poon, Z., et al., *Bone marrow regeneration promoted by biophysically sorted osteoprogenitors from mesenchymal stromal cells.* Stem Cells Transl Med, 2015. **4**(1): p. 56-65.
122. Song, H., et al., *Identification of mesenchymal stem cell differentiation state using dual-micropore microfluidic impedance flow cytometry.* Analytical Methods, 2016. **8**(41): p. 7437-7444.
123. Song, H., et al., *A microfluidic impedance flow cytometer for identification of differentiation state of stem cells.* Lab Chip, 2013. **13**(12): p. 2300-10.
124. Gong, L., et al., *Direct and Label-Free Cell Status Monitoring of Spheroids and Microcarriers Using Microfluidic Impedance Cytometry.* Small, 2021: p. e2007500.
125. Crocetti, S., et al., *Impedance flow cytometry gauges proliferative capacity by detecting TRPC1 expression.* Cytometry A, 2014. **85**(6): p. 525-36.
126. Strohm, E.M., et al., *Sizing biological cells using a microfluidic acoustic flow cytometer.* Sci Rep, 2019. **9**(1): p. 4775.
127. Moledina, F., et al., *Predictive microfluidic control of regulatory ligand trajectories in individual pluripotent cells.* Proc Natl Acad Sci U S A, 2012. **109**(9): p. 3264-9.
128. Choi, S., et al., *A cell rolling cytometer reveals the correlation between mesenchymal stem cell dynamic adhesion and differentiation state.* Lab Chip, 2014. **14**(1): p. 161-6.
129. Otto, O., et al., *Real-time deformability cytometry: on-the-fly cell mechanical phenotyping.* Nat Methods, 2015. **12**(3): p. 199-202, 4 p following 202.
130. Lin, J., et al., *High-throughput physical phenotyping of cell differentiation.* Microsyst Nanoeng, 2017. **3**: p. 17013.
131. Bagnaninchi, P.O. and N. Drummond, *Real-time label-free monitoring of adipose-derived stem cell differentiation with electric cell-substrate impedance sensing.* Proc Natl Acad Sci U S A, 2011. **108**(16): p. 6462-7.
132. DiMasi, J.A., H.G. Grabowski, and R.W. Hansen, *Innovation in the pharmaceutical industry: New estimates of R&D costs.* J Health Econ, 2016. **47**: p. 20-33.
133. Waring, M.J., et al., *An analysis of the attrition of drug candidates from four major pharmaceutical companies.* Nature Reviews Drug Discovery, 2015. **14**(7): p. 475-486.
134. Van Norman, G.A., *Limitations of Animal Studies for Predicting Toxicity in Clinical Trials: Is it Time to Rethink Our Current Approach?* JACC Basic Transl Sci, 2019. **4**(7): p. 845-854.

135. Horvath, P., et al., *Screening out irrelevant cell-based models of disease.* Nat Rev Drug Discov, 2016. **15**(11): p. 751-769.
136. Park, S.E., A. Georgescu, and D. Huh, *Organoids-on-a-chip.* Science, 2019. **364**(6444): p. 960-965.
137. Low, L.A., et al., *Organs-on-chips: into the next decade.* Nat Rev Drug Discov, 2021. **20**(5): p. 345-361.
138. Bhatia, S.N. and D.E. Ingber, *Microfluidic organs-on-chips.* Nat Biotechnol, 2014. **32**(8): p. 760-72.
139. Shrestha, J., et al., *Lung-on-a-chip: the future of respiratory disease models and pharmacological studies.* Critical Reviews in Biotechnology, 2020. **40**(2): p. 213-230.
140. Ashammakhi, N., et al., *Gut-on-a-chip: Current progress and future opportunities.* Biomaterials, 2020. **255**: p. 120196.
141. Yoon No, D., et al., *3D liver models on a microplatform: well-defined culture, engineering of liver tissue and liver-on-a-chip.* Lab Chip, 2015. **15**(19): p. 3822-37.
142. Zhao, Y., et al., *Towards chamber specific heart-on-a-chip for drug testing applications.* Adv Drug Deliv Rev, 2020. **165-166**: p. 60-76.
143. Mofazzal Jahromi, M.A., et al., *Microfluidic Brain-on-a-Chip: Perspectives for Mimicking Neural System Disorders.* Mol Neurobiol, 2019. **56**(12): p. 8489-8512.
144. Zhang, B., et al., *Advances in organ-on-a-chip engineering.* Nature Reviews Materials, 2018. **3**(8): p. 257-278.
145. Wnorowski, A., H. Yang, and J.C. Wu, *Progress, obstacles, and limitations in the use of stem cells in organ-on-a-chip models.* Adv Drug Deliv Rev, 2019. **140**: p. 3-11.
146. van den Berg, A., et al., *Personalised organs-on-chips: functional testing for precision medicine.* Lab Chip, 2019. **19**(2): p. 198-205.
147. Grizzle, W.E., W.C. Bell, and K.C. Sexton, *Issues in collecting, processing and storing human tissues and associated information to support biomedical research.* Cancer Biomark, 2010. **9**(1-6): p. 531-49.
148. Fabre, K.M., et al., *Utilizing microphysiological systems and induced pluripotent stem cells for disease modeling: a case study for blood brain barrier research in a pharmaceutical setting.* Adv Drug Deliv Rev, 2019. **140**: p. 129-135.
149. Tavakol, D.N., S. Fleischer, and G. Vunjak-Novakovic, *Harnessing organs-on-a-chip to model tissue regeneration.* Cell Stem Cell, 2021. **28**(6): p. 993-1015.
150. Pittenger, M.F., et al., *Multilineage potential of adult human mesenchymal stem cells.* Science, 1999. **284**(5411): p. 143-7.
151. Narsinh, K.H., J. Plews, and J.C. Wu, *Comparison of human induced pluripotent and embryonic stem cells: fraternal or identical twins?* Mol Ther, 2011. **19**(4): p. 635-8.
152. Sasai, Y., *Cytosystems dynamics in self-organization of tissue architecture.* Nature, 2013. **493**(7432): p. 318-26.
153. Jodat, Y.A., et al., *Human-Derived Organ-on-a-Chip for Personalized Drug Development.* Curr Pharm Des, 2018. **24**(45): p. 5471-5486.
154. Zhang, B. and M. Radisic, *Organ-on-a-chip devices advance to market.* Lab Chip, 2017. **17**(14): p. 2395-2420.

155. Ma, C., et al., *Organ-on-a-Chip: A New Paradigm for Drug Development.* Trends in Pharmacological Sciences, 2020.
156. Tsamandouras, N., et al., *Quantitative Assessment of Population Variability in Hepatic Drug Metabolism Using a Perfused Three-Dimensional Human Liver Microphysiological System.* J Pharmacol Exp Ther, 2017. **360**(1): p. 95-105.
157. van Berlo, D., et al., *Stem cells, organoids, and organ-on-a-chip models for personalized in vitro drug testing.* Current Opinion in Toxicology, 2021. **28**: p. 7-14.
158. Takahashi, K., et al., *Induction of pluripotent stem cells from adult human fibroblasts by defined factors.* Cell, 2007. **131**(5): p. 861-72.
159. Dogan, E., et al., *Cancer Stem Cells in Tumor Modeling: Challenges and Future Directions.* Advanced NanoBiomed Research, 2021. **1**(11): p. 2100017.
160. Andrysiak, K., J. Stępniewski, and J. Dulak, *Human-induced pluripotent stem cell-derived cardiomyocytes, 3D cardiac structures, and heart-on-a-chip as tools for drug research.* Pflügers Archiv - European Journal of Physiology, 2021. **473**(7): p. 1061-1085.
161. Danoy, M., et al., *Optimized protocol for the hepatic differentiation of induced pluripotent stem cells in a fluidic microenvironment.* Biotechnol Bioeng, 2019. **116**(7): p. 1762-1776.
162. Naumovska, E., et al., *Direct On-Chip Differentiation of Intestinal Tubules from Induced Pluripotent Stem Cells.* Int J Mol Sci, 2020. **21**(14).
163. Noorani, B., et al., *A Quasi-Physiological Microfluidic Blood-Brain Barrier Model for Brain Permeability Studies.* Pharmaceutics, 2021. **13**(9).
164. Fanizza, F., et al., *Induced pluripotent stem cell-based organ-on-a-chip as personalized drug screening tools: A focus on neurodegenerative disorders.* J Tissue Eng, 2022. **13**: p. 20417314221095339.
165. Du, Y., et al., *Mimicking liver sinusoidal structures and functions using a 3D-configured microfluidic chip.* Lab Chip, 2017. **17**(5): p. 782-794.
166. Sakolish, C., et al., *Analysis of reproducibility and robustness of a human microfluidic four-cell liver acinus microphysiology system (LAMPS).* Toxicology, 2021. **448**: p. 152651.
167. Yin, F., et al., *HiPSC-derived multi-organoids-on-chip system for safety assessment of antidepressant drugs.* Lab Chip, 2021. **21**(3): p. 571-581.
168. Oleaga, C., et al., *Investigation of the effect of hepatic metabolism on off-target cardiotoxicity in a multi-organ human-on-a-chip system.* Biomaterials, 2018. **182**: p. 176-190.
169. Zhang, Y.S., et al., *Multisensor-integrated organs-on-chips platform for automated and continual in situ monitoring of organoid behaviors.* Proc Natl Acad Sci U S A, 2017. **114**(12): p. E2293-e2302.
170. Qian, F., et al., *Simultaneous electrical recording of cardiac electrophysiology and contraction on chip.* Lab Chip, 2017. **17**(10): p. 1732-1739.
171. Marsano, A., et al., *Beating heart on a chip: a novel microfluidic platform to generate functional 3D cardiac microtissues.* Lab Chip, 2016. **16**(3): p. 599-610.
172. Abulaiti, M., et al., *Establishment of a heart-on-a-chip microdevice based on human iPS cells for the evaluation of human heart tissue function.* Sci Rep, 2020. **10**(1): p. 19201.

173. Christoffersson, J., et al., *A Cardiac Cell Outgrowth Assay for Evaluating Drug Compounds Using a Cardiac Spheroid-on-a-Chip Device.* Bioengineering (Basel), 2018. **5**(2).
174. Kujala, V.J., et al., *Laminar ventricular myocardium on a microelectrode array-based chip.* J Mater Chem B, 2016. **4**(20): p. 3534-3543.
175. Maoz, B.M., et al., *Organs-on-Chips with combined multi-electrode array and transepithelial electrical resistance measurement capabilities.* Lab Chip, 2017. **17**(13): p. 2294-2302.
176. Ircsak, K.M., et al., *A 3D microfluidic liver model for high throughput compound toxicity screening in the OrganoPlate®.* Toxicology, 2021. **450**: p. 152667.
177. Wang, Y., et al., *In situ differentiation and generation of functional liver organoids from human iPSCs in a 3D perfusable chip system.* Lab Chip, 2018. **18**(23): p. 3606-3616.
178. Torisawa, Y.-s., et al., *Bone marrow–on–a–chip replicates hematopoietic niche physiology in vitro.* Nature Methods, 2014. **11**(6): p. 663-669.
179. Sieber, S., et al., *Bone marrow-on-a-chip: Long-term culture of human haematopoietic stem cells in a three-dimensional microfluidic environment.* J Tissue Eng Regen Med, 2018. **12**(2): p. 479-489.
180. Aleman, J., et al., *Deconstructed Microfluidic Bone Marrow On-A-Chip to Study Normal and Malignant Hemopoietic Cell-Niche Interactions.* Small, 2019. **15**(43): p. e1902971.
181. Torisawa, Y.S., et al., *Modeling Hematopoiesis and Responses to Radiation Countermeasures in a Bone Marrow-on-a-Chip.* Tissue Eng Part C Methods, 2016. **22**(5): p. 509-15.
182. Musah, S., et al., *Directed differentiation of human induced pluripotent stem cells into mature kidney podocytes and establishment of a Glomerulus Chip.* Nature Protocols, 2018. **13**(7): p. 1662-1685.
183. Linville, R.M., et al., *Human iPSC-derived blood-brain barrier microvessels: validation of barrier function and endothelial cell behavior.* Biomaterials, 2019. **190-191**: p. 24-37.
184. Vatine, G.D., et al., *Human iPSC-Derived Blood-Brain Barrier Chips Enable Disease Modeling and Personalized Medicine Applications.* Cell Stem Cell, 2019. **24**(6): p. 995-1005.e6.
185. Wang, Y.I., H.E. Abaci, and M.L. Shuler, *Microfluidic blood-brain barrier model provides in vivo-like barrier properties for drug permeability screening.* Biotechnol Bioeng, 2017. **114**(1): p. 184-194.
186. Qi, D., et al., *Establishment of a Human iPSC- and Nanofiber-Based Microphysiological Blood-Brain Barrier System.* ACS Appl Mater Interfaces, 2018. **10**(26): p. 21825-21835.
187. Motallebnejad, P., et al., *An isogenic hiPSC-derived BBB-on-a-chip.* Biomicrofluidics, 2019. **13**(6): p. 064119.
188. Koo, Y., B.T. Hawkins, and Y. Yun, *Three-dimensional (3D) tetra-culture brain on chip platform for organophosphate toxicity screening.* Scientific Reports, 2018. **8**(1): p. 2841.
189. Osaki, T., V. Sivathanu, and R.D. Kamm, *Engineered 3D vascular and neuronal networks in a microfluidic platform.* Sci Rep, 2018. **8**(1): p. 5168.
190. Mo, S.J., et al., *A microfluidic gradient device for drug screening with human iPSC-derived motoneurons.* Analyst, 2020. **145**(8): p. 3081-3089.

191. Yang, K., et al., *Recapitulation of in vivo-like paracrine signals of human mesenchymal stem cells for functional neuronal differentiation of human neural stem cells in a 3D microfluidic system.* Biomaterials, 2015. **63**: p. 177-88.
192. Atchison, L., et al., *A Tissue Engineered Blood Vessel Model of Hutchinson-Gilford Progeria Syndrome Using Human iPSC-derived Smooth Muscle Cells.* Scientific Reports, 2017. **7**(1): p. 8168.
193. Ramme, A.P., et al., *Autologous induced pluripotent stem cell-derived four-organ-chip.* Future Sci OA, 2019. **5**(8): p. Fso413.
194. Skardal, A., et al., *Drug compound screening in single and integrated multi-organoid body-on-a-chip systems.* Biofabrication, 2020. **12**(2): p. 025017.
195. Joensson, H.N. and H. Andersson Svahn, *Droplet microfluidics--a tool for single-cell analysis.* Angew Chem Int Ed Engl, 2012. **51**(49): p. 12176-92.
196. Altschuler, S.J. and L.F. Wu, *Cellular heterogeneity: do differences make a difference?* Cell, 2010. **141**(4): p. 559-63.
197. Yang, H., et al., *Epithelial-Mesenchymal Micro-niches Govern Stem Cell Lineage Choices.* Cell, 2017. **169**(3): p. 483-496 e13.
198. Qian, M., et al., *Detection of single cell heterogeneity in cancer.* Semin Cell Dev Biol, 2017. **64**: p. 143-149.
199. Gawad, C., W. Koh, and S.R. Quake, *Single-cell genome sequencing: current state of the science.* Nature Reviews Genetics, 2016. **17**(3): p. 175.
200. Schwartzman, O. and A. Tanay, *Single-cell epigenomics: techniques and emerging applications.* Nature Reviews Genetics, 2015. **16**(12): p. 716-726.
201. Stegle, O., S.A. Teichmann, and J.C. Marioni, *Computational and analytical challenges in single-cell transcriptomics.* Nature Reviews Genetics, 2015. **16**(3): p. 133-145.
202. Rubakhin, S.S., et al., *Profiling metabolites and peptides in single cells.* Nature methods, 2011. **8**(4s): p. S20.
203. Breker, M. and M. Schuldiner, *The emergence of proteome-wide technologies: systematic analysis of proteins comes of age.* Nature reviews Molecular cell biology, 2014. **15**(7): p. 453-464.
204. Levy, E. and N. Slavov, *Single cell protein analysis for systems biology.* Essays in biochemistry, 2018. **62**(4): p. 595-605.
205. Klein, A.M., et al., *Droplet barcoding for single-cell transcriptomics applied to embryonic stem cells.* Cell, 2015. **161**(5): p. 1187-1201.
206. Ding, L., et al., *An easy-to-operate method for single-cell isolation and retrieval using a microfluidic static droplet array.* 2021. **188**(8): p. 1-11.
207. Luo, T., et al., *Microfluidic single-cell manipulation and analysis: Methods and applications.* 2019. **10**(2): p. 104.
208. Rotem, A., et al., *Single-cell ChIP-seq reveals cell subpopulations defined by chromatin state.* Nat Biotechnol, 2015. **33**(11): p. 1165-72.
209. Izzo, F., et al., *DNA methylation disruption reshapes the hematopoietic differentiation landscape.* Nature Genetics, 2020. **52**(4): p. 378-387.
210. De Micheli, A.J., et al., *Single-Cell Analysis of the Muscle Stem Cell Hierarchy Identifies Heterotypic Communication Signals Involved in Skeletal Muscle Regeneration.* Cell Rep, 2020. **30**(10): p. 3583-3595 e5.
211. An, C., et al., *Continuous microfluidic encapsulation of single mesenchymal stem cells using alginate microgels as injectable fillers for bone regeneration.* Acta Biomater, 2020. **111**: p. 181-196.

212. Sikorski, D.J., et al., *Clonal analysis of individual human embryonic stem cell differentiation patterns in microfluidic cultures.* Biotechnol J, 2015. **10**(10): p. 1546-54.
213. Zhong, J.F., et al., *A microfluidic processor for gene expression profiling of single human embryonic stem cells.* Lab Chip, 2008. **8**(1): p. 68-74.
214. Dettinger, P., et al., *Automated Microfluidic System for Dynamic Stimulation and Tracking of Single Cells.* Anal Chem, 2018. **90**(18): p. 10695-10700.
215. Lecault, V., et al., *High-throughput analysis of single hematopoietic stem cell proliferation in microfluidic cell culture arrays.* Nature methods, 2011. **8**(7): p. 581.
216. Skelley, A.M., et al., *Microfluidic control of cell pairing and fusion.* Nat Methods, 2009. **6**(2): p. 147-52.
217. Kobel, S.A., et al., *Automated analysis of single stem cells in microfluidic traps.* Lab Chip, 2012. **12**(16): p. 2843-9.
218. Faley, S.L., et al., *Microfluidic single cell arrays to interrogate signalling dynamics of individual, patient-derived hematopoietic stem cells.* Lab Chip, 2009. **9**(18): p. 2659-64.
219. Silvestris, E., et al., *In vitro differentiation of human oocyte-like cells from oogonial stem cells: single-cell isolation and molecular characterization.* Hum Reprod, 2018. **33**(3): p. 464-473.
220. Evander, M., et al., *Noninvasive acoustic cell trapping in a microfluidic perfusion system for online bioassays.* Anal Chem, 2007. **79**(7): p. 2984-91.
221. Wissemann, K.W. and B.S. Jacobson, *Pure gelatin microcarriers: synthesis and use in cell attachment and growth of fibroblast and endothelial cells.* In Vitro Cell Dev Biol, 1985. **21**(7): p. 391-401.
222. Moshaverinia, A., et al., *Dental mesenchymal stem cells encapsulated in an alginate hydrogel co-delivery microencapsulation system for cartilage regeneration.* Acta Biomater, 2013. **9**(12): p. 9343-50.
223. Zhao, X., et al., *Injectable stem cell‐laden photocrosslinkable microspheres fabricated using microfluidics for rapid generation of osteogenic tissue constructs.* 2016. **26**(17): p. 2809-2819.
224. Ng, E.X., et al., *Dissolvable Gelatin-Based Microcarriers Generated through Droplet Microfluidics for Expansion and Culture of Mesenchymal Stromal Cells.* Biotechnol J, 2021. **16**(3): p. e2000048.
225. Kim, H., et al., *Mesenchymal stem cell 3D encapsulation technologies for biomimetic microenvironment in tissue regeneration.* Stem Cell Res Ther, 2019. **10**(1): p. 51.
226. Allazetta, S., T.C. Hausherr, and M.P. Lutolf, *Microfluidic synthesis of cell-type-specific artificial extracellular matrix hydrogels.* Biomacromolecules, 2013. **14**(4): p. 1122-31.
227. Dashtimoghadam, E., et al., *Microfluidic fabrication of microcarriers with sequential delivery of VEGF and BMP-2 for bone regeneration.* Sci Rep, 2020. **10**(1): p. 11764.
228. Li, F., et al., *Microfluidic Encapsulation of Human Mesenchymal Stem Cells for Articular Cartilage Tissue Regeneration.* ACS Appl Mater Interfaces, 2017. **9**(10): p. 8589-8601.

229. Feng, S., et al., *Large-scale generation of functional and transplantable hepatocytes and cholangiocytes from human endoderm stem cells.* 2020. **33**(10): p. 108455.
230. Guerzoni, L.P.B., et al., *A Layer-by-Layer Single-Cell Coating Technique To Produce Injectable Beating Mini Heart Tissues via Microfluidics.* Biomacromolecules, 2019. **20**(10): p. 3746-3754.
231. Liu, H., et al., *A Droplet Microfluidic System to Fabricate Hybrid Capsules Enabling Stem Cell Organoid Engineering.* Adv Sci (Weinh), 2020. **7**(11): p. 1903739.
232. Chan, H.F., et al., *Rapid formation of multicellular spheroids in double-emulsion droplets with controllable microenvironment.* Sci Rep, 2013. **3**: p. 3462.
233. Onoe, H., et al., *Metre-long cell-laden microfibres exhibit tissue morphologies and functions.* Nat Mater, 2013. **12**(6): p. 584-90.
234. Wang, H., et al., *One-Step Generation of Aqueous-Droplet-Filled Hydrogel Fibers as Organoid Carriers Using an All-in-Water Microfluidic System.* ACS Appl Mater Interfaces, 2021. **13**(2): p. 3199-3208.
235. Liu, M., et al., *Synthesis of cell composite alginate microfibers by microfluidics with the application potential of small diameter vascular grafts.* Biofabrication, 2017. **9**(2): p. 025030.
236. Nguyen, T.P.T., N.X.T. Le, and N.Y. Lee, *Microfluidic Approach to Generate a Tadpole-Egg-Shaped Alginate Fiber and Its Application in Tissue Engineering.* ACS Biomater Sci Eng, 2020. **6**(3): p. 1663-1670.
237. Alessandri, K., et al., *A 3D printed microfluidic device for production of functionalized hydrogel microcapsules for culture and differentiation of human Neuronal Stem Cells (hNSC).* Lab Chip, 2016. **16**(9): p. 1593-604.
238. Kankala, R.K., et al., *Highly Porous Microcarriers for Minimally Invasive In Situ Skeletal Muscle Cell Delivery.* Small, 2019. **15**(25): p. e1901397.
239. Zhou, Z., et al., *Polymer-based porous microcarriers as cell delivery systems for applications in bone and cartilage tissue engineering.* 2021. **66**(2): p. 77-113.
240. Wang, J., et al., *Microfluidic generation of porous microcarriers for three-dimensional cell culture.* 2015. **7**(49): p. 27035-27039.
241. de Rutte, J.M., J. Koh, and D.J.A.F.M. Di Carlo, *Scalable high‐throughput production of modular microgels for in situ assembly of microporous tissue scaffolds.* 2019. **29**(25): p. 1900071.
242. Hidalgo San Jose, L., et al., *Microfluidic Encapsulation Supports Stem Cell Viability, Proliferation, and Neuronal Differentiation.* Tissue Eng Part C Methods, 2018. **24**(3): p. 158-170.
243. Kim, J., et al., *A Microfluidic Device to Fabricate One-Step Cell Bead-Laden Hydrogel Struts for Tissue Engineering.* Small, 2022. **18**(1): p. e2106487.
244. Sun, J., et al., *Mesenchymal Stem Cell‐Laden Composite β Cell Porous Microgel for Diabetes Treatment.* 2023: p. 2211897.
245. Zuo, X., et al., *A clinical feasible stem cell encapsulation ensures an improved wound healing.* 2023. **18**(2): p. 025005.
246. Giulitti, S., et al., *Direct generation of human naive induced pluripotent stem cells from somatic cells in microfluidics.* Nat Cell Biol, 2019. **21**(2): p. 275-286.

247. Gagliano, O., et al., *Microfluidic reprogramming to pluripotency of human somatic cells.* Nat Protoc, 2019. **14**(3): p. 722-737.
248. Singh, A., et al., *Adhesion strength-based, label-free isolation of human pluripotent stem cells.* Nat Methods, 2013. **10**(5): p. 438-44.
249. Luni, C., O. Gagliano, and N. Elvassore, *Derivation and Differentiation of Human Pluripotent Stem Cells in Microfluidic Devices.* Annu Rev Biomed Eng, 2022. **24**: p. 231-248.
250. Kamei, K., et al., *Microfluidic image cytometry for quantitative single-cell profiling of human pluripotent stem cells in chemically defined conditions.* Lab Chip, 2010. **10**(9): p. 1113-9.
251. Lyu, J., et al., *A microfluidics-derived growth factor gradient in a scaffold regulates stem cell activities for tendon-to-bone interface healing.* Biomater Sci, 2020. **8**(13): p. 3649-3663.
252. Tan, W.-H., et al., *A lamination micro mixer for μ-immunomagnetic cell sorter.* JSME International Journal Series C Mechanical Systems, Machine Elements and Manufacturing, 2005. **48**(4): p. 425-435.
253. Wu, H.W., et al., *An integrated microfluidic system for isolation, counting, and sorting of hematopoietic stem cells.* Biomicrofluidics, 2010. **4**(2).
254. Kane, K.I.W., et al., *Automated microfluidic cell culture of stem cell derived dopaminergic neurons.* Sci Rep, 2019. **9**(1): p. 1796.
255. Sun, G., et al., *Functional Stem Cell Sorting via Integrative Droplet Synchronization.* Anal Chem, 2020. **92**(11): p. 7915-7923.
256. Sakuma, S., et al., *Continuous mechanical indexing of single-cell spheroids using a robot-integrated microfluidic chip.* 2019. **4**(3): p. 2973-2980.
257. Fan, W., et al., *Single-cell impedance analysis of osteogenic differentiation by droplet-based microfluidics.* Biosens Bioelectron, 2019. **145**: p. 111730.
258. Valero, A., et al., *Gene transfer and protein dynamics in stem cells using single cell electroporation in a microfluidic device.* Lab Chip, 2008. **8**(1): p. 62-7.
259. Lakshmipathy, U., et al., *Efficient transfection of embryonic and adult stem cells.* Stem Cells, 2004. **22**(4): p. 531-43.
260. Jiang, A.Y.L., et al., *High-throughput continuous dielectrophoretic separation of neural stem cells.* Biomicrofluidics, 2019. **13**(6): p. 064111.
261. Schirhagl, R., et al., *Microfluidic purification and analysis of hematopoietic stem cells from bone marrow.* Lab Chip, 2011. **11**(18): p. 3130-5.
262. Gilland, B.J.F.p., *World population and food supply: can food production keep pace with population growth in the next half-century?* 2002. **27**(1): p. 47-63.
263. Alexandratos, N. and J. Bruinsma, *World agriculture towards 2030/2050: the 2012 revision.* 2012.
264. Ritchie, H. and M.J.O.w.i.d. Roser, *Land use.* 2013.
265. Shadow, F.L.s.L.J.F.R., Italy, *Environmental issues and options.* 2006.
266. Tsai, A.C., et al., *Influence of Microenvironment on Mesenchymal Stem Cell Therapeutic Potency: From Planar Culture to Microcarriers.* Front Bioeng Biotechnol, 2020. **8**: p. 640.
267. Lipsitz, Y.Y., N.E. Timmins, and P.W.J.N.b. Zandstra, *Quality cell therapy manufacturing by design.* 2016. **34**(4): p. 393-400.
268. Levine, D.W., et al., *Optimization of growth surface parameters in microcarrier cell culture.* 1979. **21**(5): p. 821-845.

269. Rodrigues, A.L., et al., *Dissolvable microcarriers allow scalable expansion and harvesting of human induced pluripotent stem cells under xeno‐free conditions.* 2019. **14**(4): p. 1800461.
270. Ding, L., R. Moloudi, and M.E. Warkiani, *Bioreactor-Based Adherent Cells Harvesting from Microcarriers with 3D Printed Inertial Microfluidics*. 2021, Springer.
271. Opalski, A.S., et al., *Grooved step emulsification systems optimize the throughput of passive generation of monodisperse emulsions.* Lab Chip, 2019. **19**(7): p. 1183-1192.
272. Dangla, R., et al., *The physical mechanisms of step emulsification.* 2013. **46**(11): p. 114003.
273. Reiss, J., S. Robertson, and M. Suzuki, *Cell Sources for Cultivated Meat: Applications and Considerations throughout the Production Workflow.* Int J Mol Sci, 2021. **22**(14).
274. Van Vlierberghe, S., et al., *Affinity study of novel gelatin cell carriers for fibronectin.* 2009. **9**(11): p. 1105-1115.
275. Tsuji, K., et al., *Effects of Different Cell-Detaching Methods on the Viability and Cell Surface Antigen Expression of Synovial Mesenchymal Stem Cells.* Cell Transplant, 2017. **26**(6): p. 1089-1102.
276. Zhang, H., et al., *Human myotube formation is determined by MyoD-Myomixer/Myomaker axis.* Sci Adv, 2020. **6**(51).
277. Olson, E.N., *Regulation of muscle transcription by the MyoD family. The heart of the matter.* Circ Res, 1993. **72**(1): p. 1-6.
278. Ganassi, M., et al., *Myogenin promotes myocyte fusion to balance fibre number and size.* Nat Commun, 2018. **9**(1): p. 4232.
279. Dedieu, S., et al., *Involvement of myogenic regulator factors during fusion in the cell line C2C12.* Int J Dev Biol, 2002. **46**(2): p. 235-41.
280. Galipeau, J., et al., *International Society for Cellular Therapy perspective on immune functional assays for mesenchymal stromal cells as potency release criterion for advanced phase clinical trials.* Cytotherapy, 2016. **18**(2): p. 151-159.
281. Baer, P.C., *Adipose-derived mesenchymal stromal/stem cells: An update on their phenotype in vivo and in vitro.* World J Stem Cells, 2014. **6**(3): p. 256-65.
282. Chamberlain, G., et al., *Concise review: mesenchymal stem cells: their phenotype, differentiation capacity, immunological features, and potential for homing.* Stem Cells, 2007. **25**(11): p. 2739-49.
283. Udani, V.M., *The continuum of stem cell transdifferentiation: possibility of hematopoietic stem cell plasticity with concurrent CD45 expression.* Stem Cells Dev, 2006. **15**(1): p. 1-3.
284. Marquez-Curtis, L.A., et al., *Mesenchymal stromal cells derived from various tissues: biological, clinical and cryopreservation aspects.* Cryobiology, 2015. **71**(2): p. 181-197.
285. Yong, K.W., et al., *Cryopreservation of Human Mesenchymal Stem Cells for Clinical Applications: Current Methods and Challenges.* Biopreserv Biobank, 2015. **13**(4): p. 231-9.

286. Akiyama, Y., et al., *Cryoprotectant-free cryopreservation of mammalian cells by superflash freezing.* Proceedings of the National Academy of Sciences, 2019. **116**(16): p. 7738-7743.
287. Lovelock, J. and M. Bishop, *Prevention of freezing damage to living cells by dimethyl sulphoxide.* Nature, 1959. **183**(4672): p. 1394-1395.
288. Kartberg, A.-J., et al., *Vitrification with DMSO protects embryo membrane integrity better than solutions without DMSO.* Reproductive biomedicine online, 2008. **17**(3): p. 378-384.
289. Rowley, S. and G.J.B.m.t. Anderson, *Effect of DMSO exposure without cryopreservation on hematopoietic progenitor cells.* 1993. **11**(5): p. 389-393.
290. Rammler, D.J.A.o.t.N.Y.A.o.S., *The effect of DMSO on several enzyme systems.* 1967. **141**(1): p. 291-299.
291. Da Violante, G., et al., *Evaluation of the cytotoxicity effect of dimethyl sulfoxide (DMSO) on Caco2/TC7 colon tumor cell cultures.* 2002. **25**(12): p. 1600-1603.
292. Bala Chandran, R., et al., *Influence of buoyancy-driven flow on mass transfer in a two-stream microfluidic channel: Introduction of cryoprotective agents into cell suspensions.* Biomicrofluidics, 2012. **6**(4): p. 44110.
293. Wang, J., et al., *Measurement of the biophysical properties of porcine adipose-derived stem cells by a microperfusion system.* Cryobiology, 2014. **69**(3): p. 442-50.
294. Song, Y.S., et al., *Microfluidics for cryopreservation.* Lab Chip, 2009. **9**(13): p. 1874-81.
295. Nguyen, N.-T. and Z. Wu, *Micromixers—a review.* Journal of micromechanics and microengineering, 2004. **15**(2): p. R1.
296. Lee, C.-Y., et al., *Microfluidic mixing: a review.* International journal of molecular sciences, 2011. **12**(5): p. 3263-3287.
297. Cai, G., et al., *A review on micromixers.* Micromachines, 2017. **8**(9): p. 274.
298. Rafeie, M., et al., *An easily fabricated three-dimensional threaded lemniscate-shaped micromixer for a wide range of flow rates.* Biomicrofluidics, 2017. **11**(1): p. 014108.
299. Ding, L., et al., *A modular 3D printed microfluidic system: a potential solution for continuous cell harvesting in large-scale bioprocessing.* Bioresources and Bioprocessing, 2022. **9**(1): p. 64.
300. Thirumala, S., W.S. Goebel, and E.J. Woods, *Clinical grade adult stem cell banking.* Organogenesis, 2009. **5**(3): p. 143-54.
301. Bazaz, S.R., et al., *Obstacle-free planar hybrid micromixer with low pressure drop.* 2020. **24**(8): p. 1-15.
302. Frangos, J.A., L.V. McIntire, and S.G. Eskin, *Shear stress induced stimulation of mammalian cell metabolism.* Biotechnol Bioeng, 1988. **32**(8): p. 1053-60.
303. Regmi, S., A. Fu, and K.Q. Luo, *High Shear Stresses under Exercise Condition Destroy Circulating Tumor Cells in a Microfluidic System.* Sci Rep, 2017. **7**: p. 39975.
304. Connolly, S., K. McGourty, and D. Newport, *The in vitro inertial positions and viability of cells in suspension under different in vivo flow conditions.* Sci Rep, 2020. **10**(1): p. 1711.
305. Huang, Y., et al., *Effects of shear stress on differentiation of stem cells into endothelial cells.* 2021. **13**(7): p. 894.

306. Sonam, S., et al., *Cell contractility arising from topography and shear flow determines human mesenchymal stem cell fate.* 2016. **6**(1): p. 1-12.
307. Marquez-Curtis, L.A., et al., *Mesenchymal stromal cells derived from various tissues: Biological, clinical and cryopreservation aspects.* Cryobiology, 2015. **71**(2): p. 181-97.
308. Levy, O., et al., *Shattering barriers toward clinically meaningful MSC therapies.* Science Advances, 2020. **6**(30): p. eaba6884.
309. Matthay, M.A., et al., *Treatment with allogeneic mesenchymal stromal cells for moderate to severe acute respiratory distress syndrome (START study): a randomised phase 2a safety trial.* The Lancet Respiratory Medicine, 2019. **7**(2): p. 154-162.
310. Moll, G., et al., *Do cryopreserved mesenchymal stromal cells display impaired immunomodulatory and therapeutic properties?* Stem cells, 2014. **32**(9): p. 2430-2442.
311. Panes, J., et al., *Expanded allogeneic adipose-derived mesenchymal stem cells (Cx601) for complex perianal fistulas in Crohn's disease: a phase 3 randomised, double-blind controlled trial.* Lancet, 2016. **388**(10051): p. 1281-90.
312. Notman, R., et al., *Molecular basis for dimethylsulfoxide (DMSO) action on lipid membranes.* 2006. **128**(43): p. 13982-13983.
313. Balint, B., et al., *The cryopreservation protocol optimal for progenitor recovery is not optimal for preservation of marrow repopulating ability.* Bone marrow transplantation, 1999. **23**(6): p. 613-619.
314. Skoric, D., et al., *Collection strategies and cryopreservation of umbilical cord blood.* Transfusion Medicine, 2007. **17**(2): p. 107-113.
315. Kreith, F. and R.M. Manglik, *Principles of heat transfer*. 2016: Cengage learning.
316. Byrne, B., S. Murray, and E.J.W. IGNASZEWSKI, DC: Good Food Institute., *State of the Industry Report: Cultivated Meat.* 2020.
317. Gomes, J., et al., *Monitoring and control of bioreactor: Basic concepts and recent advances.* 2018: p. 201-237.
318. Sensebé, L., et al., *Production of mesenchymal stromal/stem cells according to good manufacturing practices: a review.* 2013. **4**(3): p. 1-6.
319. Xie, Y., et al., *The quality evaluation system establishment of mesenchymal stromal cells for cell-based therapy products.* Stem Cell Res Ther, 2020. **11**(1): p. 176.
320. Serra, M., et al., *Advancing manufacture of human mesenchymal stem cells therapies: technological challenges in cell bioprocessing and characterization.* Current opinion in chemical engineering, 2018. **22**: p. 226-235.
321. Tsao, Y.S., et al., *Monitoring Chinese hamster ovary cell culture by the analysis of glucose and lactate metabolism.* J Biotechnol, 2005. **118**(3): p. 316-27.
322. Hassell, T., et al., *Growth inhibition in animal cell culture.* 1991. **30**(1): p. 29-41.
323. Lao, M.S. and D.J.B.p. Toth, *Effects of ammonium and lactate on growth and metabolism of a recombinant Chinese hamster ovary cell culture.* 1997. **13**(5): p. 688-691.

324. Jang, M., et al., *Serum-free cultures of C2C12 cells show different muscle phenotypes which can be estimated by metabolic profiling.* Sci Rep, 2022. **12**(1): p. 827.
325. Tsukamoto, S., et al., *Lactate Promotes Myoblast Differentiation and Myotube Hypertrophy via a Pathway Involving MyoD In Vitro and Enhances Muscle Regeneration In Vivo.* Int J Mol Sci, 2018. **19**(11).
326. Willkomm, L., et al., *Lactate regulates myogenesis in C2C12 myoblasts in vitro.* Stem Cell Res, 2014. **12**(3): p. 742-53.
327. Nalbandian, M., Z. Radak, and M. Takeda, *Lactate Metabolism and Satellite Cell Fate.* Front Physiol, 2020. **11**: p. 610983.
328. Moustogiannis, A., et al., *The Effects of Muscle Cell Aging on Myogenesis.* Int J Mol Sci, 2021. **22**(7).
329. O'Mara, P., et al., *Staying alive! Sensors used for monitoring cell health in bioreactors.* Talanta, 2018. **176**: p. 130-139.
330. Xiao, W. and Q.J.C. Dong, *The Recent Advances in Bulk and Microfluidic-Based pH Sensing and Its Applications.* 2022. **12**(10): p. 1124.
331. Zamboni, R., et al., *Opto-Microfluidic System for Absorbance Measurements in Lithium Niobate Device Applied to pH Measurements.* Sensors (Basel), 2020. **20**(18).
332. Guan, Z., et al., *A highly parallel microfluidic droplet method enabling single-molecule counting for digital enzyme detection.* Biomicrofluidics, 2014. **8**(1): p. 014110.